DISSERTATION

CHARACTERIZATION OF THE PERFORMANCE OF EXTRACTION CHROMATOGRAPHIC RESINS IN HIGH RADIATION ENVIRONMENTS

Submitted By

Rebecca Mueller

Department of Environmental and Radiological Health Sciences

In partial fulfillment of the requirements

For the Degree of Doctor of Philosophy

Colorado State University

Fort Collins, Colorado

Spring 2025

Doctoral Committee:

Advisor: Ralf Sudowe

Thomas Johnson
Alexander Brandl
Thomas Borch

ABSTRACT

CHARACTERIZATION OF THE PERFORMANCE OF EXTRACTION CHROMATOGRAPHIC RESINS IN HIGH RADIATION ENVIRONMENTS

The overall goal of this work is to analyze the impacts of ionizing radiation on extraction chromatography resins. This includes analyzing how the retention of a particular radionuclide changes as the resin is exposed to increasing doses of ionizing radiation (0 to 50 kGy). The effects of the system and strength of the aqueous mobile phase are also investigated with batch contact studies carried out on 3M nitric acid, 1M nitric acid, 3M hydrochloric acid, and 1M hydrochloric acid.

The changes to the surface functionality of the extraction chromatography resins are investigated via FTIR measurements. Changes in the physical structure of the resins and their fragmentation patterns are investigated via MALDI-TOF-MS (Matrix Assisted Laser Desorption Ionization Time of Flight Mass Spectrometry, referenced as MALDI colloquially).

ACKNOWLEDGEMENTS

There are many people without whom this dissertation wouldn't have been possible.

They include, but are not limited to, my parents, my siblings, and my dog.

I would like to make a particular acknowledgement of the late Joe Herndon, of ORNL, who helped me find a path that led me to the nuclear sciences as a study, for which I will be forever grateful.

I would like to thank Dr. Ralf Sudowe for his supervision and advice during this process. It has not been an easy or a short road, but I have grown so much as a scientist and a professional, and I would like to thank you again for your support.

Further acknowledgements include both funding sources and academic collaborations.

Academic collaborations have included the Analytical Resources Core (ARC) facility at Colorado State University—their Research Resource ID is listed here (RRID: SCR_021758). Specific acknowledgements to the FTIR and the MALDI instrumentation and maintenance teams are due. I would like to personally thank both Dr. Alyssa Winter May and Dr. Claudia Boot from the Mass Spectrometry (MS) facilities for their assistance in designing MALDI analyses, training, and troubleshooting assistance.

TABLE OF CONTENTS

LIST OF TABLES

LIST OF FIGURES

FOREWORD

This project started with a question. As, I imagine, many research projects have over the years. I read an article about irradiated extraction materials for radiochemical separations (yes, I know just how nerdy that sounds, thank you) and started wondering about materials I had worked with in the past. I had heard about columns that had turned to so much black sludge from exposure to highly radioactive analytes, but I hadn't come across a limit or benchmark for the extraction chromatography resins that are a modern radiochemist's proverbial bread and butter for laboratory scale separations. This made me quite curious and led me to do as any number of previous scientists have done in the past: I went to the literature. I looked through many articles describing what happens when you irradiate the extractants that are coated on the extraction chromatography resins (for more on this, see chapter 2), but I couldn't find any detailing how things changed when you only had a thin coating of that organic extractant on its inert polymer backbone. This led me to the second step of the classic graduate student research journey: my advisor's office. I went to my advisor's office and asked him the question I had encountered, namely: Is there a difference in how the extractants on extraction chromatography resins function under irradiation to how the organic extractants function if you irradiate them on their own? He looked at me, said he wasn't aware of anything to that effect being quantified, but he would look into it and get back with me. A few days later, he reached back out, advising me to reach out to others and ask them. The consensus from people with whom I discussed it seemed to be that differences were expected, but no one knew of work

actually published analyzing the differences. I was hooked. I knew what knowledge I would be pursuing in the near future.

CHAPTER 1: INTRODUCTION

1.1: Motivations

Radiochemical separations and the waste they generate are a contentious issue that radiochemists have faced and continue to face. Separations goals are complex and manifold in addition to being based on the end goals of that *particular* separation. The specifics inherent to a separation with defense applications differ from those with radiopharmaceutical applications. Radioactive and/or complex organic waste streams can be challenging for academic institutions but may be acceptable at a national laboratory. This is but one example of how complex radiochemical separations can be. What functions as a solution in one instance may not be an appropriate measure in another. While this can be frustrating and lead to complex challenges, this gives radiochemists such as the Ph.D. candidate writing this dissertation the opportunity to explore a variety of options that can be proposed to an institution even if they may not function within the confines necessary for a different institution. Radiochemical separations can lead to uniquely complicated waste streams with organic solvents mixing with the radioactive materials.

A major motivation behind the implementation of extraction chromatography is that it produces very small waste volumes, and the waste streams do not include organic solvents producing mixed wastes that require complex disposal procedures and are oh so difficult to dispose of. Therefore, if these separation systems could be implemented across a wider spectrum of radiochemical separations, that would be to everyone's benefit. Thus a sample of commercially available extraction chromatography resins was irradiated to determine how their

separation capability changes and determine how their functionality changed and how they broke apart under the stress of ionizing radiation.

1.2: Dissertation Goals

To explore the impacts of ionizing radiation on extraction chromatography resins, the first step is to have a well-characterized and prepared source of ionizing radiation. The lead time for such an instrument is not to be underestimated, therefore, making use of extant facilities is ideal. This project makes use of a Cesium-137 source present at Colorado State University; however, per discussions with the director of the irradiation facilities, the particular instrument best suited for batch irradiations had not been rigorously characterized recently. Therefore, the first milestone for this project is to characterize the dose rate that the instrument delivers to samples in particular geometries. This is discussed in Chapter 3 of this document. After determining the dose rate of the irradiator, a schedule of doses to deliver to the extraction chromatography resins was determined. The retention of the radioisotope of choice on the unirradiated resins was then determined and validated against literature values to ensure experimenter competence and familiarity with the separatory systems. From there, batch studies with irradiated resin were completed, irradiating the resin with the characterized instrument and then spiking it with the analyte. Batch contact studies were completed with an unirradiated control batch for every irradiated batch to ensure that effects quantified are the result of the irradiation rather than other, confounding variables. The analyte was then quantified via liquid scintillation counting. Further studies should be done to determine the changes in the irradiated resin in both surface functionality and fragmentation patterns due to the deposition of energy from ionizing radiation.

1.3: Dissertation Overview

In its totality, this dissertation aims to begin to address the question of how ionizing radiation affects extraction chromatography resins. To that end, however, all the steps through the procedural development process are detailed here. Following this introduction, the current state of the literature and a summation of the theory pertaining to radiochemical separations; extraction chromatography; radiolysis; the radiolytic degradation of separatory materials used for radiochemical separations; the theoretical underpinnings of spectrophotometry, spectroscopy, and mass spectrometry; the theory of MALDI and TOF mass spectrometry; and the theory inclement to liquid scintillation counting are detailed in Chapter 2. Chapter 3 then covers the analysis and characterization of the source of the radioactivity used to irradiate the materials in question. Further discussion of the specific extraction chromatographic resins studied in this work as well as the changes in their retention of plutonium-239 across absorbed doses of several orders of magnitude can be found in Chapter 4. Each of the experimental chapters will go into the theory about the particular method of detection employed. For example, Chapter 4 will go into the theoretical underpinnings of liquid scintillation, liquid scintillation cocktail, and liquid scintillation counters as well as giving the specifics of the particular instrument used in the course of this work. Chapter 5 thus follows with an analysis of the theoretical underpinnings of Infrared Spectroscopy as well as the changes in surface functionality of the same resins detailed in Chapter 4 as a result of a 50 kGy irradiation. Chapter 6 addresses the development of a method for the characterization of extraction chromatographic resins via MALDI-TOF-MS, and Chapter 7 uses the developed method to

analyze the resins before and after a 50 kGy irradiation to analyze their fragmentation patterns.

A discussion of overarching conclusions follows Chapter 7.

CHAPTER 2: LITERATURE REVIEW

2.1 Introduction and History of Radiochemical Separations

Before and through the dawn of anthropogenic knowledge of radiation and radioactivity, separations have been paramount to the elemental and isotopic analyses, as demonstrated both by the isolation of uranium using solvent extraction techniques, though they were not yet thus named, in the early nineteenth century (1) and by Marie and Pierre Curie's renown for the separation and identification of polonium and radium and their receipt of the related Nobel Prize (4). Tuned extractions have been used to isolate analytes of interest essentially for as long as there have been chemists. Broadly speaking, there are three main overarching methods used for radiochemical separations: precipitation, ion exchange, and solvent extraction. As solvent extraction is the method from which extraction chromatography spawned, there will be a discussion of its methods and principles below, to be followed by a discussion of extraction chromatography, i.e., the main separation method being studied in this work (5).

Here will be a quick discussion of solvent extraction, sometimes referred to as liquid-liquid extractions, because these are the qualities often exploited in today's targeted radiochemical separations (1). Solvent extraction, broadly, exploits the differences in analytes' migration from aqueous to organic substrates. Typically, this includes the contacting of an aqueous substance containing the analyte of interest with an organic extractant in a water-immiscible organic solvent. Broadly speaking, such interactions can be placed into four categories by *how* the element of interest is transferred from the aqueous to the organic substrate: chelate extraction

systems, cation-exchange extraction systems, ion-association extraction systems, and solvation extraction systems (1).

Chelate extraction systems are those in which the extracted analyte is an uncharged covalent compound, called a chelate complex. A chelate complex is a complex formed via two or more separate bindings forming between the same, central metal and a polydentate ligand. Common examples of these polydentate ligands, also called chelators or chelating agents, include organic molecules like dithizone, thenoyltrifluoroacetone (TTA), and N-benzoyl-N-phenylhydroxylamine (BPHA) (1).

Cation-exchange extraction systems are those in which the extracting agent has one hydrogen atom which can be replaced by a metal ion. They may also be described as liquid cation exchangers. The extraction agents in cation-exchange extraction systems are typically acidic organophosphorus compounds. A particularly prevalent example of such an extraction agent is di-2-ethylhexyl orthophosphoric acid (HDEHP or D2EHPA). For the sake of consistency, this text will use HDEHP. The extractants in cation-exchange extraction systems also tend to make use of P==O bonds as an additional coordination center from which to interact with the metal ion to satisfy both its charge and coordination requirements (1).

Ion-association extraction systems are those in which a variety of extractable species may form via association of the metal with oppositely charged ions present in either the organic or the aqueous phase. Examples of counter ions that aid in the formation of such pairs include hydronium ions [H^+] or [H_3O^+] or ferric chloride [$FeCl_4^-$]. A second example of such extractions is the use of high molecular weight amines in organic diluents as the amines behave like an anion exchanger (1).

Solvation extraction systems are those in which the species extracted is a coordinatively solvated salt formed by the molecules of the organic solvent which compete with surrounding water molecules for places within the first coordination shell of the cation. This then makes the metal species increasingly less hydrophilic and allows for the transfer of the metal from the aqueous layer to the organic layer. Examples of such oxygen-containing organic solvents used for similar processes generally contain some electronegative groups like (a.) ketones, ethers, and alcohols or (b.) more strongly polar neutral organophosphorus extractants that exclude water from the metal complexes. Examples of the first group include isobutyl methyl ketone (IBMK), and examples of the second group include tri-n-butyl phosphate (TBP) and trioctyl-phosphine oxide (TOPO). Especially with regards to the ion-association extractions completed via the use of organic solvents like ethers and TBP, solvation and a metal's relative solvation status play key roles in the efficacy and efficiency of the separatory process (1).

Regardless of the specific mechanism used when designing a separatory process, the selective transfer of chemical species from one immiscible phase to another is a powerful and versatile tool for separations in inorganic chemistry. The performance of a particular separation system using such a tool is generally quantified by the distribution ratio (D). D is defined as the ratio of the total concentration of that element in the organic phase to that in the aqueous phase at equilibrium (see equation 1). There are a variety of factors that must be taken into account when planning a separation scheme. Some of these are (a.) choosing the proper extractant and organic solvent, (b.) the nature and acidity of the aqueous phase in question, (c.) potential additions of masking agents, and (d.) the potential of salting out effects. The proper choice of extractant/organic solvent combination allows for a high degree of elemental selectivity. The

nature and strength of the aqueous phase can alter both the reactivity and the longevity of the extractant and the solvent. A masking agent can prevent the extraction of unwanted elements into the organic phase through the formation of strong, water-soluble complexes. In cases of ion-pair systems, the addition of optional salting out agents, i.e., salt which is not itself extracted, allows for a decrease in the activity of water and the dielectric constant of the aqueous phase. This allows for enhanced extraction of the analytes of interest into the organic phase. All of these factors can play a role in the development of an efficient solvent extraction process (1).

$$\mathrm{D} = \frac{[\mathrm{A}]_{\mathrm{org}}}{[\mathrm{A}]_{\mathrm{aq}}}$$

Equation 1: Equation defining the distribution ratio where D is the distribution ratio and A is the amount of an element of interest in the organic or aqueous phase respectively (1).

It is worth noting that D is a coefficient and not a constant. The value of D for a given system or separation varies based on several factors. First, D is dependent upon the concentration of the ion to be separated. In practice, however, this does not apply to analytes present in trace concentrations, as radionuclides often are. Thus, for radionuclides, D is generally constant with respect to the concentration of the radionuclide present in solution. This is part of what makes D such an effective quantitative measure of separation's efficiency or of the capacity of a separatory material. The distribution coefficient is also dependent on the concentration of other ions with the same charge present in the separatory solution. The presence of other, competing ions in solution decreases the efficiency and performance of the separatory system (5). D is also dependent on the pH of the separatory solution.

A radiochemical separation, however, as the name indicates, also includes a radioactive material. In other words, all of the above-listed factors must be considered along with the radioactive half-life of the analyte in question, the radiation that it emits in solution, and possible degradation of the solvent and/or the extractant (5). Since the 1960s, there have been considerable advancements made with regards to the efficiency, robustness, selectivity, and lack of toxicity of radiochemical separations (5). From the chemical separations employed at industrial scales using the PUREX process for plutonium production and forward with radiopharmaceutical separations of Technetium-99 in its metastable state (Tc-99m), the field has developed considerably in the intervening decades, with separations at the heart of the issue (6).

Radiopharmaceuticals in particular require separations that are both rapid and efficient. Radiopharmaceuticals must have rapid, effective separations because some isotopes used either therapeutically or diagnostically have short half-lives (6). Technetium-99m, which is the most commonly used diagnostic radionuclide, has a half-life of 6.0072 hours (7) and a biological half-life on the order of a day (6). A quick, effective separation is necessary to avoid excessive damage to the patient, either from exposure to excess radiation or from chemical damage from contaminants.

2.1.1 Introduction and History of Extraction Chromatography

Extraction chromatography, also called reverse-phase partition chromatography, came out of liquid-liquid or solvent extraction and ion exchange chromatography (1). Extraction chromatographic resins were introduced as commercially available radiochemical separatory

materials in the early 1990s. They have developed considerably since then. These resins play an important role in radiochemical separations due to their high retention factors for elements of interest, excellent separation performance, and the relatively small amount of waste created (2).

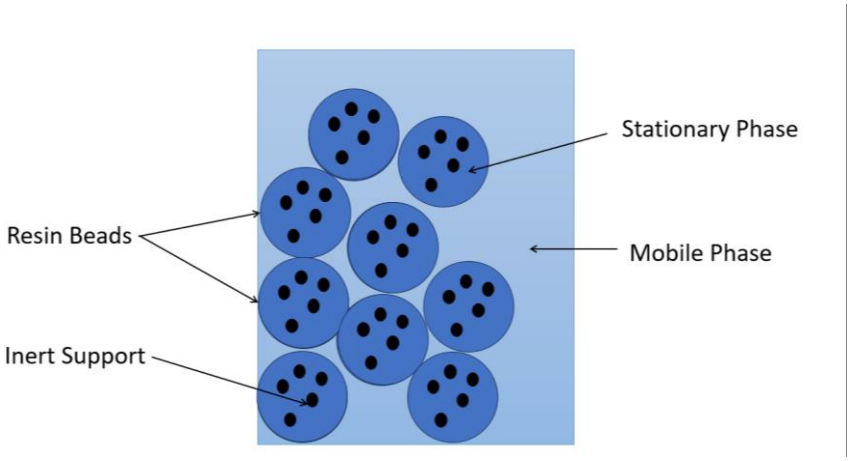

Figure 1: Diagram detailing the surface of an extraction chromatography resin bead, adapted from the Triskem International Produced document "Extraction Chromatography Technical Documentation- All Resins" (2).

An extraction chromatography resin bead is comprised of two main components: the stationary phase and the inert support. These are both highlighted in Figure 1. The inert support is a polymer that is generally highly cross linked for increased stability. The purpose of the inert support is simply to provide support and a surface on which the stationary phase can be mounted. The stationary phase is an organic extractant molecule in a diluent. The organic extractant is most commonly the main differentiating factor between resins. The mobile phase, also labelled in figure 1, is the solution that is contacted with the resin, often a mineral acid such as nitric acid. The analyte is pulled from the mobile phase onto the stationary phase during the extraction process and is then removed from the stationary phase/the resin with another, different mobile phase (2) (8).

Extraction chromatography performance can also be quantified via the distribution coefficient as a weight distribution ratio, D_w, or as a capacity factor. The capacity factor of a column, k', is the number of free column volumes (FCVs) corresponding to the volume of mobile phase contained in the column to peak maximum for a given element. The relationship of k' to the distribution coefficient (D) as defined for the corresponding liquid-liquid separations is given in the equation below.

$$k' = D\left(\frac{v_s}{v_m}\right)$$

Equation 2: Equation defining the capacity factor of a column, k', as a combination of the distribution coefficient, D, the volume of the stationary phase, v_s,, and the volume of the mobile phase, v_m (1).

For resins produced by Eichrom, the FCV corresponds to ~65-70% of the column bed volume, and it is possible to convert k' data to weight distribution ratios by using a correction factor that generally ranges from 1.7-2.0 and can be found in the technical documentation pertaining to that resin. The weight distribution ratio, D_w, is obtained by measuring the amount of a given metal ion taken up by a measured mass of resin from a given volume of aqueous solution. When radioactive species are being studied—as they are in this work—the weight distribution ratio can be calculated using the equation below.

$$D_w = \frac{A_0 - A_s}{A_s} * \frac{mL}{g}$$

Equation 3: Equation for EXC weight distribution ratios for radioactive elements where $A_0 - A_s$ is the activity sorbed on a known weight of resin (g) and A_s is the activity in a known volume (mL) of solution, reproduced from (2).

There are a variety of extraction chromatographic resins available commercially. A selection were taken and were included in the table below specifying the extractant mounted on the inert support; the diluent, if applicable; analytes that can be separated with that resin; trace and

potentially co-extracted elements; and examples of mobile phases for both loading the resin and eluting the analyte from the resin. All resins in the table use Amberchrom CG71 as the inert support (1). Amberchrom CG71 is a highly cross-linked polystyrene. This lends stability to the inert support of the resin and makes it incredibly difficult to dissolve the entire resin bead in common organic solvents used in polymeric studies such as tetrahydrofuran (THF) or chloroform. Of the resins listed in the table below, four were selected for this study of the radiolytic stability of extraction chromatography materials under gamma irradiation: TRU Resin, TEVA Resin, UTEVA Resin, and the Actinide (DIPEX) Resin.

Table 1: table identifying common EXC materials, their extracting agent, their target element/s for separation, trace impurities that can accompany the analyte, and the mobile phases for loading and extraction (1).

EXC material name (Supplier)	**Extracting Agent (Diluent, if applicable)**	**Target element/s**	**accompanying trace element/s**	**potentially extracted matrix element/s**	**mobile phase: extraction stage**	**mobile phase: back-extraction**
Sr Resin (Eichrom)	Crown ether DtBuCH18-C6 (1-Octanol)	Sr	(Ba), Pb	K	2-7 M HNO3	0.05 M HNO3 or H2O (Sr) or 6-8 M HCl (Pb)
Pb Resin (Eichrom)	Crown ether DtBuCH18-C6 (Isodecanol)	Pb	Bi		0.01-7 M HNO3	Complexing agents
TRU Resin (Eichrom)	Mixed, neutral organophosphorus (CMPO 13 wt.% + TBP 27 wt.%)	Pu, Np, Am, Th, U(VI)	Bi, lanthanides, Zr	Iron from >1 M HNO3	>1 M HNO3	very dilute [HNO3] or [HCl], complexing agents (HF)
RE Resin (Eichrom)	Mixed, neutral organophosphorus (CMPO 16 wt.% + TBP 24 wt.%)	Pu, Np, Am, Th, U, lanthanides		Iron from >1 M HNO3	>1 M HNO3	very dilute [HNO3] or [HCl], complexing agents (HF)

TEVA Resin (Eichrom)	Quaternary ammonium salt/ Aliquat 336	Pu, Np, Am, Th, U(IV)	Zr, Tc, Re		>1 M HNO3	very dilute [HNO3], dilute HF
UTEVA Resin (Eichrom)	neutral organophosphorus DAAP	Pu, Np, Am, Th, U(VI)	Zr		>2 M HNO3	very dilute [HNO3] or [HCl], dilute (HF)
Actinide (DIPEX) Resin (Eichrom)	Acidic organophosphorus H2DEHP [MDP]	actinides, lanthanides	Many (e.g., Zr, Hf, Nb, Mo)	Fe, Ti	large range of [HNO3]	di-phosphonic acid (HEDPA) or removal of stationary phase with isopropanol
Ln Resin (Eichrom)	Acidic organophosphorus HDEHP	Lanthanides	Zr, Hf	Fe, Ti	dilute HCl, HNO3, HClO4	more concentrated acids
DGA Resins (Eichrom)	Glycolamides TODGA or TEHDGA	Am(III), lanthanides	Zr, Hf	Ca	high [HNO3] or [HCl]	0.05-0.5 M HCl (lanthanides), 3 M HNO3-0.2 M HF (Zr. Hf, Th, U)
BPHA Resin	Hydroxamic acid BPHA	Nb, Ta, Mo, W	Zr, Hf	Ti	4 M HCl	2 M H2SO4-1% H2O2 (Ti), 1 M HF (Zr, Hf), 5 M HF (Ta)

Extraction chromatography systems demonstrate the selectivity of solvent extraction processes with their bespoke organic extractants and the processing speed and smaller, less complex waste generation of ion exchange processes (5) (1).

2.1.2 Drawbacks and Challenges of Extraction Chromatography

An issue that remains prevalent within the study of such materials is their durability under intense radiation exposure. Radiolytic degradation of the organic molecules used as extractants as well as the polymer backbone can have massive impacts on the efficiency of the radiochemical separation attained. Extraction chromatography provides rapid, efficient separations in analytical and laboratory scale radiochemical separations. However, procedures such as those used for preparing radioisotopes for radiopharmaceutical applications or separations involving used nuclear fuel can result in these resins being exposed to intense radiation fields. Since their durability to such radiation fields has not been explored, this research seeks to answer the questions: what happens when extraction chromatographic resins are exposed to high radiation environments, and how does their retention of analytes of interest change?

2.2 Introduction to Plutonium and its Chemistry

Plutonium is the 94th element on the periodic table, is abbreviated with the symbol Pu, and was formally created and identified in 1941 at the University of California, Berkeley (9). Its position is highlighted in figure 2. Plutonium's most common isotopes include 238, 239, 240, 241, 242, and 244, all of which have been identified from anthropogenic activities in the twentieth century (7). This work is primarily concerned with plutonium-239, an isotope of significant controversy due to its use in nuclear weapons and environmental concerns, both past and present. Plutonium-239 has a radiological half-life of 24,110 years, with an alpha emission abundance of 100 % and

an energy of 5.244 mega-electronvolts (MeV) and a spontaneous fission likelihood of 3.1×10^{-10} % abundance (7).

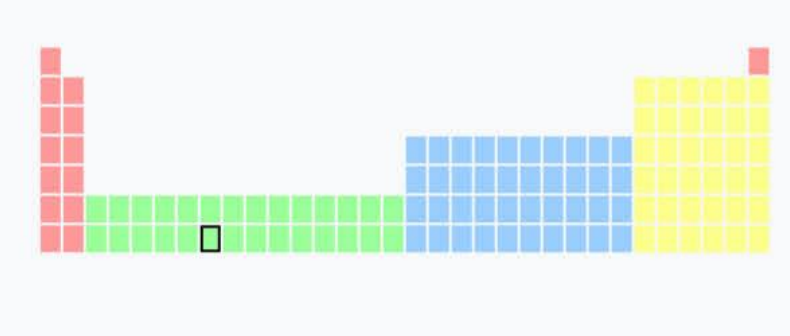

Figure 2: Figure of periodic table with actinides and lanthanides in raised position highlighting plutonium's position.

Plutonium compounds have been well-characterized in valence states from three (3+, III) to seven (7+, VII). Plutonium's chemical behavior presents challenges due to rich reduction-oxidation, or redox, chemistry. Plutonium exists in any of these oxidation states in aqueous solutions, depending on the other components of the solution and their relative reductive or oxidative character. In both 5+ and 6+ states, plutonium forms a plutonyl ion, characterized as two linearly bonded oxygen atoms double bonded to a plutonium ion in the center. A plutonyl ion is symbolically represented thus: PuO_2 and is generally hydrated in aqueous solutions like $PuO_2(H_2O)_5^q$ where q is equal to 1 or 2, with the oxygens of the waters arranged around the plutonium in a plane perpendicular to the linearly bound O==Pu==O structure. The plutonyl ion thus follows the actinide tendency for the formation of hydrated actinyl. Under acidic conditions with non-complexing acids, Pu(III) and Pu(IV) form complex, hydrated ions represented thus: $Pu(OH_2)_n^{q+}$, where q is either 3 or 4 and n is 8 or 9 (9).

Generally speaking, the tri- and tetra-valent plutonium species are less soluble than the penta- and hexa-valent. The relative tendency of a plutonium ion to form complexes or to undergo

hydrolysis follows the trend shown below. Pu^{4+} forms the strongest complexes, and PuO_2^+ forms the weakest (9).

$$Pu^{4+} > Pu^{3+} \approx PuO_2^{2+} > PuO_2^+$$

Equation 4: relation of the strength of complexes with concern to the valence state of the plutonium ions (9).

In acidic solutions containing plutonium, the energy needed to shift oxidation states is small. Therefore, even slight changes in the oxidizing power of the solution can have large impacts on the oxidation state of the plutonium in solution. It is entirely possible and, in fact, kinetically favorable, for multiple oxidation states of plutonium to exist in solution simultaneously.

Many plutonium compounds of various oxidation states can be precipitated out of solution. Plutonium forms compounds with most elements of the periodic table. Almost all of these compounds are, to some degree, ionic; however, many binary plutonium compounds are semiconductors or metallic. Plutonium borides, group 13 compounds (carbides, silicides, and germanides), pnictides (Pu-N, Pu-P, Pu-As, Pu-Sb, and Pu-Bi systems), and chalcogenides (Pu-S, Pu-Se, and Pu-Te systems) are some important, primarily refractive classes of such binary compounds that plutonium can form (9).

Currently, nuclear power plants produce plutonium on the order of 70-90 megatons per year. The total global inventory is greater than 1900 megatons. Most of this material is within spent fuel rods; however, there is also a fairly significant amount of the global plutonium inventory in the form of nuclear weapons, disassembled nuclear weapons, and recycled reactor fuel. Safeguarding this material is a significant task.

2.2.1 Extraction Chromatography of Plutonium

Extraction chromatography is well-suited for separations of plutonium from other actinide materials and/or fission products on an analytical or laboratory scale. There are several extraction chromatography resins specifically aimed at actinide, and specifically plutonium separations. A selection of commercially available resins that can target plutonium have been taken from Table 1 and reproduced in the table below.

Table 2: An excerpt taken from Table 1, adapted from (1).

EXC material name (Supplier)	**Extracting Agent (Diluent, if applicable)**	**Target element/s**	**mobile phase: extraction stage**	**mobile phase: back-extraction**
TRU Resin (Eichrom)	Mixed, neutral organophosphorus (CMPO 13 wt.% + TBP 27 wt.%)	Pu, Np, Am, Th, U(VI)	>1 M HNO3	very dilute [HNO3] or [HCl], complexing agents (HF)
RE Resin (Eichrom)	Mixed, neutral organophosphorus (CMPO 16 wt.% + TBP 24 wt.%)	Pu, Np, Am, Th, U, lanthanides	>1 M HNO3	very dilute [HNO3] or [HCl], complexing agents (HF)
TEVA Resin (Eichrom)	Quaternary ammonium salt/ Aliquat 336	Pu, Np, Am, Th, U(IV)	>1 M HNO3	very dilute [HNO3], dilute HF
UTEVA Resin (Eichrom)	neutral organophosphorus DAAP	Pu, Np, Am, Th, U(VI)	>2 M HNO3	very dilute [HNO3] or [HCl], dilute (HF)
Actinide (DIPEX) Resin (Eichrom)	Acidic organophosphorus H2DEHP [MDP]	actinides, lanthanides	large range of [HNO3]	di-phosphonic acid (HEDPA) or removal of stationary phase with isopropanol

In this study, four resins were examined for their stability and their performance with regards to plutonium retention following their irradiation: TRU, TEVA, UTEVA, and the Actinide resins were selected for this study. RE Resin was not selected for this study as multiple active extractant components were desired, and RE and TRU Resins have the same active extractants, with

different ratios of CMPO to TBP (2). TRU Resin was selected rather than RE Resin between the two because it is more frequently and commonly used.

Table 3: EXC Resins selected for this study, including their conversion factors and literature defined distribution ratios, adapted from (2).

EXC material name	Vs/Vm	To convert Dw to k', divide by	Dw, Pu 3M HNO3	Dw, Pu 1M HNO3	Dw, Pu 3M HCl	Dw, Pu 1M HCl
TRU	0.22	1.8	90000	14400	270	18
TEVA	0.23	1.9	38000	7600	171	1.9
UTEVA	0.25	1.7	1020	510		
Actinide	0.2	1.9			190000	1520000

2.3 Introduction to Radiation Chemistry, Radiolysis, and Related Products

Radiation chemistry as a field implies the study of the chemical impacts of ionizing radiation interacting with materials. Here, the term 'ionizing radiation' is "applied to photons or particles having sufficient energy to ionize the molecules of the medium: it involves photons with energies ranging from the first ionization energy of the medium (~10 eV) up to several MeV, as well as energetic charged particles, electrons, positrons, accelerated heavy ions, etc. The result of the energy absorption is breaking or rearrangement of chemical bonds" (10). It is possible for high-energy photons or charged species with sufficiently high energy to be absorbed by the nuclei of atoms and then subsequently to undergo nuclear reactions. These reactions fall under the umbrellas of nuclear physics, nuclear chemistry, and/or radiochemistry but are not considered in radiation chemistry (10).

High energy photons interact with the medium via the photoelectric effect, Compton scattering, and electron-positron pair production. From the perspective of energy absorption in a given medium, there are four main cases to consider: (a.) activated molecule formation in the

interactions of very high-energy particles such as photons or electrons with the atoms and molecules in hard collisions, (b.) interactions of fast electrons (electrons with energies ranging from several hundred to several thousand eV) with the atoms and molecules of the medium, (c.) reactions of slow electrons (electrons with energies between ~5 and 100 eV) with the atoms and molecules of the medium, and (d.) scattering of very low-energy electrons (electrons with <5 eV) in the medium (10).

In the first case listed above—that of activated molecule formation due to the interactions of very-high energy electrons with atoms and molecules of the medium in hard collisions, a large amount of energy is transferred to the electron of the interacting molecule. This system is fairly well described via the classical model with the system being comprised of a fast-moving charged particle passing near a free electron at rest. The Coulomb interaction of the free electron begins as the fast-moving charged particle loses momentum and energy. The "probability" for a charged particle to transfer energy between Q and Q + dQ to an electron of the medium when passing is given below.

$$dP = NZ\frac{2\pi e^4 z^2}{(4\pi\varepsilon_0)^2 m_e u^2} * \frac{dQ}{Q^2}$$

Equation 5: model describing the "probability" dP for a charged particle with charge ze and speed u to transfer energy between Q and Q+dQ to an electron of the medium when passing unit distance and where m_e is the electron mass, N is the number density of molecules, and Z is the number of electrons in one molecule, making NZ (the product of the two) the electron number density (10).

The quantity dP/NZ has a dimension of (length)^2 and is called the differential cross section for the events per electron (10). For low values of Q (when Q is near or comparable to the binding energy of the electron), the model of a collision with a free electron at rest is no longer correct. For such "soft collisions", a model is applied involving the resonance-like absorption of energy

by the molecules. A visual representation of such interactions is shown in the figure below. In the gas phase, the fast electron passing by the molecule (M) induces a strongly time-dependent electric polarization in the molecule. This time-dependent electric polarization presents in the molecule as electromagnetic waves over a range of frequencies. Some electrons may begin oscillating and resonant excitation or ionization may occur (10).

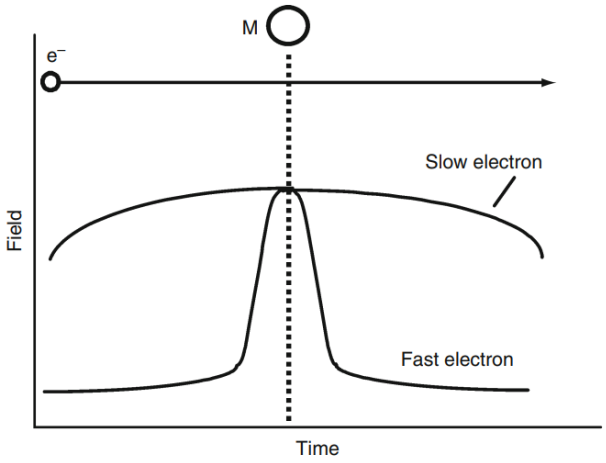

Figure 3: Figure showing interaction of a passing electron (e) with a molecule (M). Fast electrons exert an impulse action on the molecule, but the effect is elongated in the case of slow electrons (11) included in the Handbook of Nuclear Chemistry (10).

The time needed for a fast electron with kinetic energy between 10^2 and 10^4 eV (the second case listed above) to pass by a molecule is on the order of attoseconds (10^{-18} s) which is similar to the time required for the electric transition induced by the absorption of a photon of ~10 eV energy. A fast charged particle's impulse action is then generally comparable with the energy absorbed from the electromagnetic field. In the action of the charged particle, like in photolysis, selection rules and relevant versus forbidden transitions work to determine processes experienced by the molecule. There are a few key differences between photolysis and interactions with fast electrons. During the absorption of a photon, the total energy of the photon is absorbed by the molecule, leading to a given excitation or ionization. During the

interactions with the fast electrons, the energy gained by the molecule varies from the energy of the lowest excited state to the total energy involved (10).

However, the energy absorption at high energies is limited by reciprocal energy dependence. Therefore, most energy absorption occurs between the energies of 10 and 40 eV. In this energy range, there is also the possibility of the formation of so-called “super excited” molecules. These are neutral excited molecules whose excess energy is higher than the ionization threshold. These molecules thus have short lifetimes and may undergo auto-ionization, conversion to lower energy excited molecules, or in direct dissociation to fragments. As the kinetic energy of an incident particle drops below ~100 eV, reaching the third case of interactions between higher-energy particles and nearby molecules listed above, the possibility of a sudden and dramatic energy transfer decreases to near non-existence. Therefore, it is in this energy range that the optical approximation loses its relevance, and previously disallowed transitions may occur (10). When higher-energy particles transfer energy the incident radiation drops below ~5 eV, i.e., the fourth case of interactions described, energy can no longer be transferred via electron excitation processes. The electron instead undergoes extended scattering in the medium, gradually losing energy to the rotational and/or vibrational levels of the surrounding molecules (10).

The total energy lost per unit path length is described in the Linear Energy Transfer (LET) of the radiation. The LET of the radiation can be determined by taking the sum of all energy losses occurring in both hard and soft collisions over a given amount of space. The average LET for fast electrons in water is ~0.2 eV per nm. An alpha particle with ~5 MeV of energy has a considerably higher LET value of ~40 eV per nm. The linear energy transfer for a given particle

with a given energy is dependent on the square of the charge of the particle (z^2) and inversely proportional to the square of its speed (u^2). In radiation chemistry, the deposition of energy tends to lead to the formation of higher-energy intermediates that are short lived. As an electron progresses further down its track, these intermediates tend to become more densely populated (10).

Radiolysis investigations involve the identification of such intermediates and/or the changes in the medium as a result of the absorption of energy from radiation. As the yields of radiolysis experiments are generally low—on the order of 0.0001-0.01, sensitive analytical techniques are necessary. Typically, this has called for spectrophotometry, gas chromatography (GC), or high-performance liquid chromatography (HPLC) (10). The theoretical underpinnings of spectrophotometry are included in section 2.4. Radiolysis products are identified in this work via MALDI-TOF-MS, or Matrix Assisted Laser Desorption Ionization-Time of Flight-Mass Spectrometry. The theoretical underpinnings of mass spectrometry with a focus on MALDI systems are included in section 2.5. Here the focus will be on what radiolysis is accomplishing chemically whereas the later focus will be on identification and quantification of the resulting changes.

The main intermediates generated during radiolysis reactions include excited molecules, cations, free electrons, anions, and radicals. There are a few main factors that must be considered when aiming to quantify the chemical effects of ionizing radiation. These are the molecules transformed or produced and the amount of absorbed radiation energy that caused the effect. The ratio of these two values is the radiation chemical yield, also called the “G-value” and denoted G in the equation below (10). A material’s G-value can be expressed in the SI unit

of the mole per Joule (mol/J, mol J^{-1}). In earlier literature, a material's G-value was expressed in terms of how many molecules were produced, changed, or destroyed per 100 eV of energy absorbed.

$$G(X) = \frac{n(X)}{E}$$

Equation 6: equation to determine the radiation chemical yield where n is the amount of a substance, X, which is produced, destroyed, or changed by radiation by the mean energy imparted, E, into the irradiated material (10).

Since only the fraction of the energy actually absorbed by the material can lead to physical or chemical changes, an important quantity to be aware of with radiation chemical experiments is the absorbed dose. The absorbed dose, or simply the dose for the purposes of this work, is defined as the average energy imparted to an incremental quantity of matter divided by the mass of that matter (see equation below). Absorbed dose is most often quantified in the SI units of Gray (Gy), defined as 1 joule per kilogram (J/kg or $J \bullet kg^{-1}$) which is equal to 6.24 x 10^{15} electron volts per gram (10).

$$D_{abs} = \frac{dE}{dm}$$

Equation 7: equation defining the parameter absorbed dose (D_{abs}) in terms of the energy deposited in an incremental mass (dm), divided by that mass (10).

The radiolysis of water is one of the more heavily studied solvent radiolysis systems. The intermediates of water's radiolysis are well characterized and include hydrated electrons (e_{aq}^-), hydroxyl radicals (OH), and hydrogen atoms (H). These intermediates generally form as a consequence of the ionization of surrounding water molecules.

$$1: H_2O \rightsquigarrow H_2O^{+\circledast} + e^-$$

$$2: H_2O \rightsquigarrow H_2O^*$$

$$3: H_2O^{+\circledast} + H_2O \rightarrow H_3O^+ + OH$$

$$4: e^- + nH_2O \rightarrow e^-_{aq}$$

$$5: H_2O^* \rightarrow OH + H$$

$$6: e^-_{aq} + H_3O^+ \rightarrow H_2O + H$$

$$7: H + OH \rightarrow H_2O$$

$$8: H + H \rightarrow H_2$$

$$9: 2e^-_{aq} + 2H_2O \rightarrow 2OH^- + H_2$$

$$10: OH + OH \rightarrow H_2O_2$$

Equation 8: chemical reactions of water undergoing radiolysis (10).

The radical cation formed in the first step may manage to migrate a few water molecules over by resonance electron transfer; however, it functions as a strong acid and will generally give a proton to one of the nearby water molecules within ~10^{-14} s (step 3). The resultant electron released in step 1 collides with other surrounding molecules, releases its kinetic energy, and, within ~10^{-12} s, is localized in a potential energy well due to the rotation of the molecular dipoles in the presence of the negative charge. This leads to the formation of the solvated (hydrated) electron, also referred to as an aqueous electron (step 4). The excited water molecules formed in step 2 decay to a hydroxyl radical and a hydrogen atom as shown in step 5. Hydrogen atoms are also formed when the hydrated electrons interact with the hydroxonium ions, as shown in step 6. The final products of the radiolysis of water, hydrogen gas and hydrogen peroxide, are created from the reactions of the intermediates (shown in steps 7-10). It

is important to note that, while the reactions above are labelled as “steps” for ease of reference, they can and do happen concurrently during the process of radiolysis and do not necessarily lead directly into one another. They also occur on quite different time scales, which allows for multiple species to be made by the incident radiation (10), (12).

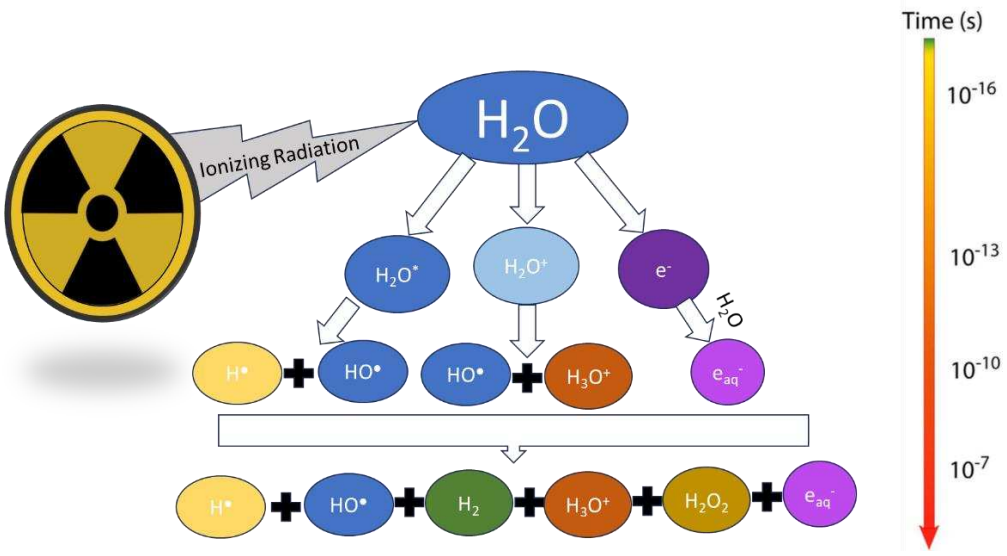

Figure 4: Pictorial representation of the radiolysis of water with time-scales, adapted from (12).

The hydroxyl radical is a strong oxidizing agent, and both the aqueous electrons and hydrogen atoms have strong reducing potential (10).

$$1: \mathrm{NO_3^-} + \mathrm{e_{aq}^-} \longrightarrow \mathrm{HNO_3^{2-\circledast}}$$

$$2: \mathrm{NO_3^-} + \mathrm{H} \longrightarrow \mathrm{HNO_3^{-\circledast}}$$

$$3: \mathrm{HNO_3} + \mathrm{OH} \longrightarrow \mathrm{NO_3^{\circledast}} + \mathrm{H_2O}$$

Equation 9: Reactions involving nitrate ions/nitric acid and radiolysis products (10)

Two additional ion systems are being queried here in addition to water due to their use in extraction chromatography systems. Both nitric and hydrochloric acids can function as the

mobile phase in extraction chromatography systems (see section 2.1.1) for finely tuned selection sensitivity (2). In nitric acid or generally in the presence of nitrate ions, these ions react with the aqueous electrons and, through intermediates, form nitrous radicals ($NO_2^{\bullet}$) which partially transform into nitrate and nitrite ions. The final products of radiolysis in concentrated nitric acid systems include HNO_2, H_2, and O_2 with yields varying with acid concentration (10). Some reactions in this process are shown in equation 9. In hydrochloric acid or generally in the presence of chloride ions, hydrogen atoms and chloride radicals are formed (shown in equation 10). As these are particularly reactive chemical species, they are short lived in solution but can cause changes and/or damage to surrounding chemical species (10) (13).

$$1\text{: } \mathrm{HCl} \rightsquigarrow \mathrm{HCl}^{\circledast\circledast}$$

$$2\text{: } \mathrm{HCl}^{\circledast\circledast} \longrightarrow \mathrm{H} + \mathrm{Cl}^{\circledast}$$

$$3\text{: } \mathrm{HCl}^{\circledast\circledast} \longrightarrow \mathrm{HCl}^{+} + \mathrm{e}_{\mathrm{aq}}^{-}$$

Equation 10: reactions describing radiolysis effects in hydrochloric acid/chloride ion systems (13).

These species can cause significant chemical damage to a tailored extraction agent present in solution for the selective separation of radionuclides (10) (5).

2.3.1 Irradiated Extraction Materials

The first part of this section will deal with different kinds of damage to materials and how the more common breakages within chemical structures occur. The second part will pull the extractants on the resins chosen in this study and identify how they have been reported to break under radiolysis in the literature when not part of an extraction chromatography system.

$$1\text{: } H + R^{\circledast} \rightarrow HR, \text{where R is any radical}$$

$$2a\text{: } CH_4 \rightarrow CH_3^{\circledast} + H$$

$$2b\text{: } CH_4 \rightarrow CH_2 + H_2$$

$$2c\text{: } CH_4 \rightarrow CH + H_2 + H$$

$$3a\text{: } H_2C = CH - CH_2CH_2CH_3^{\circledast} \rightarrow \overline{H_2C - CHCH}^{\circledast}CH_2CH_3 + H$$

$$3b\text{: } H_2C = CH - CH_2CH_2CH_3^{\circledast} \rightarrow \overline{H_2C - CHCH_2}^{\circledast} + H_2C^{\circledast}CH_3$$

Equation 11: series of chemical reactions that can occur in materials due to the presence of radiolysis products (10).

There are several main methods by which extraction materials can be damaged while undergoing irradiation. Any radical that encounters a hydrogen atom is likely to combine with that radical as shown in reaction 1 in equation 11. Reactions 2a, 2b, and 2c all show some of the ways that saturated hydrocarbons can react in the presence of incident radiation, where atoms toward the outside of the molecule tend to take in energy and splinter off. This also holds with hydrocarbon chains, with such molecules experiencing a tendency to lose an end group or a fragment. Since such released atoms, end groups, or fragments also tend to carry more of the incident energy off with them, they can also combine in interesting ways with surrounding molecules. Some can even synthesize into longer chain molecules or polymers (10). In allylic molecules, the C-H or the C-C bond in the beta position to the double bond tends to break as the π-π^* interactions allow for more favorable orbital restructuring. These two cases are shown in reactions 3a and 3b above.

2.4 Introduction to Spectrophotometry, Spectroscopy, and Spectrometry

This section deals with several similar-sounding words wherein the differences highlight some of the different analytical techniques used throughout this project. All three main terms—spectrophotometry, spectroscopy, and spectrometry—all derive from the Latin spectrum/spectra for “appearance” or “form” in the sense of looking at or regarding. Spectroscopy is “the science that deals with the use of the spectroscope and with spectrum analysis” according to dictionary.com (14). Spectrophotometry is any procedure that uses light to measure chemical concentrations (15). Spectrometry deals with the quantification of features from a generated spectrum. Thus, when spectroscopy is referenced, it is for the purposes of characterization rather than quantification; however, when spectrometry is referenced, the opposite is true. Spectrophotometry deals specifically with the behavior of a sample with the addition of light. Here, when spectrophotometry is referenced, that will indicate that light in the ultra-violet to visible range is being introduced to the sample. Figure 6 shows the regions of the electromagnetic spectrum and includes representative examples of potential inter- and intra-molecular interactions that can be examined using particular wavelengths. These differing interactions with differing wavelengths of electromagnetic energy are exploited for a variety of analytical techniques (3) (15).

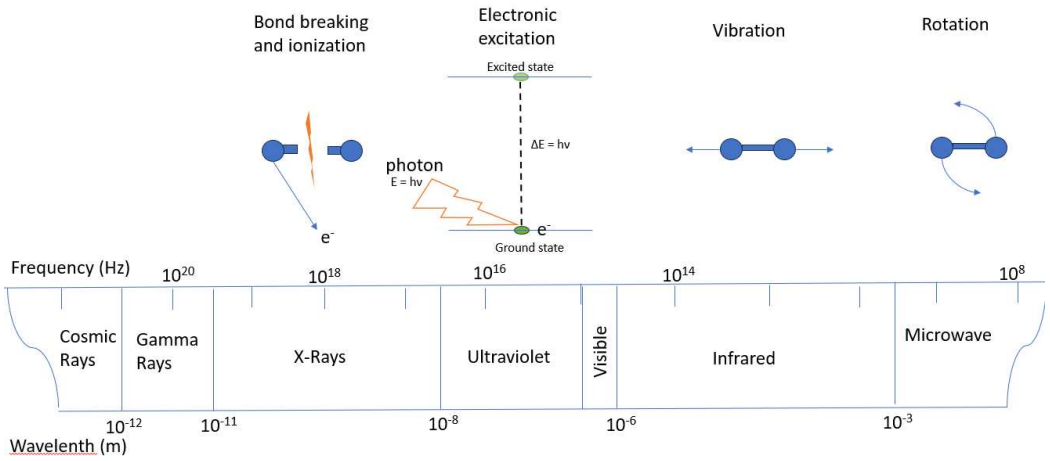

Figure 5: Electromagnetic spectrum, showing representative molecular processes that occur when light in each region is absorbed. The visible spectrum is from 380-780 nm (15).

This project uses instruments examining sample materials in the ultraviolet-visible range during the characterization of the irradiator (for more details, see Chapter 3), in the range of ionizing gamma radiation for the irradiation of the extraction chromatographic resins which is further discussed in the radiolysis section of this chapter, and in the infrared range for the characterization of the changes to the surface functionality of those irradiated resins via Fourier Transformed Infrared Spectroscopy (FTIR), which is discussed next.

FTIR, Fourier Transformed Infrared spectroscopy, makes use of infrared radiation which is broadly defined as the part of the electromagnetic spectrum between the visible and the microwave regions. Infrared radiation can be absorbed and converted within an organic molecule into molecular rotation energy. The frequency or wavelength of the absorption depends on the relative masses of the atoms, the force constants of the bonds, and the geometry of the atoms being queried (3).

Band positions in the generated spectra are presented in either wavenumbers (inverse or reciprocal centimeters, cm^{-1}) or wavelengths. As the wavenumber is directly proportional to the

energy of the vibration, this unit is used most often for reporting purposes. Band intensities are reported in either transmittance (T) or absorbance (A). Transmittance is the ratio of the radiant power transmitted by a sample to the radiant power incident on the sample. Absorbance is the base 10 logarithm of the reciprocal of the transmittance as reflected in the equation 12 below (3).

$$A = \log_{10}\left(\frac{1}{T}\right)$$

Equation 12: equation showing the relationship between absorbance (A) and transmittance (T).

There are two types of molecular vibrations: stretching and bending. A stretching vibration is a rhythmical movement along a bond axis with a change in the interatomic distance. A bending vibration may consist of a change in bond angle between bonds with a common atom or the movement of a group of atoms with respect to the remainder of the molecule without movement of the atoms in the group with respect to one another. Examples include twisting, rocking, and torsional vibrations (3).

Assignments for stretching frequencies can be estimated using an application of Hooke's Law. In this application, two atoms and their connecting bond are viewed as a simple harmonic oscillator composed of two masses joined by a spring. The equation below, derived from Hooke's Law, states the relationship between the frequency of oscillation, the atomic masses, and the force constant of the bond. The force constant of a single bond is on the order of 5×10^5 dynes per centimeter, and double and triple bonds double and triple this constant respectively (3).

$$\bar{\nu} = \frac{1}{2\pi c}\left(\frac{f}{\frac{M_X M_Y}{(M_X + M_Y)}}\right)^{1/2}$$

Equation 13: : Equation relating the frequency of oscillation, the atomic masses, and force constant of the bond between two atoms, derived from Hooke's Law, where $\bar{\nu}$ is the vibrational frequency in wavenumbers (cm^{-1}), c is the velocity of light in centimeters per second (cm/s), f is the force constant of the bond in dynes per centimeter (dynes/cm), and Mx and My are the masses of atoms x and y respectively in grams (g).

Using the above equation, some rough regions of interest for spectroscopy can be defined. A selection is shown in the table below *(3)*.

Table 4: Types of organic bonds and their regions of general placement in IR Spectroscopy (3).

Bond Type	Stretching frequencies / cm^{-1}
C—C, C—O, C—N	1300-800
C==C, C==O, C==N, N==O	1900-1500
C≡≡C, C≡≡N	2300-2000
C—H, O—H, N—H	3800-2700

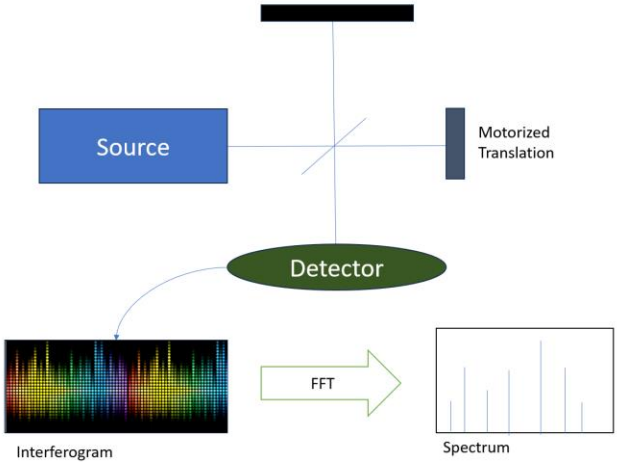

Figure 6: Schematic representation of FTIR functionality, adapted from Wikimedia commons.

2.5 Introduction to Mass Spectrometry and MALDI-TOF Systems

While the spectrometry/spectroscopy debate was touched on in the previous section, mass spectrometry makes up a significant enough portion of this project to justify its own section. Mass spectrometry involves the differentiation of ionized analytes of different masses to charge

(m/z) ratios via the application of an electromagnetic current and sufficient voltage. The differentiation of analytes by their flight paths has been used as an analytical tool since the late nineteenth or early twentieth centuries. Ionization sources differ across mass spectrometry systems (16).

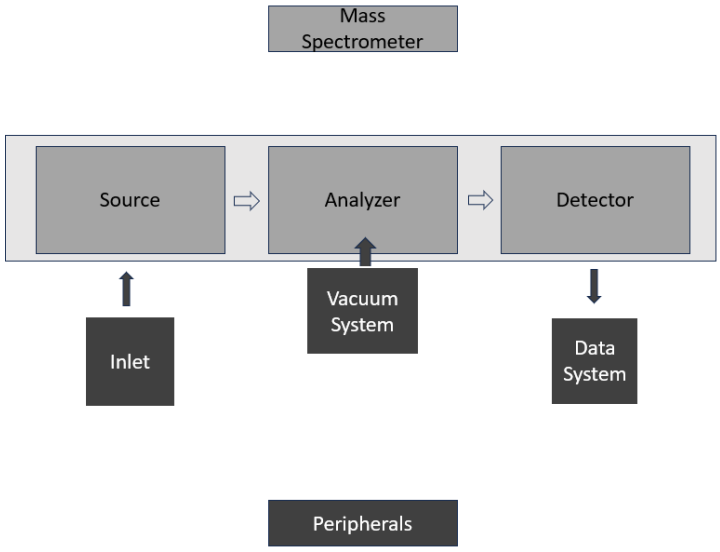

Figure 7: Fundamental components of a mass spectrometer, adapted from (16).

The three primary components necessary to produce a mass spectrometer are an ion source, a mass analyzer, and a detector, as shown in the figure above. The ion source functions to vaporize and ionize samples. The mass analyzer, broadly speaking, separates ions based on their mass to charge ratio or, more broadly, their mass. More on the specific mass analyzer used in this work is discussed later in this section, including figures 11 and 12. The detector functions to measure the separated ions as they come out of the mass analyzer. There are many variations in these components which then make up the variety of mass spectrometers (16).

The early steps necessary for obtaining a mass spectrum include analyte species being converted from a solid or liquid phase to gas phase ions which includes both the vaporization and the ionization of the species in question. Vaporization of the species has generally been accomplished via the evaporation of the sample with heating, if necessary. Many sample types have sufficient vapor pressure under the vacuum generated by the peripheral system (typically in the realm of 10^{-6} torr) for sublimation to occur directly into the ion source with little to no external heat added. However, many biological molecules, proteins, and polymers decompose prior to evaporation. For upward of seven decades, ionization in mass spectrometry was generally accomplished via the bombardment of the vaporized sample with electrons in a process called either electron bombardment (EB) or, more commonly, electron impact (EI) ionization. This ionization occurs via the interaction of a 70-eV electron and the sample which results in the sample molecule ejecting a secondary electron and forming a radical cation. This radical cation is generally in a relatively energetic state and rapidly loses its excess energy by fragmentation to produce characteristic lower mass fragments. While the 'fingerprint' of fragmentation patterns can be used to identify some molecules, this becomes incredibly difficult when analyzing larger, more complex molecules. This has led to the development of 'softer' ionization methods like MALDI.

From here, this section will narrow in on the component variants used in this project. The particular system employed during this project is known as MALDI-TOF-MS—Matrix Assisted Laser Desorption Ionization Time of Flight Mass Spectrometry. From this relatively long and confusing acronym, the main components for discussion are the MALDI, or the Matrix Assisted

Laser Desorption Ionization, which is the ionization source, and the TOF, or the Time of Flight, which is the mass analyzer.

MALDI, or Matrix Assisted Laser Desorption Ionization, is one of many methods of ionization that has developed over the years and was part of the basis for the 2002 Nobel Prize in Chemistry awarded to Koichi Tanaka. MALDI serves as both a method of vaporization and of ionization in a single step. Because MALDI accomplishes both of these processes in the same step, it is referred to as a desorption/ionization technique. MALDI has an advantage over some other ionization methods in that it provides a "soft" or relatively non-destructive mechanism of converting analytes from the solid phase into gas-phase ions while minimizing fragmentation and generally keeping molecular analytes intact (16).

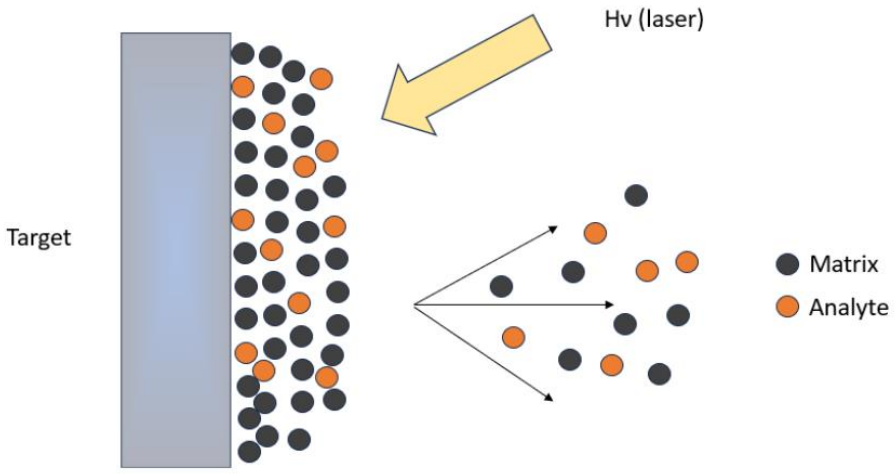

Figure 8: Principle illustration of the MALDI process, adapted from "An Introduction to MALDI-TOF MS" (16).

An illustration of the MALDI process is shown above. The three primary components of a MALDI analysis here are the analyte, the matrix, and the target. The analyte is the compound of interest for the analysis which is, with an excess of matrix compound, deposited on a target. The

target is generally a solid surface comprised of a conducting metal, like stainless steel. A variety of materials can be used as matrix materials; however, one of the more commonly used types is an aromatic organic, weak acid that absorbs light at the wavelength of the laser in the MALDI instrument. These are commonly yellow in powdered forms, and the structures of several have been included in the figure below. Lasers used in MALDI instruments are commonly modified neodymium yttrium silver (NdYAg), called neodymium yag, lasers which pulse at 305 nm (16).

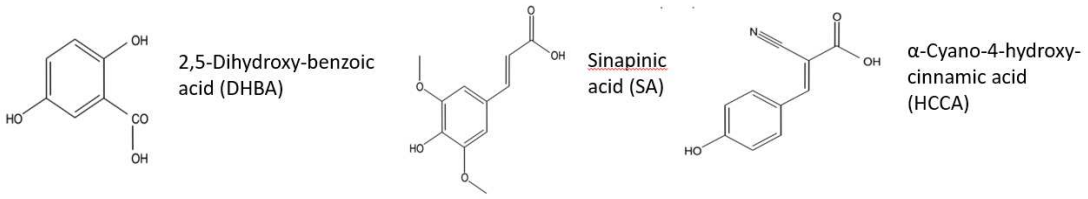

Figure 9: Structural formulae of three typical matrix compounds, replicated from "An Introduction to MALDI-TOF MA" (16).

A solution containing the analyte is generally mixed with a saturated solution containing the matrix material. The analyte, along with an excess of matrix material, is embedded on the target plate. When dry, the target plate is placed into the mass spectrometer's ion source. Because the matrix material absorbs strongly at the wavelength of the laser, a strong interaction between the matrix and the solid analyte layer occurs regardless of the light-absorbing properties of the analyte itself. Following a very brief laser pulse, the interrogated spot on the target is rapidly heated and becomes vibrationally excited. The usual common-sense notion of heating does not apply because the process involves an explosive expansion into a high-vacuum region rather than an equilibrium step. The laser energy is absorbed, and the generated vibrational energy results in material being expelled from the target in a plume just above the interrogated spot. This emission is accompanied by minimal dissociative vibrational excitation of the analyte as the expanding plume of matrix physically conveys the analyte into the vapor state with minimal

heating of the sample. This can allow for complex molecules like intact proteins or polymers to be transferred into the gas phase without experiencing the decomposition that would be expected from regular, heat-induced evaporation. As such, MALDI as a process can transfer both ionic and neutral species into a vaporous state. Depending on the selection of the particular matrix material involved, a gas-phase protonated analyte may be produced. None of the abundant desorbed neutral species are detected by the mass spectrometer. While fragmentation and the presence of multi-charged ions are both possible, they typically occur in spectra at such a magnitude as to be readily identifiable. These generated ions then depart the ion source section of the mass spectrometer and enter the mass analyzer section (16).

In a MALDI-TOF instrument like the one used in this work, the mass analyzer section of the instrument is a Time-of-Flight unit. The ions generated via the MALDI process are accelerated so that they obtain a mass-dependent velocity and move from the ion source and into a "separation" region. The ions separate in the drift or "field-free" region in which the ions attain different velocities based on their mass and charge—i.e., their mass-to-charge, *m/z*, ratio—which allows for separation as the ions "race" toward the detector, as shown in the figure below. TOF mass spectrometers operate in a pulsed mode. Therefore, each spectrum is produced from a discrete "event" in which a group, or packet, of ions is formed and accelerated. All of these ions, being either positively or negatively charged, formed in the original packet are separated in time (by their time of flight) and registered by the detector. Since basically all ions from each pulse eventually reach the detector to be recorded, the mass spectrum produced has very high sensitivity. This approach is called "separation in time". The main alternative to this approach is "separation in space" and is used in magnetic and quadrupole-based mass analyzers

to differentiate one *m/z* value—in its certain location or "space"—from all others by discarding all the unselected values. This approach results in the detection of only that small fraction of ions being detected in the scanning mode. This difference in separations via "time" or "space" serves as one of the major differences between TOF instruments and many other mass spectrometers. With Time-of-Flight mass spectrometers, the whole process can be repeated very rapidly. Many spectra can be determined in a few seconds which can then be averaged to produce a final recorded mass spectrum with an enhanced signal-to-noise ratio (16).

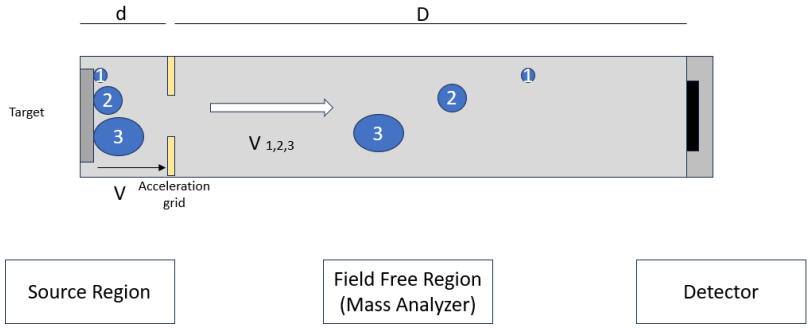

Figure 10: Principle of a time-of-flight mass spectrometer, adapted from (16).

In an absence of collisions as ions traverse the instrument, ion flight times can be directly related to *m/z* values. Ions must be formed in a specific region of the ion source because ions formed in different regions could experience a different accelerating potential. With a desorption/ionization system coupled with a TOF mass spectrometer, the ion formation usually occurs on the target, labelled in previous figures. Ions formed near or on this surface in the ion source are accelerated across a potential difference (V) created within this region, see figure above. The voltage difference results from the different potentials applied to the target and an acceleration grid at opposite ends of the ion source region. This voltage creates an electric field

that imparts energy of motion equal to the product of the number of charges on each ion (z), the magnitude of the charge of a single electron (*e*), and the overall voltage difference of the region designated (d) in the figure above. This energy of motion is a kinetic energy (KE) given by equation 2 in the equation series below. Combining equations 1 and 2 gives equation 3. In equation 3, the mass and velocity of the ions generated in the ion source are m and v. Mass spectrometry data are usually plotted with ion abundance on the vertical axis and the mass-to-charge (*m/z*) ratio on the horizontal axis. Solving for the mass-to-charge ratio gives equation 4. Since the charge of the electron and, in many experimental set-ups, the voltage applied across the ion source region are both constant, equation 4 can be simplified to equations 5 and 6. Equation 4 shows that ions leaving the source region have velocities inversely related to the square root of their mass-to-charge ratios. As long as collisions do not occur, these ions will maintain a constant velocity across the field-free region enroute to the detector. The most convenient manner for discerning the *m/z* values is by indirectly measuring the velocities of the ions. The detector of the ions is at a fixed location in the mass spectrometer at a distance, D, from the ion source (see above figure). The time taken by ions to reach the detector can be related to velocity and is given by equation 7. Substituting for v and recognizing that D is also a constant gives equation 8. This shows that ion arrival times at the detector can be related to the square root of their mass-to-charge ratios, which can then be rearranged into equation 9 to once more solve for *m/z*. Equation 9 can have the constants substituted back into it; however, it is more common to use as an experimentally determined calibration parameter, k (sometimes listed as a), and "offset" *m/z* value, b, shown in equation 10. The equation series below governs a fairly simple linear time-of-flight mass spectrometry system. Additional resolving power can

be generated by reflector systems which include a turn, multiple detectors, and multiple free field regions to increase the separation of ions generated in the ion source, shown in the figure following the equation series below.

$$1.\ \text{Energy} = zeV$$

$$2.\ KE = \frac{mv^2}{2}$$

$$3.\ \frac{mv^2}{2} = zeV$$

$$4.\ \frac{m}{z} = \frac{2eV}{v^2}$$

$$5.\ \frac{m}{z} = \frac{k}{v^2}$$

$$6.\ v = \sqrt{\frac{kz}{m}} = \frac{k}{\sqrt{\left(\frac{m}{z}\right)}}$$

$$7.\ t = \frac{D}{v}$$

$$8.\ t = \frac{D\sqrt{m}}{\sqrt{k'z}} = k'\sqrt{\frac{m}{z}}$$

$$9.\ \frac{m}{z} = k't^2$$

$$10.\ \frac{m}{z} = kt^2 + b$$

Equation 14: Equations related to time-of-flight mass spectrometry (16).

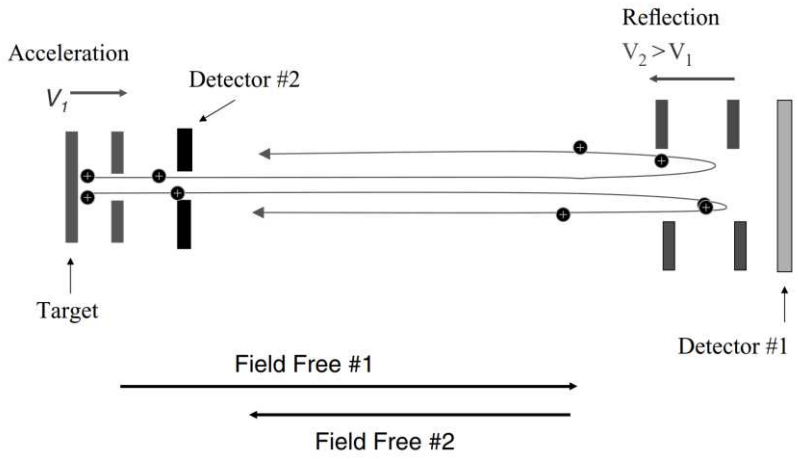

Figure 11: Principle of a reflectron/reflector mass spectrometer, reproduced from (16).

In summary, there are several advantages to Time-of-Flight mass spectrometry: sensitivity, mass range, and speed. A TOF instrument detects all ions of like charge, rather than only a particular pre-selected mass-to-charge value. Time of Flight mass spectrometers also pair exceptionally well with Matrix Assisted Laser Desorption Ionization systems as both function well in pulsed modes.

2.6 Introduction to Liquid Scintillation Counting

An introduction to liquid scintillation counting is best begun with an introduction to scintillation counting. Scintillation is, itself, a release of energy as light. Radiometric scintillation counting takes advantage of the property of some materials to emit light when exposed to excess energy, from ionizing radiation. There are two basic steps to radiometric scintillation detection: light production and signal detection. Light photons are produced from the interaction of the radiation field with the scintillating material. The number of photons produced is proportional to the energy deposited from the initial radiation. The visible light is converted to an electric signal by a dedicated electronic instrument—usually a photomultiplier tube (PMT) or a solid-state photodetector optically coupled to the scintillator (17). This is pictorially represented in the figure below.

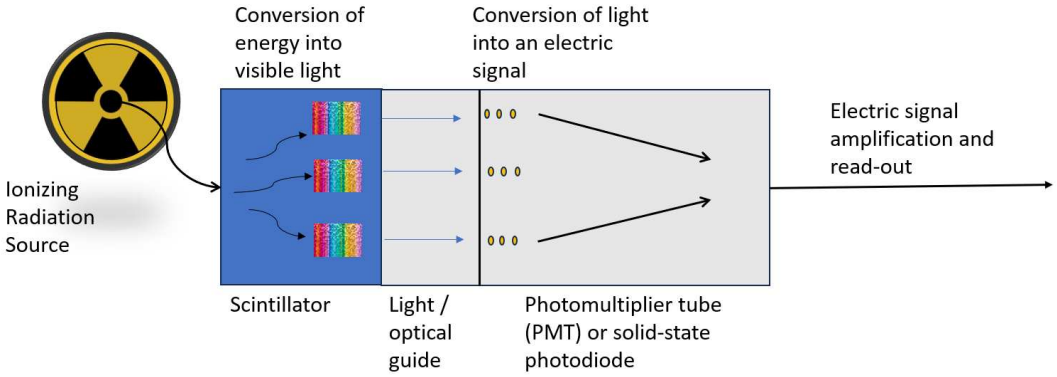

Figure 12: Pictorial representation of the radiometric scintillation process, adapted from (17).

Scintillator materials can be organic or inorganic; however, this section will focus on organic scintillator materials as those are the materials used in liquid scintillation counting. The process through which organic scintillation occurs begins when the primary incident radiation promotes one or more valence electron/s to a higher energy level in the π-molecular orbitals characteristic to organic scintillators. The typical energy level structure of an organic scintillator is shown in the figure below. An integral feature of π-molecular orbitals of the organic scintillators is the presence of a fine structure which relates to differing vibrational states of each energy level. The de-excitation of an excited electron to the ground state usually involves an excited vibrational level. Therefore, the energy of the visible photon associated with the de-excitation of the electron is less than the energy of the primary excitation energy. As a result, the organic scintillating material is functionally transparent to the visible photons associated with the scintillation process (17).

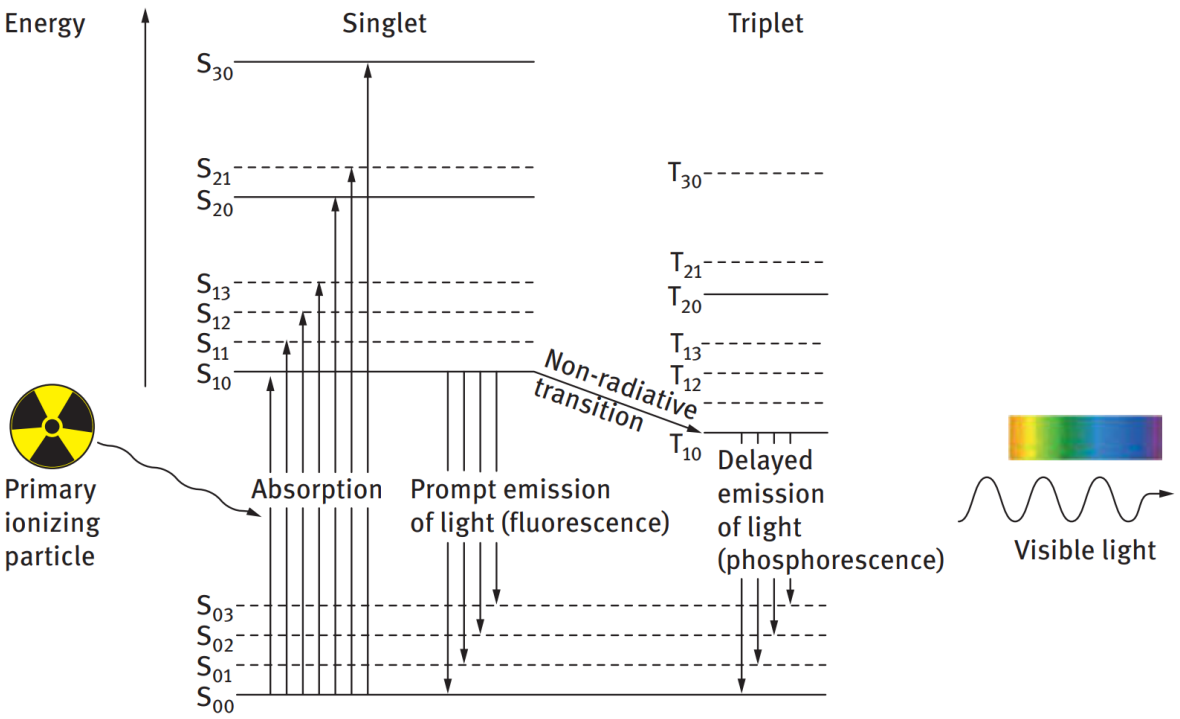

Figure 13: Typical scheme of the energy structure of an organic scintillator. The fine structure associated with each level is denoted in dashed lines, reproduced from (17).

Organic scintillators can be either crystalline solids or dissolved in an organic solvent. There are several parameters that are important to bear in mind when selecting among scintillator materials: the time-shape of the light produced in the scintillation event, the number of visible photons produced per unit energy deposited by the incident radiation, and the stopping power for charged particles or the attenuation coefficient for photons of the material. The spectral characteristics of the visible light produced and the refractive index of the material should both be in line with the PMT or other photodiode to prevent efficiency loss. Since organic scintillators are comprised of relatively low Z elements, they have poor attenuation for photons but can work well with charged particle detection (17).

Since alpha and beta emissions have very low penetrative potential—especially alpha emissions—counting them from external geometries can be difficult. However, putting the sample in direct contact with a liquid containing a scintillator can be an effective method of counting. Such cocktails contain three main parts: an organic scintillator solute, a solvent, and a wavelength shifter and are commonly referred to as “scintillation cocktails”.

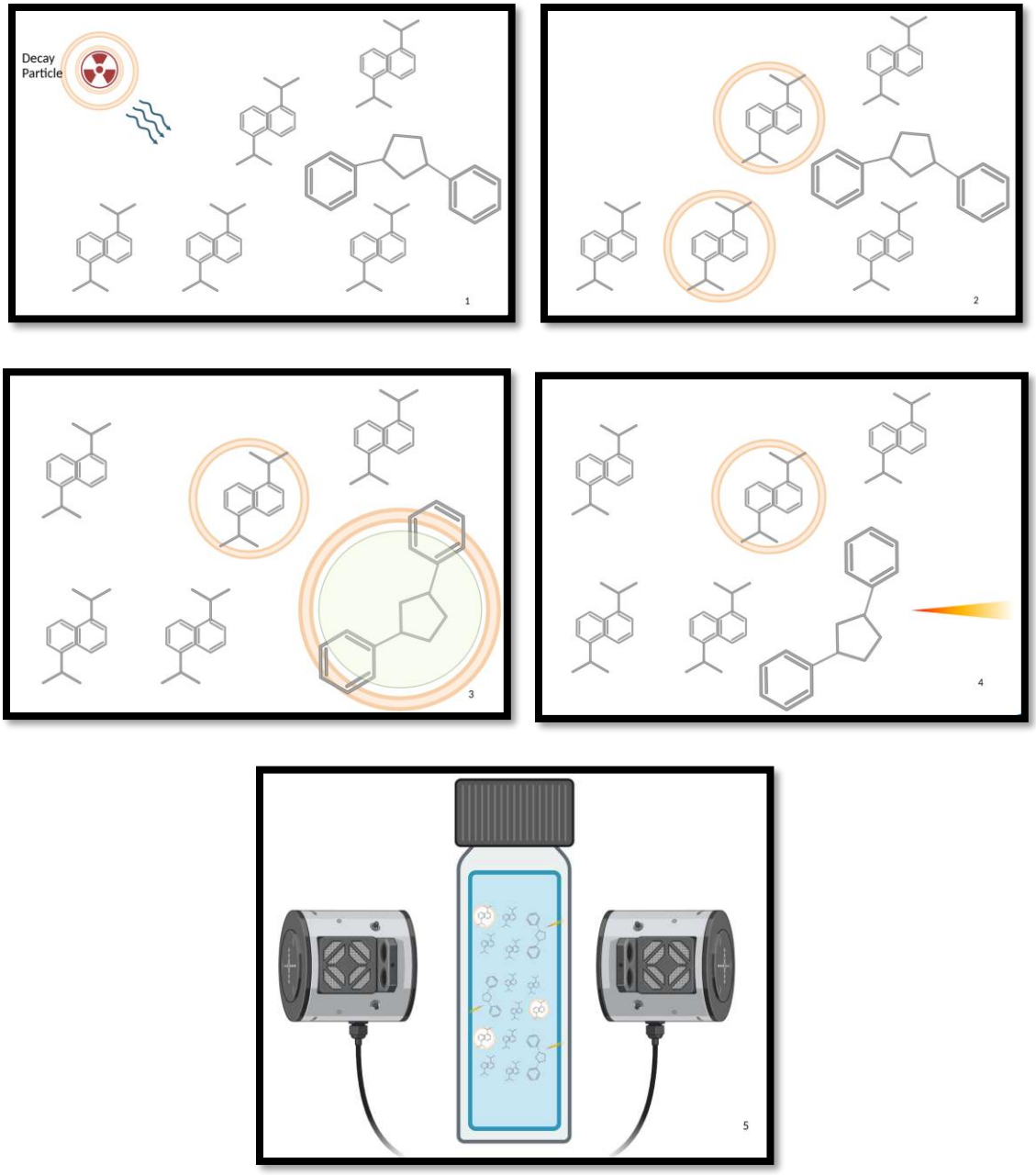

Figure 14: Figure showing the radioactive sample mixed with the liquid scintillation cocktail and emission of decay particles with kinetic energy (top left), kinetic energy exciting the solvent molecules to higher energy states (top right), and the transfer of the excitation energy to another solvent molecule or to a fluorescent molecule dissolved in the solvent (middle left), the fluorescent molecule scintillating (middle right), and a representation of the sample between two PMTs in coincidence (bottom), adapted from (18).

Radiometric instruments counting in this manner generally use multiple photomultiplier tubes (PMT)—usually two but sometimes three—in coincidence to decrease the potential of a false positive count. A scintillation event must register with both PMTs to continue to the amplifier and be recorded as a count (18) (17). Since liquid scintillation counting is highly efficient for detecting the emission of charged particles, it is employed in this project for the detection of alpha particle emission.

CHAPTER 3: CHARACTERIZING THE IRRADIATOR

3.1: Introduction and Theory

The first step to irradiating the selected extraction chromatographic resins was to characterize the irradiator utilized. The irradiator used in this project was a J.L. Sheppard and Associates Cesium-137 (Cs-137) source installed in Room 470 in the Molecular and Radiological Biosciences Building at Colorado State University. It contains a Cs-137 source that had an activity of 6000 Curie (Ci) on 7 September 1989. Based on the methods used in the characterization of other irradiators used for similar radiolytic degradation studies, Fricke dosimetry was employed (7) (19) (20).

Fricke dosimetry is a chemical dosimetry technique. The equations for the chemical reactions that occur during the irradiation of the Fricke solution are shown below.

$$Fe^{2+} + \bullet OH \implies Fe^{3+} + OH^{-}$$

$$H + O_2 \implies HO_2$$

$$Fe^{2+} + HO_2 + H^{+} \implies Fe^{3+} + H_2O_2$$

$$Fe^{2+} + H_2O_2 \implies Fe^{3+} + OH + OH^{-}$$

Equation 15: Reaction Mechanisms for Fricke Dosimetry, a chemical dosimeter

The simplified radioactive and chemical interaction is shown in figure 15.

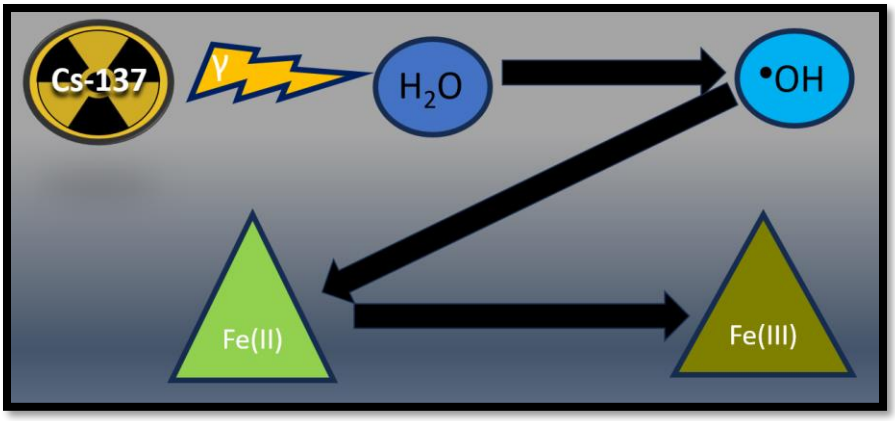

Figure 15: Pictorial Representation of Chemical Mechanism underlaying Fricke Dosimetry

Per discussion with the manager of the irradiation facilities at CSU, experimentally determining both the dose rate and the position of the source when extended from its shielding should be experimentally validated.

The reduction/oxidation shift in iron from the divalent to the trivalent form can be quantified via its change in color. For this purpose, an Ultraviolet-Visible Spectrophotometer, most commonly referred to simply as a "UV-Vis", was used. Spectrophotometry as a concept and the region of electromagnetic radiation involved is discussed in the previous chapter (15). Specifically for applications of Ultraviolet-Visible Spectrophotometry with Fricke dosimetry, the energy deposited in the solution and the resulting shift of the iron ions in solution from a divalent to a trivalent state (as described in figure 15) involves a corresponding shift in color (19). A common real-world example of reductive/oxidative related color shifting can be observed with rust. Iron has a well-characterized color shift as a result of the deposition of ionizing radiation in solution, which allows for the quantification of the absorbed dose delivered to the sample in a given geometry. This is the backbone of the Fricke chemical dosimetry system (19) (20).

3.2: Materials and Methods

The irradiator that was selected for use in this project was a J.L. Sheppard and Associates Cs-137 source installed in Room 470 in the Molecular and Radiological Biosciences Building at Colorado State University with an activity of 6000 Curie (Ci) on 7 September 1989 (decay corrected to 2736 Curies as of 7 September 2023). A virtual model of the irradiation chamber was prepared using Free CAD software. To best quantify the dose received by the extraction chromatographic resins during irradiation, microcentrifuge tubes were used for the Fricke solution. These tubes are smaller than the slots in the sample carousel (see images in Appendix) were designed to hold, however, the rotation of the samples was still determined to be necessary to achieve even irradiation across a batch of samples. Thus, sample holder inserts were produced via additive manufacturing (see Appendix for images of produced sample holders) with a MakerBot: Replicator Desktop 3D Printer, serial no. R50030047 and white 2.85 mm diameter IC3D ABS Acrylonitrile-Butadiene-Styrene copolymer. A picture of a sample carousel with microcentrifuge tubes of Fricke solution held in the sample holders is shown in figure 16.

Figure 16: Sample carousel with top and bottom rows holding additively manufactured sample holders (white) and microcentrifuge tubes containing Fricke solution.

In the preparation of the Fricke solution, the following reagents were used:

Sulfuric Acid: Macron fine chemicals AR (ACS grade: 95-98% purity), Batch No. 0000188148, manufactured date: 27 October 2017, CAS No: 7664-93-9 (sulfuric acid) and 7732-18-5 (water). Avantor Performance Materials, Avantor Performance Materials, LLC, 3477 Corporate Parkway, Center Valley, PA 18034. +1-610/573-2600.

Water: OmniSolv Water (LC-MS grade), CAS No. 7732-18-5. EMD Millipore Corporation, an affiliate of Merck KGaA, Darmstadt, Germany. 290 Concord Rd, Billerica, MA 01821, USA. +1-978/715-4321.

Ferrous Ammonium Sulfate hexahydrate, fine crystals (GR ACS grade). Product No. FX0245-1. Lot No. 2016062199. CAS No. 7783-85-9. Made in USA. EMD Millipore Corporation, an affiliate of Merck KGaA, Darmstadt, Germany. 290 Concord Rd, Billerica, MD 01821, USA. +1-978/715-4321.

Sodium Chloride, anhydrous, Redi-Dri™, free-flowing (ACS grade, ≥99% pure). Product No. 746398-500G. CAS No. 7647-14-5. Sigma Aldrich.

To best simulate the conditions to be experienced by the resin in prospective irradiations, Fricke solution was prepared with the above-listed reagents and then pipetted using a 5 mL pipette. The solution was agitated prior to pipetting to allow for more complete aeration of the solution, and then 2 mL portions were pipetted into each microcentrifuge tube.

The first experimental goal was, thus, to determine the dose rate delivered by the Cs-137 source when both the top and bottom rows of the sample carousel (shown in Fig. 16) are filled with

Fricke solution. Irradiations over multiple time periods were completed to determine the dose rate in gray per min (Gy/min) with the sample carousel in the position closest to the source (see figure 17). The radioactive source (shown in figure 17 as a circle with the radiation symbol inscribed) was deployed from the shielding which is below the irradiation chamber (symbolized by the blue arrow upwards in figure 17). The green cylinder represents the sample carousel in the location proximal to the source. Samples were assumed to be irradiated from the center of the sample carousel (represented by the cylinders) due to the rotational mechanism enabled during irradiation. The mechanism spins at a frequency of 0.2 Hz. The average position of every sample from the source in either row of the sample carousel is the center of the sample carousel itself as the samples rotate around the central axis of the sample carousel.

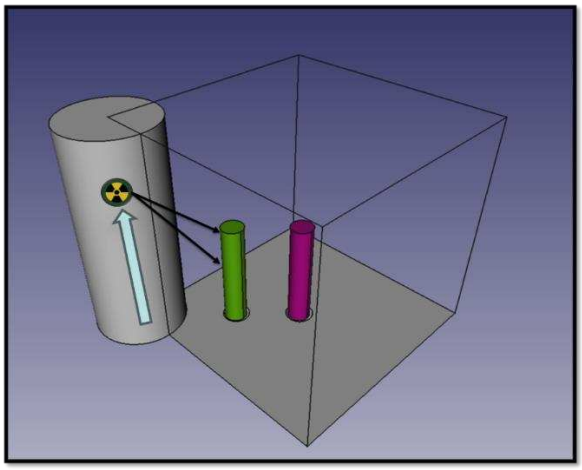

Figure 17: Model of the irradiation chamber of the 6000 Ci Cs-137 source in Room 470 of the Molecular and Radiological BioSciences Building.

As the Fricke chemical dosimetry system is applicable in the 10-400 Gy range, several hour-long irradiations were completed to verify the capacity of the solution. A selection of shorter irradiations was completed to derive the dose rate in each row of the sample carousel. Irradiations were completed in 3-minute intervals, i.e., 3, 6, …, 18-minute irradiations. These

dose rates, their relative distances to the source, the Pythagorean theorem, the quadratic equation, and the inverse square law were used to triangulate the location to which the source deploys.

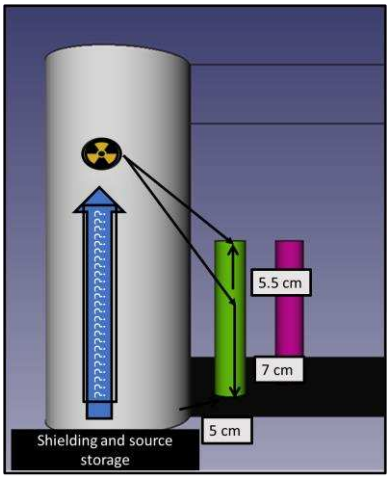

Figure 18: Pictorial representation of the approach to determining the deployed geometry of the source, made using Free CAD software.

3.3: Data

Shown below is a summary of the data gathered via ultra-violet visible spectrophotometry. Eight samples of Fricke solution were irradiated on each level of the sample carousel at each designated irradiation time. As the wavelength of peak absorbance fluctuates in the 302-305 nm range, 0.1 nm measurements were taken from 300-310 nm. The 302-305 nm range was then pulled out and averaged across the set of samples at each wavelength. The standard deviations across each set of eight samples at each 0.1 nm were calculated using Microsoft Excel. The average absorbance and the standard deviations across the 302-305 nm range were also calculated using Microsoft Excel. As an example, the data from the 18-minute irradiation on the top rack of the sample carousel is shown in Table 5. The highlighted values from the table below are what go on to represent those conditions in the subsequent table. The data from the

other irradiation times for the top and bottom rows of the sample carousel are excluded from the body of this chapter due to size considerations, but they are included in Appendix B.

Table 5: Raw data and averages taken for the 8 samples (here labelled 1, 2, ..., 8) that experienced an 18 minute irradiation condition in the top row of the sample carousel in the Cs-137 Irradiator in Room 470 in the Molecular and Radiological Biosciences Building. The data in the last row of the table shows the average of the absorbance of each sample over the selected range. This was used as a check with the sample processing. The yellow highlighted values are the averages of those average values and were used as a check to ensure that all data was processed and included in the calculations.

	1	2	3	4	5	6	7	8	average	std dev
Wavelengt	Abs	Abs	Abs	Abs	Abs	Abs	Abs	Abs	Abs	
305	0.809332	0.764575	0.843757	0.848194	0.850992	0.847934	0.855006	0.861229	0.835127	0.03247
304.9	0.810619	0.765619	0.845266	0.84963	0.85237	0.849626	0.856666	0.862621	0.836552	0.032637
304.8	0.811795	0.766983	0.846722	0.850688	0.853694	0.850906	0.857827	0.864106	0.83784	0.032633
304.7	0.813341	0.76799	0.848156	0.851973	0.854794	0.852233	0.859253	0.865297	0.83913	0.032687
304.6	0.813823	0.76905	0.849537	0.853518	0.856579	0.853595	0.860718	0.866777	0.84045	0.032944
304.5	0.815643	0.770217	0.850835	0.854681	0.857895	0.855297	0.861955	0.868552	0.841885	0.032991
304.4	0.816962	0.771216	0.852282	0.856011	0.859148	0.856417	0.863367	0.869747	0.843144	0.033074
304.3	0.818141	0.772477	0.853514	0.857319	0.860475	0.85798	0.864773	0.871299	0.844497	0.033153
304.2	0.819728	0.773831	0.854961	0.858685	0.861885	0.85968	0.866386	0.872953	0.846014	0.033212
304.1	0.821252	0.775561	0.856776	0.860498	0.863744	0.861575	0.867869	0.874704	0.847747	0.033243
304	0.822788	0.776579	0.858024	0.861781	0.865295	0.862804	0.86899	0.875746	0.849001	0.033269
303.9	0.824059	0.777993	0.859518	0.863451	0.866658	0.864553	0.870515	0.877438	0.850523	0.03336
303.8	0.825435	0.779582	0.860946	0.864905	0.868363	0.866048	0.871997	0.878976	0.852032	0.033358
303.7	0.827073	0.780627	0.862945	0.866446	0.869793	0.867863	0.873483	0.880438	0.853583	0.033514
303.6	0.828515	0.782144	0.864247	0.868019	0.870996	0.868911	0.874876	0.881964	0.854959	0.033458
303.5	0.829982	0.783177	0.8654	0.869113	0.872511	0.870581	0.876555	0.883083	0.8563	0.033554
303.4	0.831521	0.784599	0.867284	0.871081	0.874636	0.872428	0.878066	0.884438	0.858007	0.033664
303.3	0.832954	0.786019	0.86879	0.872406	0.876175	0.873838	0.879785	0.886694	0.859583	0.033788
303.2	0.834553	0.78727	0.870651	0.87409	0.877662	0.875631	0.881604	0.888253	0.861214	0.03393
303.1	0.836066	0.788639	0.872234	0.87536	0.879227	0.877071	0.883135	0.889921	0.862707	0.033983
303	0.837231	0.790087	0.874268	0.877568	0.880831	0.879079	0.884827	0.892009	0.864487	0.034218
302.9	0.839083	0.79169	0.875834	0.879041	0.882509	0.880951	0.88659	0.893751	0.866181	0.034233
302.8	0.840897	0.79309	0.87741	0.880819	0.884452	0.882837	0.888167	0.895609	0.86791	0.034348
302.7	0.842562	0.794518	0.879274	0.882359	0.886074	0.884616	0.889597	0.8974	0.86955	0.034423
302.6	0.844183	0.796037	0.881063	0.884435	0.887976	0.886552	0.891703	0.899211	0.871395	0.034587
302.5	0.845834	0.797553	0.882787	0.886272	0.889976	0.888332	0.893226	0.900888	0.873108	0.034666
302.4	0.847676	0.799116	0.884662	0.887912	0.891853	0.890263	0.895118	0.902864	0.874933	0.034771
302.3	0.849284	0.800687	0.886356	0.889862	0.893555	0.892022	0.897135	0.904613	0.876689	0.03487
302.2	0.850826	0.802313	0.888242	0.891623	0.895521	0.893776	0.898763	0.906335	0.878425	0.03494
302.1	0.853032	0.80366	0.89008	0.893352	0.897284	0.896251	0.900679	0.908408	0.880343	0.035115
302	0.854786	0.805587	0.891745	0.895349	0.899355	0.89794	0.902803	0.910146	0.882214	0.035117
	0.830612	0.783822	0.866567	0.870208	0.873622	0.871535	0.877466	0.88437	**0.857275**	**0.033749**
								0.857275		

Table 6 shows the tabulated average absorbances for multiple irradiation durations for the top row of the sample carousel.

Table 6: Tabulated average absorbances and associated standard deviations from 0 to 18 minutes irradiation time for both the top and bottom rows of the sample carousel.

irradiation time / min	Absorbance—top row	std dev—top row	Absorbance—bottom row	std dev—bottom row
0	0.300	0.00777	0.300	0.00777
3	0.391	0.0101	0.390	0.0296
6	0.393	0.0897	0.486	0.0315
9	0.521	0.0870	0.515	0.0518
12	0.654	0.0399	0.544	0.169
15	N/A	N/A	0.632	0.191
18	0.857	0.0337	0.758	0.136

3.4: Calculations

The data from the above tables was then used to determine the net absorbance using the equation below.

$$\Delta A = A_i - A_0$$

Equation 16: Net Absorbance, where ΔA is the net absorbance, A_i is the experimentally determined absorbance, and A_0 is the absorbance of the blank, i.e. the unirradiated Fricke solution.

Furthermore, the net absorbance is then plugged into the basic equation for the calculation of absorbed dose in the dosimeter solution, D_F as shown below.

$$D_F = \frac{\Delta A}{(\varepsilon * G * \rho * d)}$$

Equation 17: Absorbed Dose in dosimeter solution in Gy, where D_F is the absorbed dose to the Fricke solution in Gray (Gy), ΔA is the net absorbance, ε is the molar linear absorption coefficient of the ferric ions (Fe^{3+}) in m^2*mol^{-1}, G is the radiation chemical yield of ferric ions (Fe^{3+}) in $mol*J^{-1}$, ρ is the density of the dosimetric solution equal to 1.024 x 10^3 $kg*m^{-3}$ at 25°C, and d is the optical pathlength of the dosimetric solution in the cuvette in m. The recommended value of εG at room temperature is 3.52x10^{-4} m^2/J due to the potential for large uncertainties in the experimental verification of εG. The pathlength is 10 mm (20).

Therefore, at room temperature, the calculation for the absorbed dose can be simplified to equation 18, which can be used to determine the absorbed dose of the Fricke solution from the

calculated net absorbance at a particular location in the sample carousel (i.e. top or bottom row) and at a particular irradiation time.

$$D_F = 278\Delta A$$

Equation 18: Simplified equation for the experimental determination of absorbed dose in Gy to Fricke solution (20).

The further experimental goal, beyond determining the dose rate at multiple locations within the irradiation chamber, was to use those dose rates and their locations in space relative to each other and to the location of the Cs-137 source when deployed to triangulate the position of the source when it is fully deployed via the pneumatic lift within its cylinder of containment. This is represented above pictorially.

3.5: Results

The table below shows the tabulated absorbed doses of the Fricke solution for the top and bottom rows of the sample carousel at multiple irradiation times.

Table 7: Tabulated net absorbance values in nm with error calculations at irradiation times for both the top and bottom rows of the sample carousel.

irradiation time / min	Net absorbance, top row	uncertainty, top row	Net Absorbance, bottom row	uncertainty, bottom row
0	0	0.0110	0	0.0110
3	0.0911	0.0128	0.0903	0.0306
6	0.0933	0.0900	0.186	0.0325
9	0.222	0.0873	0.215	0.0524
12	0.354	0.0406	0.244	0.170
15	N/A	N/A	0.333	0.191
18	0.557	0.0346	0.458	0.136

The data in table 7 is plotted in figure 20, with the error bars denoting one sigma uncertainties from the standard deviation of the 8 replicated trials at each irradiation time.

Figure 19: Graph showing the experimentally determined and calculated net absorbance in nanometers (nm) for the top row of the sample carousel versus the length of the irradiation in minutes (min) presented with an uncertainty of 2σ, where σ is the standard deviation among the samples that were irradiated for the same amount of time.

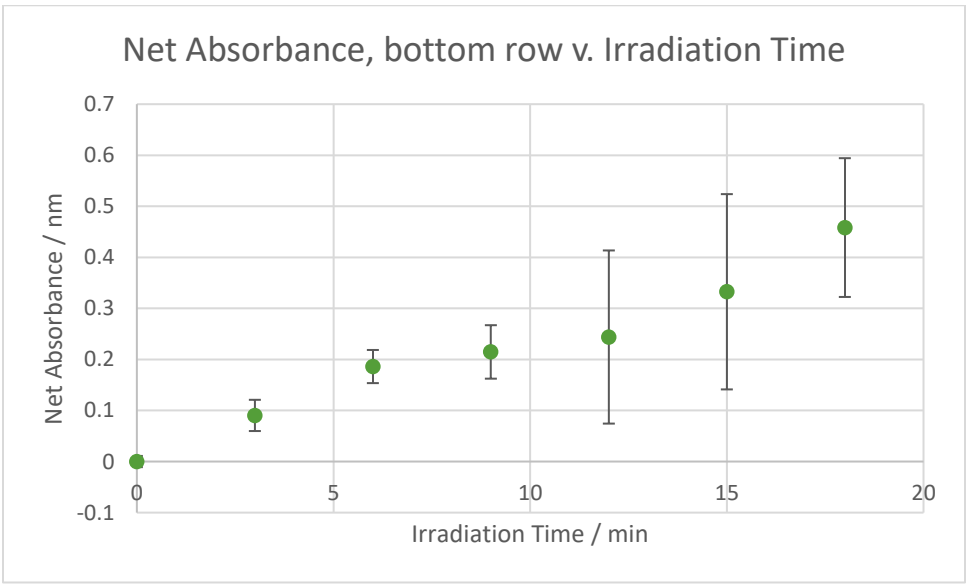

Figure 20: Graph showing the experimentally determined and calculated net absorbance in nanometers (nm) for the bottom row of the sample carousel versus the length of the irradiation in minutes (min) presented with an uncertainty of 2σ, where σ is the standard deviation among the samples that were irradiated for the same amount of time.

The net absorbance with no irradiation is, by definition, zero (0). The changes in absorbance over longer irradiation times show that the chemical reaction is proceeding as expected.

Table 8: Calculated absorbed doses in Gray (Gy) associated with both the top and bottom rows of the sample carousel at multiple irradiation times.

irradiation time / min	dose, top row	uncertainty, top row	dose, bottom row	uncertainty, bottom row
0	0	0.0110	0	0.0110
3	25.24	0.0128	25.03	0.0306
6	25.86	0.0900	51.55	0.0325
9	61.39	0.0873	59.48	0.0524
12	98.03	0.0406	67.57	0.170
15	N/A	N/A	92.12	0.191
18	154.415	0.0346	126.96	0.136

As demonstrated by the equations above, there should be a linear relationship between the change of the net absorbance and the absorbed dose to the Fricke solution. Thus, by plotting multiple absorbed dose measurements at multiple time intervals, the slope of a linear trendline, generated with Microsoft Excel software, with its y-intercept set to zero (0), gives the dose rate to each row of the sample carousel in Gray per minute (Gy/min).

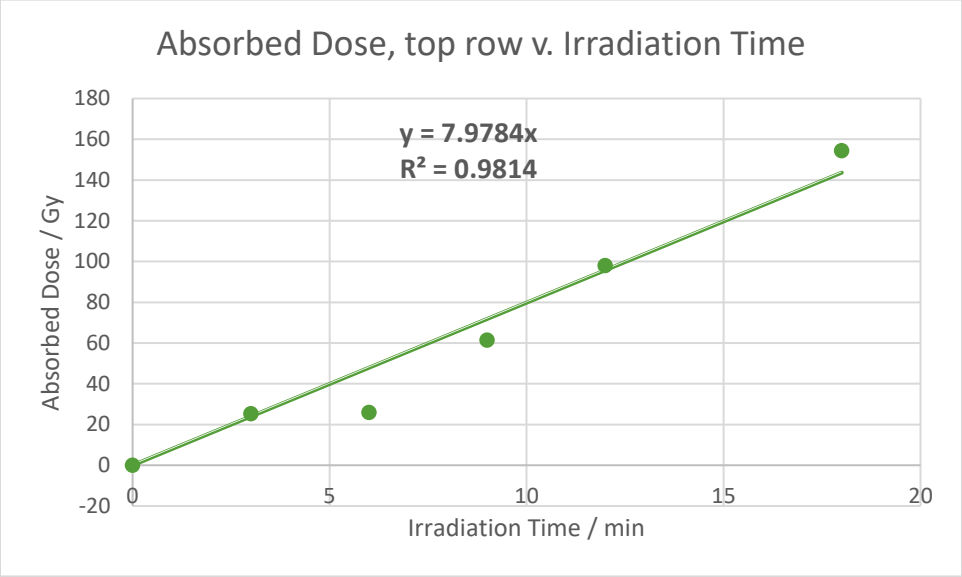

Figure 21: Graph showing the relation of the calculated absorbed dose in Gray (Gy) experienced by the top row of the sample carousel versus the length of the irradiation in minutes (min).

The ideal R^2 value for a generated linear regression is 1. Figure 21 shows a generated R^2 value of 0.9814, which shows that the data does fit the linear regression well. The slope of the generated linear regression, as mentioned above, is the dose rate experienced in the particular conditions seen by the top row of the sample carousel. This means that samples in the top row of the sample carousel are exposed to 8.0 Gy/min.

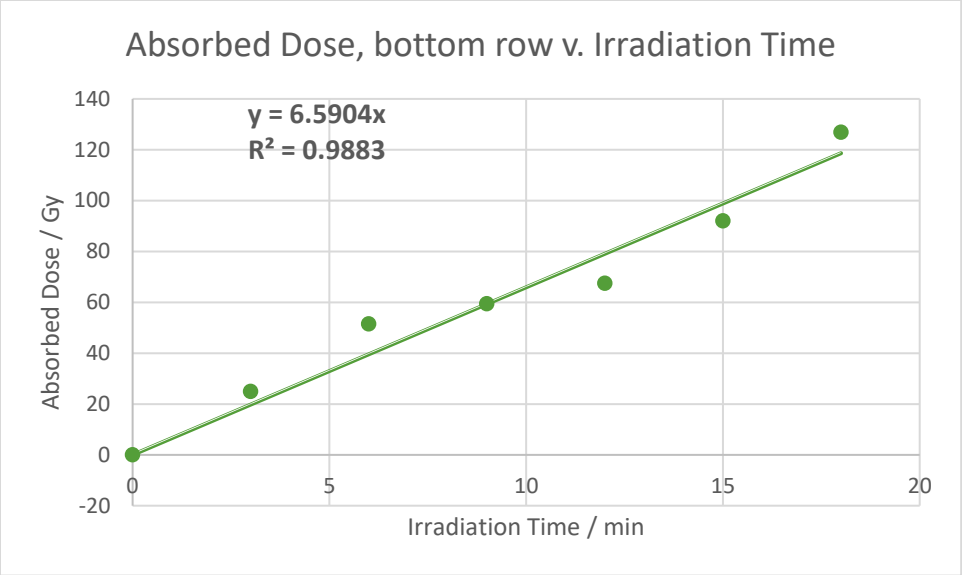

Figure 22: a graph showing the relation of the calculated absorbed dose in Gray (Gy) experienced by the bottom row of the sample carousel versus the length of the irradiation in minutes (min).

Figure 22 shows a generated R^2 value of 0.9883, which shows that the data does fit the linear regression well. The slope of the generated linear regression, as mentioned above, is the dose rate experienced in the particular conditions seen by the bottom row of the sample carousel. This means that samples in the bottom row of the sample carousel are exposed to 6.6 Gy/min.

Using both of these experimentally verified dose rates, the location of the source when deployed can be calculated. Since the intensity of the radiation follows the inverse square law and the experimental locations of the two dose rates are known, the location of the source was calculated using the inverse square law and the Pythagorean theorem. The cesium-137 source deploys 16.0 cm from the base of the irradiation chamber and 3.5 cm above the top row of the sample carousel.

3.6 Conclusions

Fricke dosimetry is an effective, well-suited method for characterizing the dose rate within the Cesium-137 source's irradiation chamber and for experimentally determining the location of the source when deployed. When the sample carousel is in its location most proximal to the source, the top row experiences a dose rate of 8.0 Gy/min, and the bottom row experiences a dose rate of 6.6 Gy/min, which is averaged for the rotation of the sample carousel. When it is deployed, the height of the source is 16.0 cm from the floor of the irradiation chamber.

4.1: TRU Resin

4.1.1: Introduction

Introduced in the late 1980s, TRU resin is one of the originals as far as extraction chromatographic resins go. TRU resin contains a mixture of octyl phenyl-N, N-di-isobutyl carbamoyl phosphine oxide (abbreviated CMPO) and tri-n-butyl phosphate (TBP) as extractant (8) (2). It is generally utilized for the extraction and separation of tetra- and hexa-valent actinides including plutonium, neptunium, thorium, and uranium as well as americium. Typical mobile phases for chemical separations involving TRU Resin are nitric acid at concentrations greater than 1 molar. Typical mobile phases utilized for back-extraction are nitric acid at very dilute concentrations, hydrochloric acid, and complexing agents such as hydrofluoric acid (1).

4.1.1.1: Structure

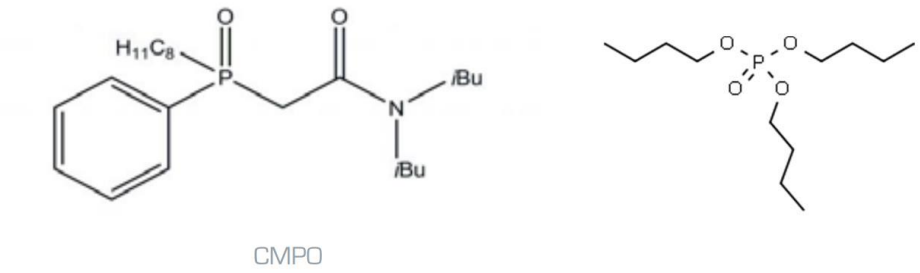

Figure 23: Chemical structure of octyl phenyl-N, N-di-isobutyl carbamoyl phosphine oxide (abbreviated CMPO), reproduced from (2), left, and of tri-n-butyl phosphate (abbreviated TBP), produced using SciFinder, right.

4.1.1.2: Experimentally Defined k'

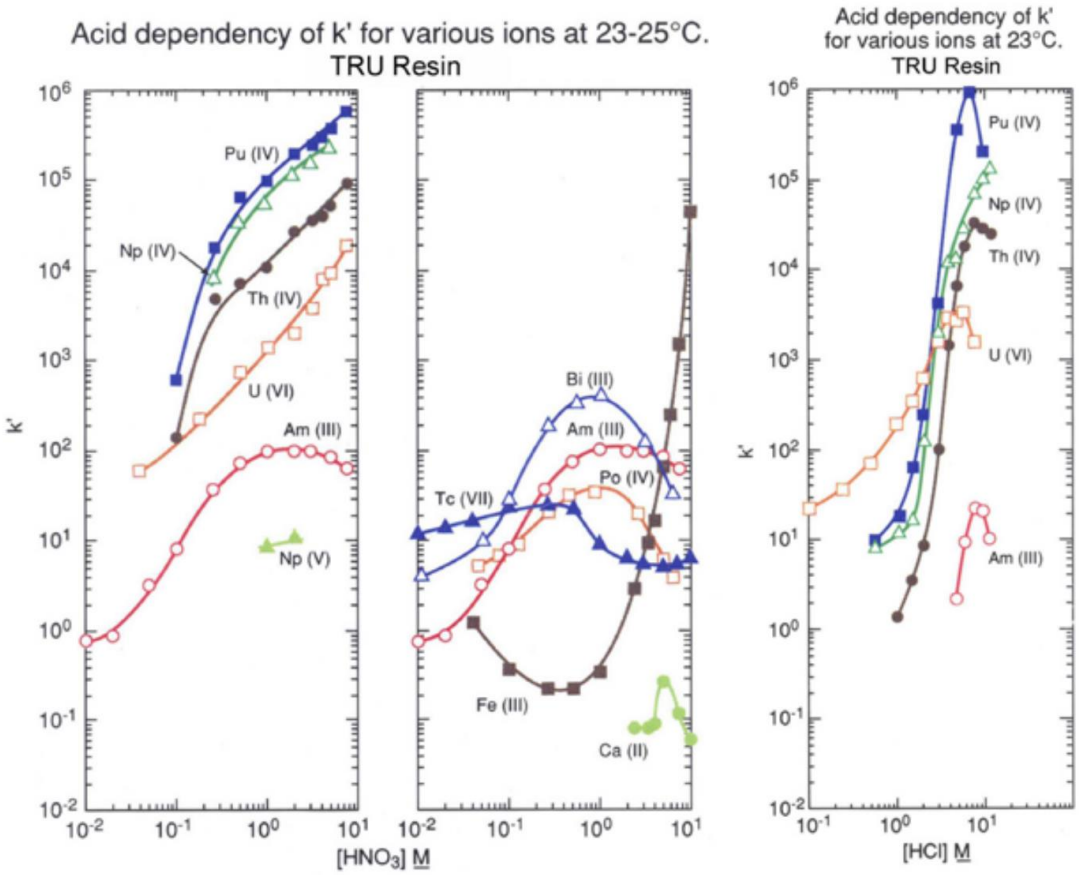

Figure 24: k' values of different elements in nitric and hydrochloric acids on TRU Resin, reproduced from (2).

Plutonium (IV) is well retained on TRU Resin in both nitric and hydrochloric acid systems, as shown by the plots in figure 24, with maximum k' values at least on the order of 10^5 from >1 M nitric acid and >3 M hydrochloric acid.

4.1.2: Materials and Methods

Plutonium retention was measured via a method of batch-contact study that is commonly used in the Sudowe Research Group. The steps of this process are shown in the figure below. 50 mg (±0.5 mg) of TRU Resin was weighed out into microcentrifuge tubes. To each microcentrifuge

1.5 mL acid—3 M HNO_3, 3 M HCl, 1 M HNO_3, or 1 M HCl—was added. The tube was then shaken for at least one hour on a shaker table. After shaking, each group of four microcentrifuge tubes containing both 50 mg resin and 1.5 mL acid was taken to the irradiation facilities and exposed to its associated dose of ionizing radiation.

Sample groups in quadruplicate were batched with an unirradiated sample group (also in quadruplicate) that went through identical chemical processing to ensure that any changes in plutonium retention are due to the exposure of the resin to ionizing radiation rather than other, unrelated factors. Exposure duration was calculated using the highest level of the sample carousel in the location most proximal to the source within the irradiator (see chapter 3 for more details). Absorbed doses in gray were selected on logarithmic scales: 10, 100, 1000, 10000, and 50,000. Since the 10, 100, and 1000 gray exposures were relatively short, they were batched with a single unirradiated control group. As determined in chapter 3, the dose rate in the top row of the sample carousel in the location most proximal to the source of the Cesium-137 irradiator is 8 Gy per minute. Thus, the 10, 100, and 1000 gray doses were delivered in 1.25-, 12.5-, and 125-minute irradiation intervals. The 10 kGy irradiation took 1250 minutes or 20 hours and 50 minutes and was thus generally completed overnight. The 50 kGy irradiation in the same microcentrifuge tubes took 6250 minutes or 4 days, 8 hours, and 10 minutes; however, it was determined that the microcentrifuge tubes suffered too much embrittlement from this dose of ionizing radiation. They began to crumble and had their lids fall apart when manipulated after the extended irradiation. Thus thicker 5 mL centrifuge tubes were used for the 50 kGy measurements. The sample in the bottom of the tube was farther from the cesium source so, using the geometry of the irradiation chamber, the location of the source, and the inverse

square law, these 50 kGy irradiations were calculated to run for 6622.5 minutes or 4 days, 14 hours, and 22.5 minutes.

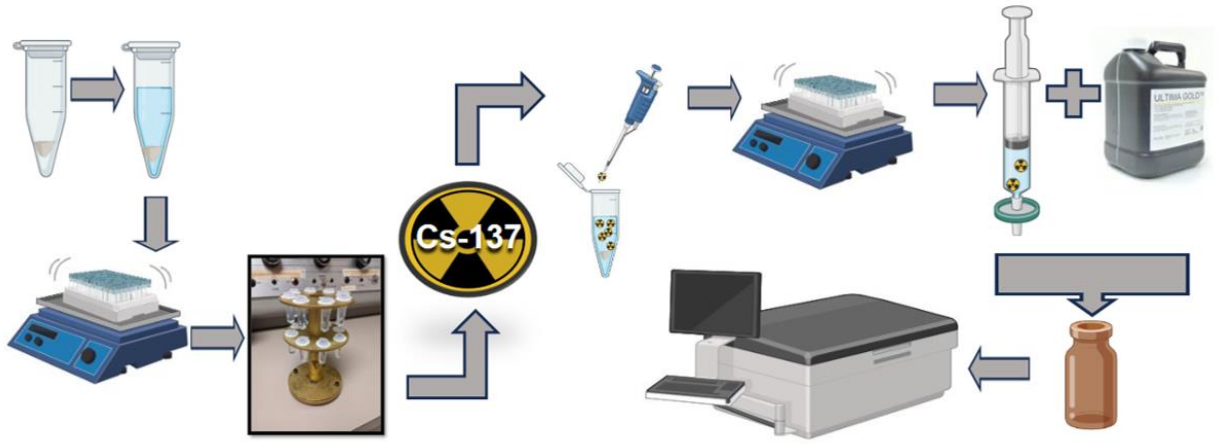

Figure 25: Pictorial representation of batch-contact studies used for contacting plutonium-239 with EXC resins post-irradiation.

Post-irradiation, 50 µL of a working solution of ~1000 Bq/mL plutonium-239 in the same acid with which the resin was pre-conditioned was added to each microcentrifuge tube—irradiated and unirradiated control groups alike. These samples were then agitated on a shaker table for one hour. Following their agitation, a 1 mL aliquot was taken from each sample and filtered through a 0.45-micron pore Luer-lock syringe filter. This aliquot was then added to a plastic scintillation vial along with 15 mL Ultima Gold scintillation cocktail. The sample was taken to the liquid scintillation counter and counted for one hour. The initial activity added to each sample from the working solution was experimentally verified by measuring a group of four standards from the same working solution that was used to spike the samples. These standards were prepared via a direct addition of 50 µL of the working solution, 950 µL of the same acid, and 15 mL Ultima Gold cocktail. These standards were then counted with the same counting protocol on the liquid scintillation counter.

4.1.3: Data and Calculations

Data was collected via reports generated by the liquid scintillation counter that were then collated in Microsoft Excel. An example of part of one such collation from a generated report is included in the table below. The remainder of the raw count data is included in Appendix C of this document.

Table 9: A selection of raw data taken from the first table containing plutonium retention data in Appendix C.

S#	SAMPLE ID	COUNT TIME / MIN	CPMA	SIS	MESSAGES	Group
1	HNO3 STD-1	60	4193	243.22		1
2	HNO3 STD-2	60	4190	236.39		1
3	HNO3 STD-3	60	4183	235.25		1
4	HNO3 STD-4	60	4200	232.15		1
5	HCl STD-1	60	3180	678.86		2
6	HCl STD-2	60	3182	684.63		2
7	HCl STD-3	60	3163	685.47		2
8	HCl STD-4	60	3178	688.8		2
9	TRU081	60	110	453.28		3
10	TRU082	60	109	484.33		3
11	TRU083	60	109	461.46		3
12	TRU084	60	111	495.31		3
13	TRU085	60	110	512.57		4
14	TRU086	60	112	466.93		4
15	TRU087	60	110	512.45		4
16	TRU088	60	108	487.05		4
17	TRU089	60	107	447.03		5
18	TRU090	60	110	486.64		5
19	TRU091	60	109	468.22		5
20	TRU092	60	109	500.46		5
21	TRU093	60	107	461.08		6
22	TRU094	60	107	433.96		6
23	TRU095	60	108	477.75		6
24	TRU096	60	108	442.31		6
25	TRU097	60	105	432.94		7
26	TRU098	60	104	410.41		7
27	TRU099	60	105	426.29		7
28	TRU100	60	109	424.4		7
29	TRU101	60	111	479.19		8

30	TRU102	60	103	427.1		8
31	TRU103	60	105	433.55		8
32	TRU104	60	113	526.67		8

The equation below was used to calculate the distribution ratio from the initial activity added to the sample and the activity that remained in the aqueous portion of the sample. The distribution ratio for every sample was calculated.

$$\mathrm{D_w} = \frac{\mathrm{A_0} - \mathrm{A_s}}{\mathrm{A_s}} * \frac{\mathrm{mL}}{\mathrm{g}}$$

Equation 19: Equation for EXC weight distribution ratios for radioactive elements where $A_0 - A_s$ is the activity sorbed on a known weight of resin (g) and A_s is the activity in a known volume (mL) of solution, reproduced from (2). The related theory is explained in more depth in section 2.1.1.

The average value for each group, i.e., each condition relative to acid, acid concentration, and absorbed dose, was calculated using the "AVERAGE" function in Microsoft Excel. The standard deviation of each group was calculated using the "STDEV.S" function in Microsoft Excel. An example of the data tables generated is shown below. Each unirradiated control group is listed conventionally as having received a dose of 1 Gy so that values can be plotted logarithmically. Each acid condition has three values listed as having received 1 Gy. The first is the unirradiated control group related to the 10, 100, and 1000 Gy irradiated groups. The second value listed as having received 1 Gy is related to the group that received the 10,000 Gy (or 10 kGy) irradiation, and the third value listed is related to the group that received the 50,000 Gy (or 50 kGy) dose. Each experimental group was normalized relative to its own related unirradiated control group, and those normalized distribution ratios were calculated using the formula below.

$$\text{Normalized } \mathrm{D_w} = \frac{\mathrm{D_{w,for\ a\ particular\ experimental\ group}}}{\mathrm{D_{w,for\ the\ related\ unirradiated\ control\ group}}}$$

Equation 20: Equation for normalizing the experimentally determined distribution ratio

Normalized distribution ratios are included for each acid, acid concentration, and irradiation condition included in the table below. By definition, each unirradiated control group has a normalized distribution ratio of 1.

Table 10: Data showing absorbed dose in gray, computed distribution ratios, and distribution ratios normalized to an unirradiated control batch with identical chemical processing for TRU Resin in 3 M nitric acid, 3 M hydrochloric acid, 1 M nitric acid, and 1 M hydrochloric acid.

	TRU
acid:	3 M HNO3

dose / Gy	Dw	Sdev	p-value from two-tailed t.test with unequal variances (dose to control)	Normalized Dw
1	489.25	4.43		1.00
1	498.22	22.86		1.00
1	452.63	14.20		1.00
10	488.14	7.55	0.811	0.998
100	493.95	5.99	0.257	1.01
1000	499.89	2.79	0.009	1.02
10000	508.65	10.89	0.453	1.02
50000	477.92	14.19	0.045	1.06

resin:	TRU
acid:	3 M HCl

dose / Gy	Dw	Sdev	p-value from two-tailed t.test with unequal variances (dose to control)	Normalized Dw
1	49.02	13.81		1.00
1	13.39	3.86		1.00
1	15.43	6.15		1.00
10	49.57	8.81	0.007	1.01
100	73.14	4.66	0.014	1.49
1000	96.67	20.92	0.001	1.97
10000	54.27	23.54	0.001	4.05
50000	80.14	103.94	0.394	5.19

resin:	TRU
acid:	1 M HNO3

dose / Gy	Dw	Sdev	p-value from two-tailed t.test with unequal variances (dose to control)	Normalized Dw
1	231.03	4.25		1.00
1	221.30	7.29		1.00
1	206.08	8.90		1.00
10	235.18	7.49	0.381	1.02
100	230.17	10.32	0.885	0.996

1000	231.17	8.02	0.977	1.00
10000	222.95	8.71	0.780	1.01
50000	242.51	3.77	0.002	1.18

resin: TRU
acid: 1 M HCl

dose / Gy	Dw	Sdev	p-value from two-tailed t.test with unequal variances (dose to control)	Normalized Dw
1	18.44	7.54		1.00
1	20.68	5.85		1.00
1	7.56	1.47		1.00
10	17.21	5.03	0.797	0.933
100	18.47	4.01	0.994	1.00
1000	19.76	8.29	0.822	1.07
10000	20.70	2.45	0.993	1.00
50000	91.97	46.71	0.036	12.16

4.1.4: Results and Discussion

The data gathered in section 4.1.3 is plotted here in section 4.1.4. Each acid condition is plotted with a pair of graphs to show the changes in distribution ratio versus the absorbed dose to the resin in gray. Each figure in this section contains two graphs. The first graph shows the calculated distribution ratio versus the absorbed dose to the resin in gray. The second graph in each pair illustrates the normalized distribution ratio plotted versus the absorbed dose to the resin in gray. Both graphs are shown with an uncertainty budget of two experimentally determined standard deviations, i.e., at a 95% confidence interval. Plotting both figures and presenting them as a pair is done as a check to ensure there were no confounding variables that affected both the unirradiated control group and the irradiated group since more time elapsed between the acid preconditioning and the addition of the plutonium. The p-values for the two-tailed t.test with unequal variances are listed with the raw data in Appendix C.

The first pair of graphs (shown in figure 26) are for the retention of plutonium-239 on TRU Resin in 3 M nitric acid. The distribution ratio is around 500 and remains fairly stable across 0 to 50 kGy irradiations. The literature value for the distribution ratio of the retention of plutonium on TRU Resin in 3 M nitric acid is 90,000 (2). The second graph showing the normalized distribution ratios shows a stable result with the largest fluctuation being less than 6% (a normalized distribution ratio of ~1.056).

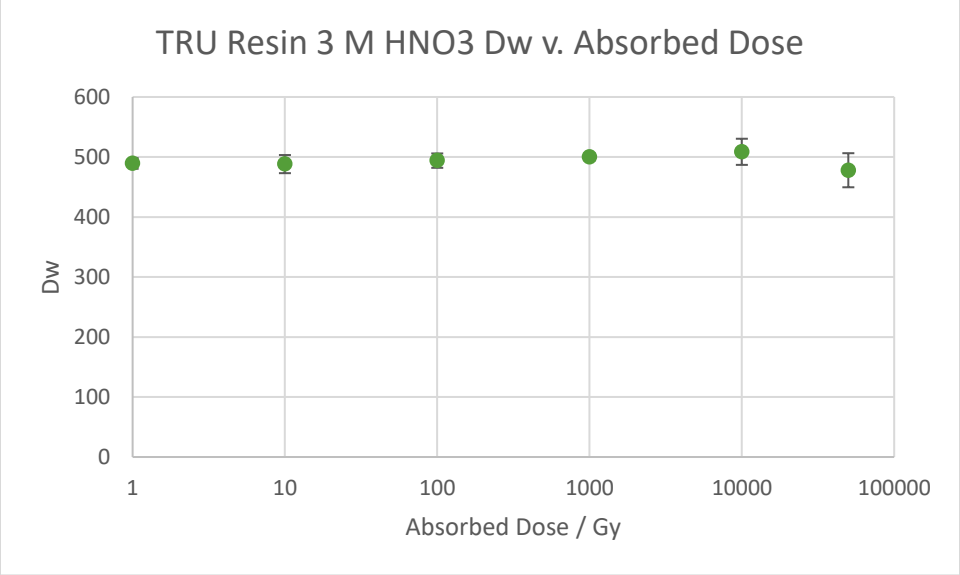

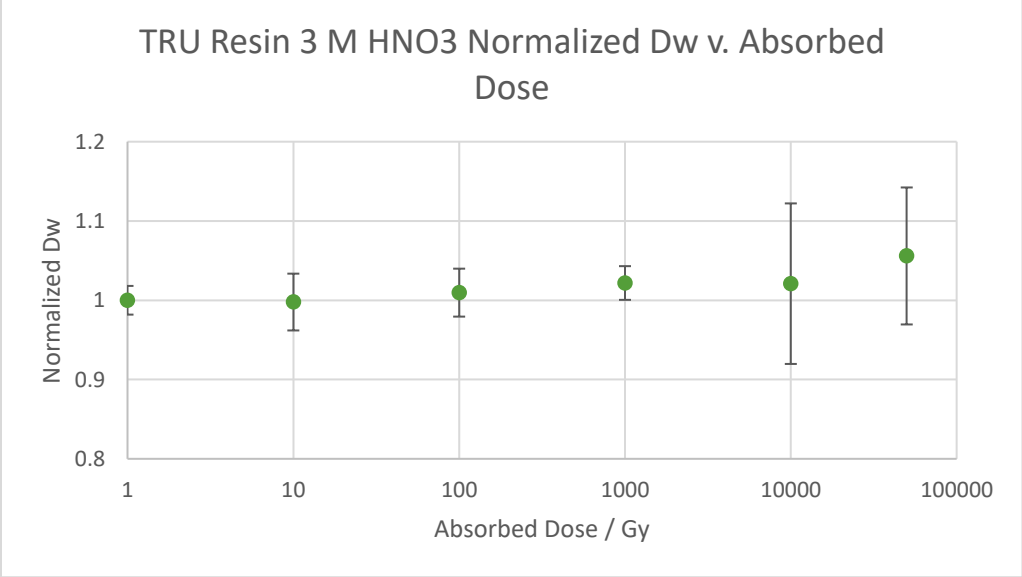

Figure 26: Contains two graphs showing the retention of plutonium-239 on TRU Resin irradiated in 3 M nitric acid. The top graph shows the experimentally determined distribution ratio (Dw) v. the absorbed dose to the EXC Resin in Gray. The bottom graph shows the normalized experimentally determined distribution ratio v. the absorbed dose to the EXC Resin in Gray.

Figure 27 shows the retention of plutonium-239 on TRU Resin in 3 M hydrochloric acid. The distribution ratio in the first graph shows some fluctuations but generally remains between 50-100 over the entire irradiation range. The literature value for the distribution ratio of the retention of plutonium on TRU Resin in 3 M hydrochloric acid is around 270 (2). There is, to be noted, a large uncertainty associated with the 50 kGy measurement. The second graph of the graphs in figure 27 however, shows a markedly different trend with increasing values of the normalized distribution ratio across the irradiations. To that end, there is some compounding factor affecting the unirradiated control groups that should be investigated.

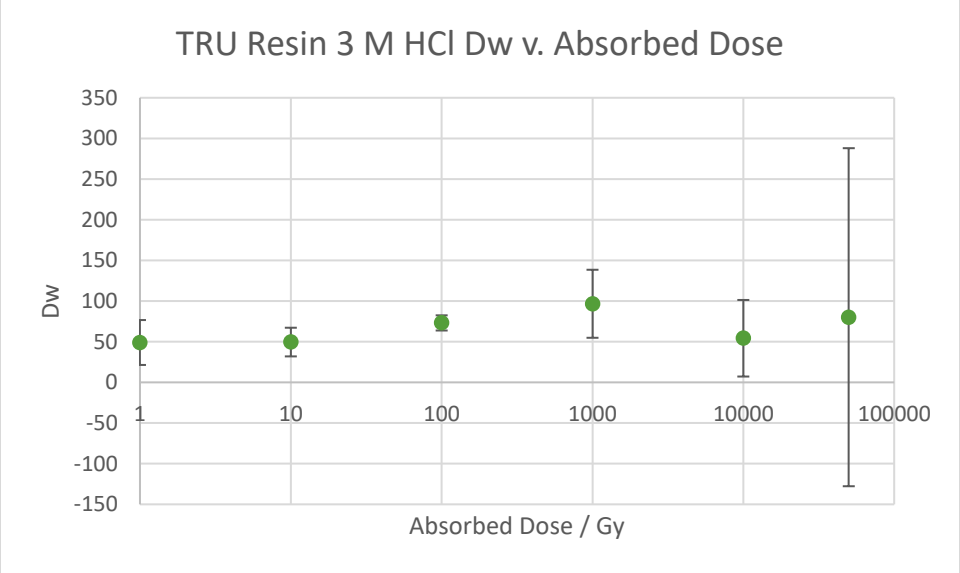

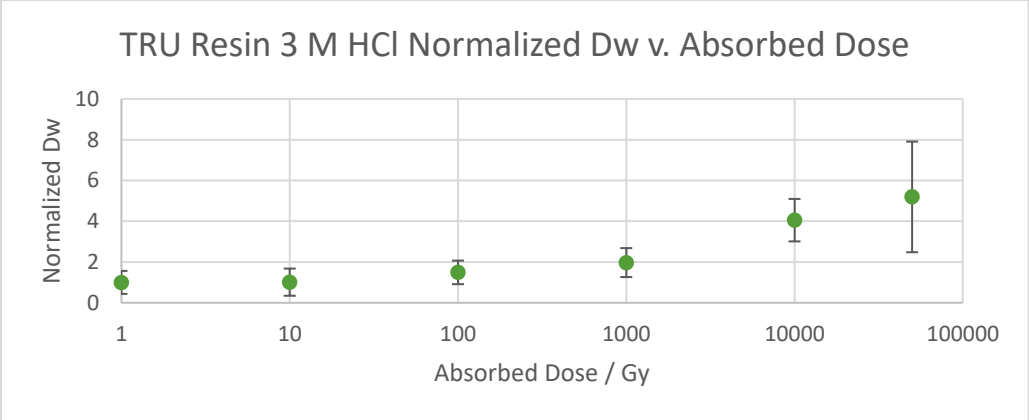

Figure 27: Contains two graphs showing the retention of plutonium-239 on TRU Resin irradiated in 3 M hydrochloric acid. The top graph shows the experimentally determined distribution ratio (Dw) v. the absorbed dose to the EXC Resin in gray. The bottom graph shows the normalized experimentally determined distribution ratio v. the absorbed dose to the EXC Resin in gray.

The pair of graphs in figure 28 show the retention of plutonium-239 on TRU Resin in 1 M nitric acid. In the first graph, the distribution ratio shows some minor fluctuations but generally remains steady around 230. The literature value for the distribution ratio of the retention of plutonium on TRU Resin in 1 M nitric acid is 14,400 *(2)*. There is a slight increase in the retention of plutonium at the 50 kGy mark that shows in both the calculated distribution ratio and the normalized distribution ratio, but the increase is small.

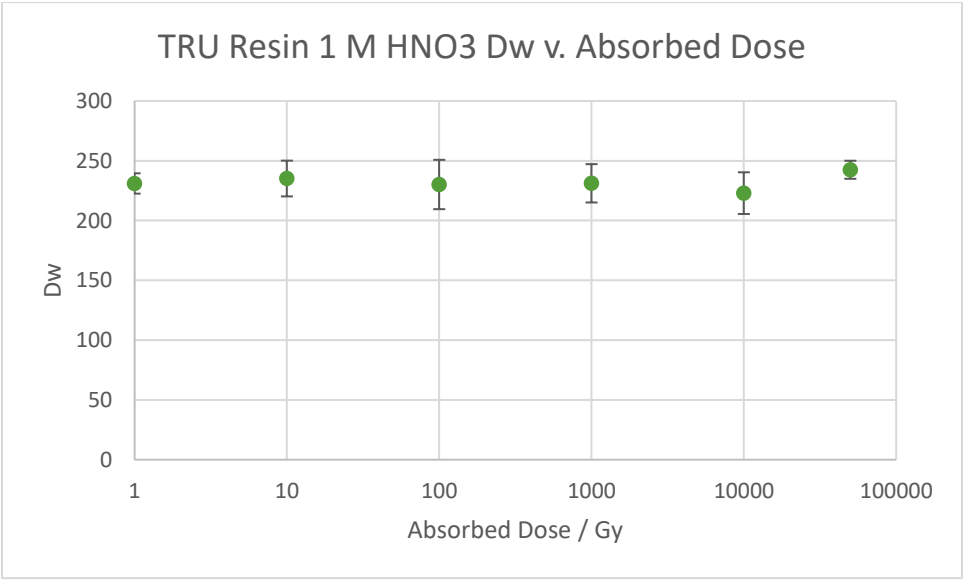

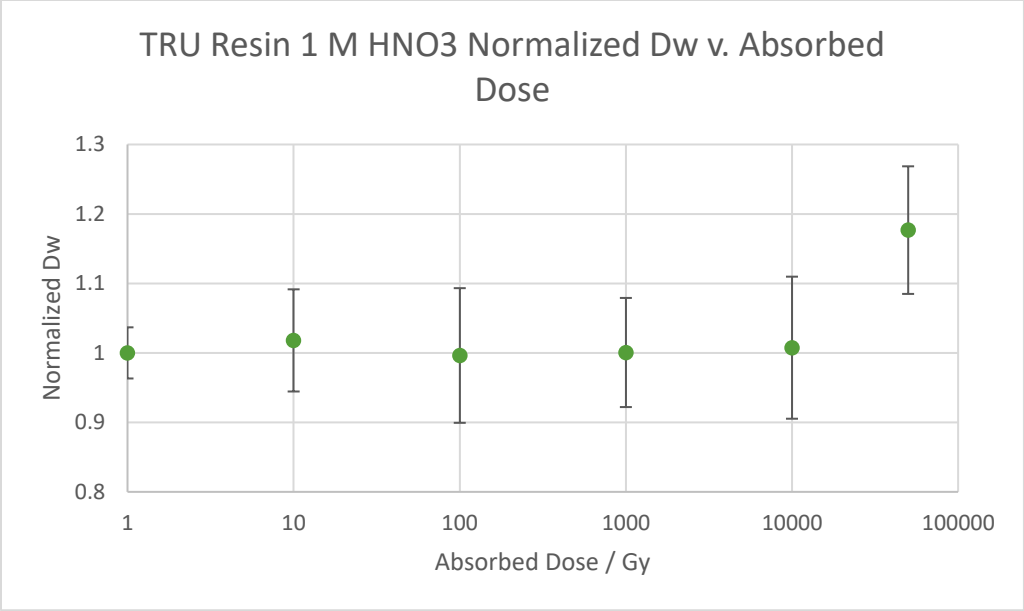

Figure 28: Contains two graphs showing the retention of plutonium-239 on TRU Resin irradiated in 1 M nitric acid. The top graph shows the experimentally determined distribution ratio (Dw) v. the absorbed dose to the EXC Resin in gray. The bottom graph shows the normalized experimentally determined distribution ratio v. the absorbed dose to the EXC Resin in gray.

The pair of graphs in figure 29 show the retention of plutonium-239 on TRU Resin in 1 M hydrochloric acid, which has an average distribution ratio of around 10. The literature value for the distribution ratio of plutonium on TRU Resin in 1 M hydrochloric acid is 18 *(2)*. There is an increase in the retention of plutonium-239 observed at the 50 kGy measurement in both the distribution ratio and the normalized distribution ratio; however, there is a large uncertainty associated with the measurement.

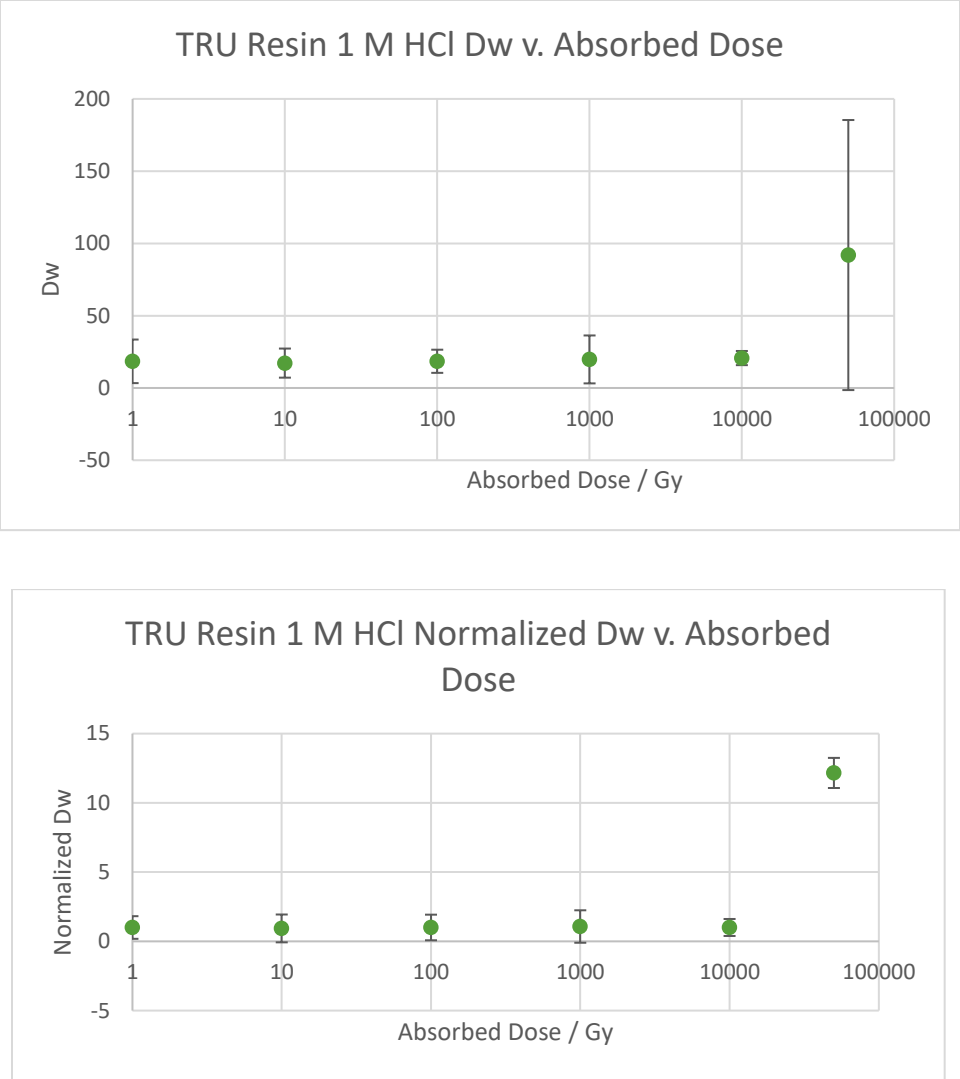

Figure 29: Contains two graphs showing the retention of plutonium-239 on TRU Resin irradiated in 1 M hydrochloric acid. The top graph shows the experimentally determined distribution ratio (Dw) v. the absorbed dose to the EXC Resin in gray. The bottom graph shows the normalized experimentally determined distribution ratio v. the absorbed dose to the EXC Resin in gray.

4.1.5: Conclusions

The two graphs shown in figure 30 display all four of the previous analyses onto common sets of axes.

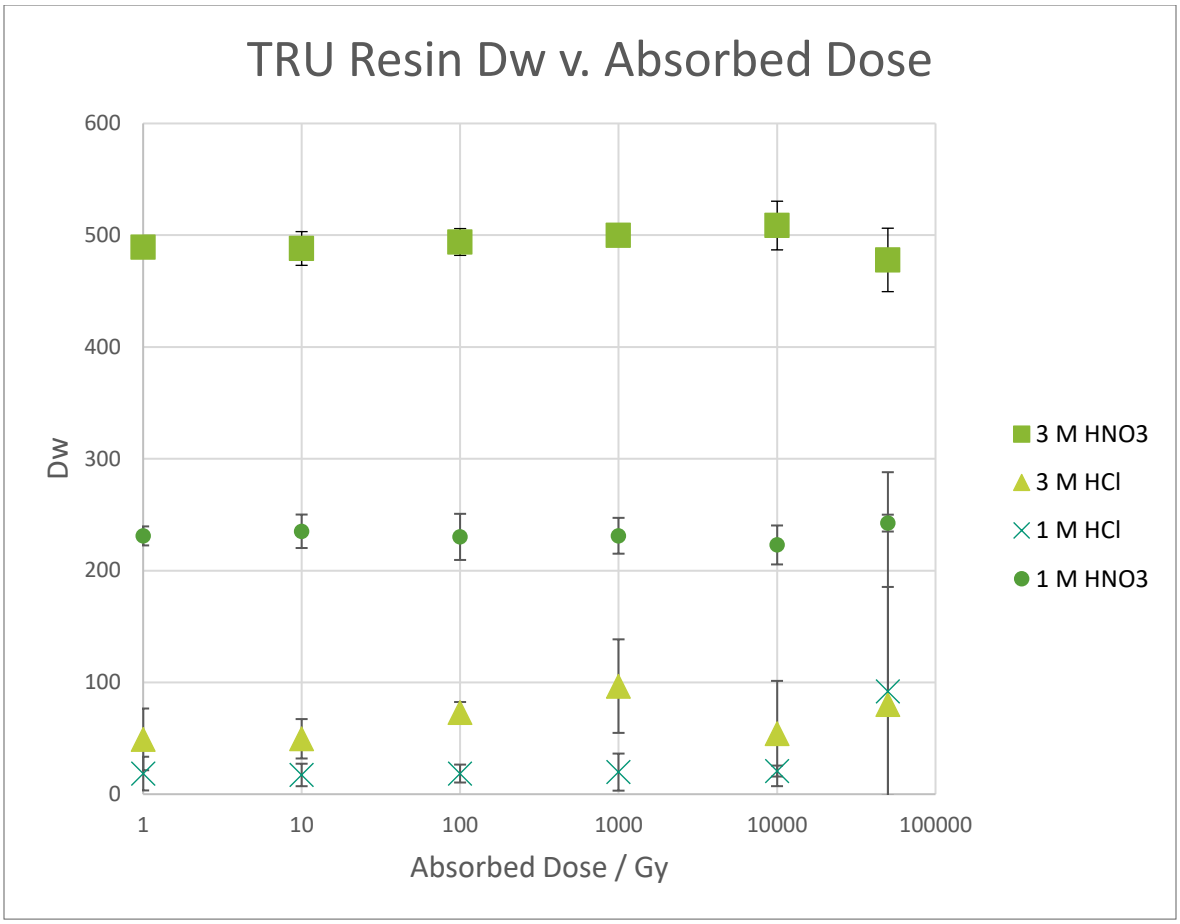
TRU Resin Dw v. Absorbed Dose
Dw
600
500
400
300
200
100
0
1
10
100
1000
10000
100000
Absorbed Dose / Gy
3 M HNO3
3 M HCl
1 M HCl
1 M HNO3

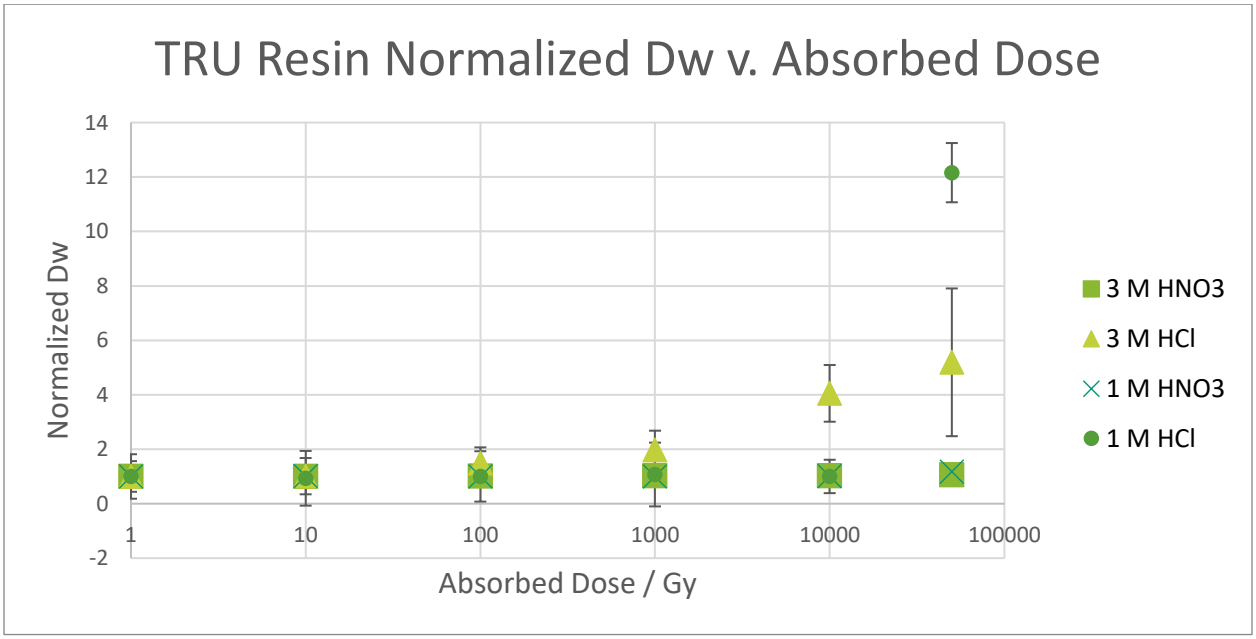
TRU Resin Normalized Dw v. Absorbed Dose
Normalized Dw
14
12
10
8
6
4
2
0
-2
1
10
100
1000
10000
100000
Absorbed Dose / Gy
3 M HNO3
3 M HCl
1 M HNO3
1 M HCl

Figure 30: Figure showing two graphs showing the compiled results the retention of plutonjium-239 on TRU Resin versus all the acid concentrations in this study. The top graph shows the distribution ratio versus the absorbed dose in gray, and the bottom graph shows the normalized distribution ratio versus the absorbed dose in gray.

Overall, there is minimal change observed in the retention of plutonium-239 on TRU Resin up to 10 kGy gamma irradiation. All of the 50 kGy irradiations saw some fluctuation in the retention of plutonium on the resin and generally saw larger experimental uncertainties as well. Generally, the TRU Resin in nitric acid saw less impact from the irradiation than the TRU Resin in hydrochloric acid. There appears to be a potential compounding factor impacting the unirradiated control groups associated with various 50 kGy measurements. Examining the effect of time between the acid preconditioning and the plutonium-239 contacting via kinetics studies is necessary and will be addressed in section 4.5. It should be noted that the literature values for the distribution ratios of plutonium in these acid conditions were determined with redox-controlled, tetravalent plutonium. Since the plutonium-239 used for these experiments did not have its oxidation state chemically controlled, it is possible that this plays a part in the large deviations from literature values.

4.2: TEVA Resin

4.2.1: Introduction

Introduced in the 1990s, TEVA is named for the TEtraValent Actinides that are its primary separation targets (2). TEVA is also used for extracting technetium (21). The extractant that is used in TEVA Resin is Aliquat 336, which is a quaternary ammonium salt. Differences in the distribution ratios in nitric and hydrochloric acids can make TEVA an effective separation media for separating thorium, neptunium, and plutonium from other actinides. In the 2-4 molarity range of nitric acid, tetravalent plutonium, neptunium, and thorium show maximum retention

with minimal retention of trivalent americium and hexavalent uranium. Under specific conditions, americium can be retained on TEVA Resin and separated from trivalent lanthanides (2).

4.2.1.1: Structure

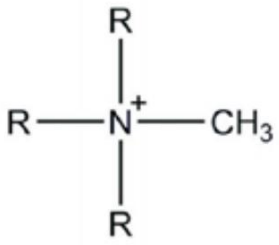

Quaternary ammonium salt Aliquat® 336,
R = octyl or decyl

Figure 31: Chemical structure of quaternary ammonium salt Aliquat 336, reproduced from (2).

4.2.1.2: Experimentally Defined k'

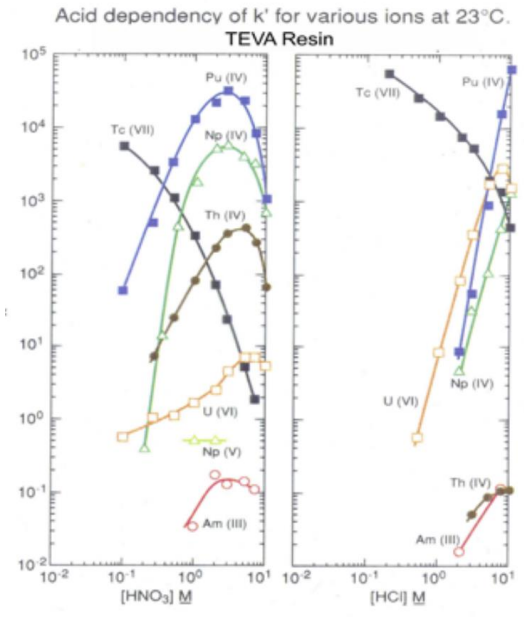

k' values, TEVA Resin, various elements, HNO_3 and HCl

Figure 32: k' values of different elements in nitric and hydrochloric acids on TEVA Resin, reproduced from (2).

4.2.2: Materials and Methods

Plutonium retention was measured via a method of batch-contact study that is commonly used in the Sudowe Research Group. This method is described at length in section 4.1.2.

4.2.3: Data and Calculations

The method by which the data was generated and reduced is discussed in section 4.1.3. All raw count data is included in Appendix C.

Table 11: Data showing absorbed dose in gray, computed distribution ratios, and distribution ratios normalized to an unirradiated control batch with identical chemical processing for TEVA Resin in 3 M nitric acid, 3 M hydrochloric acid, 1 M nitric acid, and 1 M hydrochloric acid.

resin: TEVA
acid: 3 M HNO3

dose / Gy	Dw	Sdev	p-value from two-tailed t.test with unequal variances (dose to control)	Normalized Dw
1	711.85	16.45		1.00
1	753.67	19.55		1.00
1	299.30	83.03		1.00
10	691.48	54.07	0.515	0.971
100	781.10	45.86	0.050	1.10
1000	871.84	7.47	0.000	1.22
10000	916.05	29.59	0.000	1.22
50000	503.62	10.14	0.015	1.68

resin: TEVA
acid: 3 M HCl

dose / Gy	Dw	Sdev	p-value from two-tailed t.test with unequal variances (dose to control)	Normalized Dw
1	10.70	1.64		1.00
1	10.59	0.59		1.00
1	12.62	4.37		1.00
10	10.04	1.87	0.617	0.939
100	10.17	0.79	0.587	0.950
1000	8.59	0.92	0.078	0.803
10000	10.51	0.48	0.016	0.992
50000	12.17	2.59	0.868	0.965

resin: TEVA
acid: 1 M HNO3

dose / Gy	Dw	Sdev	p-value from two-tailed t.test with unequal variances (dose to control)	Normalized Dw
1	30.51	3.81		1.00
1	39.95	13.57		1.00
1	52.97	16.42		1.00
10	34.33	3.90	0.210	1.13
100	59.52	32.29	0.170	1.95
1000	94.05	57.79	0.115	3.08
10000	190.86	23.48	0.000	4.78
50000	226.60	5.53	0.000	4.28

resin: TEVA
acid: 1 M HCl

dose / Gy	Dw	Sdev	p-value from two-tailed t.test with unequal variances (dose to control)	Normalized Dw
1	14.48	11.81		1.00
1	7.61	1.08		1.00
1	11.41	7.42		1.00
10	12.16	10.11	0.775	0.839
100	9.94	3.21	0.505	0.686
1000	8.43	1.14	0.382	0.582
10000	9.24	0.97	0.066	1.21
50000	18.23	9.26	0.296	1.60

4.2.4: Results and Discussion

The data gathered in section 4.2.3 is plotted here in section 4.2.4. Each acid condition is plotted with a pair of graphs to show the changes in distribution ratio versus the absorbed dose to the resin in Gray. Each figure in this section contains two graphs. The first graph shows the calculated distribution ratio versus the absorbed dose to the resin in gray. The second graph in each pair illustrates the normalized distribution ratio plotted versus the absorbed dose to the resin in gray. Both graphs are shown with an uncertainty budget of two experimentally determined standard deviations, i.e., at a 95% confidence interval. Plotting both figures and presenting them as a pair is done as a check to ensure there were no confounding variables that

affected both the unirradiated control group and the irradiated group since more time elapsed between the acid preconditioning and the addition of the plutonium. The p-values for the two-tailed t.test with unequal variances are listed with the raw data in Appendix C.

The first pair of graphs (figure 33) are for the retention of plutonium-239 on TEVA Resin in 3 M nitric acid. The distribution ratio is around 700 and increases from 0 to 10 kGy; however, the distribution ratio at 50 kGy shows a marked decrease. The literature value for the distribution ratio of plutonium on TEVA Resin in 3 M nitric acid is 38,000 (2). The second graph showing the normalized distribution ratios shows a continual trend of increasing normalized distribution ratios, leading to the hypothesis that a potentially confounding chemical factor might also affect the extraction over time.

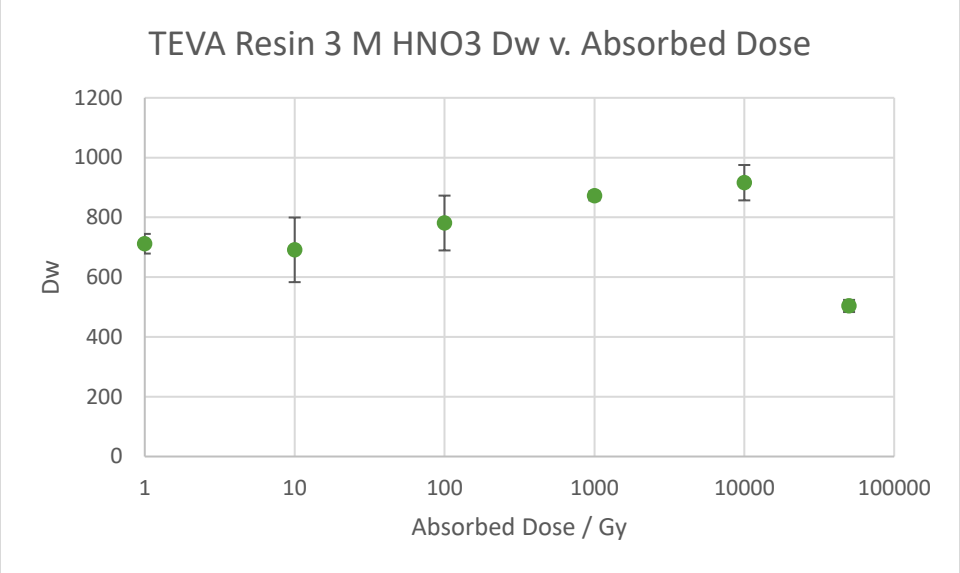

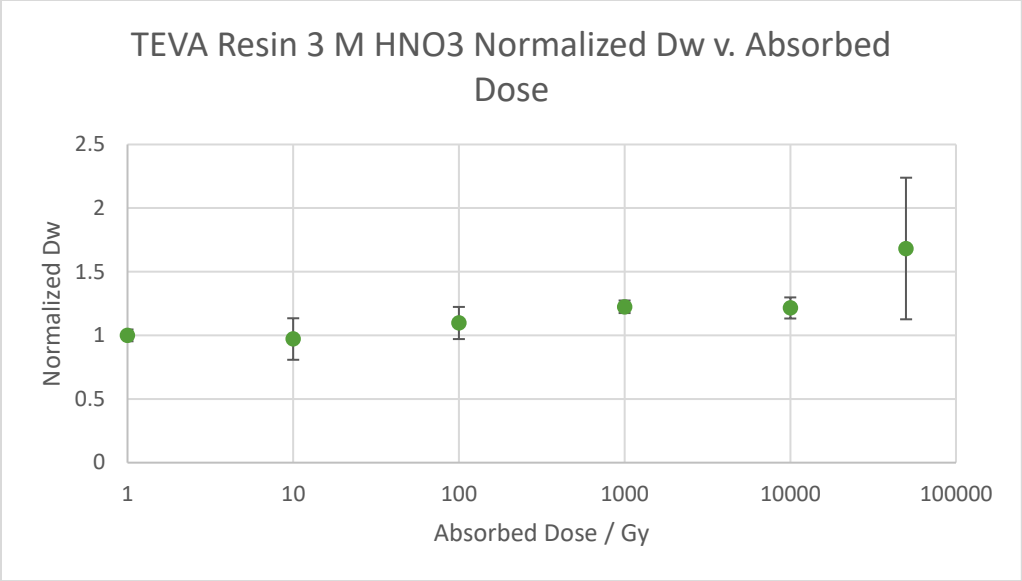

Figure 33: Contains two graphs showing the retention of plutonium-239 on TEVA Resin irradiated in 3 M nitric acid. The top graph shows the experimentally determined distribution ratio (Dw) v. the absorbed dose to the EXC Resin in gray. The bottom graph shows the normalized experimentally determined distribution ratio v. the absorbed dose to the EXC Resin in gray.

The two graphs in figure 34 show the retention of plutonium-239 on TEVA Resin in 3 M hydrochloric acid. The literature value for the distribution ratio of plutonium on TEVA Resin in 3 M hydrochloric acid is 170 (2). While there appears to be a slight dip in plutonium retention at the 10 kGy point, it is not statistically significant. The bigger takeaway from this graph is that plutonium is simply not particularly well retained on TEVA resin in 3 M hydrochloric acid, with or without radiation being applied to the extraction chromatographic resin.

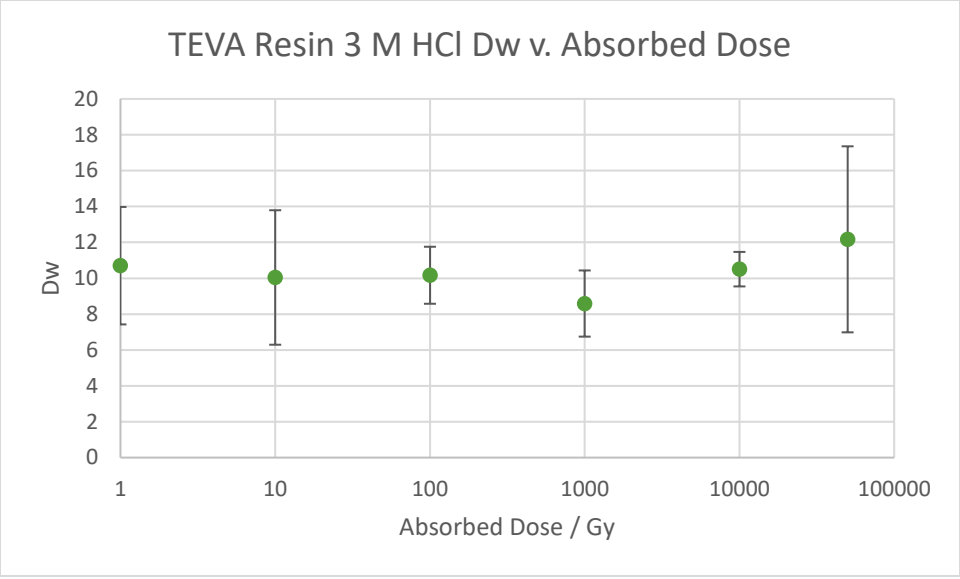

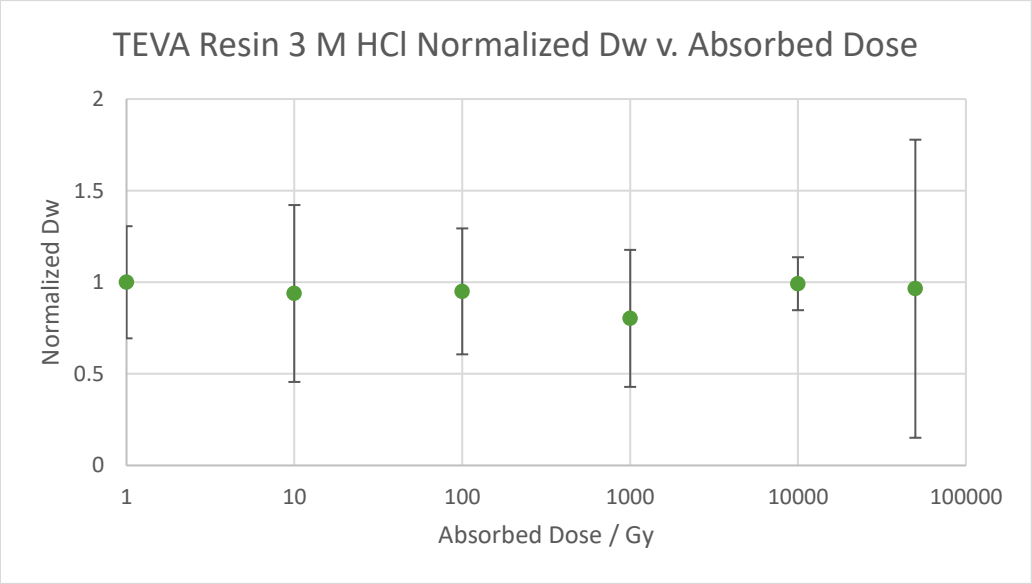

Figure 34: Contains two graphs showing the retention of plutonium-239 on TEVA Resin irradiated in 3 M hydrochloric acid. The top graph shows the experimentally determined distribution ratio (Dw) v. the absorbed dose to the EXC Resin in gray. The bottom graph shows the normalized experimentally determined distribution ratio v. the absorbed dose to the EXC Resin in gray.

The two graphs in figure 35 show the retention of plutonium-239 on TEVA Resin in 1 M nitric acid. The literature value for the distribution ratio of plutonium on TEVA Resin in 1 M nitric acid is 7,600 (2). Both graphs show an increase in retention of plutonium-239 with increasing radiation dose.

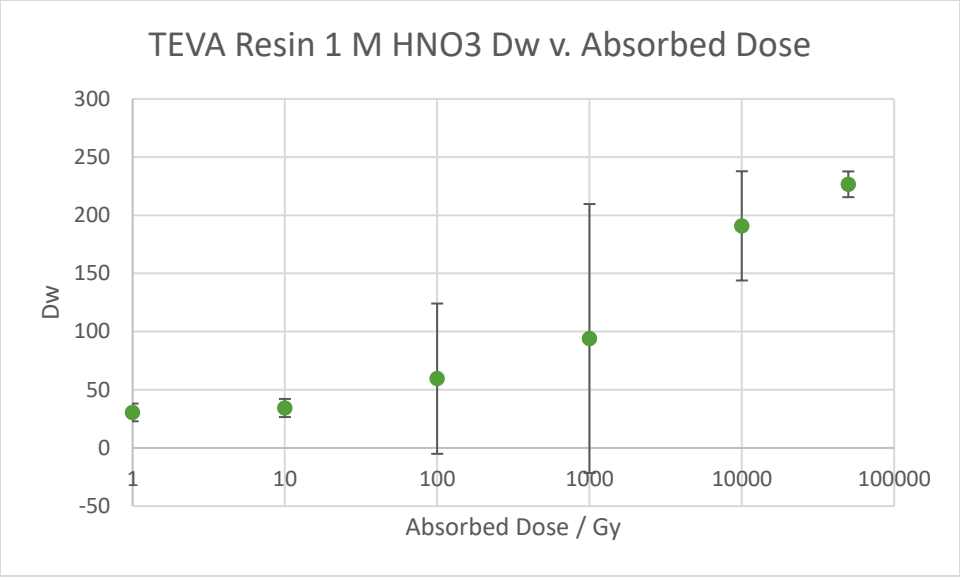

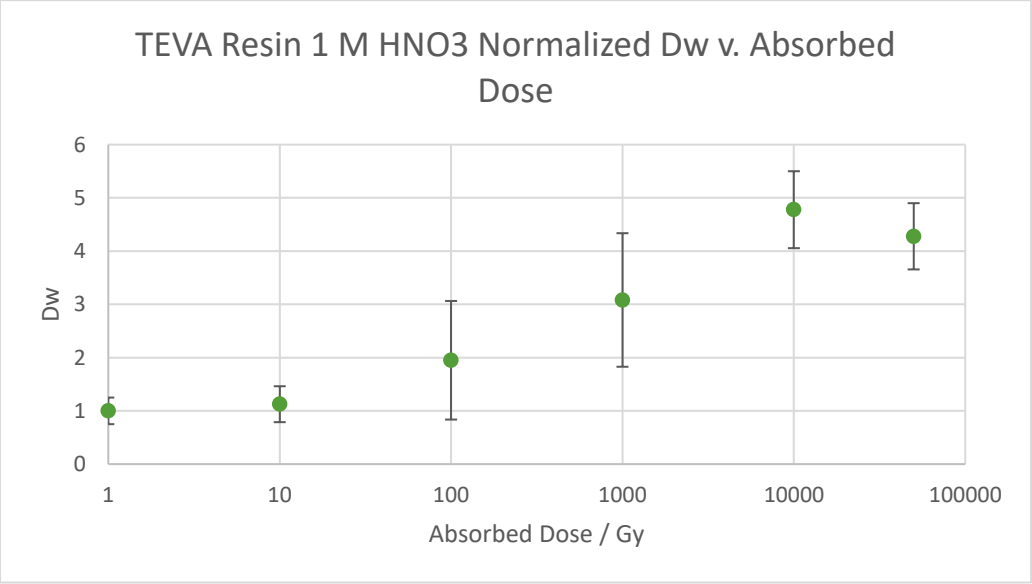

Figure 35: Contains two graphs showing the retention of plutonium-239 on TEVA Resin irradiated in 1 M nitric acid. The top graph shows the experimentally determined distribution ratio (Dw) v. the absorbed dose to the EXC Resin in gray. The bottom graph shows the normalized experimentally determined distribution ratio v. the absorbed dose to the EXC Resin in gray.

The two graphs in figure 36 show the retention of plutonium-239 on TEVA Resin in 1 M hydrochloric acid. The literature value of the distribution ratio of plutonium on TEVA Resin in 1 M hydrochloric acid is 2 (2). While there appears to be a slight dip in plutonium retention at the 10 kGy point, particularly in the normalized distribution ratio, it is not statistically significant.

The bigger takeaway from this graph is that plutonium is not well retained on TEVA Resin in 1 M hydrochloric acid, with or without radiation being applied to the extraction chromatographic resin.

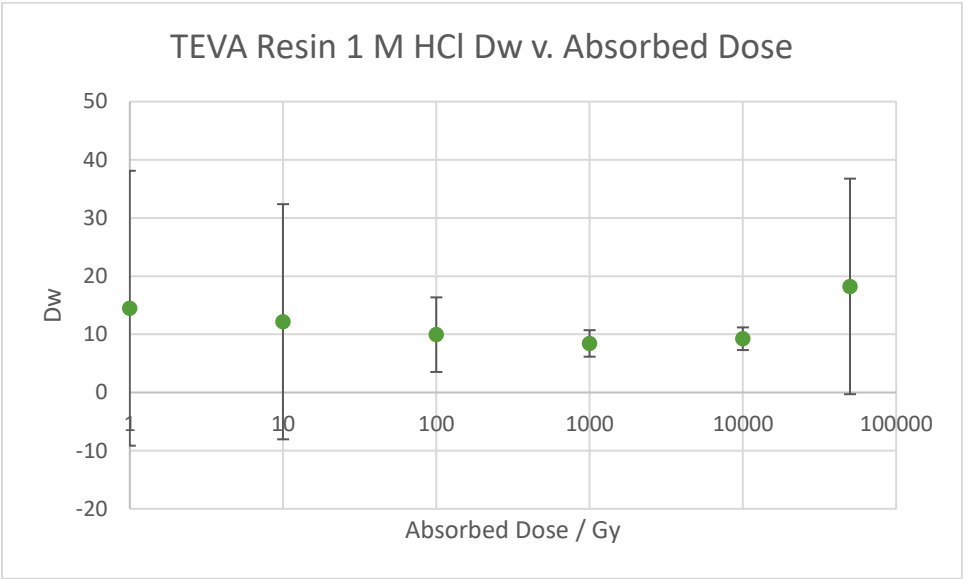

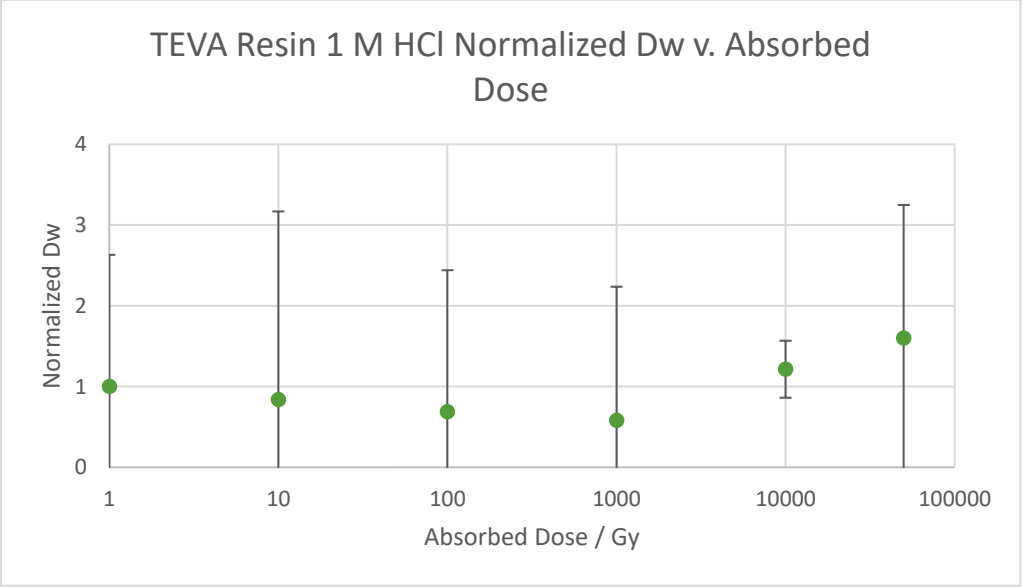

Figure 36: Contains two graphs showing the retention of plutonium-239 on TEVA Resin irradiated in 1 M hydrochloric acid. The top graph shows the experimentally determined distribution ratio (Dw) v. the absorbed dose to the EXC Resin in gray. The bottom graph shows the normalized experimentally determined distribution ratio v. the absorbed dose to the EXC Resin in gray.

4.2.5: Conclusions

The two graphs shown in figure 37 display all four of the previous analyses onto common sets of axes.

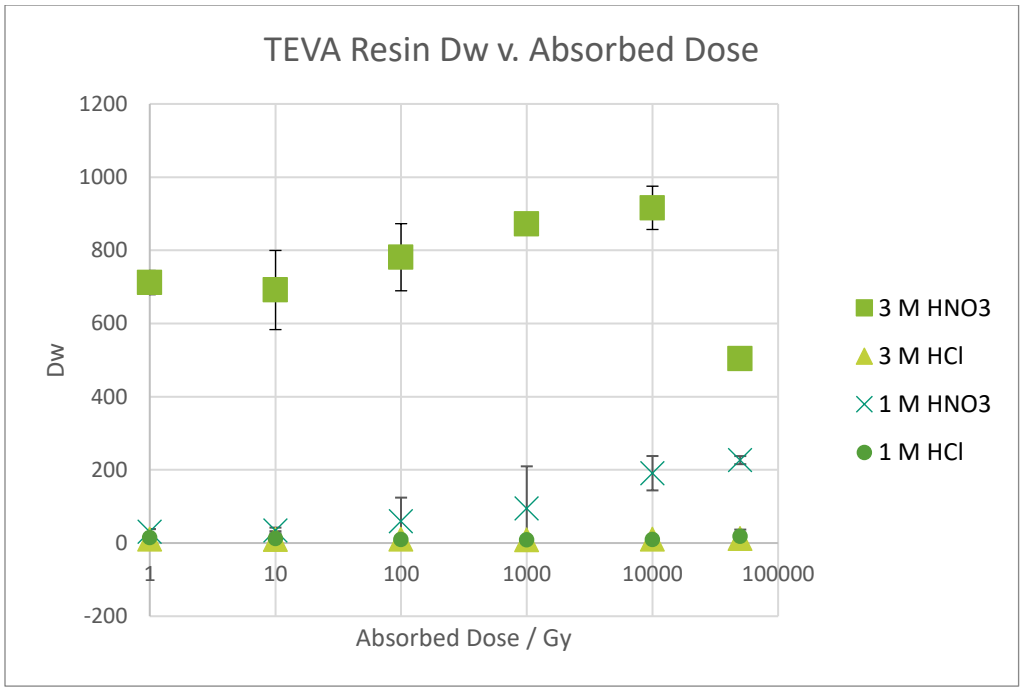

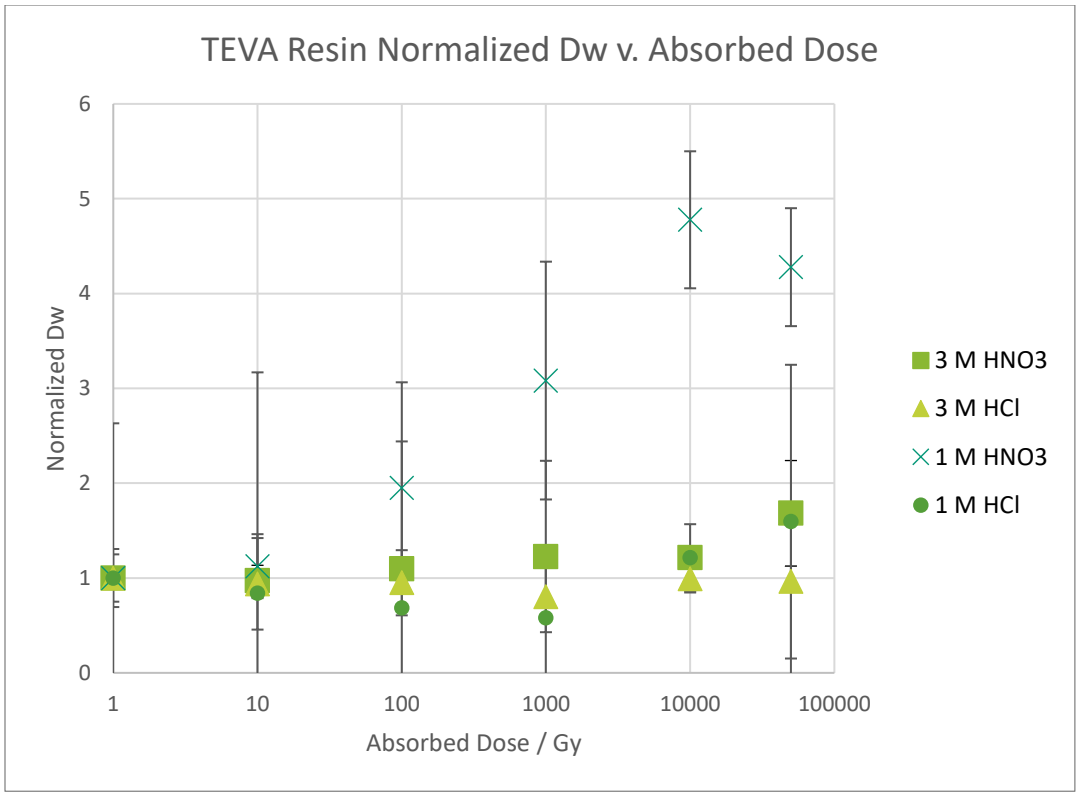

Figure 37: Figure showing two graphs showing the compiled results the retention of plutonium-239 on TEVA Resin versus all the acid concentrations in this study. The top graph shows the distribution ratio versus the absorbed dose in gray, and the bottom graph shows the normalized distribution ratio versus the absorbed dose in gray.

The retention of plutonium on TEVA Resin in 3 M nitric acid increases with increasing radiation dose to 10 kGy; however, the trend of increasing retention carries over to the 50 kGy measurement in the normalized distribution ratios, making this a condition that should be further investigated in the kinetics studies in section 4.5. The 1 M nitric acid irradiated sample groups show an increased retention of plutonium from 1 kGy and through the 10 and 50 kGy benchmarks. Neither of the experimental groups in hydrochloric acid show marked changes in performance under irradiation up to 50 kGy; however, this could be confounded by their relatively low plutonium retention under regular circumstances, i.e., generally under a distribution ratio of twenty. Overall, more changes that were potentially a result of the ionizing radiation were observed in TEVA Resin in nitric acid than in hydrochloric acid.

4.3: UTEVA Resin

4.3.1: Introduction

Introduced in the early 1990s, UTEVA Resin is also named for its primary analytes, as the Uranium and TEtraValent Actinides Resin (22) (2). UTEVA Resin is primarily used for the separation of uranium and tetravalent actinides like neptunium, thorium, and plutonium. The extractant coated on the inert polymer backbone is dipentyl pentyl phosphonate, abbreviated DP[PP] or DPPP, which can also be called diamyl amyl phosphonate, abbreviated DAAP. DPPP shows a marked preferential affinity for U(VI), Th (IV), Np (IV), and Pu (IV) over common matrix constituents like aluminum, iron, and group 1 and 2 elements. UTEVA Resin can also be used for the separation of zirconium from various matrices (2).

4.3.1.1: Structure

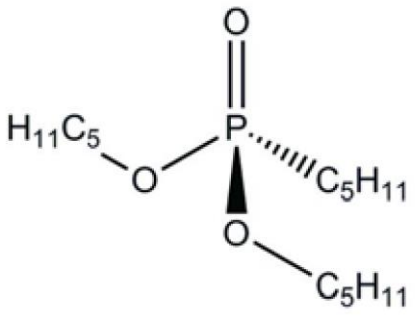

Dipentyl pentylphosphonate (DP[PP]) also called Diamyl amylphosphonate (DAAP)

Figure 38: Chemical structure of dipentyl pentyl phosphonate (DPPP) which is also called diamyl amyl phosphonate (DAAP), reproduced from (2).

4.3.1.2: Experimentally Defined k'

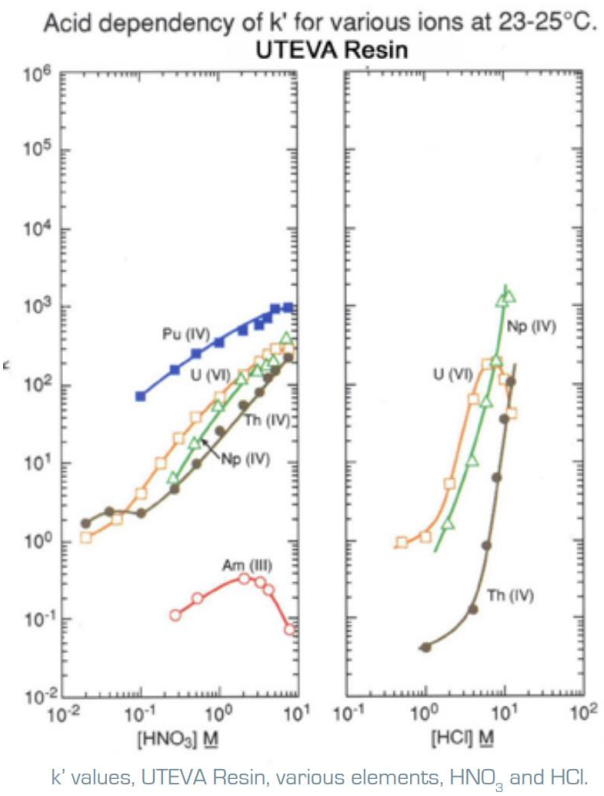

Figure 39: k' values of different elements in nitric and hydrochloric acids on UTEVA Resin, reproduced from (2).

4.3.2: Materials and Methods

Plutonium retention was measured via a method of batch-contact study that is commonly used in the Sudowe Research Group. This method is described in section 4.1.2.

4.3.3: Data and Calculations

The method by which the data was generated and reduced is discussed in section 4.1.3. All raw count data is included in Appendix C.

Table 12: Data showing absorbed dose in gray, computed distribution ratios, and distribution ratios normalized to an unirradiated control batch with identical chemical processing for UTEVA Resin in 3 M nitric acid, 3 M hydrochloric acid, 1 M nitric acid, and 1 M hydrochloric acid.

resin: UTEVA
acid: 3 M HNO3

dose / Gy	Dw	Sdev	p-value from two-tailed t.test with unequal variances (dose to control)	Normalized Dw
1	98.99	17.13		1.00
1	140.42	22.99		1.00
1	161.41	25.42		1.00
10	102.88	34.26	0.848	1.04
100	162.66	18.47	0.002	1.64
1000	109.66	14.16	0.375	1.11
10000	211.63	27.26	0.008	1.51
50000	314.70	38.48	0.001	1.95

resin: UTEVA
acid: 3 M HCl

dose / Gy	Dw	Sdev	p-value from two-tailed t.test with unequal variances (dose to control)	Normalized Dw
1	13.46	1.00		1.00
1	12.45	1.95		1.00
1	35.69	10.39		1.00
10	14.90	1.49	0.168	1.11
100	16.63	3.44	0.162	1.24
1000	14.08	1.49	0.517	1.05
10000	14.51	2.04	0.194	1.17
50000	41.73	14.54	0.527	1.17

resin: UTEVA
acid: 1 M HNO3

dose / Gy	Dw	Sdev	p-value from two-tailed t.test with unequal variances (dose to control)	Normalized Dw
1	21.26	11.15		1.00
1	34.41	5.21		1.00
1	29.24	10.36		1.00
10	23.50	13.70	0.809	1.10
100	28.25	20.47	0.577	1.33
1000	43.44	15.73	0.066	2.04
10000	67.58	11.65	0.006	1.96
50000	56.34	15.52	0.032	1.93

resin: UTEVA
acid: 1 M HCl

dose / Gy	Dw	Sdev	p-value from two-tailed t.test with unequal variances (dose to control)	Normalized Dw
1	10.24	1.73		1.00

1	8.71	0.80		1.00
1	13.45	1.35		1.00
10	8.88	0.22	0.212	0.866
100	9.67	1.76	0.656	0.944
1000	9.47	1.86	0.562	0.924
10000	9.26	1.38	0.518	1.06
50000	17.31	3.01	0.077	1.29

4.3.4: Results and Discussion

The data gathered in section 4.3.3 is plotted here in section 4.3.4. Each acid condition is plotted with a pair of graphs to show the changes in distribution ratio versus the absorbed dose to the resin in gray. Each figure in this section contains two graphs. The first graph shows the calculated distribution ratio versus the absorbed dose to the resin in gray. The second graph in each pair illustrates the normalized distribution ratio plotted versus the absorbed dose to the resin in gray. Both graphs are shown with an uncertainty budget of two experimentally determined standard deviations, i.e., at a 95% confidence interval. Plotting both figures and presenting them as a pair is done as a check to ensure there were no confounding variables that affected both the unirradiated control group and the irradiated group since more time elapsed between the acid preconditioning and the addition of the plutonium. The p-values for the two-tailed t.test with unequal variances are listed with the raw data in Appendix C.

The first pair of graphs (shown in figure 40) are for the retention of plutonium-239 on UTEVA Resin in 3 M nitric acid. UTEVA Resin shows an increase in plutonium retention with increased radiation in 3 M nitric acid dose to the EXC resin. The literature value for the distribution ratio of plutonium on UTEVA Resin in 3 M nitric acid is 1000 (2). The experimental group that was irradiated to 50 kGy saw a threefold increase in the plutonium retention in the distribution ratio

and twofold in the normalized distribution ratio. The fact that both of these show a marked increase, but the normalized distribution ratio has less of an increase confirms some confounding effects also seen in other acid conditions.

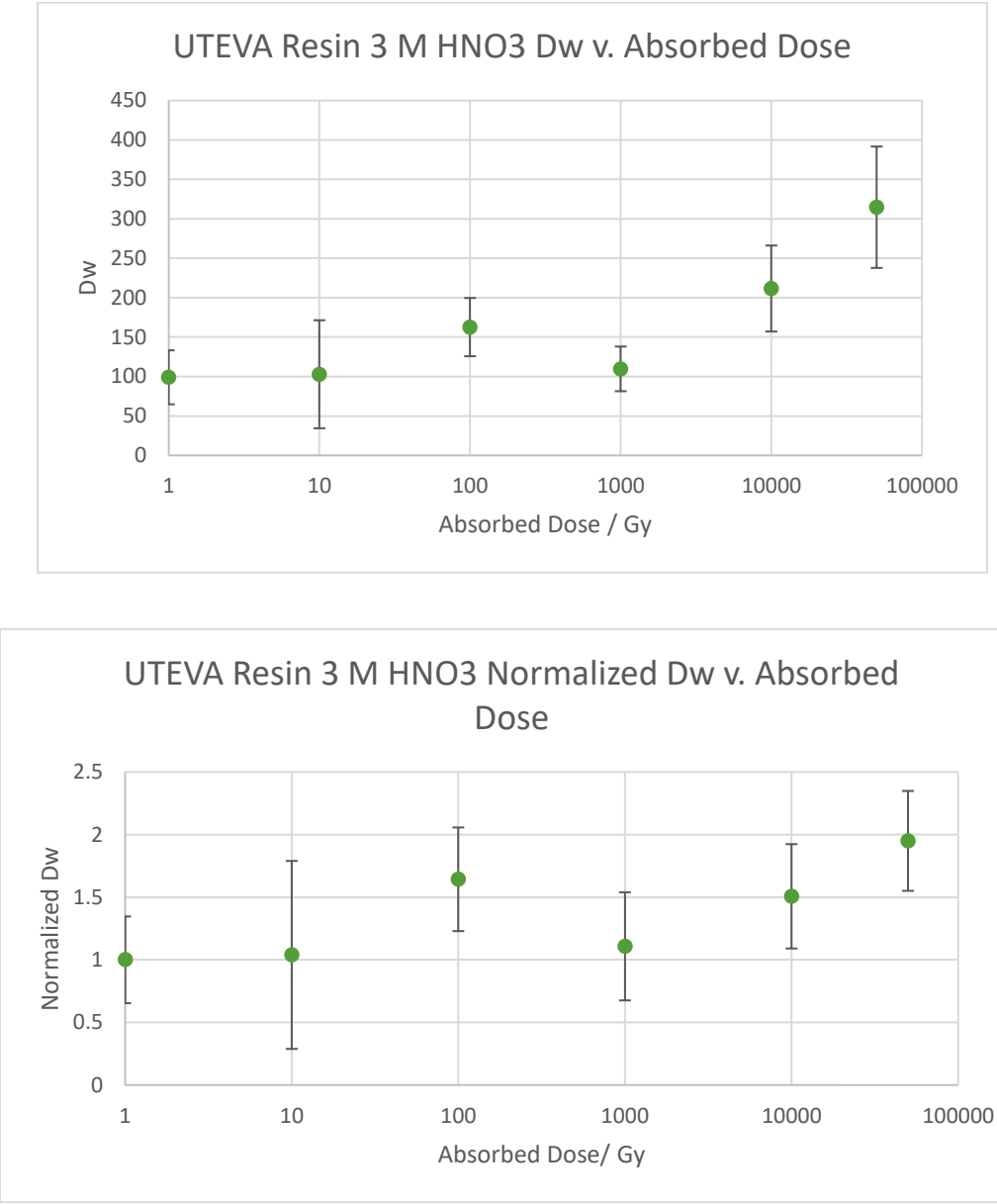

Figure 40: Contains two graphs showing the retention of plutonium-239 on UTEVA Resin irradiated in 3 M nitric acid. The top graph shows the experimentally determined distribution ratio (Dw) v. the absorbed dose to the EXC Resin in gray. The bottom graph shows the normalized experimentally determined distribution ratio v. the absorbed dose to the EXC Resin in gray.

The two graphs in figure 41 show the retention of plutonium-239 on UTEVA Resin in 3 M hydrochloric acid. Plutonium retention stays fairly constant up to a dose of 10 kGy. At the 50 kGy point, there is a roughly fourfold observed uptick in the retention of plutonium on the UTEVA Resin; however, the increase is less than 1.25 times in the normalized distribution ratio, indicating that there is a confounding chemical factor affecting metal retention on the resin in that experimental condition. Generally, low plutonium retention with this resin and acid condition can also make it so smaller differences appear to have more impact.

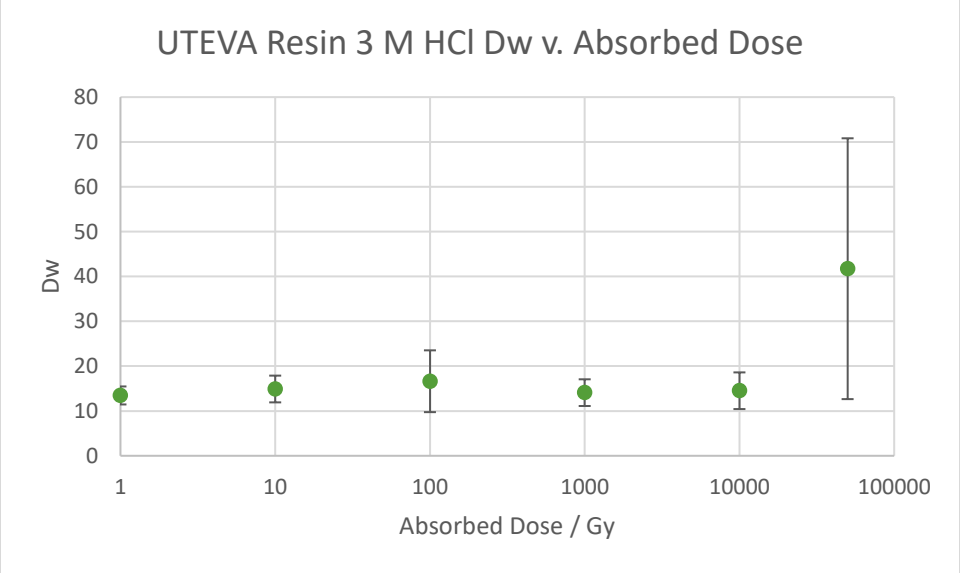

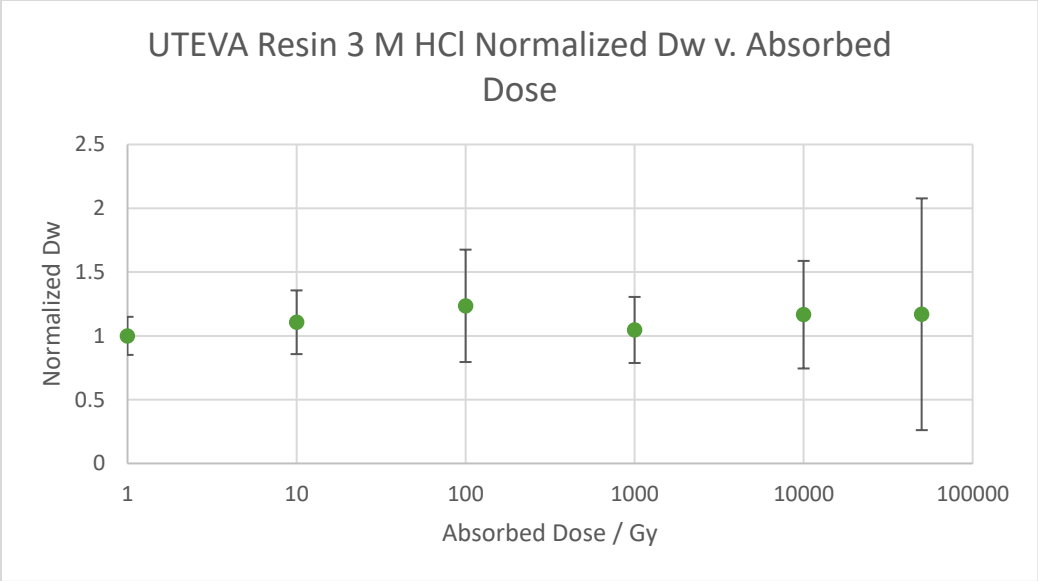

Figure 41: Contains two graphs showing the retention of plutonium-239 on UTEVA Resin irradiated in 3 M hydrochloric acid. The top graph shows the experimentally determined distribution ratio (Dw) v. the absorbed dose to the EXC Resin in gray. The bottom graph shows the normalized experimentally determined distribution ratio v. the absorbed dose to the EXC Resin in gray.

The two graphs in figure 42 show the retention of plutonium on UTEVA Resin in 1 M nitric acid. The literature value for the distribution ratio of plutonium on UTEVA Resin in 1 M nitric acid is 500 (2). Increasing the absorbed radiation dose to the resin also increases the retention of plutonium on the resin. Preferred uncertainties would certainly have standard deviations less than the magnitude of the experimentally determined distribution ratios. The uncertainties are larger than preferred; however, the relatively low magnitude of the distribution ratio does make this seem to have a disproportionately large impact. The trends in the calculated distribution ratio and the normalized distribution ratio are similar. While the magnitude of the differences could indicate that there are some effects of confounding chemical behavior as seen in the 3 M nitric acid batches, it was not a statistically significant factor.

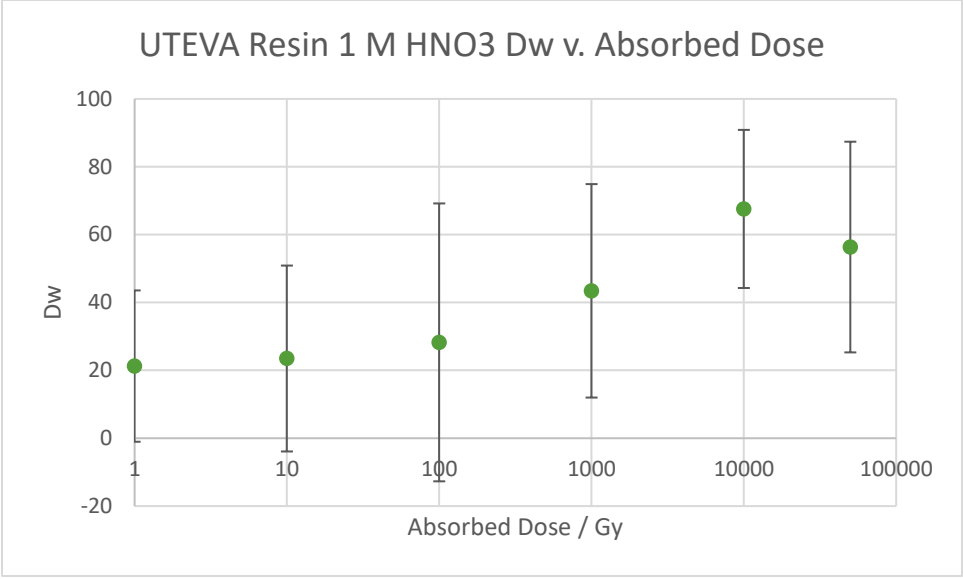

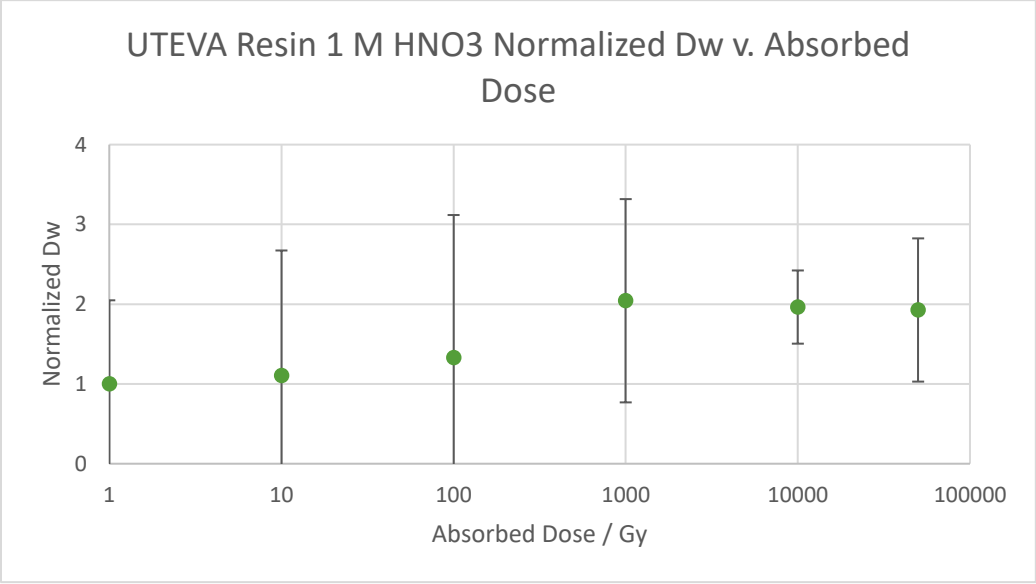

Figure 42: Contains two graphs showing the retention of plutonium-239 on UTEVA Resin irradiated in 1 M nitric acid. The top graph shows the experimentally determined distribution ratio (Dw) v. the absorbed dose to the EXC Resin in gray. The bottom graph shows the normalized experimentally determined distribution ratio v. the absorbed dose to the EXC Resin in gray.

The graphs in figure 43 show the retention of plutonium on UTEVA Resin in 1 M hydrochloric acid. The trends shown in the calculated distribution ratio and the normalized distribution ratio match. While there is a slight increase of the observed plutonium retention for the experimental group that had an absorbed dose of 50 kGy and a slight decrease for those with an absorbed

dose of 10, 100, and 1000 Gray, none of these are statistically significant at 95% confidence. All of them remain below 20 which indicates that this would not be a particularly favorable separation condition.

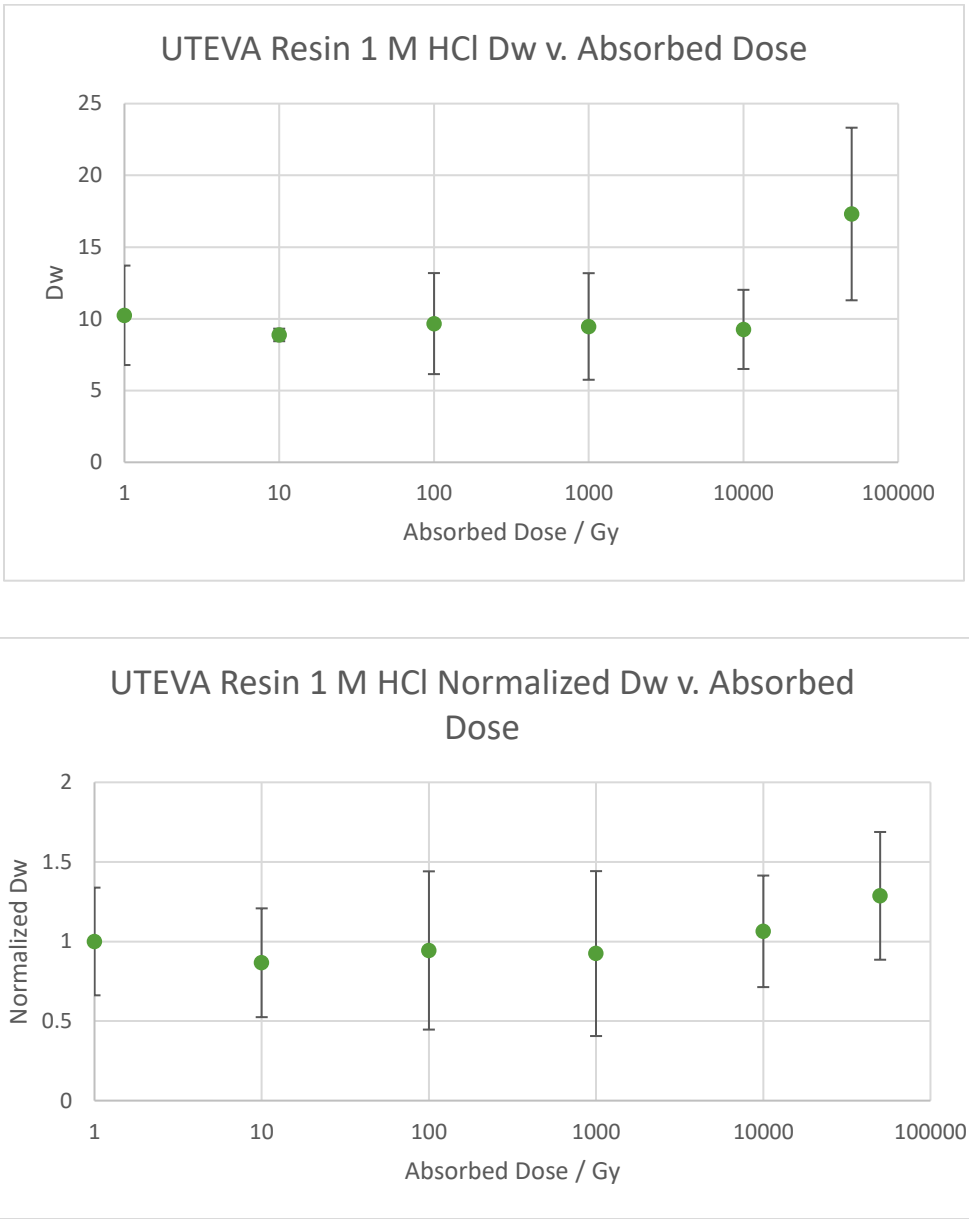

Figure 43: Contains two graphs showing the retention of plutonium-239 on UTEVA Resin irradiated in 1 M hydrochloric acid. The top graph shows the experimentally determined distribution ratio (Dw) v. the absorbed dose to the EXC Resin in gray. The bottom graph shows the normalized experimentally determined distribution ratio v. the absorbed dose to the EXC Resin in gray.

4.3.5: Conclusions

The two graphs shown in figure 44 pull all four of the previous analyses onto common sets of axes.

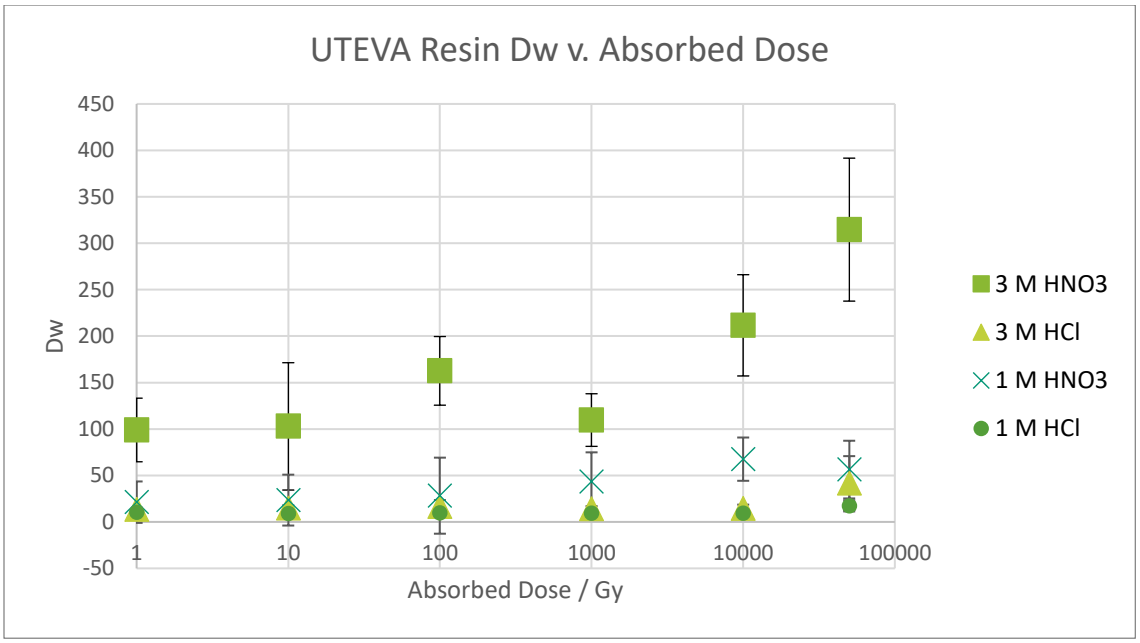

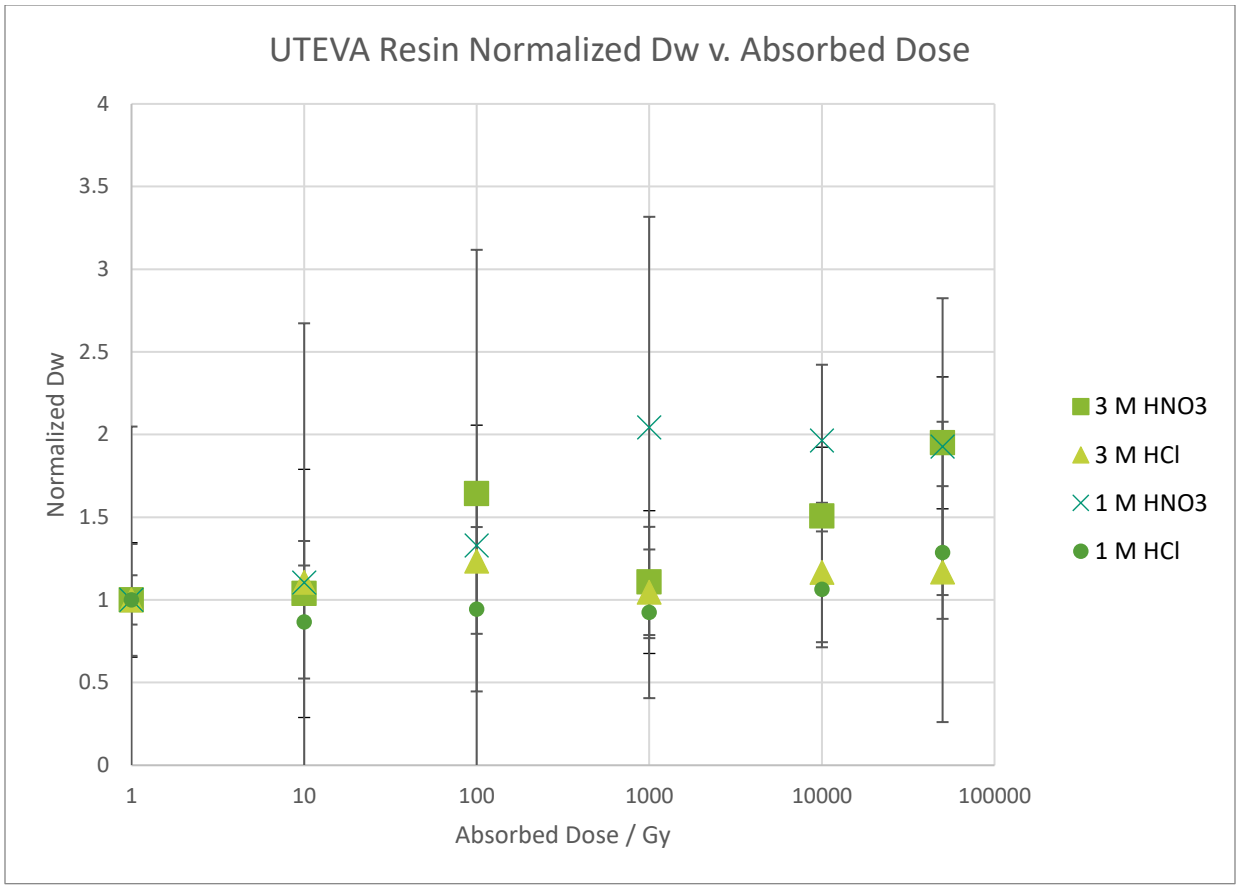

Figure 44: Figure showing two graphs showing the compiled results the retention of plutonium-239 on UTEVA Resin versus all the acid concentrations in this study. The top graph shows the distribution ratio versus the absorbed dose in gray, and the bottom graph shows the normalized distribution ratio versus the absorbed dose in gray.

A greater effect is seen on the retention of plutonium on UTEVA Resin in nitric acid than on UTEVA Resin in hydrochloric acid. There are potentially confounding chemical factors that should be considered in a kinetics study presented in the 50 kGy experimental group and its related unirradiated control group, especially for the 3 M nitric acid experimental condition. UTEVA Resin in hydrochloric acid does not see significant impacts from ionizing gamma radiation up to 50 kGy. UTEVA Resin in nitric acid generally sees increasing plutonium retention with the addition of ionizing gamma radiation, but the 3 M nitric acid condition should be further interrogated in a kinetics study.

4.4: Actinide (DIPEX) Resin

4.4.1: Introduction

Introduced in the late 1980s, the Actinide Resin produced by Eichrom Technologies and Triskem International uses DIPEX as extractant. Actinide Resin is also referenced as AC Resin and DIPEX Resin. DIPEX is an abbreviation for P, P'-di(2-ethylhexyl) methane-di-phosphonic acid which may also be named bis(2-ethylhexyl) methane-di-phosphonic acid (H_2DEH[MDP], DIPEX®) (23) (2). DIPEX shows a strong affinity for actinides and lanthanides. Typical mobile phases for extraction include a large range of nitric acid concentrations. Typical mobile phases for back-extraction include di-phosphonic acid (HEDPA) or the removal of the organic extractant from the extraction chromatography resin with isopropanol (1).

4.4.1.1: Structure

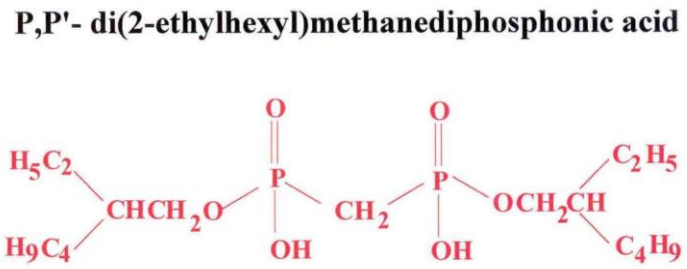

Figure 45: Chemical structure of P, P'-di(2-ethylhexyl) methane-di-phosphonic acid, more commonly referenced as DIPEX, reproduced from (23).

4.4.1.2: Experimentally Defined k'

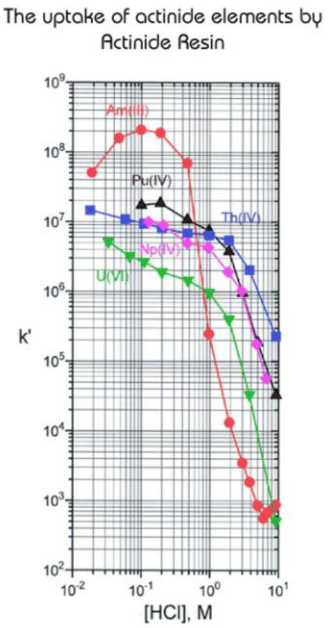

Figure 46: k' values of different elements in nitric and hydrochloric acids on Actinide Resin, reproduced from (23).

4.4.2: Materials and Methods

Plutonium retention was measured via a method of batch-contact study that is commonly used in the Sudowe Research Group. This method is described in section 4.1.2.

4.4.3: Data and Calculations

The method by which the data was generated and reduced is discussed in section 4.1.3. All raw count data is included in Appendix C.

Table 13: Data showing absorbed dose in gray, computed distribution ratios, and distribution ratios normalized to an unirradiated control batch with identical chemical processing for Actinide (DIPEX) Resin in 3 M nitric acid, 3 M hydrochloric acid, 1 M nitric acid, and 1 M hydrochloric acid.

resin: Actinide/DIPEX
acid: 3 M HNO3

dose / Gy	Dw	Sdev	p-value from two-tailed t.test with unequal variances (dose to control)	Normalized Dw
1	521.10	7.84		1.00

1	521.05	5.04		1.00
1	507.27	10.88		1.00
10	521.20	11.57	0.989	1.00
100	522.36	4.30	0.791	1.00
1000	519.87	10.87	0.861	0.998
10000	522.36	4.30	0.708	1.00
50000	508.39	4.77	0.860	1.00

resin: Actinide/DIPEX
acid: 3 M HCl

dose / Gy	Dw	Sdev	p-value from two-tailed t.test with unequal variances (dose to control)	Normalized Dw
1	393.13	5.67		1.00
1	395.08	2.32		1.00
1	385.32	4.96		1.00
10	389.24	7.12	0.426	0.990
100	388.25	6.67	0.308	0.988
1000	391.20	7.60	0.550	0.995
10000	390.22	7.53	0.292	0.988
50000	386.07	9.66	0.911	1.00

resin: Actinide/DIPEX
acid: 1 M HNO3

dose / Gy	Dw	Sdev	p-value from two-tailed t.test with unequal variances (dose to control)	Normalized Dw
1	245.62	3.88		1.00
1	246.28	4.68		1.00
1	246.38	4.84		1.00
10	248.84	3.66	0.273	1.01
100	247.52	2.61	0.451	1.01
1000	246.28	4.68	0.836	1.00
10000	241.85	3.72	0.191	0.982
50000	248.91	2.57	0.403	1.01

resin: Actinide/DIPEX
acid: 1 M HCl

dose / Gy	Dw	Sdev	p-value from two-tailed t.test with unequal variances (dose to control)	Normalized Dw
1	495.67	4.70		1.00
1	499.43	7.13		1.00
1	503.39	4.15		1.00
10	503.47	15.45	0.396	1.02
100	492.01	4.90	0.322	0.993
1000	490.86	8.20	0.358	0.990
10000	494.51	8.00	0.394	0.990
50000	498.43	8.14	0.333	0.990

4.4.4: Results and Discussion

The data gathered in section 4.4.3 is plotted here in section 4.4.4. Each acid condition is plotted with a pair of graphs to show the changes in distribution ratio versus the absorbed dose to the resin in gray. Each figure in this section contains two graphs. The first graph shows the calculated distribution ratio versus the absorbed dose to the resin in gray. The second graph in each pair illustrates the normalized distribution ratio plotted versus the absorbed dose to the resin in gray. Both graphs are shown with an uncertainty budget of two experimentally determined standard deviations, i.e., at a 95% confidence interval. Plotting both figures and presenting them as a pair is done as a check to ensure there were no confounding variables that affected both the unirradiated control group and the irradiated group since more time elapsed between the acid preconditioning and the addition of the plutonium. The p-values for the two-tailed t.test with unequal variances are listed with the raw data in Appendix C.

The first pair of graphs (figure 47) show the retention of plutonium-239 on Actinide (DIPEX) Resin in 3 M nitric acid. There are no significant changes in the retention of plutonium-239 on Actinide (DIPEX) Resin in 3 M nitric acid over the whole irradiation range of 0-50 kGy.

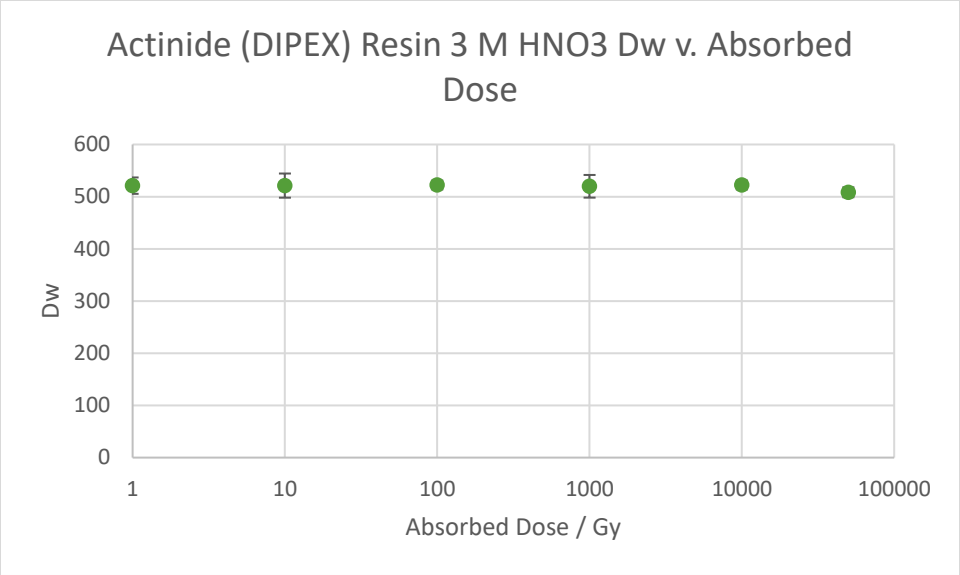

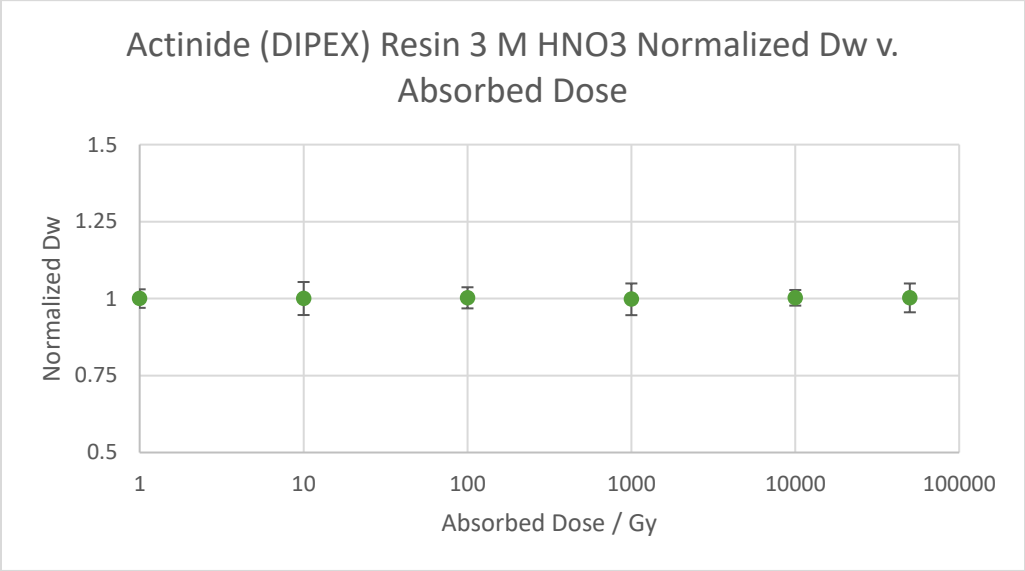

Figure 47: Contains two graphs showing the retention of plutonium-239 on Actinide (DIPEX) Resin irradiated in 3 M nitric acid. The top graph shows the experimentally determined distribution ratio (Dw) v. the absorbed dose to the EXC Resin in gray. The bottom graph shows the normalized experimentally determined distribution ratio v. the absorbed dose to the EXC Resin in gray.

The next pair of graphs (figure 48) display the retention of plutonium-239 on Actinide (DIPEX) Resin in 3 M hydrochloric acid. The literature value for the distribution ratio of plutonium on AC Resin in 3 M hydrochloric acid is 190,000 (2). There are no significant changes in the retention of

plutonium-239 on Actinide (DIPEX) Resin in 3 M hydrochloric acid over the whole irradiation range of 0-50 kGy.

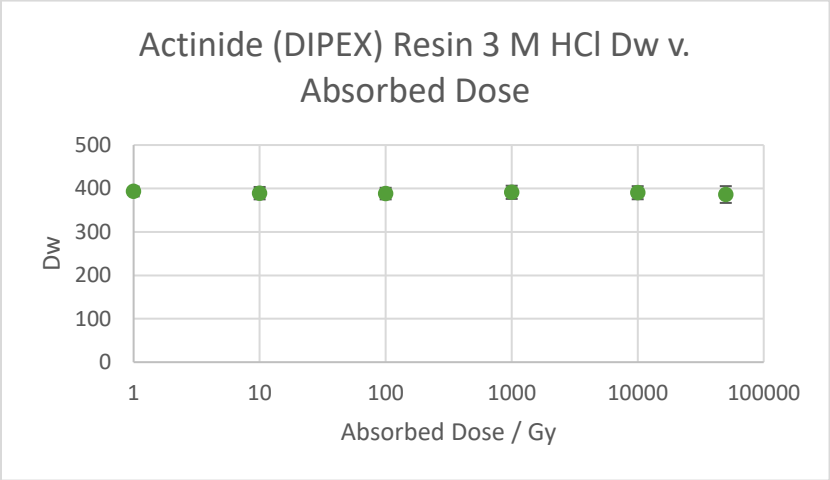

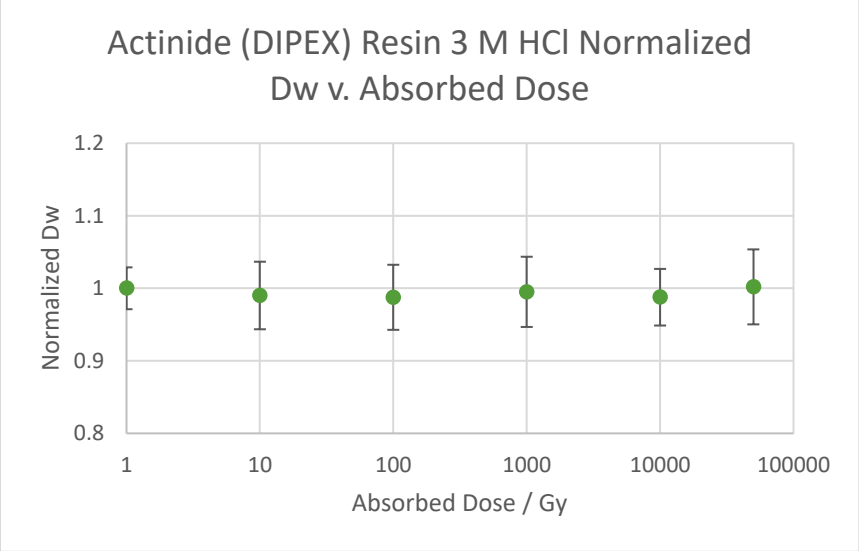

Figure 48: Contains two graphs showing the retention of plutonium-239 on Actinide (DIPEX) Resin irradiated in 3 M hydrochloric acid. The top graph shows the experimentally determined distribution ratio (Dw) v. the absorbed dose to the EXC Resin in gray. The bottom graph shows the normalized experimentally determined distribution ratio v. the absorbed dose to the EXC Resin in gray.

The next pair of graphs (figure 49) display the retention of plutonium-239 on Actinide (DIPEX) Resin in 1 M nitric acid. There are no significant changes in the retention of plutonium-239 on Actinide (DIPEX) Resin in 1 M nitric acid over the whole irradiation range of 0-50 kGy.

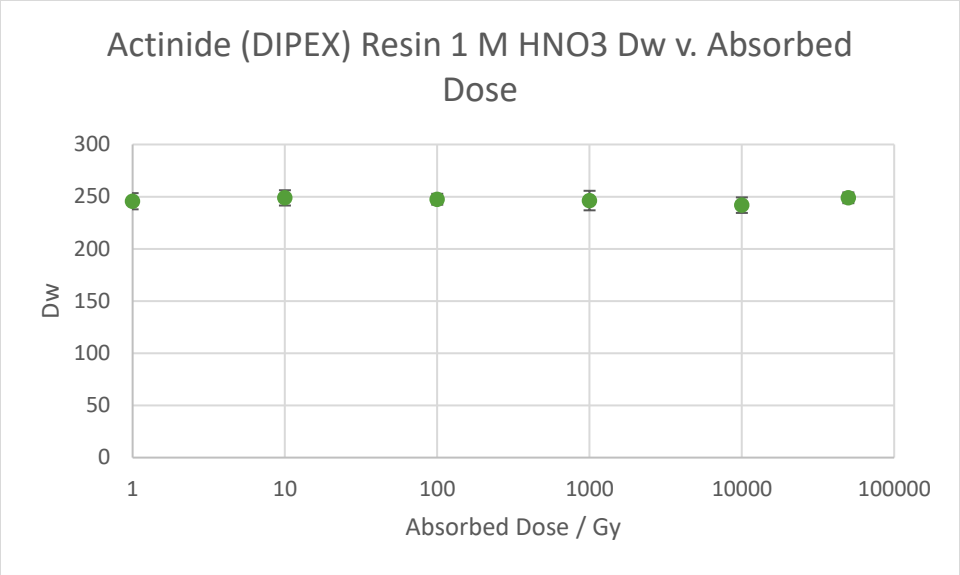

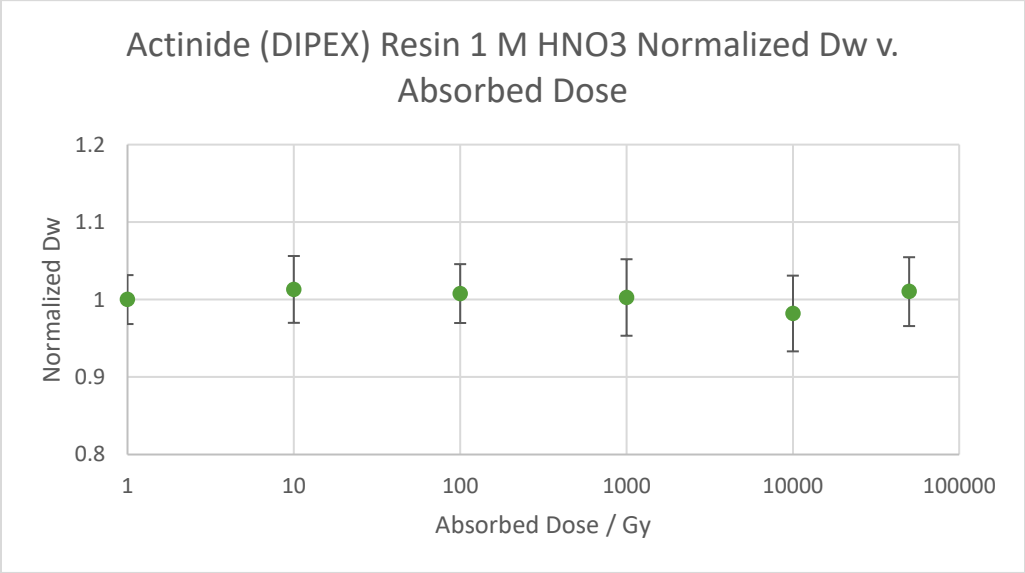

Figure 49: Contains two graphs showing the retention of plutonium-239 on Actinide (DIPEX) Resin irradiated in 1 M nitric acid. The top graph shows the experimentally determined distribution ratio (Dw) v. the absorbed dose to the EXC Resin in gray. The bottom graph shows the normalized experimentally determined distribution ratio v. the absorbed dose to the EXC Resin in gray.

Figure 50 displays the retention of plutonium-239 on Actinide (DIPEX) Resin in 1 M hydrochloric acid. The literature value of the distribution ratio for plutonium on AC Resin in 1 M hydrochloric acid is 1,520,000 (2). There are no significant changes in the retention of plutonium-239 on

Actinide (DIPEX) Resin in 1 M hydrochloric acid with the addition of 0-50 kGy of ionizing gamma radiation.

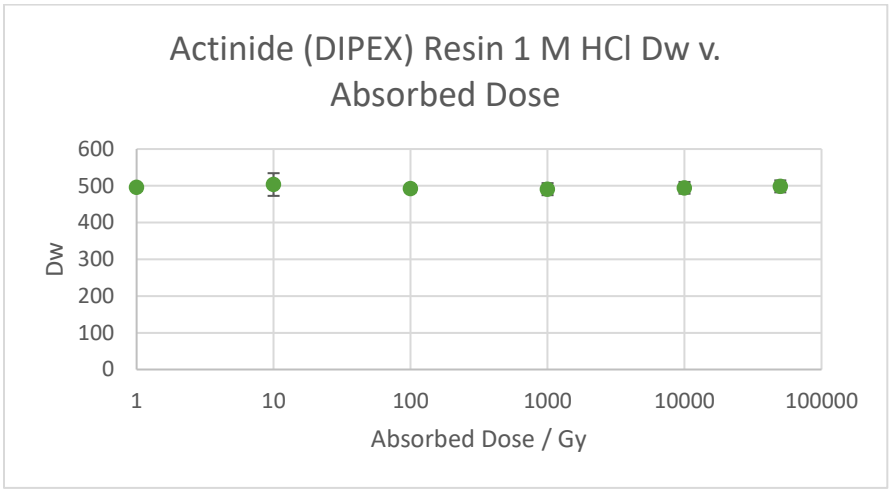

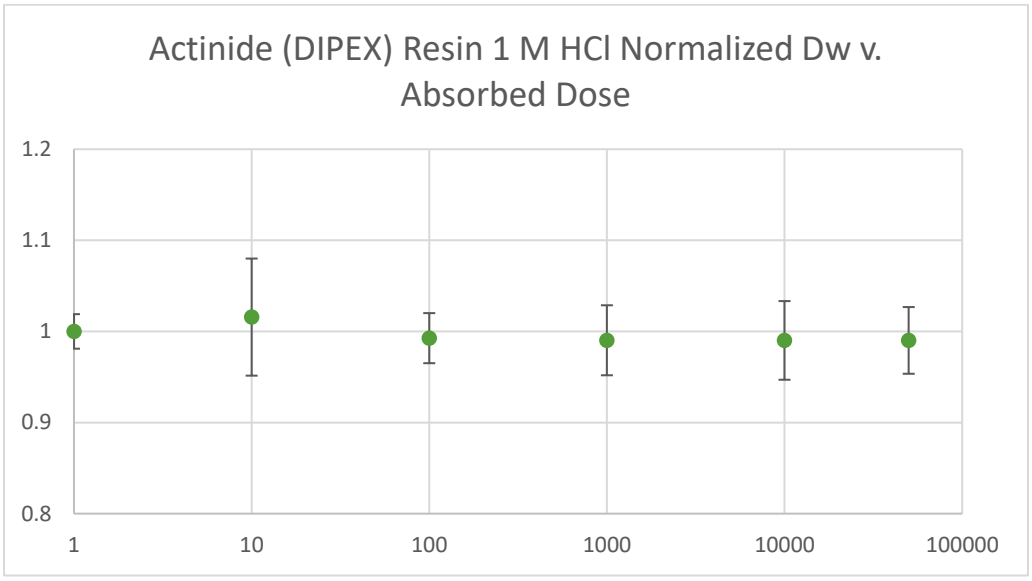

Figure 50: Contains two graphs showing the retention of plutonium-239 on Actinide (DIPEX) Resin irradiated in 1 M hydrochloric acid. The top graph shows the experimentally determined distribution ratio (Dw) v. the absorbed dose to the EXC Resin in gray. The bottom graph shows the normalized experimentally determined distribution ratio v. the absorbed dose to the EXC Resin in gray.

4.4.5: Conclusions

The two graphs shown in figure 51 display all four of the previous analyses onto common sets of axes.

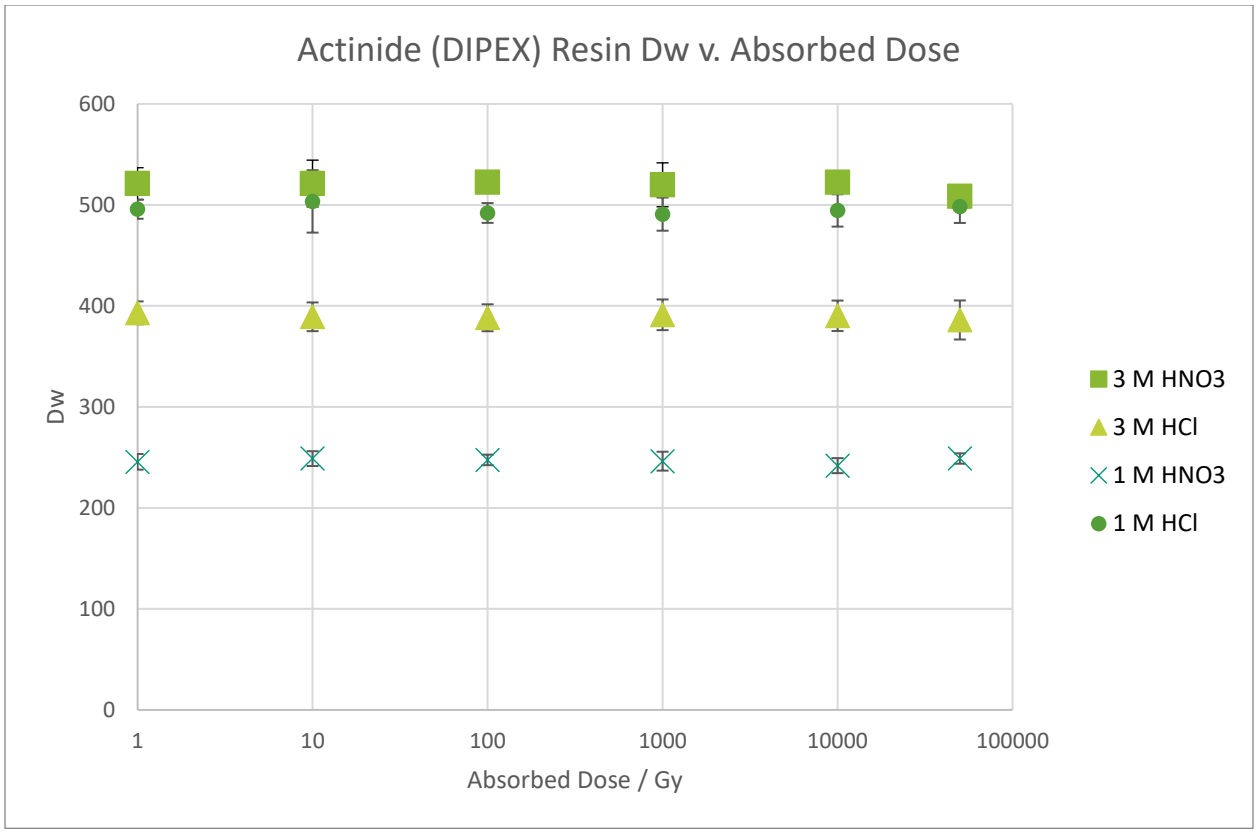

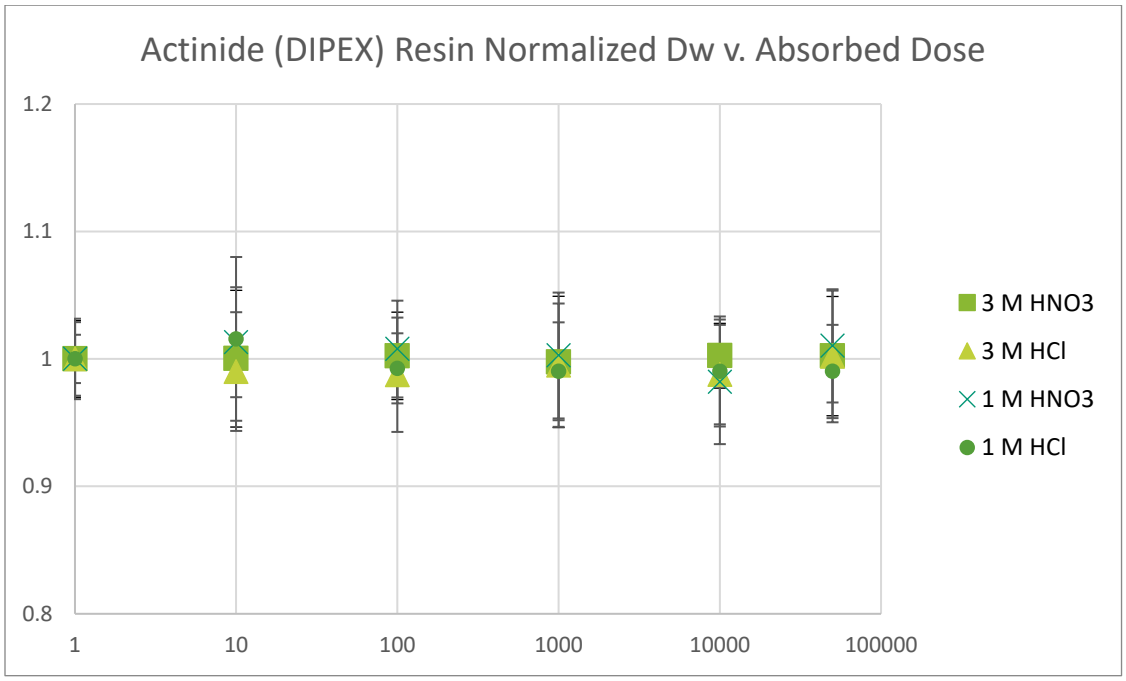

Figure 51: Figure showing two graphs showing the compiled results the retention of plutonium-239 on Actinide (DIPEX) Resin versus all the acid concentrations in this study. The top graph shows the distribution ratio versus the absorbed dose in gray, and the bottom graph shows the normalized distribution ratio versus the absorbed dose in gray.

The overall takeaway from this series of studies of the retention of plutonium-239 on Actinide (DIPEX) Resin is that the retention of plutonium is not largely impacted by 0-50 kGy of ionizing gamma radiation. This resin holds up well to radiation exposure, at least in terms of plutonium retention, up to 50 kGy. None of the acid conditions have a significant impact upon that.

4.5: Kinetics Studies

4.5.1: Introduction

The purpose of these studies is to investigate potentially confounding chemical processes that showed up in the batch-contact studies of the retention of plutonium-239 on the extraction chromatography resins described in the previous sections of this chapter. Since the anomaly most commonly presented itself in the unirradiated control group associated with the 50 kGy irradiations and those take roughly 4.5 days when only counting irradiation time, the kinetics studies were planned to examine a time frame of roughly 3 weeks. These studies were planned to identify any potentially interfering chemical reactions and to determine whether the EXC resins spending extended time in contact with the mineral acid is contributing to the experimental anomalies observed.

4.5.2: Materials and Methods

The retention of plutonium-239 on extraction chromatography resins was measured via batch-contact studies. Similar to the batch-contact studies in the rest of this chapter, these experiments (methodology shown in figure 52) also call for 50 mg (±0.5 mg) of resin contacted with 1.5 mL of the selected acid, 3 M nitric acid, 3 M hydrochloric acid, 1 M nitric acid, or 1 M hydrochloric acid, for one hour. The independent variable in these batch-contact studies is the

number of days between the acid pre-conditioning and the addition of plutonium to the solution and subsequent mixing. Experimental groups in quadruplicate were contacted with plutonium-239 at 0-, 1-, 3-, 7-, 14-, and 22-days post-acid pre-conditioning.

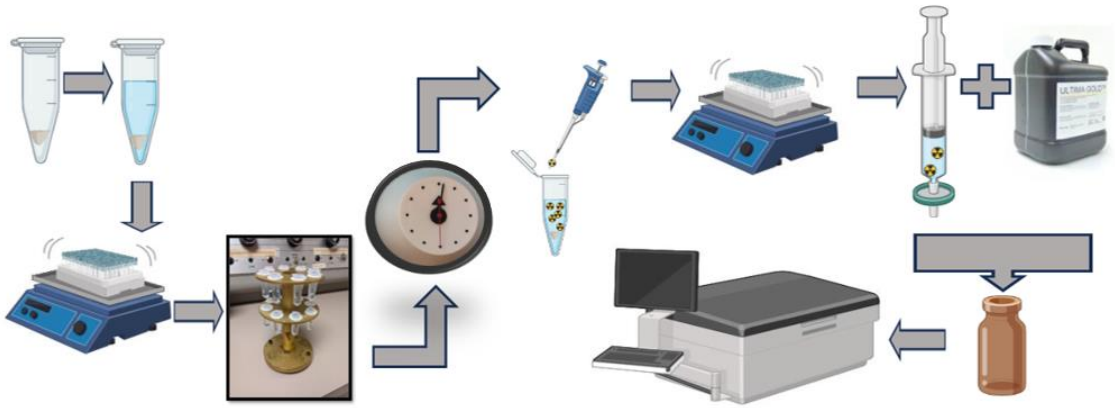

Figure 52: Pictorial representation of batch-contact studies used for contacting plutonium-239 with EXC resins with increasing time between the acid-preconditioning step and the addition of the plutonium.

After the allotted waiting time for each experimental group, 50 µL of a working solution of ~1000 Bq/mL plutonium-239 in the same acid with which the resin was pre-conditioned were added to each microcentrifuge tube. These samples were then agitated on a shaker table for one hour. Following their agitation, a 1 mL aliquot was taken from each sample and filtered through a 0.45-micron pore Luer-lock syringe filter. This aliquot was then added to a plastic scintillation vial along with 15 mL Ultima Gold scintillation cocktail. This sample was counted in a liquid scintillation counter for one hour. The initial activity added to each sample from the working solution was experimentally verified by a standard group of four standards from the same working solution that was used to spike the samples. These standards were prepared via a direct addition of 50 µL of the working solution, 950 µL of the same acid, and 15 mL Ultima Gold

cocktail. These standards were then counted with the same counting protocol on the liquid scintillation counter during the sample collection.

All four acid conditions for TRU Resin were subjected to a full kinetics study. Other resin and acid combinations were selected through an analysis of the calculated distribution ratios of their unirradiated control batches, shown in the table below. Sample conditions that were selected for kinetics studies where selected based on a large variability in the average value of the distribution ratio for the unirradiated sample batches. The decision threshold was set so that 1.) if any resin and acid condition showed a spread greater than the average of the three calculated measurements ± 115% of the standard deviation of those measurements, 2.) then that resin and acid combination would enter the kinetics study to determine whether there was a confounding effect present.

Table 14: The batch-contact studies used for contacting plutonium-239 with EXC resins to determine the impact of an extended waiting period between the acid pre-conditioning and the contacting with the plutonium-239.

resin:	TRU	resin:	TEVA	resin:	UTEVA	resin:	Actinide
acid:	3 M HNO3	acid:	3 M HNO3	acid:	3 M HNO3	acid:	3 M HNO3
associated experimental group	Dw	associated experimental group	Dw	associated experimental group	Dw	associated experimental group	Dw
10/100/1000	489.25	10/100/1000	711.85	10/100/1000	98.99	10/100/1000	521.10
10000	498.22	10000	753.67	10000	140.41	10000	521.05
50000	452.63	50000	299.30	50000	161.41	50000	507.27
average	480.03	Average	588.27	average	133.61	average	516.48
Sdev	24.15	Sdev	251.13	sdev	31.76	Sdev	7.97
range low	452.26	range low	299.47	range low	97.08	range low	507.31
range high	507.81	range high	877.08	range high	170.13	range high	525.64
resin:	TRU	resin:	TEVA	resin:	UTEVA	resin:	Actinide
acid:	3 M HCl	acid:	3 M HCl	acid:	3 M HCl	acid:	3 M HCl
associated experimental group	Dw	associated experimental group	Dw	associated experimental group	Dw	associated experimental group	Dw
10/100/1000	49.03	10/100/1000	10.70	10/100/1000	13.46	10/100/1000	393.13
10000	13.39	10000	10.59	10000	12.45	10000	395.08
50000	15.43	50000	12.62	50000	35.69	50000	385.32
average	25.95	Average	11.30	average	20.53	average	391.18
Sdev	20.01	Sdev	1.14	sdev	13.13	Sdev	5.17
range low	2.94	range low	9.99	range low	5.43	range low	385.24
range high	48.96	range high	12.61	range high	35.64	range high	397.12
resin:	TRU	resin:	TEVA	resin:	UTEVA	resin:	Actinide
acid:	1 M HNO3	acid:	1 M HNO3	acid:	1 M HNO3	acid:	1 M HNO3
associated experimental group	Dw	associated experimental group	Dw	associated experimental group	Dw	associated experimental group	Dw
10/100/1000	231.03	10/100/1000	30.51	10/100/1000	21.26	10/100/1000	245.62
10000	221.30	10000	39.95	10000	34.41	10000	246.28
50000	206.08	50000	52.97	50000	29.24	50000	246.38
average	219.47	Average	41.14	average	28.30	average	246.09
Sdev	12.57	Sdev	11.27	sdev	6.62	Sdev	0.41
range low	205.01	range low	28.18	range low	20.69	range low	245.62
range high	233.93	range high	54.11	range high	35.92	range high	246.57
resin:	TRU	resin:	TEVA	resin:	UTEVA	resin:	Actinide

acid:	1 M HNO3	acid:	1 M HNO3	acid:	1 M HNO3	acid:	1 M HNO3
associated experimental group	Dw	associated experimental group	Dw	associated experimental group	Dw	associated experimental group	Dw
10/100/1000	231.03	10/100/1000	30.51	10/100/1000	21.26	10/100/1000	245.62
10000	221.30	10000	39.95	10000	34.41	10000	246.28
50000	206.08	50000	52.97	50000	29.24	50000	246.38
average	219.47	Average	41.14	average	28.30	average	246.09
Sdev	12.57	Sdev	11.27	sdev	6.62	sdev	0.41
range low	205.01	range low	28.18	range low	20.69	range low	245.62
range high	233.93	range high	54.11	range high	35.92	range high	246.57
resin:	TRU	resin:	TEVA	resin:	UTEVA	resin:	Actinide
acid:	1 M HCl	acid:	1 M HCl	acid:	1 M HCl	acid:	1 M HCl
associated experimental group	Dw	associated experimental group	Dw	associated experimental group	Dw	associated experimental group	Dw
10/100/1000	18.44	10/100/1000	14.49	10/100/1000	10.24	10/100/1000	495.67
10000	20.68	10000	7.61	10000	8.71	10000	499.43
50000	7.56	50000	11.41	50000	13.45	50000	503.39
average	15.56	Average	11.17	average	10.80	average	499.50
Sdev	7.015	Sdev	3.44	sdev	2.42	sdev	3.86
range low	7.49	range low	7.21	range low	8.02	range low	495.06
range high	23.63	range high	15.13	range high	13.58	range high	503.94

The resin and acid condition combinations that met these criteria are highlighted in table 14. The resin and acid combinations are TRU Resin in 3 M HCl, TEVA Resin in 3 M HNO_3, UTEVA Resin in 3 M HCl, Actinide Resin in 3 M HNO_3, and Actinide Resin in 3 M HCl. Both of the selections of the actinide resin are a product of very tight groupings in the data and thus very small standard deviations; however, the 3 M hydrochloric acid condition was included in the kinetics study to ensure that there was one resin and acid combination of each resin in this study. Thus, the conditions examined in the kinetics study are TRU Resin in all four acid conditions: 3 M nitric acid, 1 M nitric acid, 3 M hydrochloric acid, and 1 M hydrochloric acid, TEVA Resin in 3 M nitric acid, UTEVA in 3 M hydrochloric acid, and Actinide Resin in 3 M hydrochloric acid.

4.5.3: Data and Calculations

The data was reduced in the same manner as the data generated in the other batch-contact studies. This batch contact experimental method is discussed in section 4.1.3. All raw count and statistical testing data is included in Appendix C.

Table 15: Table showing data for time post-acid pre-conditioning in days (0-22), computed distribution ratios, and the related calculated standard deviations for TRU Resin in 3 M nitric acid, 3 M hydrochloric acid, 1 M nitric acid, and 1 M hydrochloric acid.

TRU Resin	Dw							
days post acid preconditioning	3 M HNO3	Sdev	3 M HCl	sdev	1 M HNO3	sdev	1 m HCl	sdev
0	472.09	9.59	19.69	8.70	217.45	15.79	11.38	2.53
1	451.55	15.69	10.49	1.09	221.10	10.71	13.51	4.54
3	469.60	24.54	11.64	3.34	203.13	9.94	10.80	5.11
7	462.41	5.39	14.84	8.09	209.34	4.85	7.79	2.18
14	487.98	15.21	11.40	1.65	217.46	10.06	12.67	1.42
22	495.93	6.69	13.89	2.75	223.13	9.32	17.71	6.30

Table 16: Table showing data for time post-acid pre-conditioning in days (0-22), computed distribution ratios, and the related calculated standard deviations for TEVA Resin in 3 M nitric acid.

TEVA 3 M HNO3

days post acid preconditioning	Dw	sdev
0	380.75	12.11
1	391.65	35.86
3	444.36	16.10
7	628.20	16.34
14	626.91	62.51
22	666.71	54.25

Table 17: Table showing data for time post-acid pre-conditioning in days (0-22), computed distribution ratios, and the related calculated standard deviations for UTEVA Resin in 3 M hydrochloric acid.

UTEVA 3 M HCl

days post acid preconditioning	Dw	sdev
0	8.42	1.60
1	7.75	1.06
3	5.95	0.76
7	7.30	0.60
14	8.86	2.87
22	6.52	0.65

Table 18: Table showing data for time post-acid pre-conditioning in days (0-22), computed distribution ratios, and the related calculated standard deviations for Actinide Resin in 3 M hydrochloric acid.

AC 3 M HCl

days post acid preconditioning	Dw	sdev
0	522.96	4.98
1	509.61	7.25
3	511.02	4.77
7	769.96	32.93
14	762.49	77.64
22	792.61	23.15

4.5.4: Results and Discussion

The data gathered in section 4.5.3 is plotted and discussed in this section. Each resin and acid condition combination is plotted to show the changes in distribution ratio versus the time elapsed since the resin was pre-conditioned with the acid condition in days in figures 53-59. On each graph, the data is plotted with an uncertainty budget of two standard deviations.

The first of these graphs is shown in figure 53, indicating the distribution ratio (D_w) versus the time after the acid pre-conditioning. The time between the initial acid pre-conditioning and the addition and contacting of the plutonium varied from 0 to 22 days. The first graph of the kinetics studies shows the distribution ratio (D_w) versus the time after the acid pre-conditioning for TRU Resin in 3 M nitric acid. Overall, there is little to no statistically significant effect of an extended time between the acid pre-conditioning and the plutonium contacting on this resin and acid condition combination.

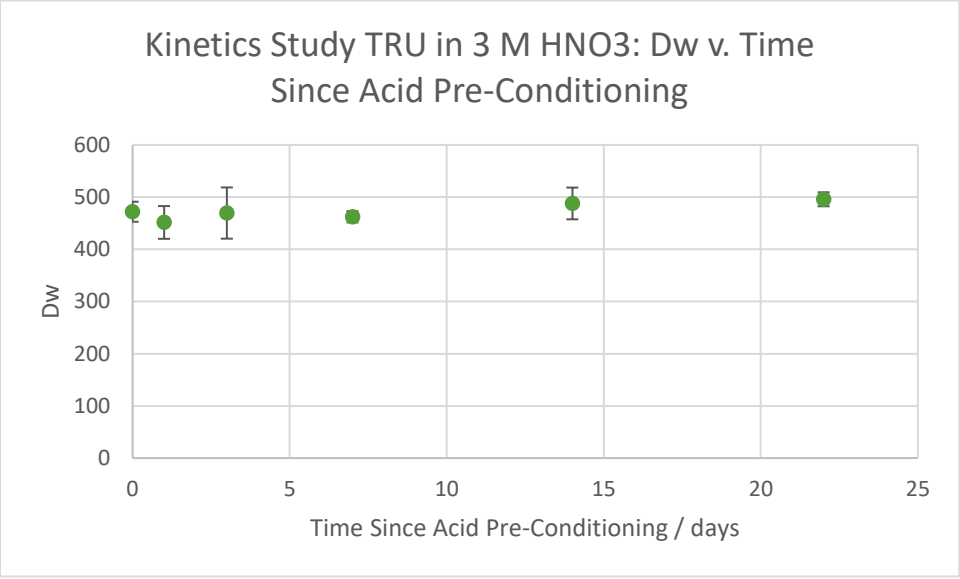

Figure 53: Graph showing the results the retention of plutonium-239 on TRU Resin in 3 M nitric acid versus the time elapsed since acid pre-conditioning in days.

The next graph (figure 54) shows the distribution ratio (D_w) versus the time after the acid pre-conditioning for TRU Resin in 1 M nitric acid. Overall, there is little to no statistically significant effect of an extended time between the acid pre-conditioning and the plutonium contacting on this resin and acid condition combination.

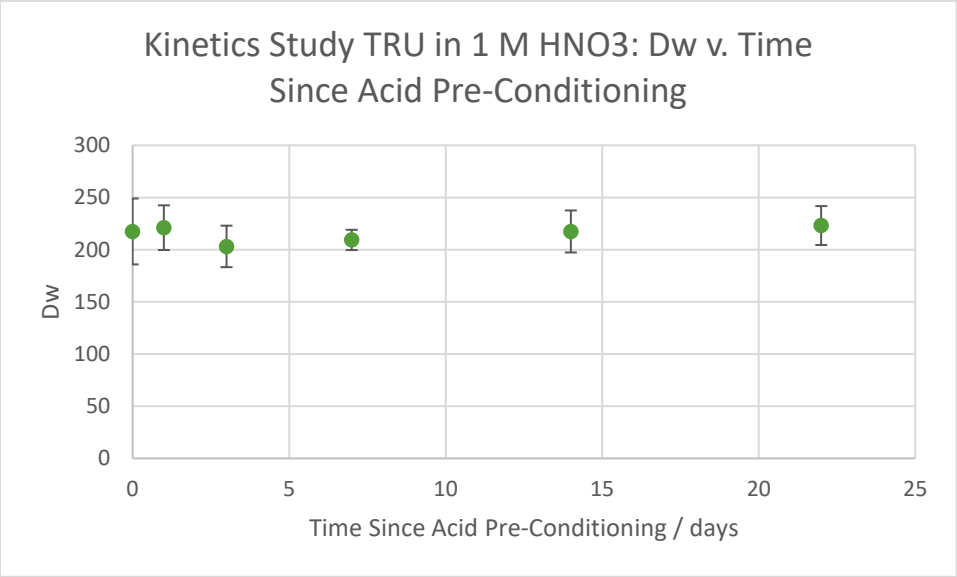

Figure 54: Graph showing the results the retention of plutonium-239 on TRU Resin in 1 M nitric acid versus the time elapsed since acid pre-conditioning in days.

Figure 55 shows the distribution ratio (D_w) versus the time after the acid pre-conditioning for TRU Resin in 3 M hydrochloric acid. Overall, there appears to be a slight decrease in distribution ratio as an effect of an extended time between the acid pre-conditioning and the plutonium contacting on this resin and acid condition combination; however, this “trend” is more likely to be an artifact resulting from the low magnitude of the distribution ratio at this combination of resin and acid concentration. The effect is also not statistically significant.

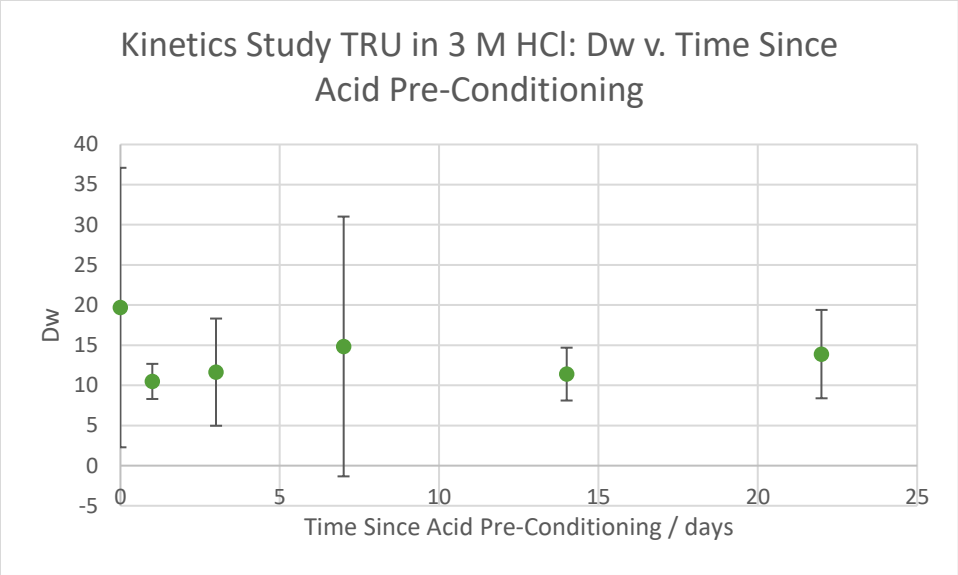

Figure 55: Graph showing the results the retention of plutonium-239 on TRU Resin in 3 M hydrochloric acid versus the time elapsed since acid pre-conditioning in days.

The next graph (figure 56) of the kinetics studies shows the distribution ratio (D_w) versus the time after the acid pre-conditioning for TRU Resin in 1 M hydrochloric acid. Overall, there is little to no effect of an extended time between the acid pre-conditioning and the plutonium contacting on this resin and acid condition combination.

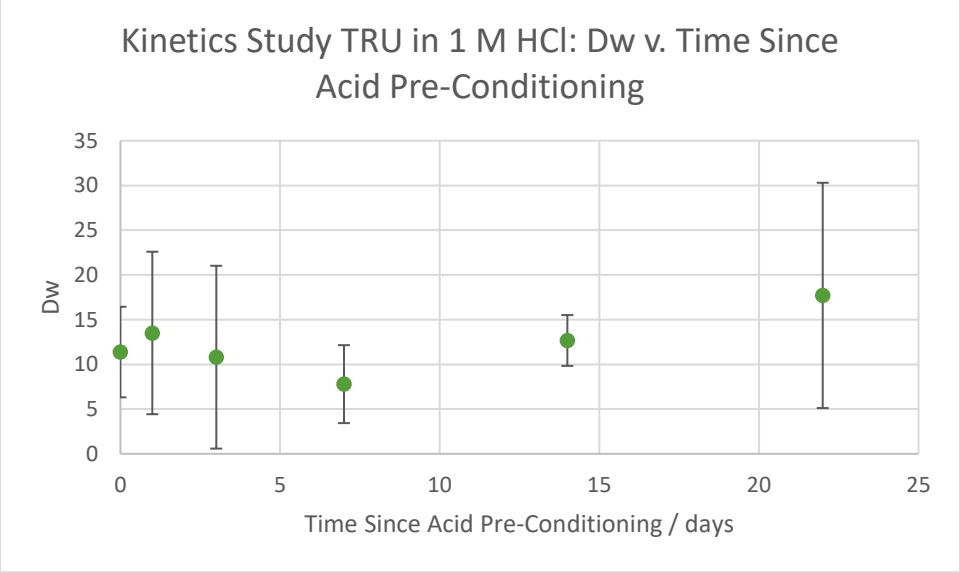

Figure 56: Graph showing the results the retention of plutonium-239 on TRU Resin in 1 M hydrochloric acid versus the time elapsed since acid pre-conditioning in days.

Figure 57 shows the distribution ratio (D_w) versus the time after the acid pre-conditioning for TEVA Resin in 3 M nitric acid. There is a significant increase in plutonium retention when more time is allowed between a one-hour acid pre-conditioning and plutonium contacting that occurs in the 1-to-7-day range. The increase remains constant after 7 days from 7 to 22 days.

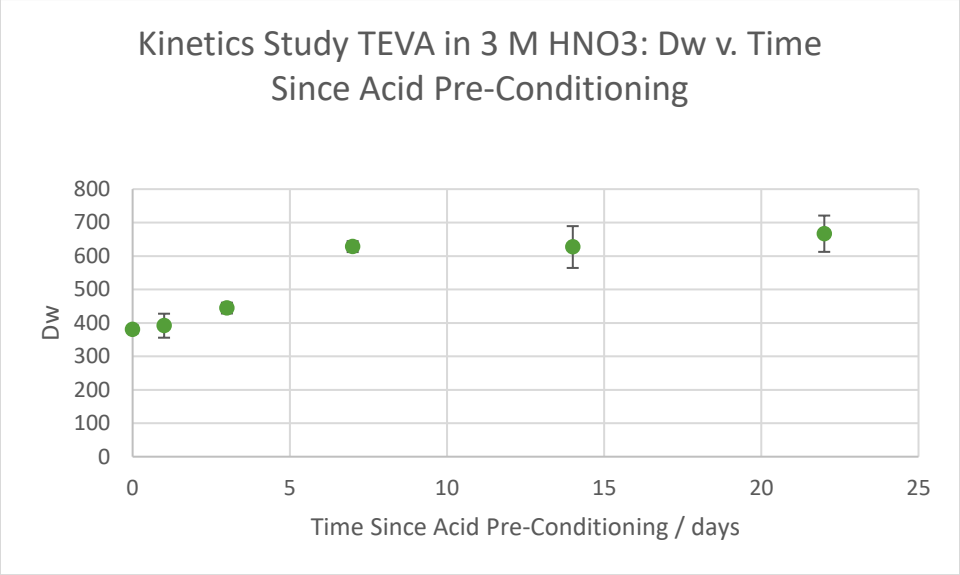

Figure 57: Graph showing the results the retention of plutonium-239 on TEVA Resin in 3 M nitric acid versus the time elapsed since acid pre-conditioning in days.

The graph in figure 58 shows the distribution ratio (D_w) versus the time after the acid pre-conditioning for UTEVA Resin in 3 M hydrochloric acid. Overall, there is perhaps a slight decrease in distribution ratio as an effect of an extended time between the acid pre-conditioning and the plutonium contacting on this resin and acid condition combination; however, this “trend” is more likely to be an artifact resulting from the low magnitude of the distribution ratio at this combination of resin and acid concentration. The effect is also not statistically significant.

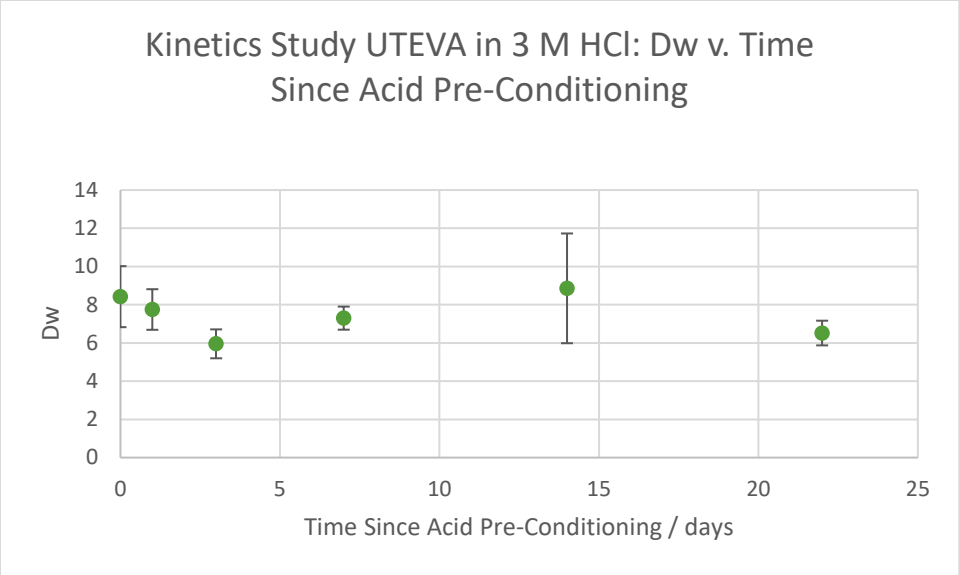

Figure 58: Graph showing the results the retention of plutonium-239 on UTEVA Resin in 3 M hydrochloric acid versus the time elapsed since acid pre-conditioning in days.

Figure 59 shows the distribution ratio (D_w) versus the time after the acid pre-conditioning for Actinide (DIPEX) Resin in 3 M hydrochloric acid. There is a significant increase in plutonium retention when more time is allowed between a one-hour acid pre-conditioning and plutonium contacting that occurs at day 7. The increase remains constant after 7 days from 7 to 22 days.

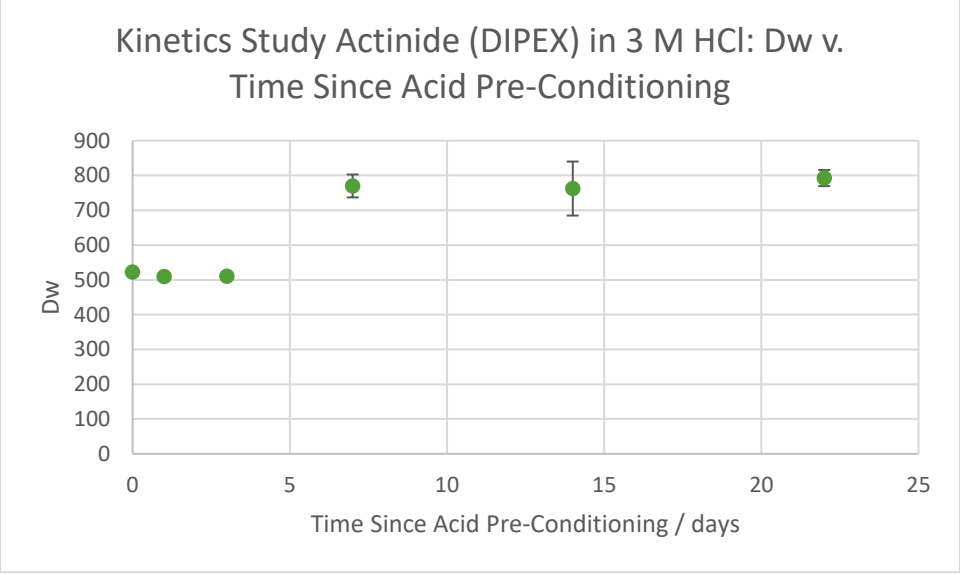

Figure 59: Graph showing the results the retention of plutonium-239 on Actinide (DIPEX) Resin in 3 M hydrochloric acid versus the time elapsed since acid pre-conditioning in days.

4.5.5: Conclusions

There is little to no statistically significant effect of extending the time between the acid pre-conditioning and the plutonium contacting for the following resin and acid condition combinations: TRU Resin in 3 M nitric acid, TRU Resin in 1 M nitric acid, TRU Resin in 3 M hydrochloric acid, TRU Resin in 1 M hydrochloric acid, and UTEVA in 3 M hydrochloric acid. There were also conditions for which a statistically significant effect was observed. TEVA Resin in 3 M nitric acid had increasing plutonium retention for the first seven days of the study and then that increased retention held constant from day 7 through day 22. Actinide (DIPEX) Resin in 3 M hydrochloric acid had an increase in plutonium retention that occurred after day 7 of the study and that then held constant from day 7 to day 22. To achieve maximum metal retention with future extraction chromatography experiments, the acid pre-conditioning step should be re-examined.

4.6: Cross-Resin Comparisons

Since this experimental work contains multiple resins and multiple acidic conditions, another comparison to be made is how different resins fare under a particular acid condition when exposed to ionizing radiation. However, since the retention of plutonium on different resins is different, sometimes by multiple orders of magnitude, these comparisons are only carried out with the distribution ratios that have been normalized to the associated experimental control group. This normalization is described and its equation listed in section 4.1.3. For the 3 M nitric acid condition, UTEVA and TEVA Resins showed the most effect across these exposure doses.

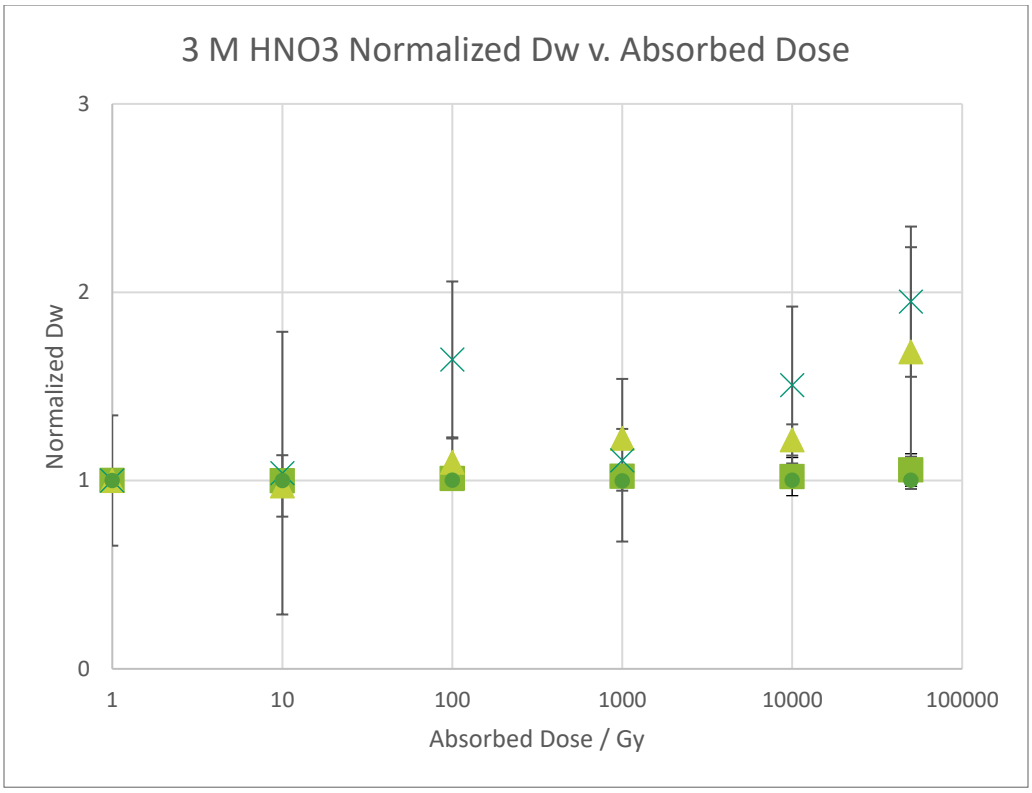

Figure 60: Figure showing the graph showing the compiled results the retention of plutonium-239, quantified as the normalized distribution ratio, on all four resins: TRU Resin, TEVA Resin, UTEVA Resin, and Actinide (DIPEX) Resin versus a single acid concentration, here 3 M nitric acid.

For the 3 M hydrochloric acid condition, TRU Resin was the only resin to show significant changes over this exposure range.

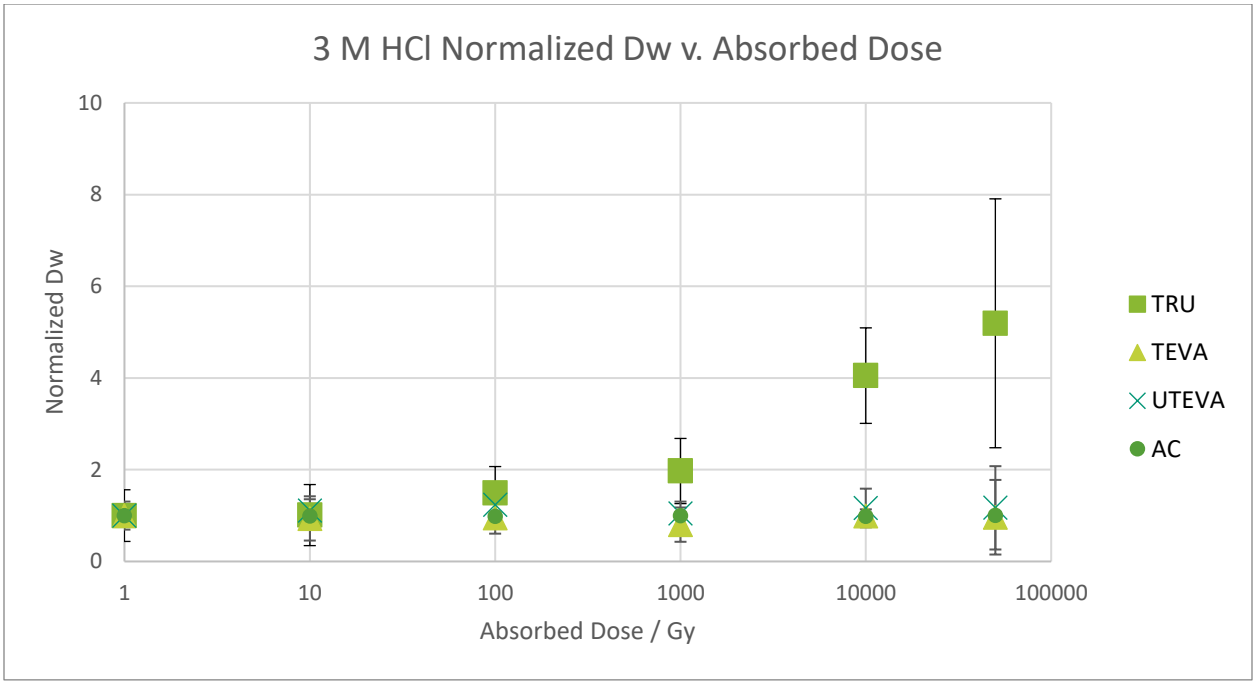

Figure 61: Figure showing the graph showing the compiled results the retention of plutonium-239, quantified as the normalized distribution ratio, on all four resins: TRU Resin, TEVA Resin, UTEVA Resin, and Actinide (DIPEX) Resin versus a single acid concentration, here 3 M hydrochloric acid.

For the 1 M nitric acid condition, TEVA Resin showed the most fluctuation across these dose ranges, followed by UTEVA Resin.

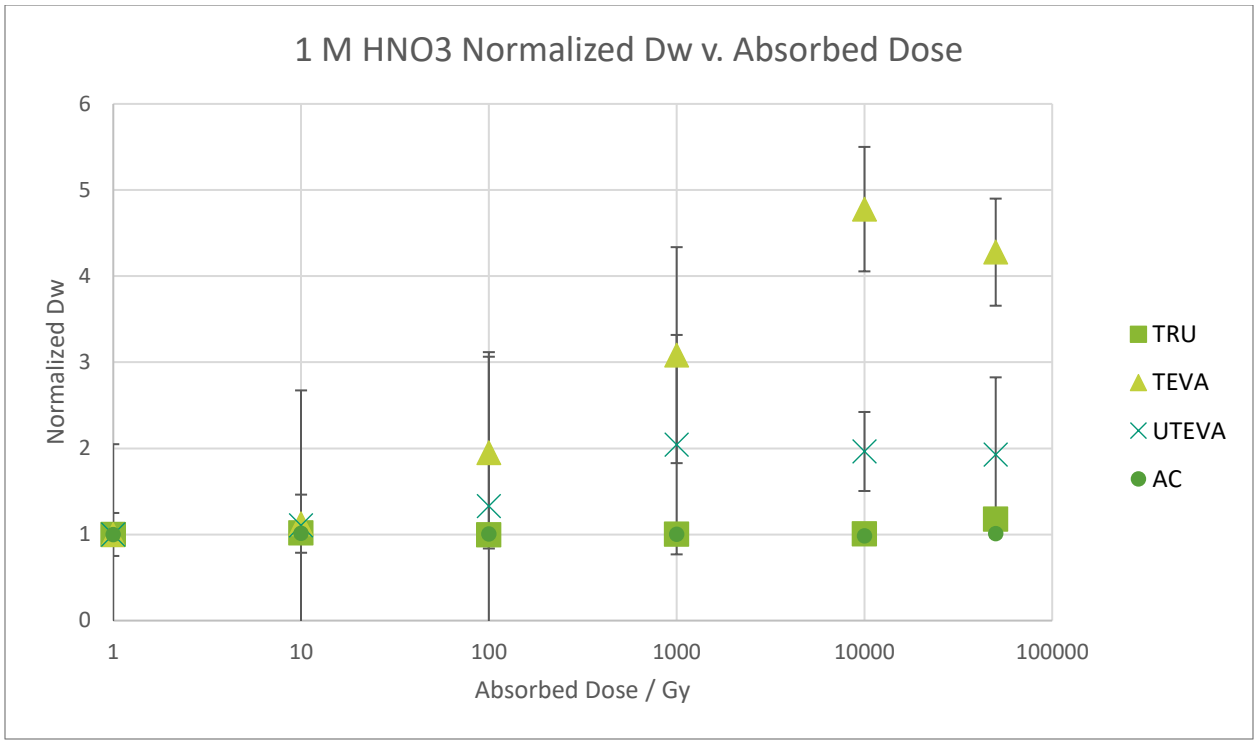

Figure 62: Figure showing the graph showing the compiled results the retention of plutonium-239, quantified as the normalized distribution ratio, on all four resins: TRU Resin, TEVA Resin, UTEVA Resin, and Actinide (DIPEX) Resin versus a single acid concentration, here 1 M nitric acid.

For the 1 M hydrochloric acid condition, the only significant deviation from the normalization point of 1 across all the resins and all the exposure doses therein was TRU Resin at the 50 kGy exposure point.

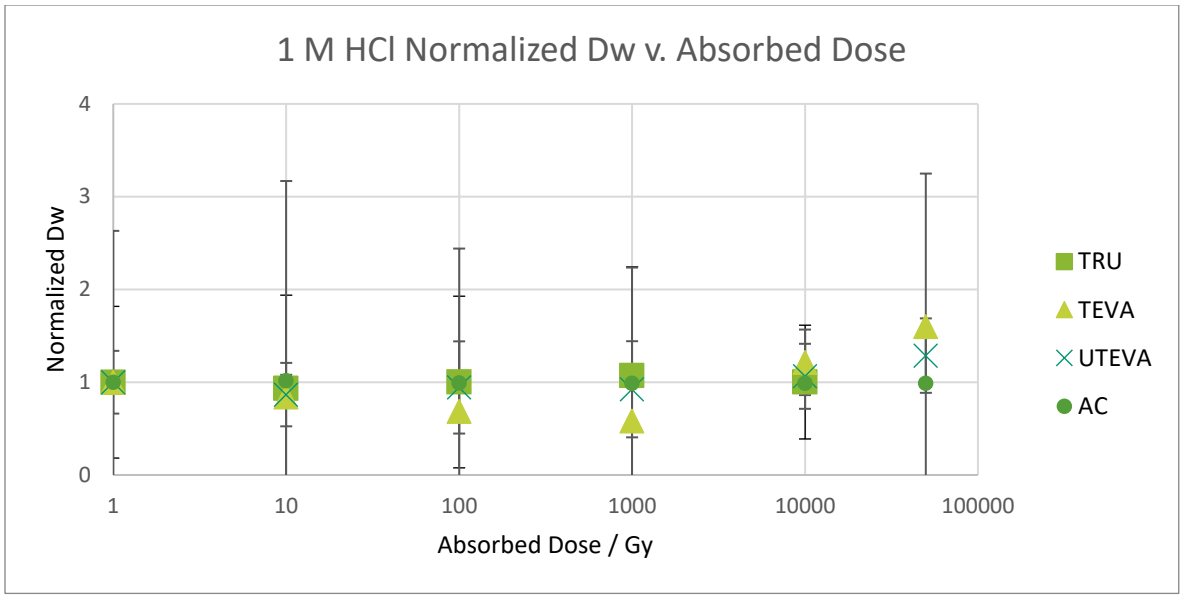

Figure 63: Figure showing the graph showing the compiled results the retention of plutonium-239, quantified as the normalized distribution ratio, on all four resins: TRU Resin, TEVA Resin, UTEVA Resin, and Actinide (DIPEX) Resin versus a single acid concentration, here 1 M hydrochloric acid.

In both nitric acid concentrations, more effects of the ionizing radiation on the retention of plutonium presented on TEVA and UTEVA Resins. In both hydrochloric acid concentrations, more effects of the ionizing radiation on the retention of plutonium presented on TRU Resin.

4.7: Conclusions and Recommendations

The disparate conclusions from across all of the parts of this study quantifying plutonium retention will be summarized here. Generally, the retention of plutonium on extraction chromatographic resins was bolstered by the resin being exposed to ionizing radiation or unchanged. This conclusion comes with caveats, however. This study is only examining the loading, or extracting, phase of extraction chromatography separations. Whether the plutonium can be stripped off the resin in the back-extraction step was not examined as part of this study. TEVA and UTEVA Resins are more impacted by ionizing radiation in nitric acid. TRU Resin is more impacted by ionizing radiation in hydrochloric acid than in nitric acid. Additionally, TRU Resin is

the only resin to show marked effects from exposure to ionizing radiation in hydrochloric acid. Actinide (DIPEX) Resin is not significantly impacted by the doses of radiation from xx Gy to XX kGy. There is an anomaly that presents in some of the experimental sets that had extended time in contact with their acid phase before plutonium contacting. TEVA Resin in 3 M nitric acid and Actinide Resin in 3 M hydrochloric acid present higher distribution ratios of plutonium, i.e., more metal is retained on the resin, than expected. The acid pre-conditioning step of the standard Sudowe batch study should be examined to determine whether anomalies present in other resins and/or acid conditions.

CHAPTER 5: FTIR ANALYSIS OF IRRADIATED RESIN

5.1: Introduction

The theoretical underpinnings of FTIR, or Fourier Transformed Infrared spectroscopy are discussed in section 2.4.

5.2: Materials and Methods

The instrument used for these analyses is a Thermo Scientific Nicolet iS50 FT-IR (serial number A4Pi200130, installed in the ARC 16 February 2013) with the ATR (Attenuated Total Reflectance) attachment (figure 64).

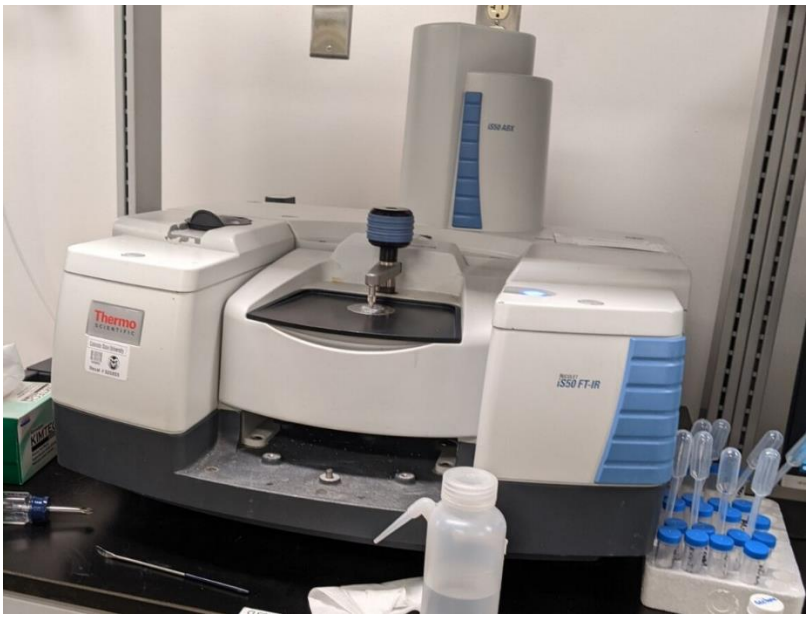

Figure 64: Thermo Scientific Nicolet iS50 FT-IR (serial no. A4Pi200130), with ATR attachment. Located in the ARC. Image acquired by Ph.D. Candidate Mueller.

Figure 65 describes the process used for each sample. Two 50 (±0.5) mg samples of each resin were weighed out and contacted with the selected mobile phase. The four possible mobile phases are different for this process than the ones selected for the plutonium retention study: 3

M nitric acid, 3 M hydrochloric acid, water, and none. After being contacted with the mobile phase, the samples were split into two groups, each containing one of each resin and the mobile phase of choice. One group was irradiated to an absorbed dose of 50 kGy, the other remained as the unirradiated control group. After irradiation, the samples were centrifuged at 3000 rotations per minute (rpm) for 30 minutes. The aqueous layer was then decanted and stored separately for analysis. A sub-sample of both the irradiated resin and the resin from the unirradiated control group was taken, ground down in a mortar with a pestle, and transferred to a new vial with acetone for storage. The sample was transferred to the ATR sample attachment in the Analytical Resources Core (ARC) at CSU and 128 scans were taken to increase the power of the data.

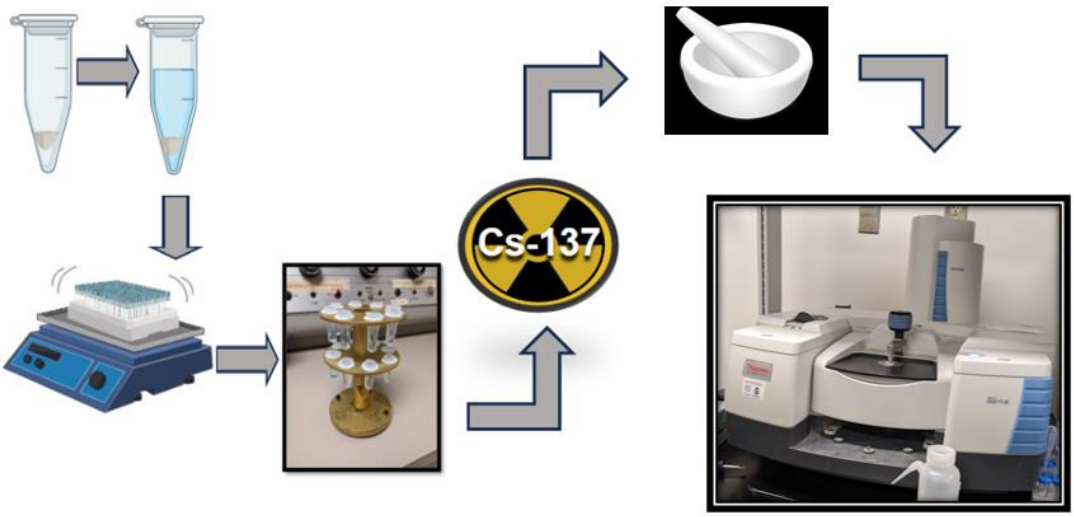

Figure 65: Pictorial representation of batch studies with the irradiation of EXC resins and FTIR analysis.

5.3: Results and Discussion

Each graph in this section contains the absorbance generated from the FTIR instrument for a sample that was irradiated with an absorbed dose of 50 kGy in a particular acid condition as

well as the associated, identically processed unirradiated control sample. A spectral feature of a peak around 2360 cm^{-1} is the result of fluctuations in the carbon dioxide microenvironment surrounding the sample in the ARC laboratory. The spectra for all four conditions: 3 M nitric acid, 3 M hydrochloric acid, water, and dry are included for TRU Resin as examples. For the three remaining resins, if a spectrum adds no new data to the analysis it is moved to Appendix D. The first spectrum (figure 66) has two samples presented on it: TRU.A and TRU.B. The TRU.A sample is the TRU Resin that was irradiated in 3 M nitric acid. The TRU.B sample is the TRU Resin that was kept back as the unirradiated control sample in 3 M nitric acid. Both are shown on the same graph to showcase their differences or, in the case of this figure, their lack of differences. Major spectral features were integrated with the regions and resulting magnitudes shown in table 19. This holds with the fact that plutonium retention was not particularly affected by the effect of ionizing radiation on TRU Resin in 3 M nitric acid.

Table 19: Integrated Peak Areas for TRU.A and TRU.B FTIR spectra.

Wavenumbers	Integration of TRU.A	Integration of TRU.B
900-975	3.70E+00	2.45E+00
975-1100	7.57E+00	4.86E+00
1100-1200	8.33E+00	5.68E+00
1300-1500	8.32E+00	6.51E+00
1600-1800	9.57E+00	6.61E+00
2250-2400	9.33E+00	1.21E+01
2800-3030	8.42E+00	9.77E+00
T.Test of Integrated Peak Areas	0.477	

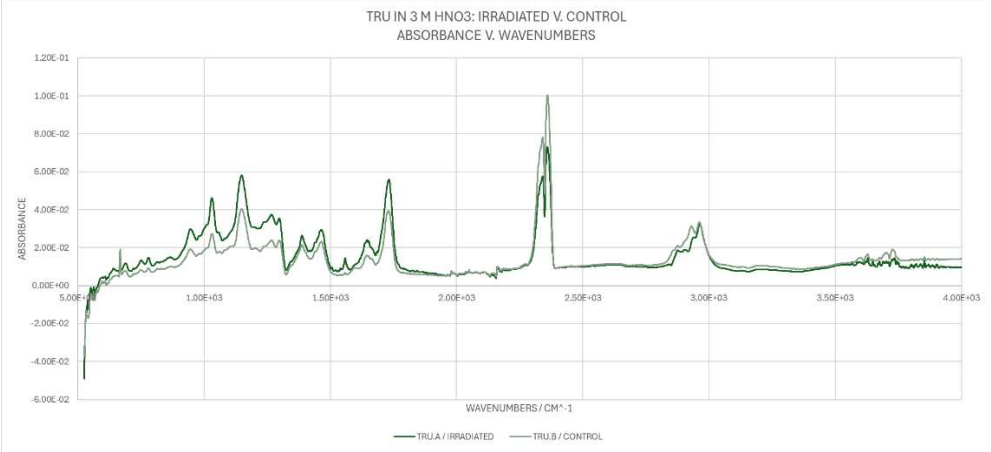

Figure 66: Graph showing FTIR absorbance for 50 kGy irradiated and unirradiated TRU Resin in 3 M nitric in absorbance versus wavenumbers.

The next spectrum shown (figure 67) has two samples presented on it: TRU.C and TRU.D. The TRU.C sample is the TRU Resin that was irradiated in 3 M hydrochloric acid. The TRU.D sample is the unirradiated control sample in 3 M hydrochloric acid. Both are shown on the same graph to display differences. In this case, the relative magnitudes of the peaks in the 1000-1500 wavenumber region are increased which may play into the increased retention of plutonium on TRU Resin in 3 M hydrochloric acid after exposure to ionizing radiation. Peaks in this region are likely to be a result of the asymmetrical C—C—O stretching, which could well happen from a stressed CMPO molecule if the carbonyl's double bonds fell prey to radiolytic damage, see the structure in section 4.1.1.1 *(3) (2)*.

Table 20: Integrated Peak Areas for TRU.C and TRU.D FTIR spectra.

Wavenumbers	Integration of TRU.C	Integration of TRU.D
900-975	5.29E+00	1.35E+00
975-1100	1.73E+01	2.87E+00
1100-1200	1.52E+01	3.10E+00
1300-1500	9.45E+00	2.35E+00
1600-1800	1.25E+01	3.11E+00
2250-2400	1.60E+01	8.93E+00
2800-3030	1.99E+01	6.78E+00
T.Test of Integrated Peak Areas	0.001	

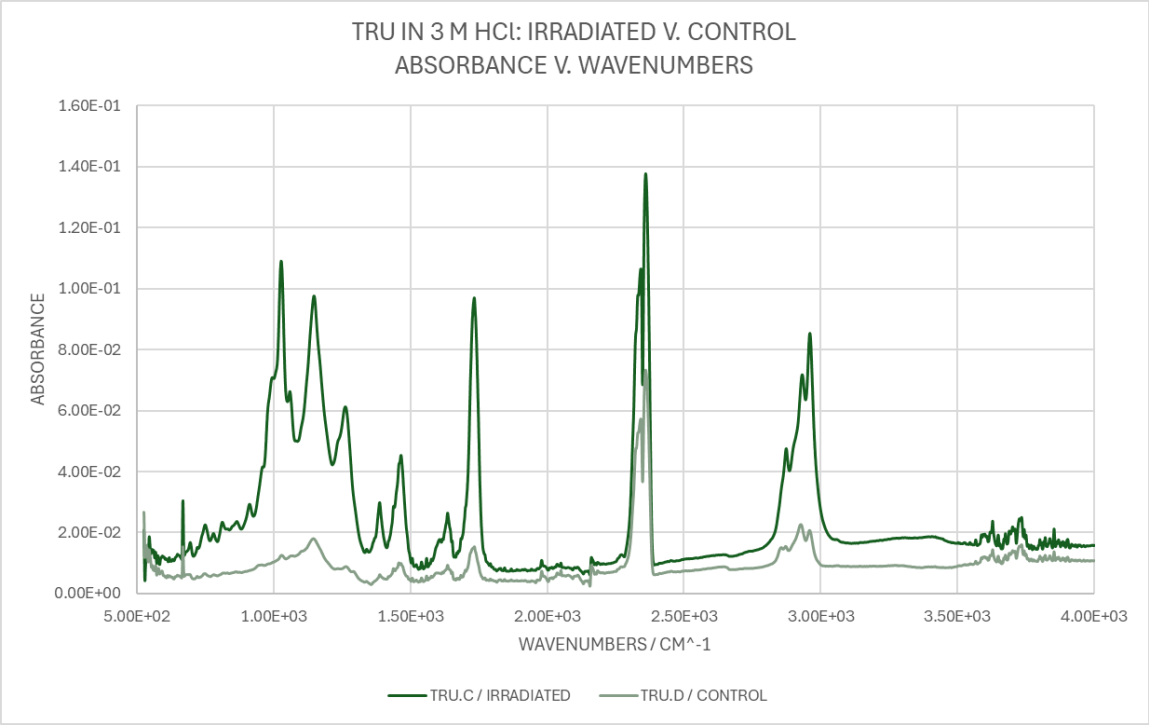

Figure 67: Graph showing FTIR absorbance for 50 kGy irradiated and unirradiated TRU Resin in 3 M hydrochloric in absorbance versus wavenumbers.

The spectrum shown in figure 68 contains two samples' spectra: TRU.I and TRU.J. The TRU.I sample was irradiated in water. The TRU.J sample is the unirradiated control sample in water. Both are shown on the same graph to showcase their differences or, in the case of this figure, their lack of differences. These two spectra are not statistically significantly different according to the t.test of their integrated peak magnitudes, shown in table 21.

Table 21: Integrated Peak Areas for TRU.I and TRU.J FTIR spectra.

wavenumbers	Integration of TRU.I	Integration of TRU.J
900-975	1.38E+01	2.29E+01
975-1100	3.18E+01	4.67E+01
1100-1200	4.21E+01	5.02E+01
1300-1500	2.38E+01	3.17E+01
1600-1800	3.38E+01	4.23E+01
2250-2400	5.51E+00	1.15E+01
2800-3030	3.81E+01	5.47E+01

T.Test of Integrated Peak Areas	0.218

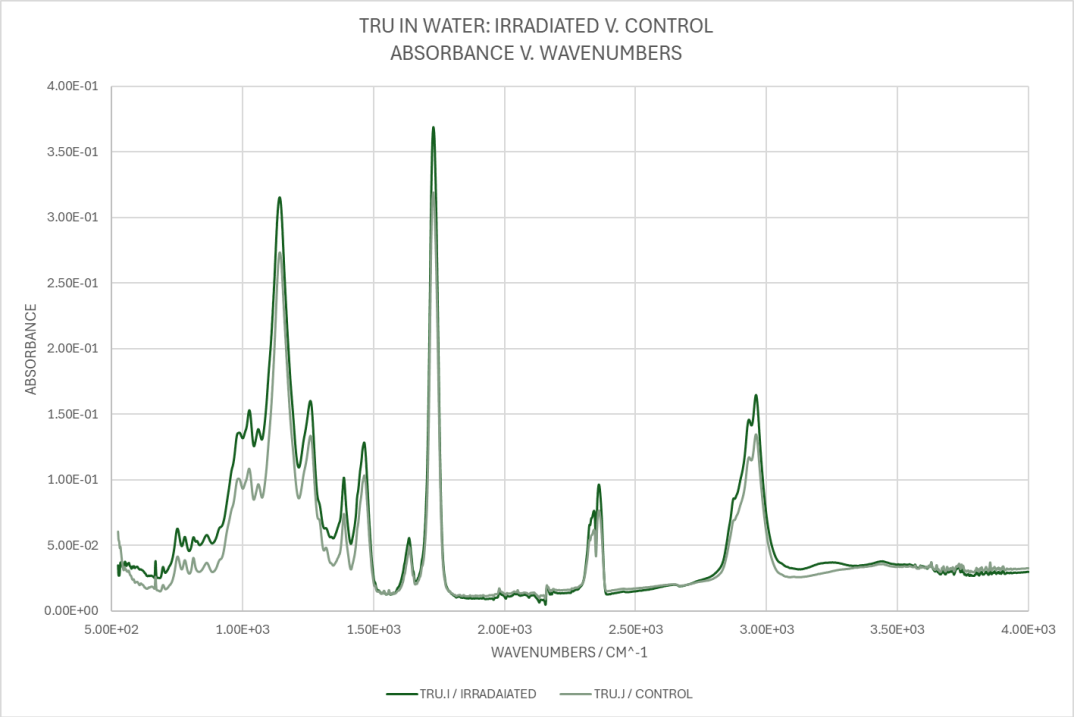

Figure 68: Graph showing FTIR absorbance for 50 kGy irradiated and unirradiated TRU Resin in water in absorbance versus wavenumbers.

The spectrum shown below has two samples presented on it: TRU.K and TRU.L. The TRU.K sample was irradiated dry. The TRU.L sample is the unirradiated control sample. Both are shown on the same graph (figure 69) to illustrate differences or, in the case of this figure, their lack of differences. These two spectra in figure 71 track well compared to each other, with the exception of the peak around 1000 cm^{-1}, which is likely some asymmetric C—C—O stretching (3).

Table 22: Integrated Peak Areas for TRU.K and TRU.L FTIR spectra.

wavenumbers	Integration of TRU.K	Integration of TRU.L
900-975	4.12E+01	3.37E+01
975-1100	7.87E+01	6.86E+01
1100-1200	6.22E+01	6.20E+01
1300-1500	4.29E+01	3.90E+01

1600-1800	5.47E+01	5.19E+01
2250-2400	2.51E+01	1.89E+01
2800-3030	9.43E+01	8.10E+01
T.Test of Integrated Peak Areas	0.614	

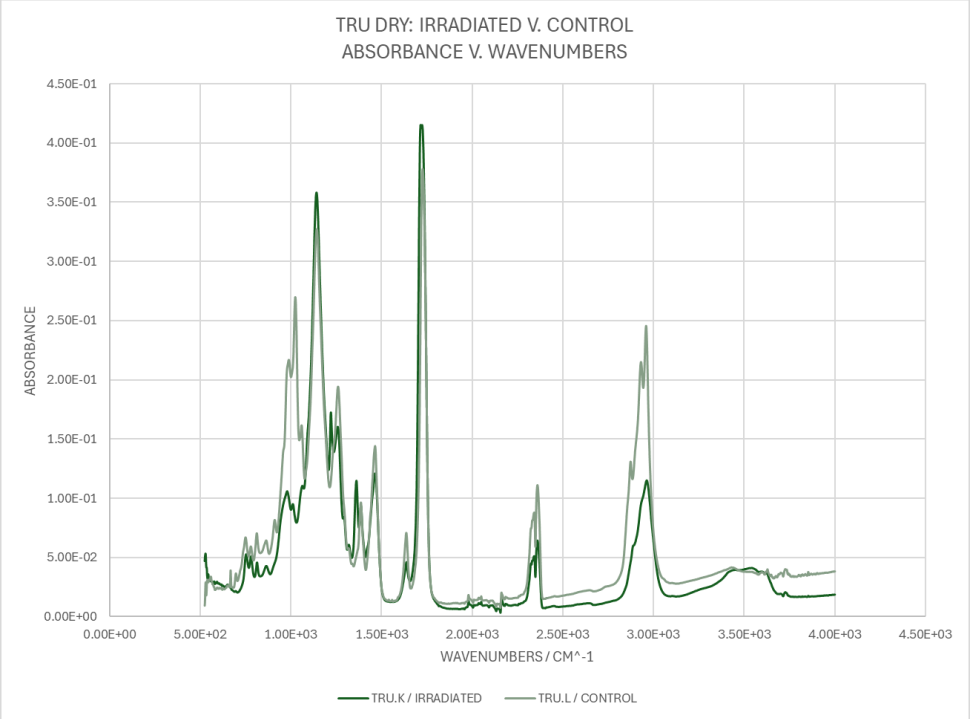

Figure 69: Graph showing FTIR absorbance for 50 kGy irradiated and unirradiated TRU Resin dry in absorbance versus wavenumbers.

The following graph (figure 70) has two samples presented on it: TEVA.A and TEVA.B. The TEVA.A sample was irradiated in 3 M nitric acid. The TEVA.B sample is the unirradiated control sample in 3 M nitric acid. Both are shown on the same graph to illustrate differences, which are primarily shown in the peaks at 1160 and 1740 cm^{-1}. The peak at 1160 cm^{-1} is likely one of the smaller peaks arising from an aliphatic amine, such as the tertiary amine that is the extractant in TEVA. The peak at 1740 cm^{-1} is likely a temporary, short-lived double bonded carbon-nitrogen pair formed as an intermediate *(3)*.

Table 23: Integrated Peak Areas for TEVA.A and TEVA.B FTIR spectra.

wavenumbers	Integration of TEVA.A	Integration of TEVA.B
1000-1250	3.88E+00	7.95E+00
1500-1800	3.95E+00	5.43E+00
2230-2400	1.18E+01	4.85E+00
2800-3000	1.19E+01	5.10E+00
T.Test of Integrated Peak Areas	0.448	

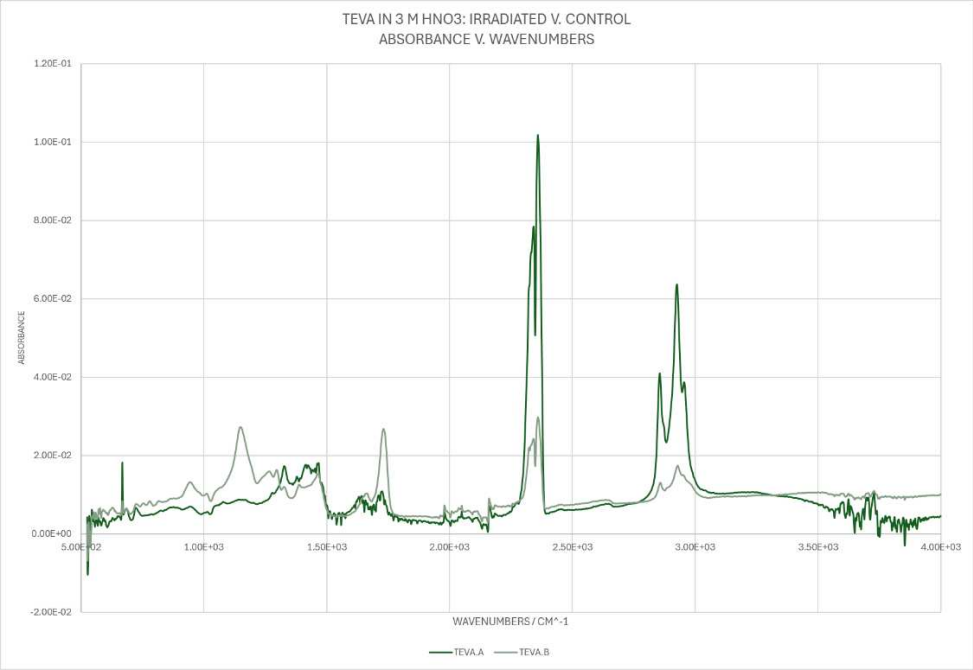

Figure 70: Graph showing FTIR absorbance for 50 kGy irradiated and unirradiated TEVA Resin in 3 M nitric in absorbance versus wavenumbers.

The following graph (figure 71) has two samples presented on it: TEVA.C and TEVA.D. The TEVA.C sample was irradiated in 3 M hydrochloric acid. The TEVA.D sample is the unirradiated control sample in 3 M hydrochloric acid. Both are shown on the same graph to illustrate differences, which are primarily shown in the magnitude of the absorbance of the control being higher. Both spectra show the same peaks at the same locations and the same or very similar ratios of peak intensities.

Table 24: Integrated Peak Areas for TEVA.C and TEVA.D FTIR spectra.

wavenumbers	Integration of TEVA.C	Integration of TEVA.D
1000-1250	6.54E+00	1.44E+01

1500-1800	3.38E+00	6.71E+00
2230-2400	1.49E+00	2.73E+00
2800-3000	6.37E+00	8.26E+00
T.Test of Integrated Peak Areas	0.251	

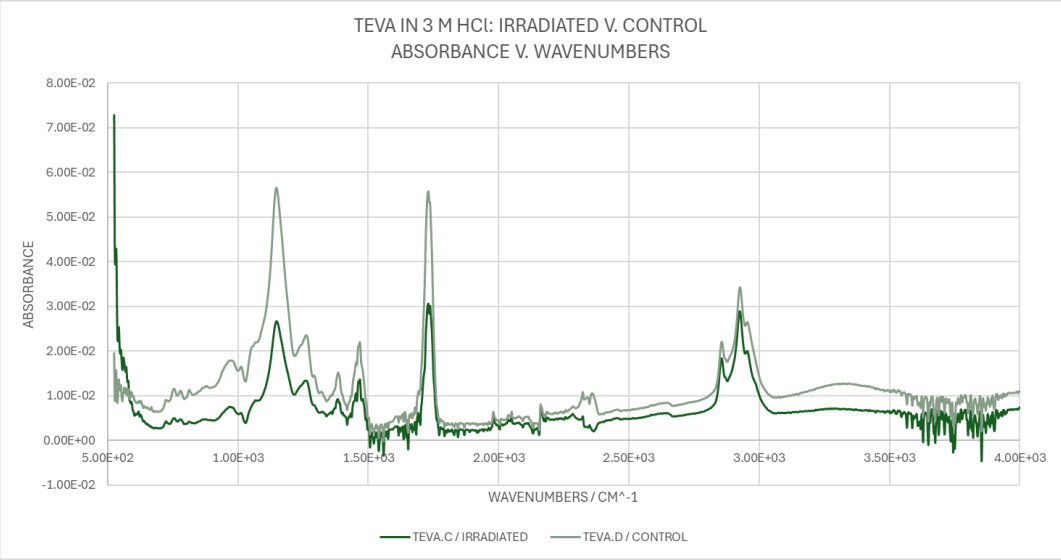

Figure 71: Graph showing FTIR absorbance for 50 kGy irradiated and unirradiated TEVA Resin in water in absorbance versus wavenumbers.

The trend shown by TEVA.I and TEVA.J, showing the changes in surface functionality of TEVA Resin irradiated in water is similar to TEVA irradiated in hydrochloric acid. The graph showing TEVA.I and TEVA.J was thus moved to Appendix D. The trend shown by TEVA.K and TEVA.L, showing the changes in surface functionality of TEVA Resin irradiated dry is similar to that shown by TEVA irradiated in hydrochloric acid. The graph showing TEVA.K and TEVA.L is in Appendix D.

The spectrum shown in figure 72 has two samples: UTEVA.A and UTEVA.B. The UTEVA.A sample was irradiated in 3 M nitric acid. The UTEVA.B sample is the unirradiated control sample in 3 M nitric acid. Both are shown on the same graph to illustrate differences with the peak at 2970 cm^{-1}. The changes seen in the 2970 cm^{-1} vicinity are likely a result of changes in the P—O—H bonds,

and the anomalous peak in the vicinity of 3420 cm^{-1} is likely a result of changing water pressure in the air during sample collection.

Table 25:Integrated Peak Areas for UTEVA.A and UTEVA.B FTIR spectra.

wavenumbers	Integration of UTEVA.A	Integration of UTEVA.B
975-1500	1.99E+01	8.38E+01
1500-1800	3.86E+00	2.58E+01
2800-3000	1.59E+00	1.95E+01
T.Test of Integrated Peak Areas	0.229	

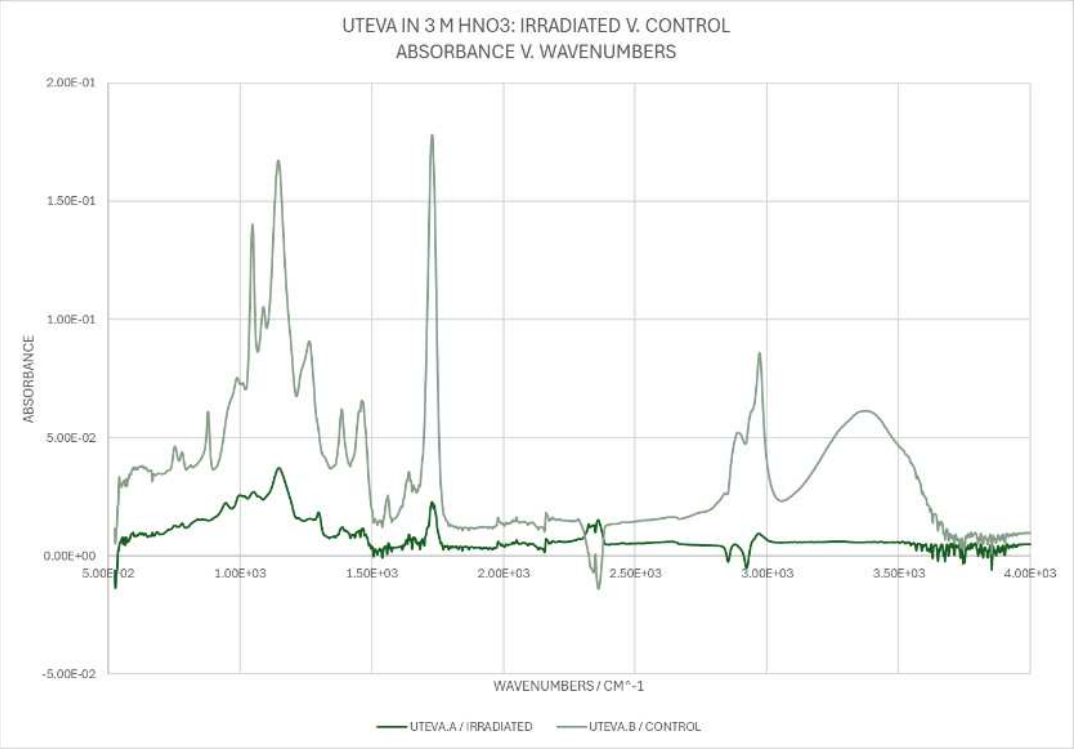

Figure 72: Graph showing FTIR absorbance for 50 kGy irradiated and unirradiated UTEVA Resin in 3 M nitric acid in absorbance versus wavenumbers.

The spectrum shown below in figure 73 has two samples presented on it: UTEVA.C and UTEVA.D. The UTEVA.C sample was irradiated in 3 M hydrochloric acid. The UTEVA.D sample is the unirradiated control sample in 3 M hydrochloric acid. Both are shown on the same graph to illustrate their differences which are generally in the magnitude of the spectra shown together

rather than any individual features. UTEVA.C and UTEVA.D spectra correlate well with the experimental data that showed a general lack of change in plutonium retention on UTEVA Resin in hydrochloric acid systems, post-irradiation.

Table 26: Integrated Peak Areas for UTEVA.C and UTEVA.D FTIR spectra.

wavenumbers	Integration of UTEVA.C	Integration of UTEVA.D
975-1500	2.74E+01	1.47E+01
1500-1800	1.02E+01	4.80E+00
2800-3000	1.10E+00	1.07E-02
T.Test of Integrated Peak Areas	0.520	

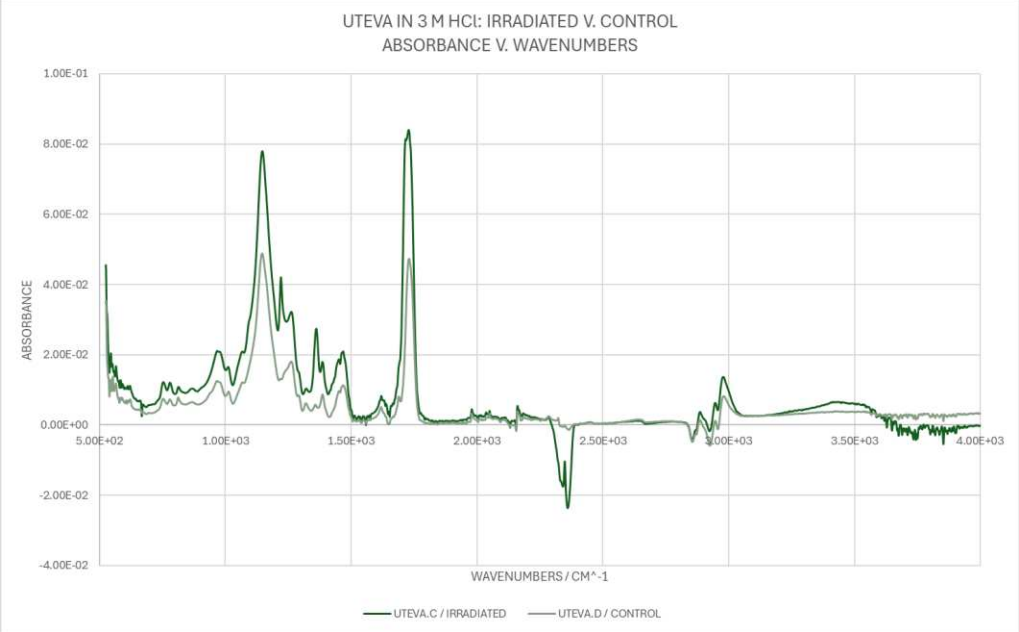

Figure 73: Graph showing FTIR absorbance for 50 kGy irradiated and unirradiated TEVA Resin in 3 M hydrochloric acid in absorbance versus wavenumbers.

The graph in figure 74 shows two samples: UTEVA.I and UTEVA.J. UTEVA.I was irradiated in water. The UTEVA.J sample is the unirradiated control sample in water. Both are shown on the same graph to illustrate their differences which are predominately in the 900-1500 wavenumber region which is likely due to changes in the asymmetric C—C—O stretching that

can be present in a stressed DAAP molecule and/or its daughter fragments where the pentyl-groups meet the phosphonate center, see section 4.2.1.1 (3) (2). The anomalous peak in the vicinity of 3420 cm^{-1} is likely a result of changing water pressure in the air during sample collection.

Table 27: Integrated Peak Areas for UTEVA.I and UTEVA.J FTIR spectra.

wavenumbers	Integration of UTEVA.I	Integration of UTEVA.J
975-1500	1.72E+02	1.53E+02
1500-1800	4.29E+01	4.84E+01
2800-3000	6.58E+01	4.83E+01
T.Test of Integrated Peak Areas	0.856	

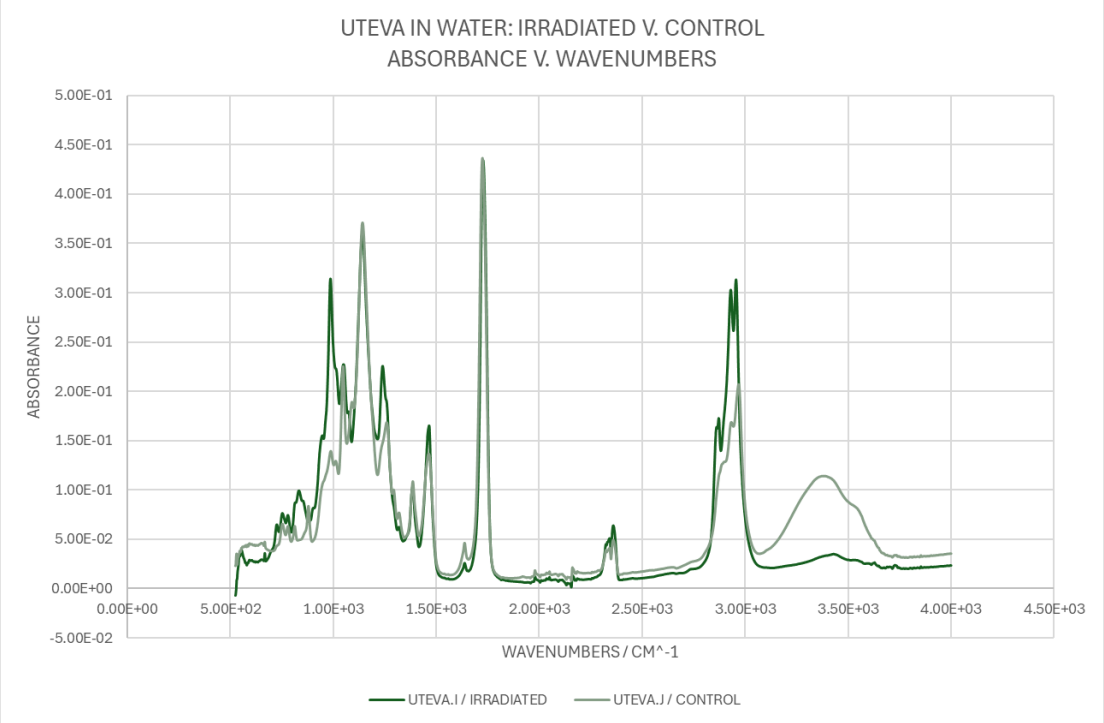

Figure 74: Graph showing FTIR absorbance for 50 kGy irradiated and unirradiated UTEVA Resin in water in absorbance versus wavenumbers.

The graph containing UTEVA.K and UTEVA.L was removed to Appendix D and is similar to the spectra of UTEVA.C and UTEVA.D in figure 73. UTEVA.K is the resin that was irradiated dry. The UTEVA.L sample is the unirradiated dry control sample. Both are shown on the same graph to

illustrate their differences which, for these samples, present only in the magnitude of their absorbance as their spectra follow near identical trends.

Figure 75 illustrates the first two samples of the Actinide (DIPEX) resin, AC.A and AC.B. The sample AC.A is the sample of the Actinide Resin that was irradiated in 3 M nitric acid. The AC.B sample is the unirradiated control sample in 3 M nitric acid. Both are shown on the same graph to showcase their differences, which are primarily shown in the peaks at 1020 and 2930 cm^{-1}. The peak at 1020 wavenumbers is likely the result of some asymmetric stretching of C—C—O bonds. The peak at 2930 cm^{-1} is likely a result of P—O—H bonds undergoing increased stretching and/or twisting as a response to the stimulus of ionizing radiation introduced to that sample (3).

Table 28: Integrated Peak Areas for AC.A and AC.B FTIR spectra.

Wavenumbers	Integration of AC.A	Integration of AC.B
900-1350	5.56E+01	2.33E+01
1350-1500	1.02E+01	3.42E+00
1650-1800	1.17E+01	5.64E+00
2800-3000	4.57E+01	3.35E+00
T.Test of Integrated Peak Areas	0.157	

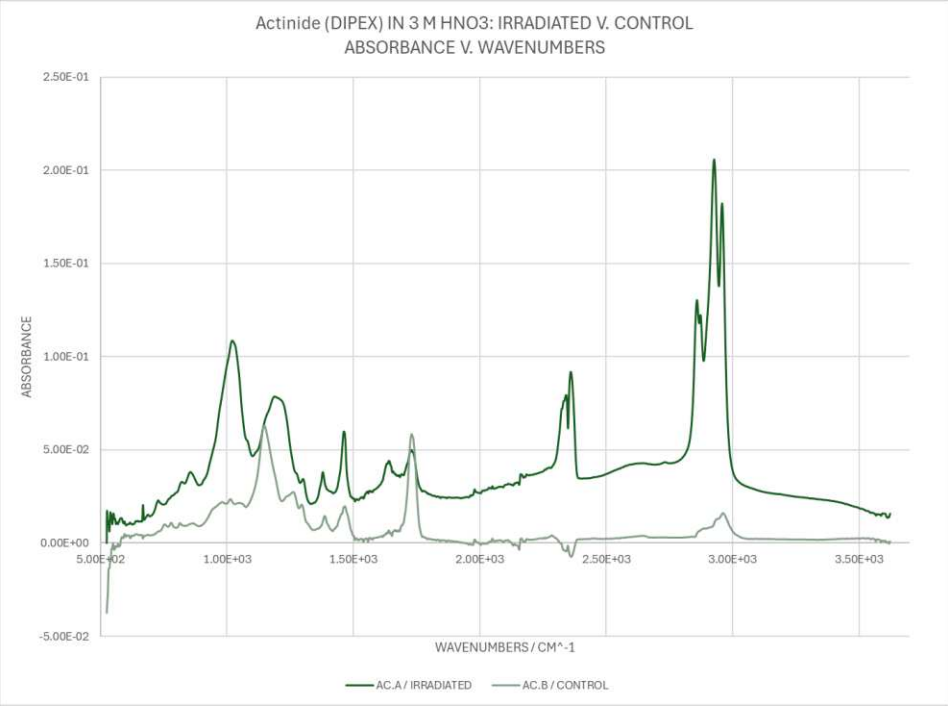

Figure 75: Graph showing FTIR absorbance for 50 kGy irradiated and unirradiated Actinide Resin in 3 M nitric acid in absorbance versus wavenumbers.

The next spectrum (figure 76) shows the first two samples of the Actinide (DIPEX) resin, AC.C and AC.D. The AC.C sample was irradiated in 3 M hydrochloric acid. The AC.C sample is the unirradiated control sample in 3 M hydrochloric acid. Both are shown on the same graph to showcase their differences or, as in the case of this graph, their lack of differences. The only difference between the two illustrated spectra, other than a slight difference in magnitude between the two, is at 2630 wavenumbers which generally denotes the presence of carbon dioxide in the microenvironment surrounding the sample.

Table 29: Integrated Peak Areas for AC.C and AC.D FTIR spectra.

Wavenumbers	Integration of AC.C	Integration of AC.D
900-1350	2.84E+01	2.36E+01
1350-1500	4.08E+00	3.32E+00
1650-1800	7.02E+00	5.49E+00
2800-3000	6.42E+00	5.26E+00
T.Test of Integrated Peak Areas	0.791	

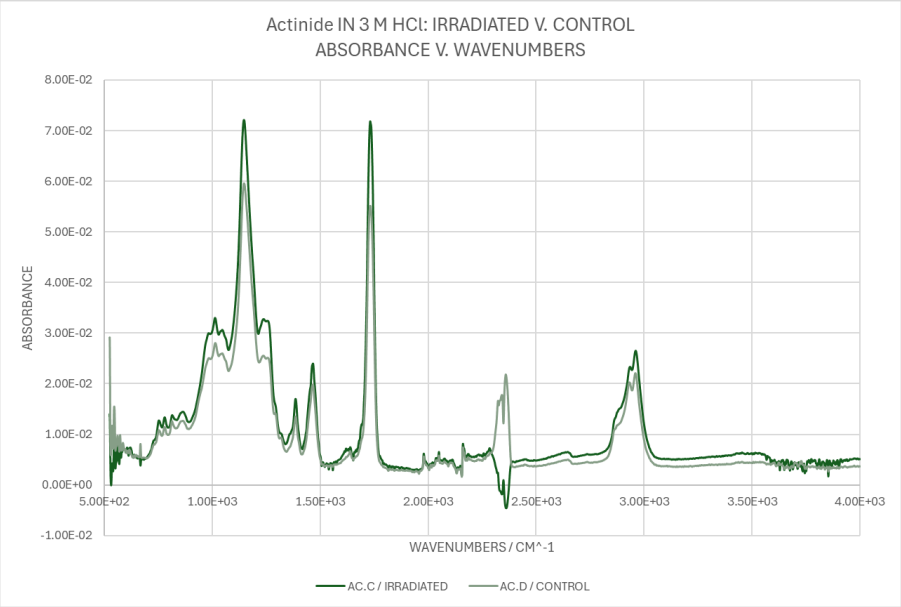

Figure 76: Graph showing FTIR absorbance for 50 kGy irradiated and unirradiated Actinide Resin in 3 M hydrochloric acid in absorbance versus wavenumbers.

The spectrum showing samples AC.I and AC.J is similar to figure 78 and is in Appendix D. Figure 77 is of samples AC.K and AC.L FTIR. The AC.K sample was irradiated dry. The AC.L sample is the unirradiated dry control sample. Both are shown on the same graph to showcase their differences which primarily appear in some peak magnitude enhancement of those peaks in the 900-1300 and the 2700-2900 wavenumber regions, compared to the peak at 1730 cm^{-1} in the irradiated sample which is likely a result of some enhanced detection of the P—C and P—O—H bonds *(3)*.

Table 30: Integrated Peak Areas for AC.K and AC.L FTIR spectra.

Wavenumbers	Integration of AC.K	Integration of AC.L
900-1350	2.33E+02	2.11E+02
1350-1500	3.41E+01	3.12E+01
1650-1800	4.63E+01	4.51E+01
2800-3000	8.88E+01	7.63E+01
T.Test of Integrated Peak Areas	0.880	

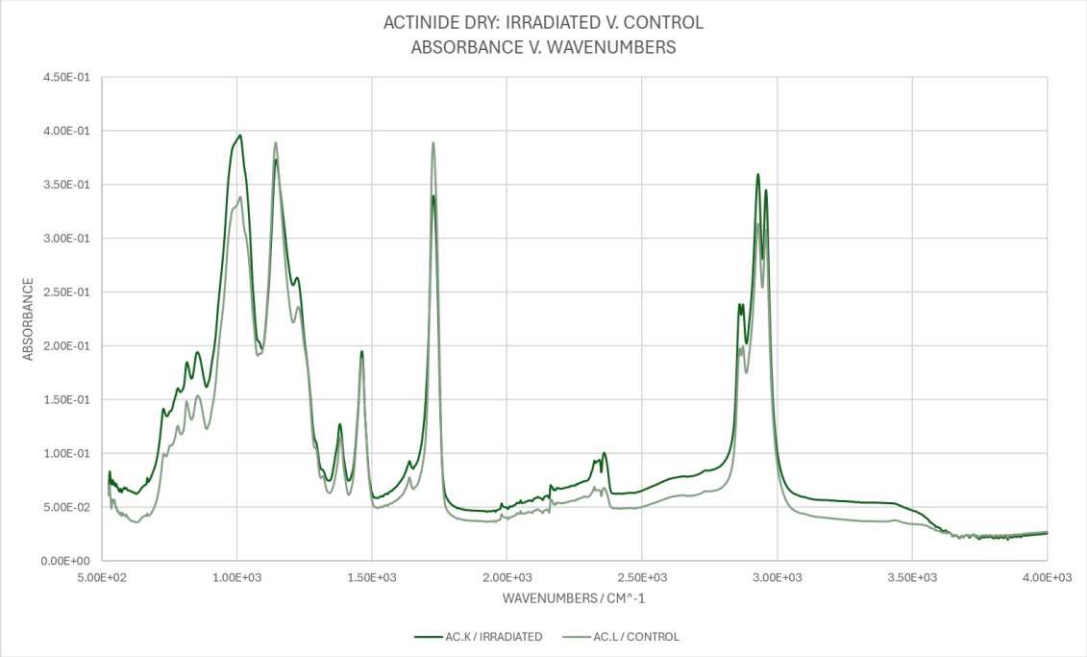

Figure 77: Graph showing FTIR absorbance for 50 kGy irradiated and unirradiated Actinide Resin dry in absorbance versus wavenumbers.

5.4: Conclusions

Overall, the surface functionality of the extraction chromatography resins is mostly unchanged after being irradiated with an absorbed gamma irradiation dose of 50 kGy. The conclusions are summarized in the table below.

Table 31: Summary table of observed changes in FTIR observations of irradiated EXC resins.

identification	Wavenumber / cm^{-1}	Interaction
Background	2630	carbon dioxide
Background	3420	water pressure
TRU: 3 M HCl	1000-1500	C—C—O asymmetric stretching
TRU: dry	1000-1500	C—C—O asymmetric stretching
TEVA: 3 M HNO3	1160	aliphatic amine, some lost in the irradiated sample
TEVA: 3 M HNO3	1740	short lived C==N
UTEVA: 3 M HNO3	2970	P—O—H asymmetric stretching
UTEVA: water	900-1500	C—C—O asymmetric stretching
AC: 3 M HNO3	1020	C—C—O asymmetric stretching
AC: 3 M HNO3	2930	P—O—H asymmetric stretching
AC: 3 M HCl	900-1300	C—P—O asymmetric stretching
AC: 3 M HCl	2700-2900	P—O—H asymmetric stretching

CHAPTER 6: DEVELOPMENT OF METHOD FOR USING MALDI TO ANALYZE EXTRACTION CHROMATOGRAPHY RESINS

6.1: Introduction and Theory

The goals of using extraction chromatography resins are discussed at length in sections 2.1.1, 2.1.2, and 2.2.1. Mass spectrometry, MALDI, and TOF systems are discussed in section 2.5. The focus of this chapter is to determine the utility of a MALDI-TOF-MS for the analysis of extraction chromatography materials and, should its utility be deemed sufficient, to develop a method for such an analysis.

6.2: Materials and Methods

The primary instrument used for this study is the Bruker UltraFlextreme (Bruker Corporation, UltraFlextreme MALDI-TOF, Billerica, MA) shown in figure 78. This instrument resides in the Analytical Resources Core (the ARC) in the basement of Colorado State University's chemistry building.

Figure 78: Bruker UltraFlextreme MALDI-TOF-MS. Located in the ARC. Image acquired by Ph.D. Candidate Mueller.

Solubility studies were completed to determine whether the resin beads could be dissolved in their entirety, using solvents commonly used for polymeric chemistry analyses such as chloroform and tetrahydrofuran. No solvent under gently heating or extended exposure was able to fully dissolve the resin beads. Thus, the focus was shifted to introducing the resin in its full bead form to the mass spectrometer as the target analyte material. A suspension of red phosphorus in methanol was used as the calibrant, given the relatively low mass range—for MALDI purposes—being investigated here (24).

Fifty mg of the resin was shaken in contact with 1.5 mL of the mineral acid and concentration of choice for one hour, and then a 20-microliter aliquot containing suspended solids was pipetted on to the stainless-steel target plates for introduction to the MALDI's high vacuum. Both positive and negative high voltage systems were investigated for optimal mass spectrum generation. The mass spectrometer's linear mode was used primarily in initial studies to determine required laser power and gain settings for that sample. The mass spectrometer's reflector mode was generally used to generate the cleaner, less messy spectra with decreased background that were gathered. The spectra were generated and processed using Bruker's flexControl and flexAnalysis software (flexAnalysis version 3.4, copyright Bruker Daltonik GmbH).

6.3: Results and Discussion

A suspension of red phosphorus clusters in methanol was used as the calibrant for these MALDI experiments. The spectra of the calibrant in each disparate processing condition are shown in figure 79.

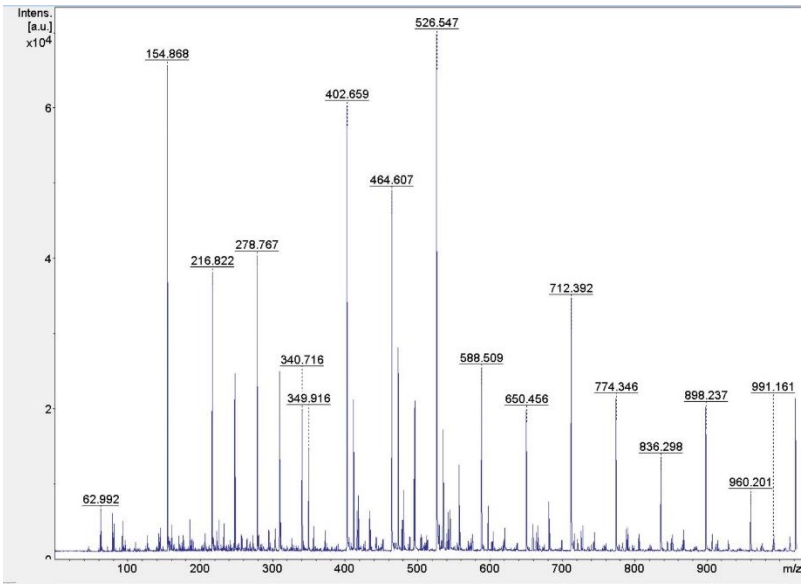
Intens.
[a.u.]
x10^4
526.547
154.868
402.659
464.607
278.767
216.822
712.392
340.716
588.509
774.346
898.237
991.161
650.456
349.916
836.298
960.201
62.992
m/z

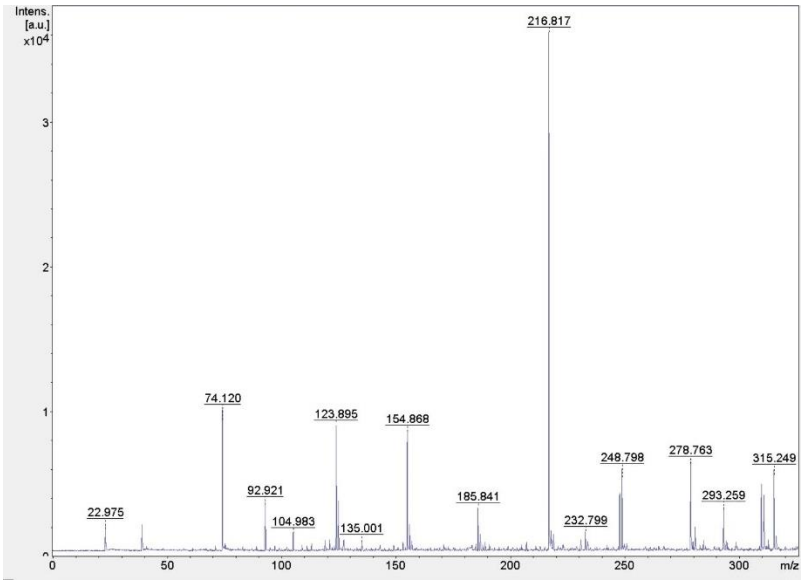
Intens.
[a.u.]
x10^4
216.817
74.120
123.895
154.868
248.798
278.763
315.249
92.921
185.841
293.259
22.975
104.983
135.001
232.799
m/z

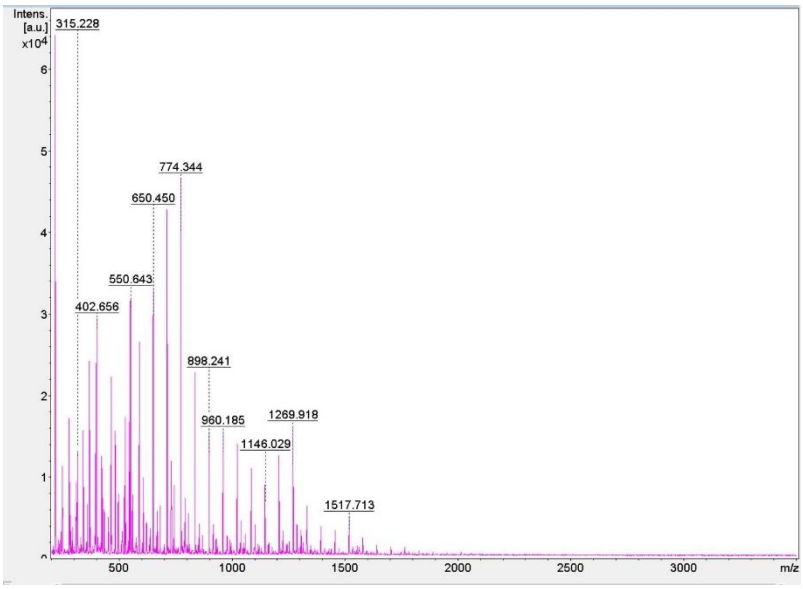

Figure 79: Figure containing three mass spectra of red phosphorus clusters suspended in methanol analyzed using MALDI-TOF-MS, plotted as m/z or mass-to-charge ratio versus intensity. The first graph is for the mass spectrometer with negative high voltage applied, the middle graph illustrates the same region with positive high voltage applied, and the last graph examines a wider mass range using the positive high voltage.

The extractants on the TRU Resin are discussed at length, including chemical structures, in section 4.1.1. The required knowledge of these extractants necessary to determine whether the MALDI can analyze TRU Resin as an extraction chromatography resin is their respective molecular weights: for CMPO—407.6 g/mol and for TBP—266.3 g/mol. Spectra were collected in four solution conditions 1: water, 2: 3 M nitric acid, 3: 3 M hydrochloric acid, and 4: dry. Figure 80 contains the spectra generated for TRU Resin in water. A peak that is likely a protonated form of TBP can be seen at 269 m/z in both reflector negative and positive modes. The peak that is likely a protonated form of CMPO is present at 408 m/z in the reflector positive mode. The peaks at 444 and 446 m/z are likely protonated CMPO molecules complexed with two water molecules. Peaks at 368, 396, and 424 m/z are likely related to the inert support and

are present to some extent in MALDI spectra generated for all four of the extraction chromatographic resins.

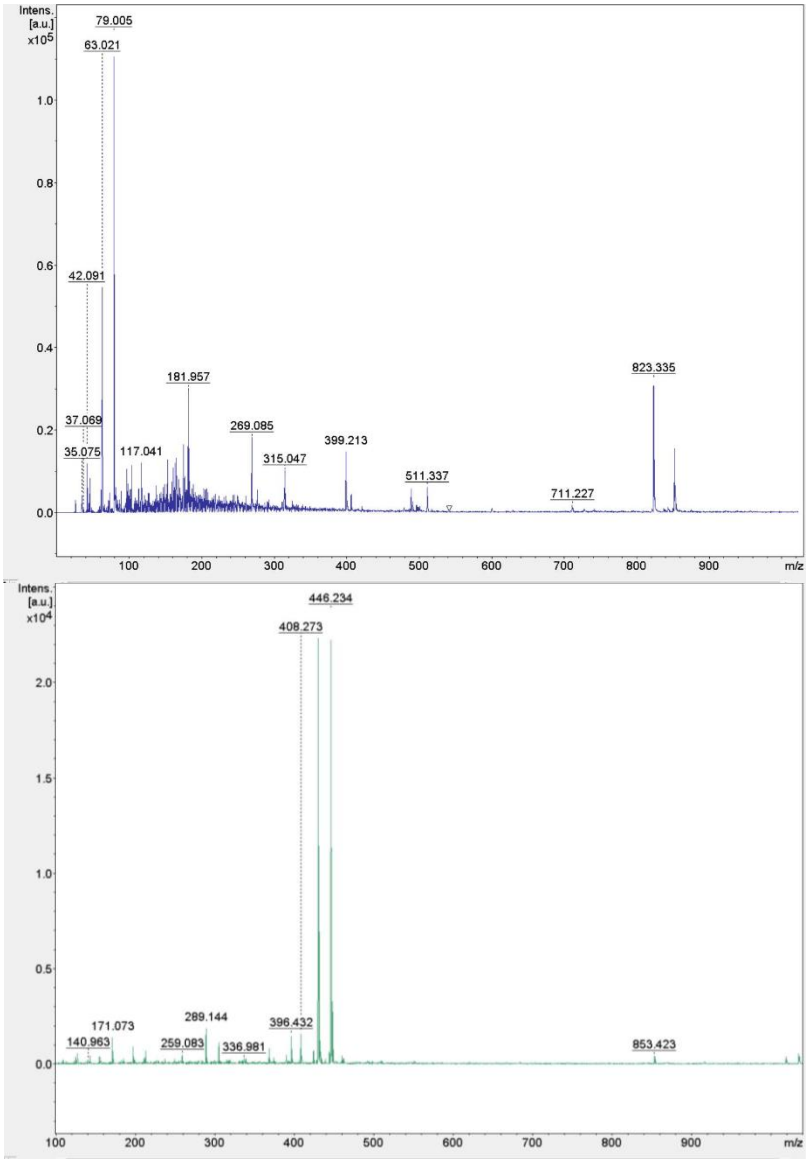

Figure 80: Figure containing two mass spectra of TRU Resin in water analyzed using MALDI-TOF-MS, plotted as m/z or mass-to-charge ratio versus intensity. The top graph is with the mass spectrometer with negative high voltage applied, and the bottom graph has positive high voltage applied.

Figure 81 shows mass spectra generated for TRU Resin in 3 M nitric acid. The reflector negative (top) graph shows a notable peak at 406 m/z correlating to CMPO. The reflector positive (bottom) graph shows notable peaks at 408, 430, and 446 m/z likely correlating to a CMPO

molecule, a protonated CMPO complexed with a water molecule, and CMPO complexed with two water molecules.

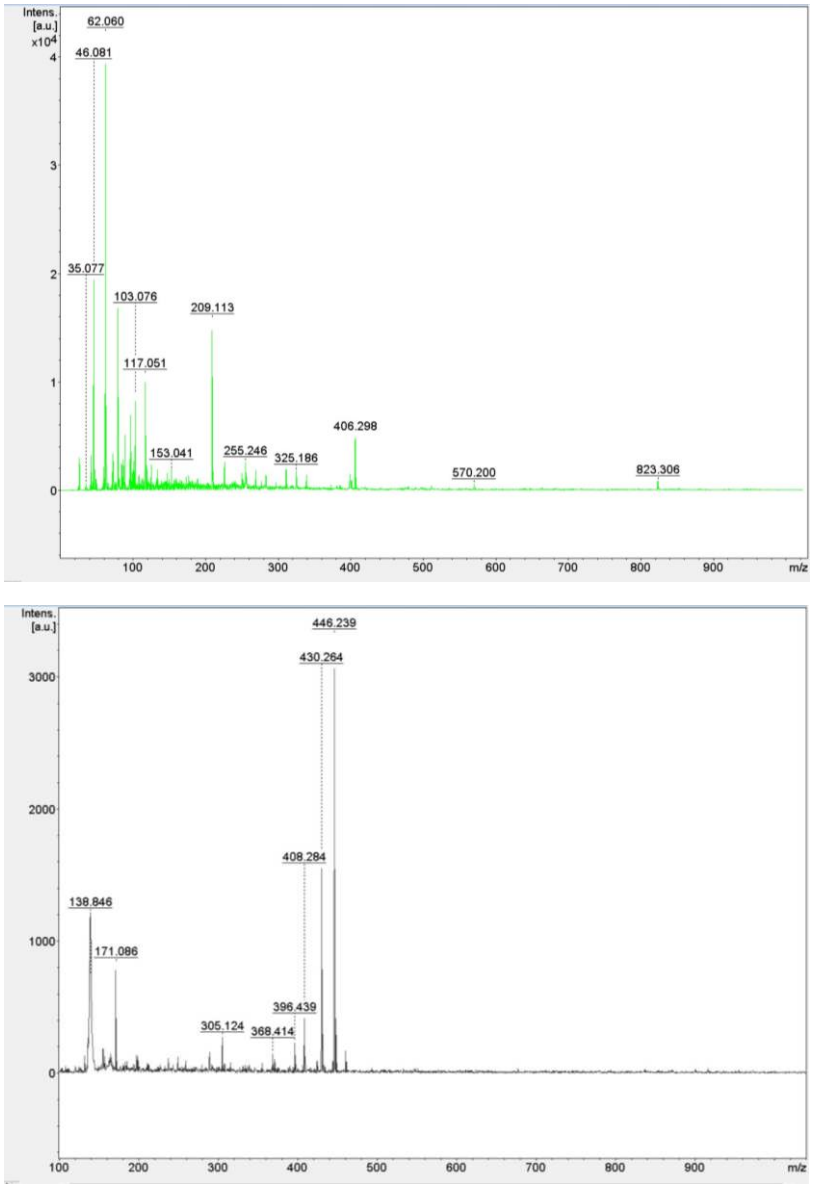

Figure 81: Figure containing two mass spectra of TRU Resin in 3 M nitric acid analyzed using MALDI-TOF-MS, plotted as m/z or mass-to-charge ratio versus intensity. The first graph is with the mass spectrometer with negative high voltage applied, and the bottom graph examines the same region with positive high voltage applied.

The spectra generated for TRU Resin in 3 M hydrochloric acid and TRU Resin without an aqueous phase (i.e., dry) show similar spectral features to those of the spectra shown above in figure 81 and are in Appendix D.

The extractant on the TEVA Resin is discussed at length, including chemical structures, in section 4.2.1. The necessary knowledge of these extractants to determine whether the MALDI can analyze TEVA Resin as an extraction chromatography resin is the molecular weight for Aliquat 336—404.2 g/mol. Spectra were collected in four solution conditions 1: water, 2: 3 M nitric acid, 3: 3 M hydrochloric acid, and 4: dry. Figure 82 contains the spectra generated for TEVA Resin in water. While there is no peak for the Aliquat 336 extractant in the reflector negative spectrum generated, the shape of the spectrum holds relatively steady across all aqueous phase profiles examined in this study. This spectrum (figure 82) allows for the characterization of changes in the breakdown structure of the extractant. In the reflector positive spectra, the main spectral features are the peaks at 368, 396, 424, and 452 relating to the inert backbone of the resin bead.

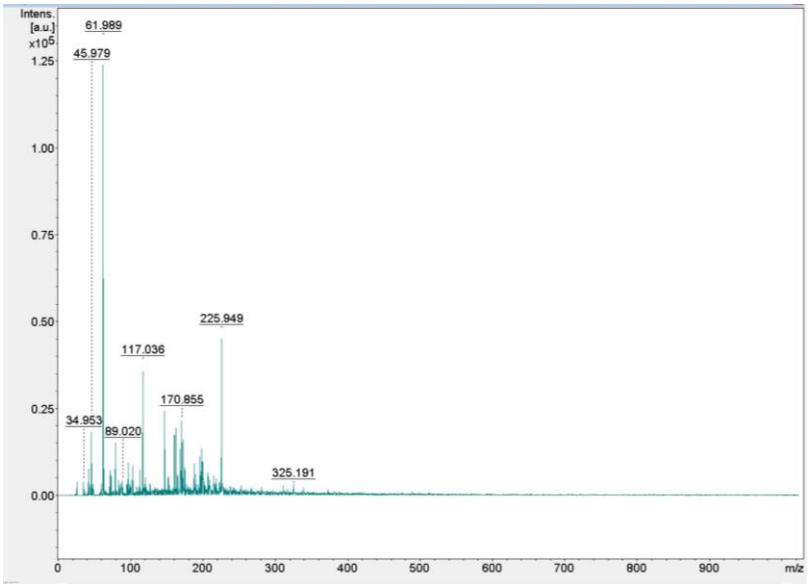

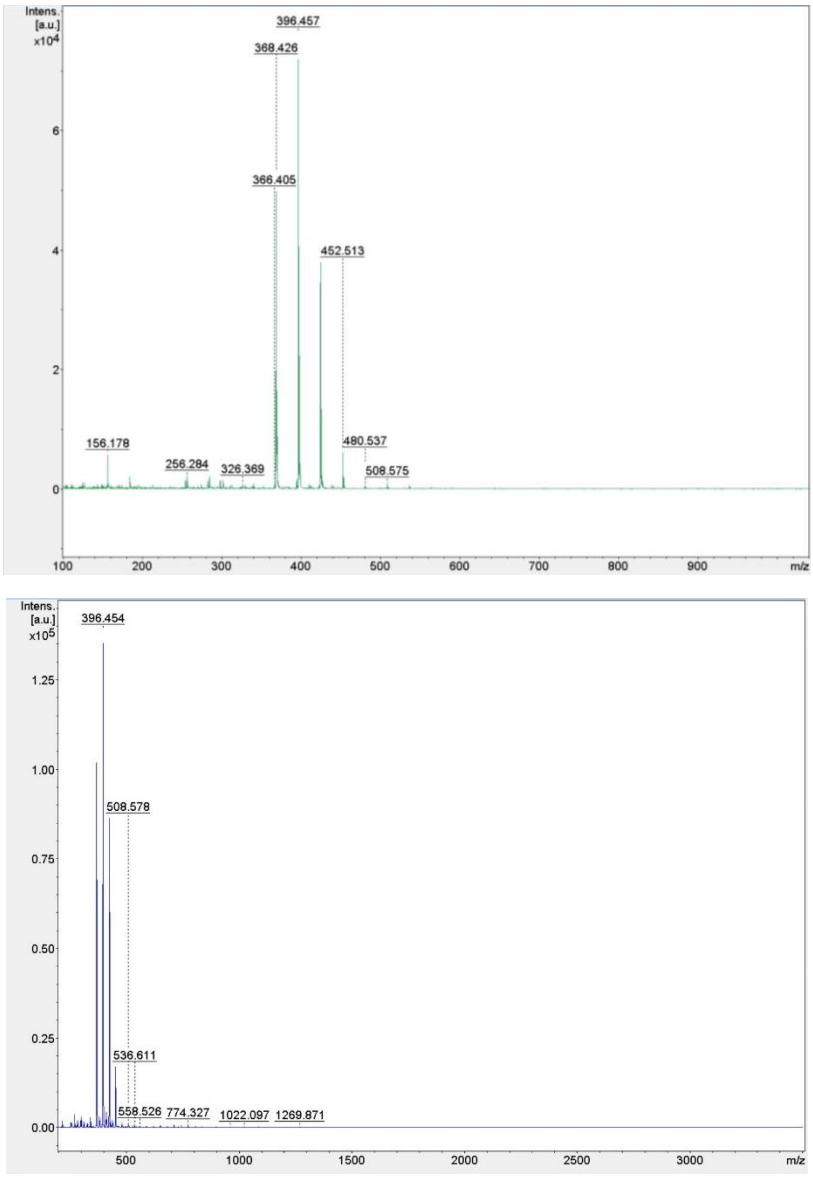

Figure 82: Figure containing three mass spectra of TEVA Resin in water analyzed using MALDI-TOF-MS, plotted as m/z or mass-to-charge ratio versus intensity. The first graph is with the mass spectrometer with negative high voltage applied, the second graph illustrates the same region with positive high voltage applied, and the third examines an expanded region of interest with the positive high voltage applied.

The MALDI mass spectra generated for TEVA Resin in 3 M nitric acid, 3 M hydrochloric acid, and dry TEVA Resin were moved to Appendix D as they present similar spectral features to those shown above. There is a notable increase in the background noise present in the spectra collected from dry TEVA Resin; however, the overall spectral features remain constant.

The extractant on the UTEVA Resin is discussed at length, including chemical structures, in section 4.3.1. The necessary knowledge of these extractants to determine whether the MALDI can analyze UTEVA Resin as an extraction chromatography resin is the molecular weight: for DAAP—292.4 g/mol. Spectra were collected in four solution conditions 1: water, 2: 3 M nitric acid, 3: 3 M hydrochloric acid, and 4: dry. Figure 83 contains the spectra generated for UTEVA Resin in water. The reflector positive spectrum contains the features characteristic of the inert polymer backbone of the resin bead. The reflector negative spectrum shows a notable peak at 283 m/z which is likely the diamyl amyl phosphonate complexed with two water molecules that has lost a C_3H_9 group from one of its amyl groups.

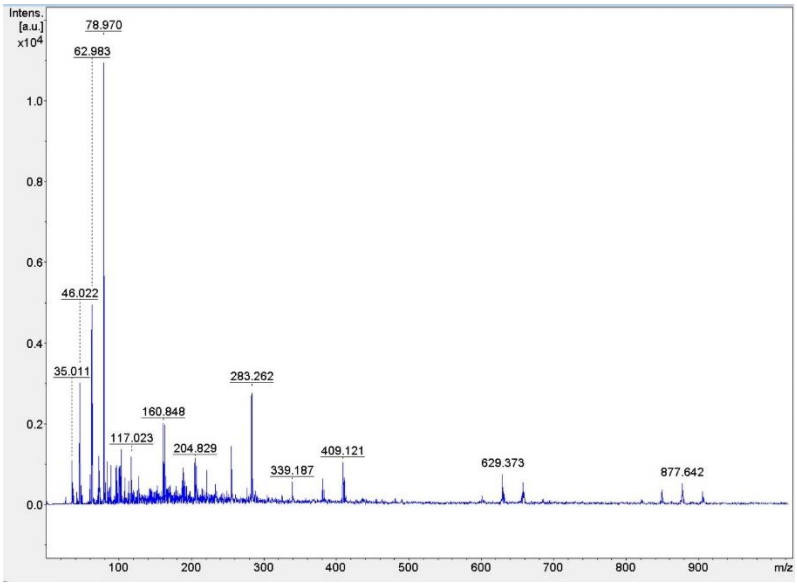

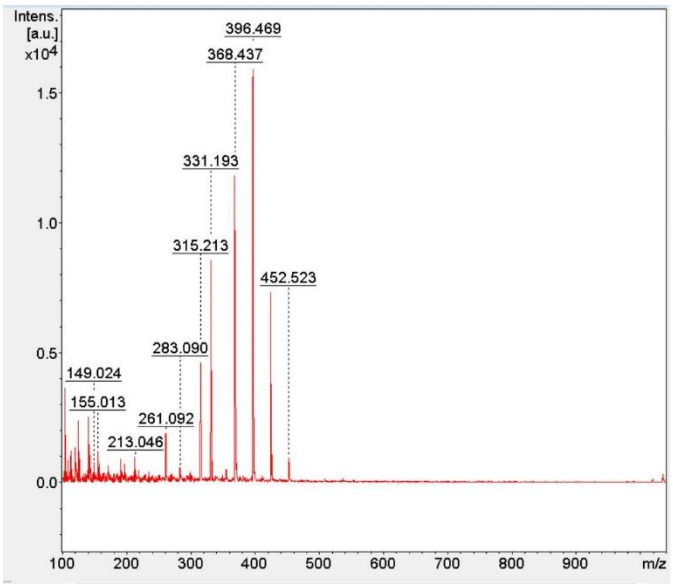

Figure 83: Figure containing two mass spectra of UTEVA Resin in water analyzed using MALDI-TOF-MS, plotted as m/z or mass-to-charge ratio versus intensity. The first graph is with the mass spectrometer with negative high voltage applied, and the second graph examines the same region with positive high voltage applied.

Figure 84 shows the gathered mass spectra of UTEVA Resin in 3 M nitric acid. The reflector positive spectrum shows those features likely attributable to the inert support of the resin bead; however, there is also a peak at 331 m/z which could be a protonated DAAP molecule complexed with two water molecules and a peak at 261 m/z which could be a DAAP molecule that lost a C_2H_7 section from an amyl group. There is also a marked increase in the background noise in the reflector negative spectrum; however, it remains the same general shape as the spectrum gathered for UTEVA Resin in water except that some of the higher m/z peaks are not detected in the sample that was conditioned with 3 molar nitric acid.

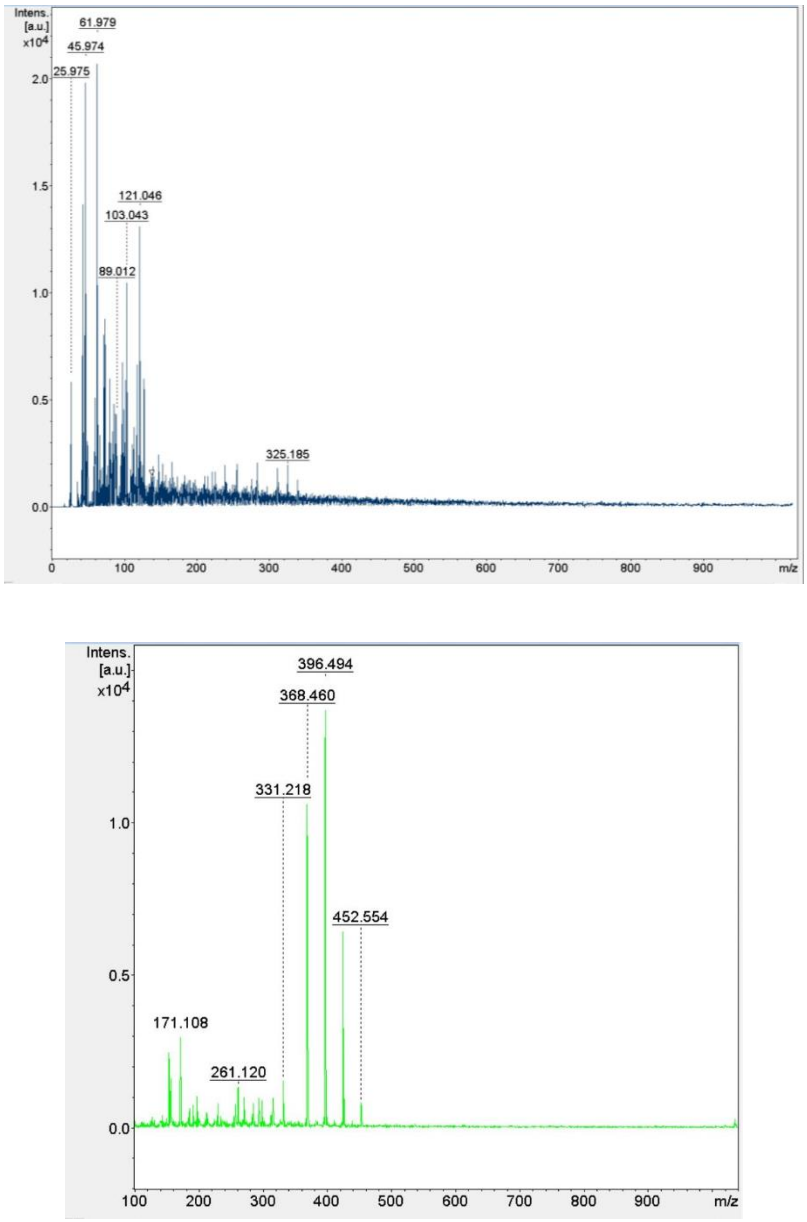

Figure 84: Figure containing two mass spectra of UTEVA Resin in 3 M nitric acid analyzed using MALDI-TOF-MS, plotted as m/z or mass-to-charge ratio versus intensity. The first graph is with the mass spectrometer with negative high voltage applied, and the second graph examines the same region with positive high voltage applied.

Figure 85 shows the gathered mass spectra of UTEVA Resin in 3 M hydrochloric acid. The reflector negative spectrum collected of UTEVA Resin in hydrochloric acid more closely resembles that of the UTEVA Resin in water than that of the UTEVA Resin in nitric acid. The reflector positive spectrum shows both the features of the inert polymer backbone (peaks

including those at 368, 396, and 424 m/z) and those of the UTEVA Resin (peaks at 261, 283, and 331 m/z).

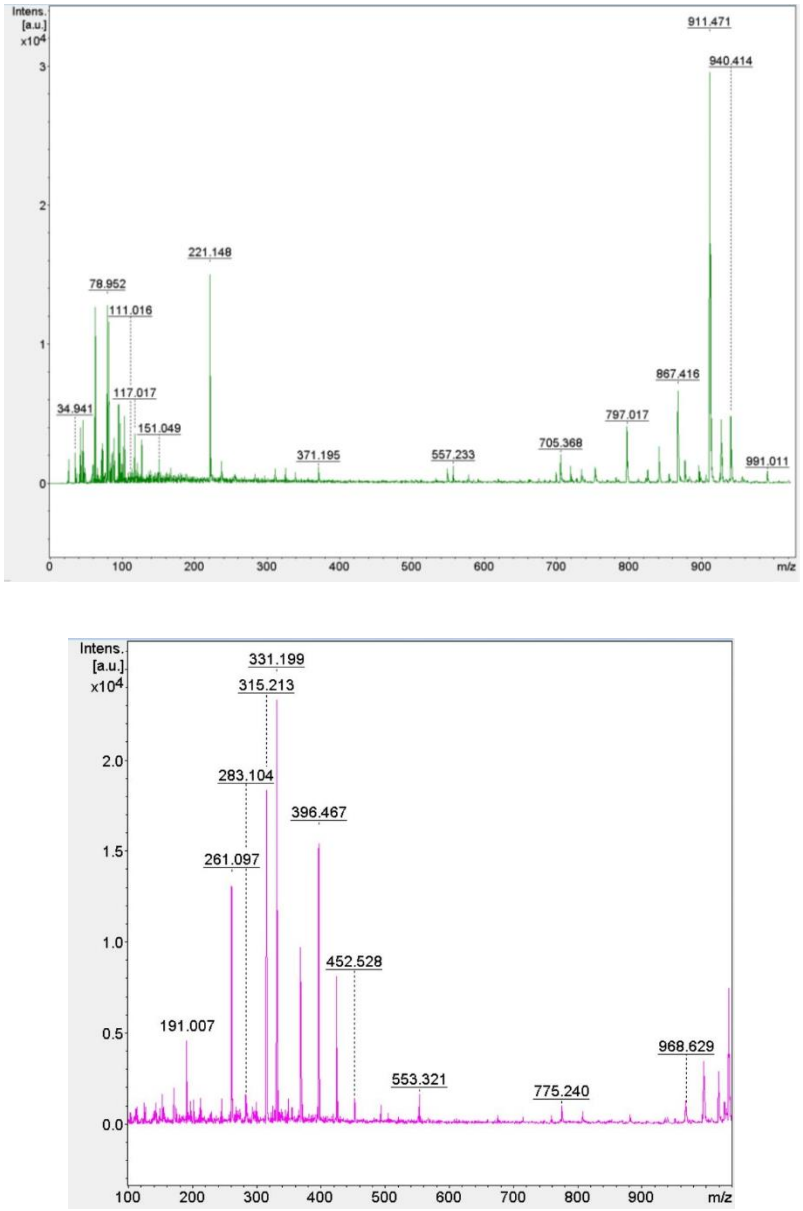

Figure 85: Figure containing two mass spectra of UTEVA Resin in 3 M hydrochloric acid analyzed using MALDI-TOF-MS, plotted as m/z or mass-to-charge ratio versus intensity. The first graph is with the mass spectrometer with negative high voltage applied, and the second graph illustrates the same region with positive high voltage applied.

The spectra generated from dry UTEVA Resin more closely resemble those of UTEVA Resin in water or 3 M hydrochloric acid than those of UTEVA Resin in 3 M nitric acid, shown in Appendix D.

The DIPEX extractant on the Actinide Resin is discussed at length, including chemical structures, in section 4.4.1. The necessary knowledge of these extractants to determine whether the MALDI can analyze Actinide Resin as an extraction chromatography resin is the molecular weight: for DIPEX—400.4 g/mol. Spectra were collected in four solution conditions 1: water, 2: 3 M nitric acid, 3: 3 M hydrochloric acid, and 4: dry.

Figure 86 below contains the spectra generated for the Actinide Resin in water. There is a small peak present in the reflector negative spectrum at 399 m/z which is likely a deprotonated DIPEX molecule. The peaks at 852, 855, and 859 m/z are likely two DIPEX molecules complexed with three waters in various states of protonation. The peak at 823 m/z is likely two DIPEX molecules complexed with parts of water molecules included in the complex generated during the desorption/ionization process. The reflector positive spectrum shows the characteristic peaks for the inert polymer backbone at 368, 396, 424, and 452 m/z. This reflector negative spectrum includes additional peaks at 480 and 508 m/z which line up with the trend of the polymer backbones of the peaks being ±Zn, where Z is an integer and n is 28.0.

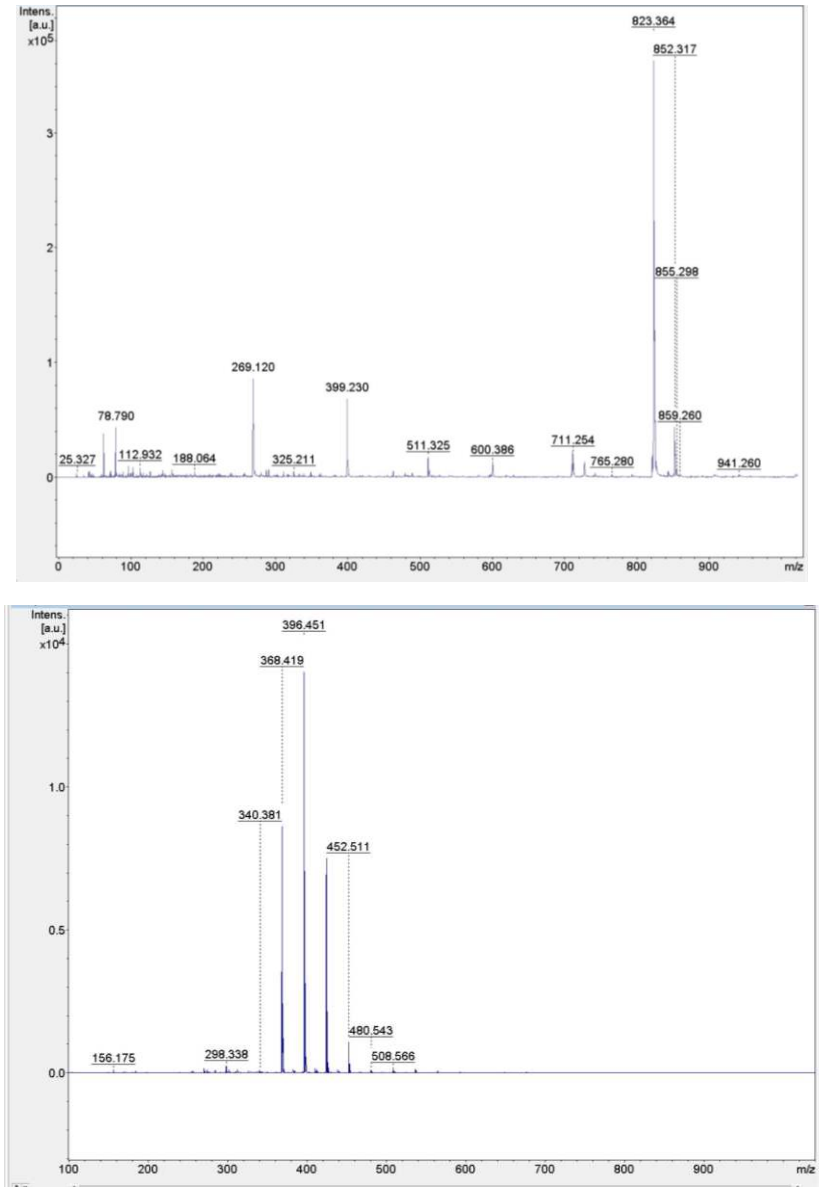

Figure 86: Figure containing two mass spectra of the Actinide Resin in water analyzed using MALDI-TOF-MS, plotted as m/z or mass-to-charge ratio versus intensity. The first graph is with the mass spectrometer with negative high voltage applied, and the second graph examines the same region with positive high voltage applied.

Figure 87 contains the spectra generated for the Actinide Resin in 3 M nitric acid. The reflector negative spectrum shows the peak at 399 m/z that is likely the deprotonated DIPEX molecule as well as the previously discussed (from the spectrum of Actinide Resin in water) peaks at 823 and 852 m/z. The reflector positive spectrum of AC Resin in 3 M nitric acid also shows the same

characteristic and expanded range of peaks linked to the inert support discussed above the previous figure (peaks at 368, 396, 424, 452, 480, 508 m/z).

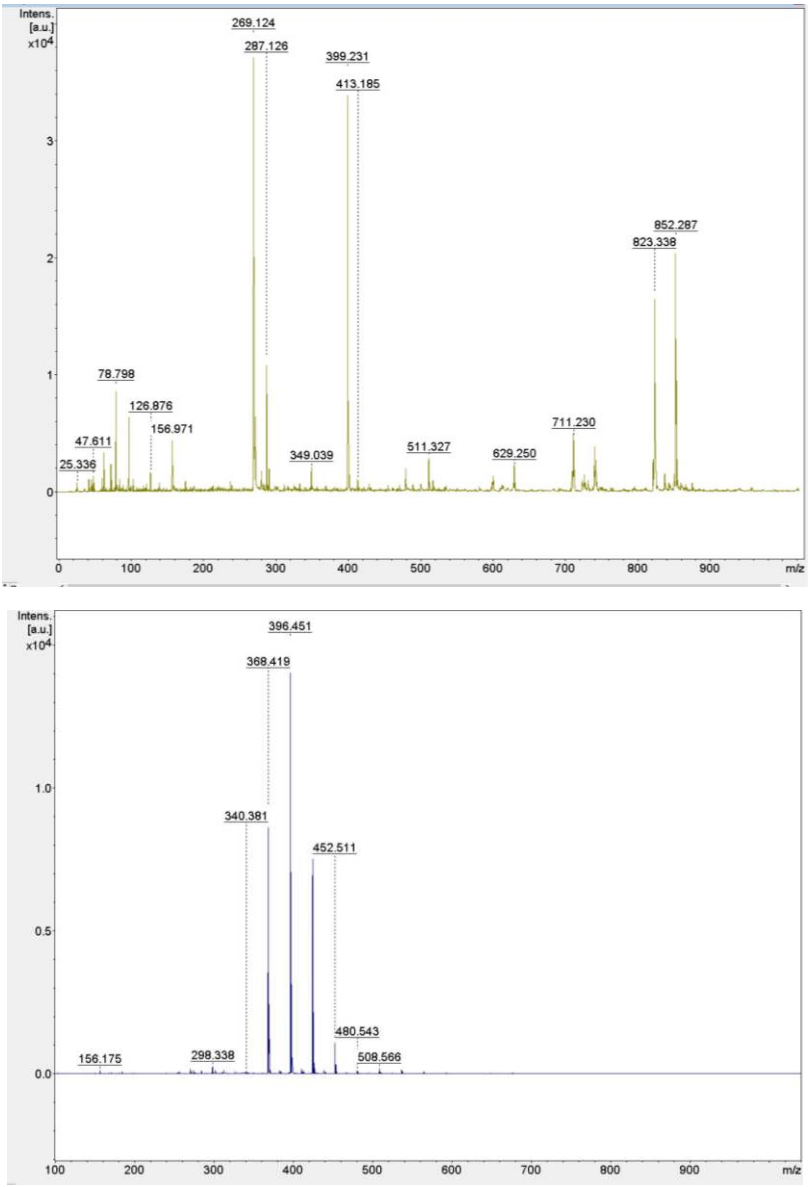

Figure 87: Figure containing two mass spectra of the Actinide Resin in 3 M nitric acid analyzed using MALDI-TOF-MS, plotted as m/z or mass-to-charge ratio versus intensity. The first graph is with the mass spectrometer with negative high voltage applied, and the second graph illustrates the same region with positive high voltage applied.

The spectra gathered of the Actinide Resin in 3 M hydrochloric acid and dry Actinide Resin present in the same fashion as those of the Actinide Resin in water or nitric acid. They were therefore moved to Appendix D.

6.4: Conclusions

Spectra from the samples of the resin that were not pre-conditioned or irradiated in contact with an aqueous layer were more difficult to collect and analyze. The samples seemed to be less readily ionized via the MALDI process. Each resin does generate characteristic spectra that can be used to determine whether the structure of the resin has changed under irradiation. In the reflector positive spectra, there are characteristic peaks that appear in all spectra of all four resins: TRU, TEVA, UTEVA, and Actinide. Thus, reflector positive peaks are most likely the result of the inert polymer support that all four resins share—Amberchrom CG71. All four resins' spectra show the peaks at 368, 396, and 424 m/z, with others also having peaks at 452, 480, and 508 m/z. Since all these peaks are 28 m/z units apart, it is likely that the peaks detected are of polymers from the inert support of the resin beads, likely plus or minus a C_2H_4 or ethylene group, which likely means that the breaks are occurring at the cross linkages of the polymer.

MALDI is an effective method for diagnosing changes in the resins such as after irradiation with increasing dose. MALDI can also be used to determine the functionalization of extraction chromatographic resins; however, the experimenter must know desired and possible outcomes, as is typical with MALDI spectrometry since a wide range of mass to charge ratios can be interrogated with this experimental technique.

CHAPTER 7: ANALYSIS OF IRRADIATED EXTRACTION CHROMATOGRAPHY RESINS USING MALDI

7.1: Introduction and Theory

The goals of using extraction chromatography resins are discussed at length in sections 2.1.1, 2.1.2, and 2.2.1. Mass spectrometry, MALDI, and TOF systems are discussed at length in section 2.5. The development of the method for the analysis of EXC materials via MALDI-TOF-MS is discussed in Chapter 6. This chapter deals with identifying the differences between unirradiated control samples of extraction chromatographic resins and samples that were exposed to 50 kGy of gamma radiation using the Cs-137 source in room 470 of the Molecular and Radiological Biosciences Building at Colorado State University.

7.2: Materials and Methods

The primary instrument used for this study is the Bruker UltraFlextreme shown in the image below. This instrument resides in the Analytical Resources Core (ARC) in the basement of Colorado State University's chemistry building.

A suspension of red phosphorus in methanol was used as the calibrant, given the relatively low mass range, for MALDI purposes, being investigated here (24). Spectra of the calibrant are presented in section 6.3.

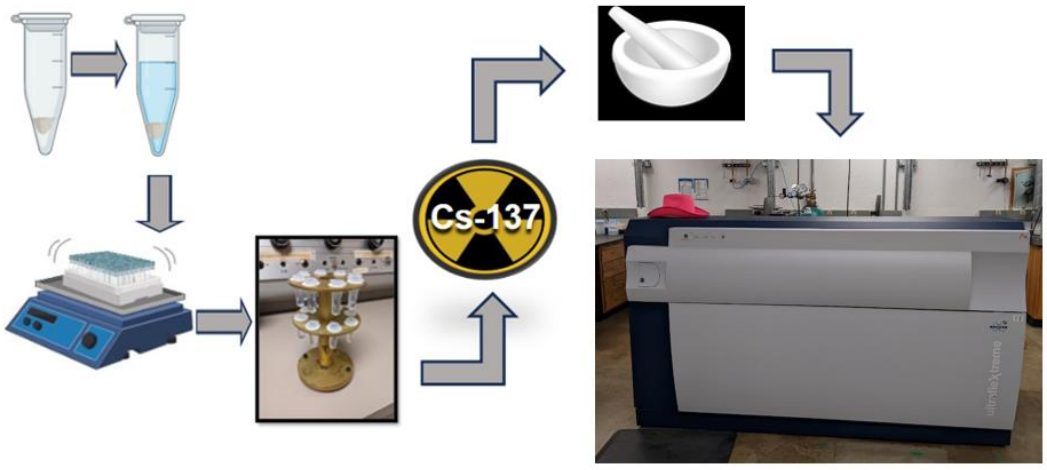

Figure 88: Pictorial representation of general sample processing used in this chapter.

Fifty mg of the resin was contacted with 1.5 mL of the mineral acid and concentration of c20-microliterd to the irradiator, centrifuged at 3000 rpm for 30 minutes, separated into resin and mobile phase samples, ground in a mortar and pestle, transferred using acetone and then a 20 microliter aliquot containing suspended solids was pipetted on to the stainless steel target plates for introduction to the MALDI's high vacuum. The steps of this procedure are shown pictorially in the figure above. Both positive and negative high voltage systems were interrogated for optimal mass spectrum generation. The mass spectrometer's linear mode was used primarily in initial studies to determine required laser power and gain settings for each particular sample. The mass spectrometer's reflector mode was generally used to generate the cleaner spectra with a lower background present that were gathered. The spectra were generated and processed using Bruker's flexControl and flexAnalysis software (flexAnalysis version 3.4, copyright Bruker Daltonik GmbH).

7.3: Results and Discussion

A suspension of red phosphorus clusters in methanol was used as the calibrant for these MALDI experiments. The spectra of the calibrant in each disparate processing condition are shown in section 6.3.

7.3.1: Fragmentation of TRU Resin

Specifics of the more general analysis of TRU Resin via MALDI-TOF-MS are in section 6.3. The figure below shows the effect of irradiation on TRU Resin. Each pair of spectra is comprised of the mass spectrum generated from the sample irradiated with 50 kGy gamma radiation (top) and the unirradiated control (bottom). Since TRU Resin in 3 M nitric acid is largely not affected by gamma irradiation to 50 kGy (conclusion from chapter 4) but does show effects in 3 M hydrochloric acid, the TRU Resin irradiated in 3 M hydrochloric acid spectra and respective unirradiated controls are presented first in this section. The TRU Resin in 3 M nitric acid spectra are in Appendix D; however, there were no overarching conclusions that could be gleaned from them, as they show minimal differences between the spectra of the irradiated and unirradiated control samples.

Figure 89 contains the paired mass spectra of irradiated TRU Resin (top) and an unirradiated control TRU Resin (bottom) that went through identical chemical processing. The first pair of spectra contains a comparatively wider range of m/z gathered in reflector mode with the negative high voltage applied. There are several higher m/z ratio peaks—notably at 283 and 406 m/z—that are present in the unirradiated control spectrum but not in the irradiated sample. It is possible that fewer intact CMPO molecules are present in the extracted sample resulting in

losses of complexed TBP molecules as well. There is a shift in the reflector positive spectra gathered where the main peak presents at 446 m/z rather than 396 m/z; however, this is likely a result of the chemical processing since the unirradiated control sample has a similar spectrum.

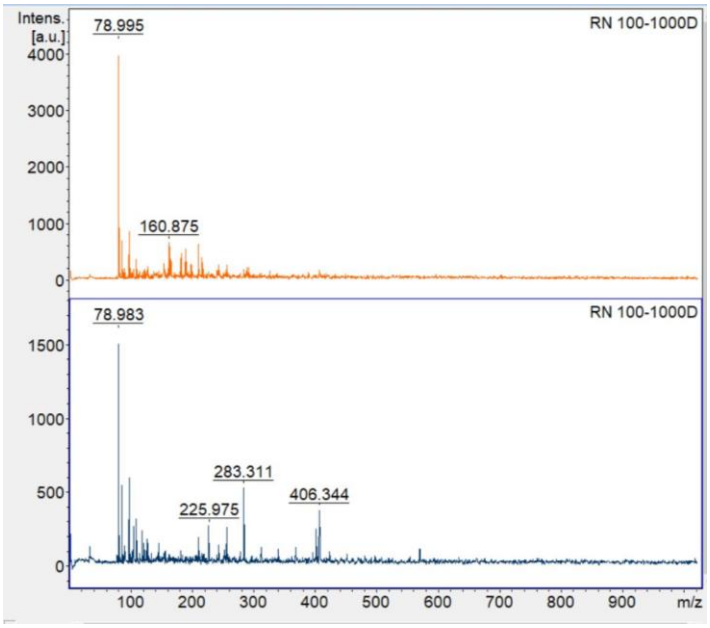

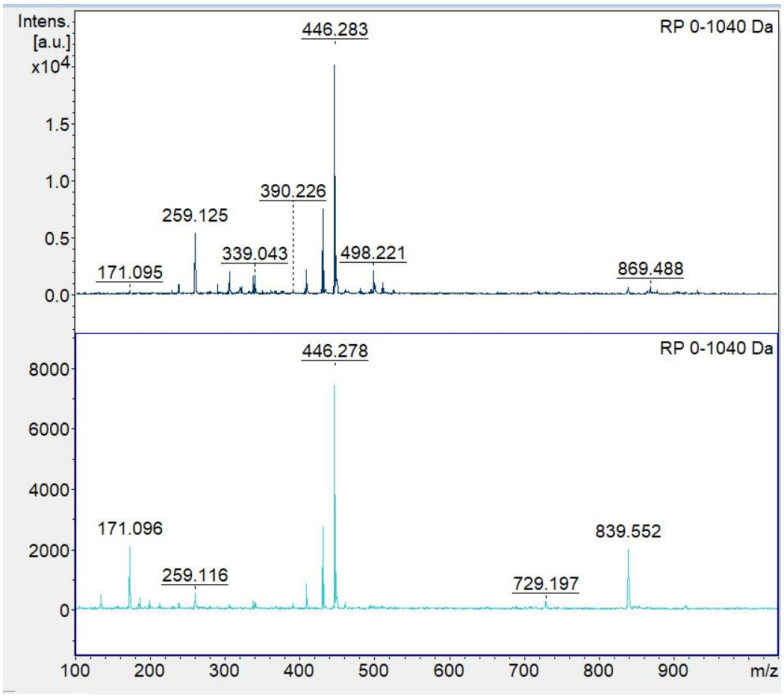

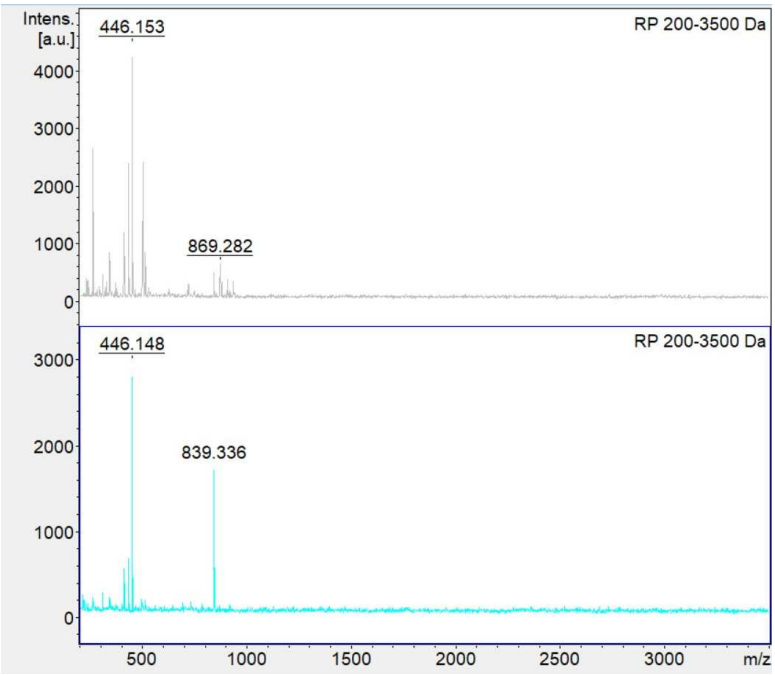

Figure 89: Figure containing three pairs of mass spectra of TRU Resin in 3 M hydrochloric acid analyzed using MALDI-TOF-MS, plotted as m/z or mass-to-charge ratio versus intensity. The top graph in each pair is the sample that received 50 kGy gamma exposure. The first pair of graphs is with the mass spectrometer with negative high voltage applied, the middle pair illustrates the same region with high voltage applied, and the last pair examines a wider mass range using the positive high voltage.

Figure 90 specifically examines low mass-to-charge ratio fragments of TRU Resin in 3 M hydrochloric acid, with irradiated and unirradiated paired spectra for ease of comparison. In figure 90, the first pair of spectra demonstrate that the differences between the irradiated and the unirradiated samples is in the mid- to upper-200s range of the mass to charge ratio. The lower mass range queried in the reflector negative and reflector positive modes both show that there are minimal changes detected below a mass to charge ratio of 150.

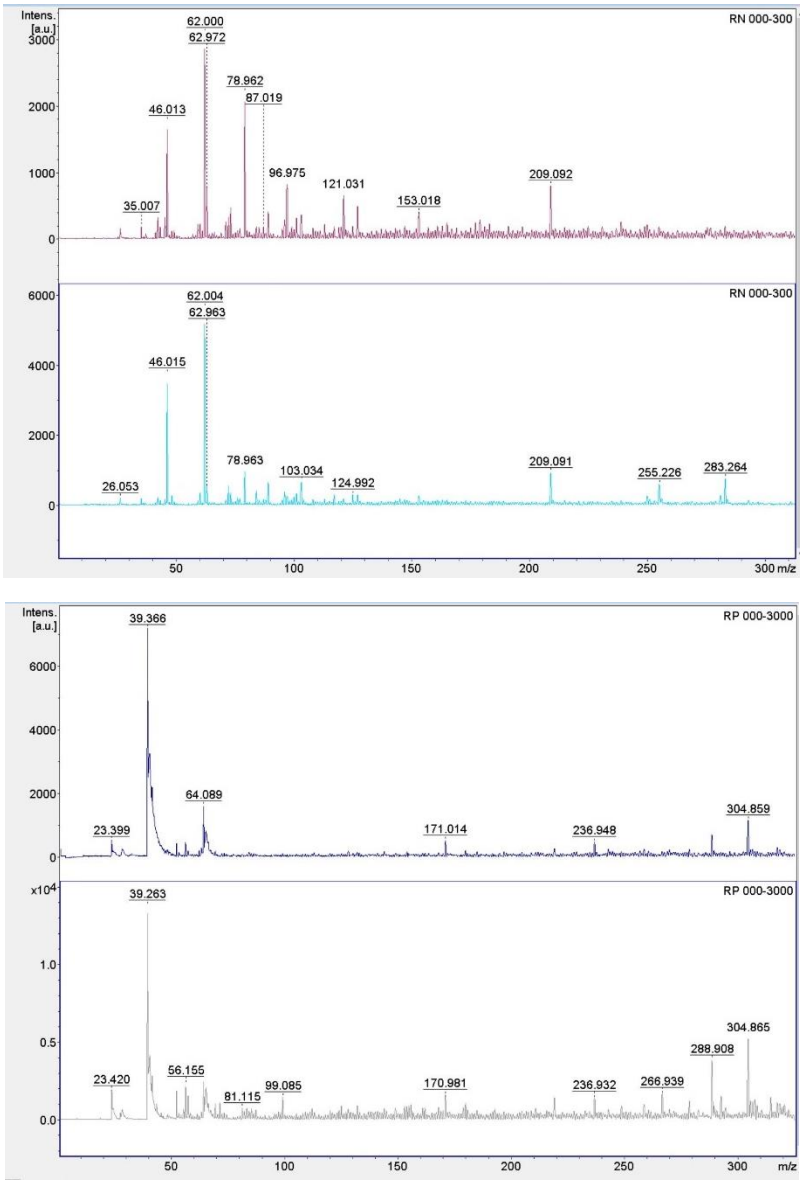

Figure 90: Figure containing two pairs of mass spectra of TRU Resin in 3 M hydrochloric acid analyzed using MALDI-TOF-MS, plotted as m/z or mass-to-charge ratio versus intensity. The top graph in each pair is the sample that received 50 kGy gamma exposure. The first pair of graphs is with the mass spectrometer with negative high voltage applied, and the bottom pair examines the same region with positive high voltage applied.

The MALDI spectra gathered for samples of TRU Resin irradiated in water show similar results to those of presented of the TRU Resin irradiated in 3 M nitric acid (Appendix D). Figure 91 shows the dry TRU Resin, with paired spectra of the irradiated sample and the unirradiated control baseline sample. There are few to no perceptible differences between the spectra of the irradiated and unirradiated baseline samples for TRU Resin irradiated dry, in both those spectra

gathered with the negative high voltage and those gathered with the positive high voltage. This supports the hypothesis that most radiolytic damage or changes to the resin are from the gamma irradiation, and a result of the interactions of the generated reactive species in solution, rather than the ionizing radiation directly impacting the resin itself.

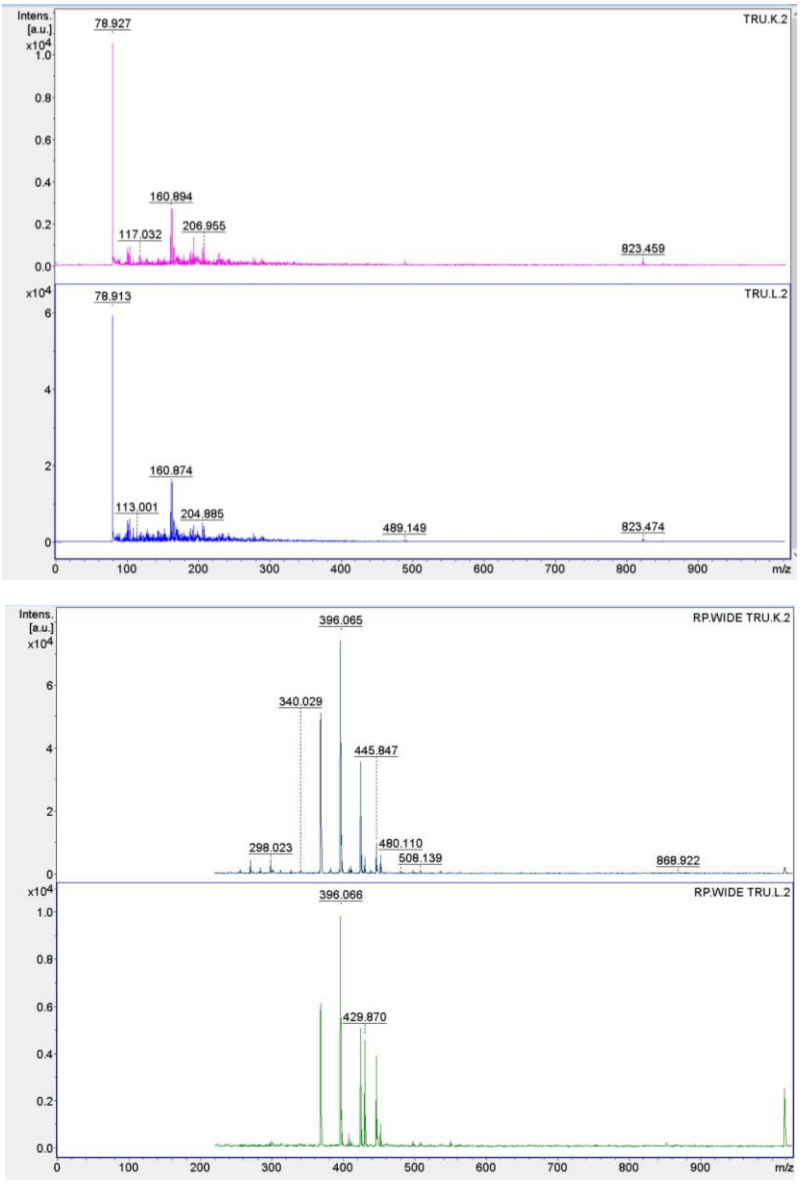

Figure 91: Figure containing two pairs of mass spectra of dry TRU Resin analyzed using MALDI-TOF-MS, plotted as m/z or mass-to-charge ratio versus intensity. The top graph in each pair is the sample that received 50 kGy gamma exposure. The first pair of graphs is with the mass spectrometer with negative high voltage applied, and the second pair illustrates the same region with positive high voltage applied.

Figure 92 specifically examines low mass-to-charge ratio fragments of dry TRU Resin, with irradiated and unirradiated paired spectra for ease of comparison. Both pairs of spectra illustrate similarities, further supporting the argument that more of the changes to the resin are caused by the reactive chemical species generated in the solution rather than the radiation directly.

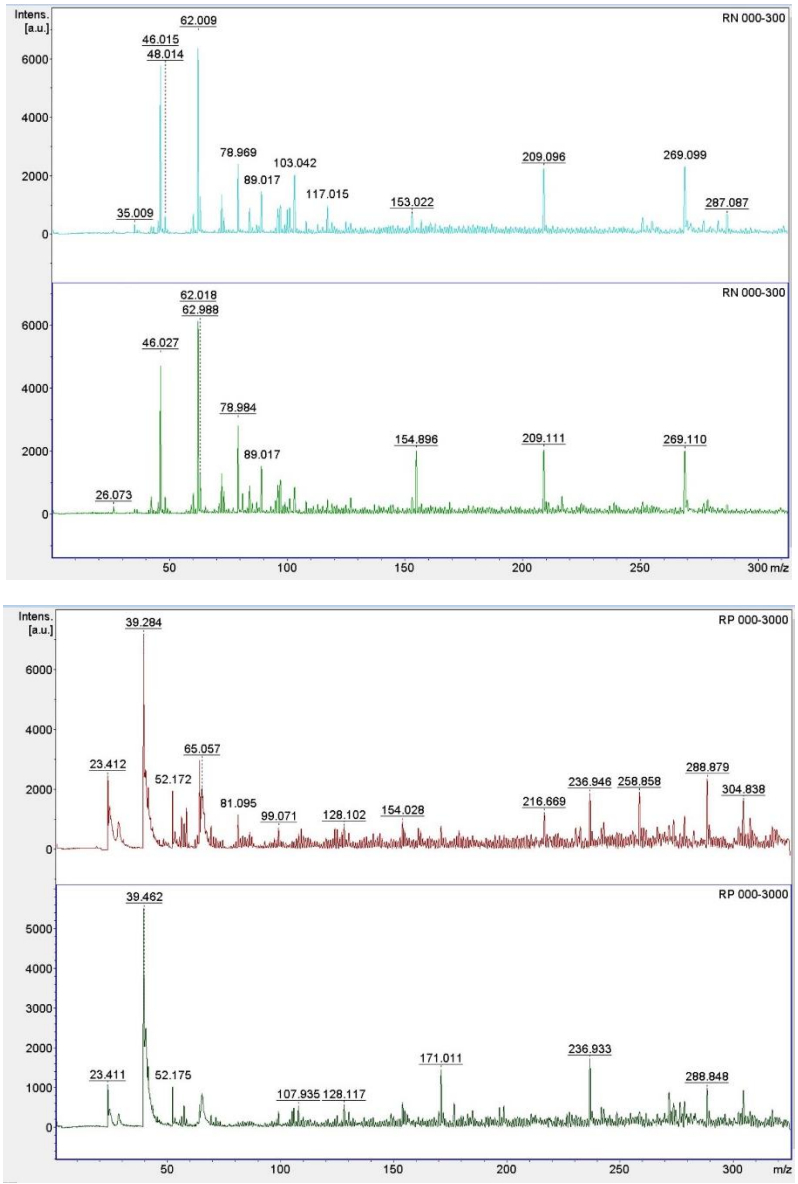

Figure 92: Figure containing two pairs of mass spectra of dry TRU Resin analyzed using MALDI-TOF-MS, plotted as m/z or mass-to-charge ratio versus intensity. The top graph in each pair is the sample that received 50 kGy gamma exposure. The first pair of

graphs is with the mass spectrometer with negative high voltage applied, and the bottom pair examines the same region with positive high voltage applied.

7.3.2: Fragmentation of TEVA Resin

Specifics of the more general analysis of TEVA Resin via MALDI-TOF-MS are in section 6.3. Figure 95 shows the effect of irradiation on TEVA Resin. Each pair of spectra is comprised of the mass spectrum generated from the sample irradiated with 50 kGy gamma radiation (top) and the unirradiated control that went through identical chemical processing (bottom). Figure 93 illustrates a wide mass range for TEVA Resin in 3 M nitric acid. The irradiated sample with the negative high voltage applied does not show the same peaks at 361 and 597 m/z that the unirradiated sample shows. The gathered spectrum for TEVA in nitric acid with the negative high voltage applied gathered and discussed in chapter 6 does not show these features. The peaks could be spurious due to the relatively low magnitude of peaks across the spectrum. However, the peaks at 361 and 597 m/z could be a fragment generated from Aliquat 336 and a molecule of Aliquat 336 complexed with molecules from the mineral acid as matrix. Furthermore, the reflector positive spectra (figure 93) do not contain the disruption to/shift in the polymer backbone that the irradiated sample of TRU Resin in 3 M hydrochloric acid presented in figure 90.

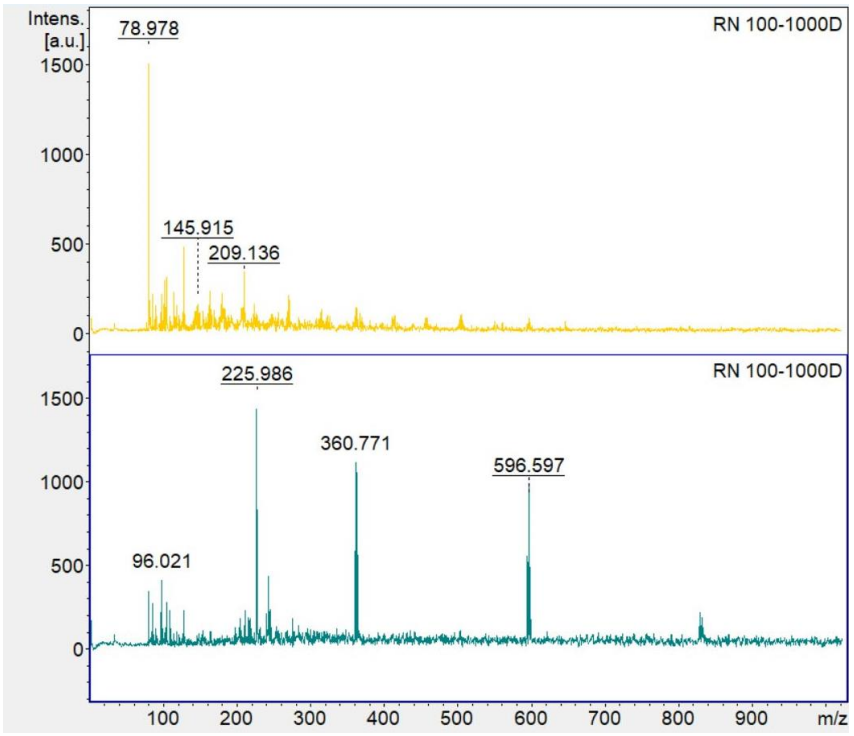
Intens.
[a.u.]
78.978
RN 100-1000D
145.915
209.136
225.986
360.771
596.597
96.021
100
200
300
400
500
600
700
800
900
m/z

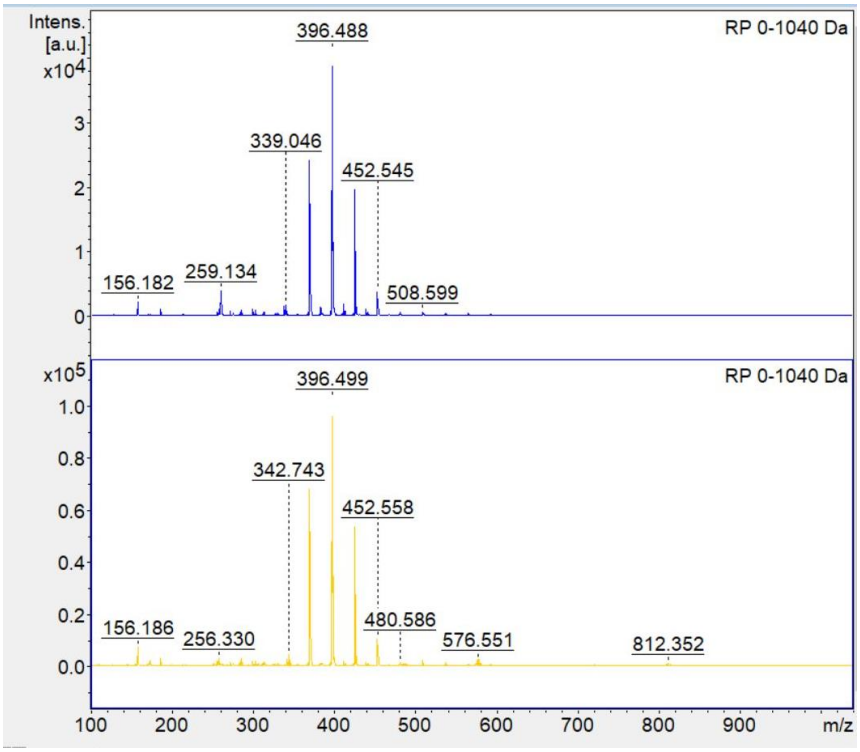
Intens.
[a.u.]
x10^4
396.488
RP 0-1040 Da
339.046
452.545
156.182
259.134
508.599
x10^5
396.499
342.743
452.558
156.186
256.330
480.586
576.551
812.352
100
200
300
400
500
600
700
800
900
m/z

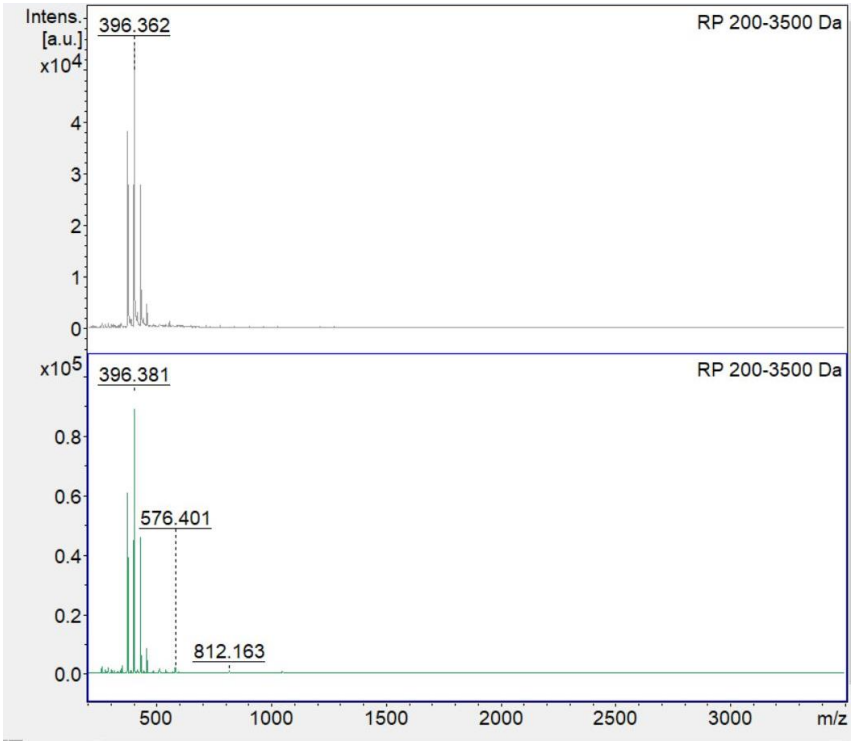

Figure 93: Figure containing three pairs of mass spectra of TEVA Resin in 3 M nitric acid analyzed using MALDI-TOF-MS, plotted as m/z or mass-to-charge ratio versus intensity. The top graph in each pair is the sample that received 50 kGy gamma exposure. The first pair of graphs is with the mass spectrometer with negative high voltage applied, the middle pair illustrates the same region with positive high voltage applied, and the last pair examines a wider mass range using the positive high voltage.

Figure 94 specifically examines low mass-to-charge ratio fragments of TEVA Resin in 3 M nitric acid, with irradiated and unirradiated paired spectra for ease of comparison. In the reflector positive mode, the magnitude of the peak at 39 m/z is markedly larger in the unirradiated sample. Few other differences between the unirradiated and the irradiated spectra are detectable at the low mass to charge ratio range.

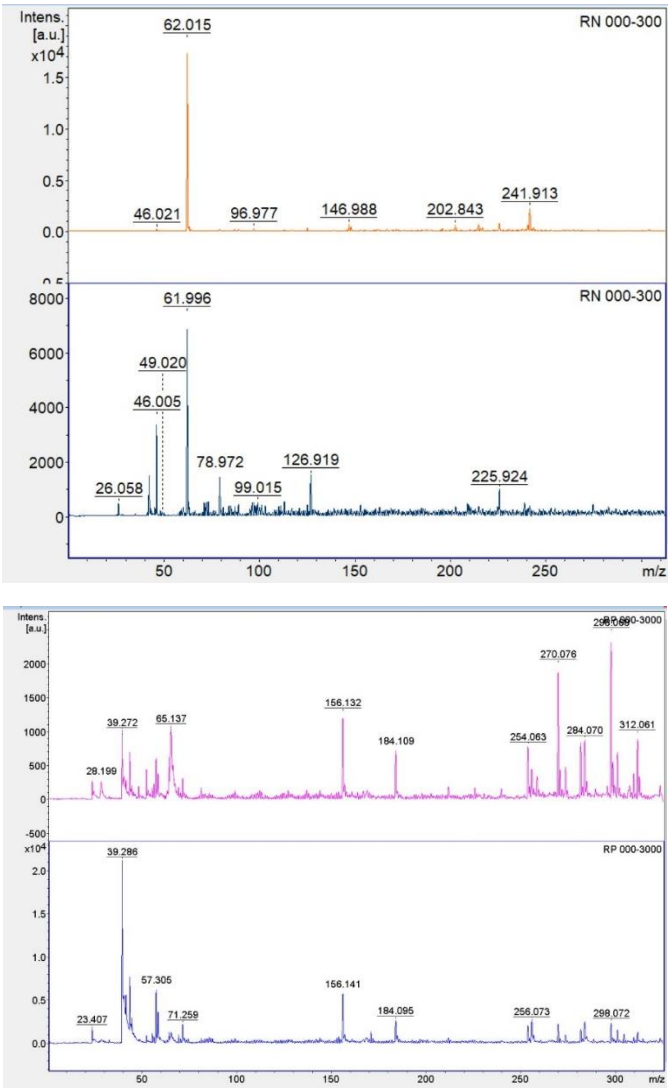

Figure 94: Figure containing two pairs of mass spectra of TEVA Resin in 3 M nitric acid analyzed using MALDI-TOF-MS, plotted as m/z or mass-to-charge ratio versus intensity. The top graph in each pair is the sample that received 50 kGy gamma exposure. The first pair of graphs is with the mass spectrometer with negative high voltage applied, and the bottom pair examines the same region with positive high voltage applied.

Figure 95 shows the TEVA Resin in 3 M hydrochloric acid, with paired spectra of the irradiated sample and the unirradiated control baseline sample. In the reflector negative spectrum in figure 95, the peaks in the 300-550 m/z range are present in the irradiated sample rather than the unirradiated control sample. This shows the opposite trend from that shown in figure 94 in the spectra gathered for TEVA Resin in 3 M nitric acid. Neither pair of reflector positive spectra in figure 95 show differences between the irradiated and unirradiated samples.

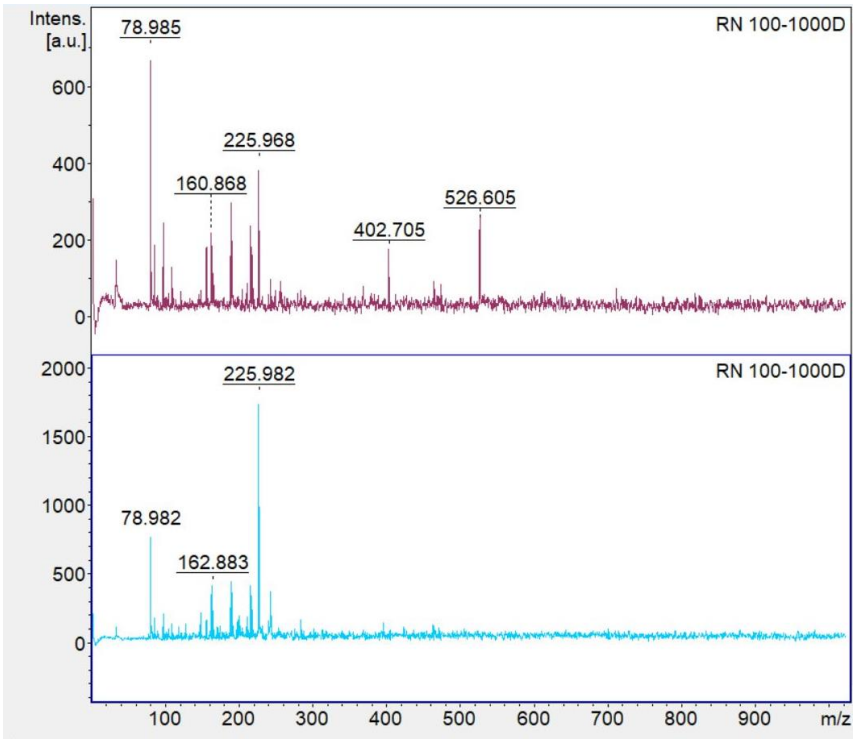
Intens.
[a.u.]
78.985
225.968
160.868
526.605
402.705
RN 100-1000D
225.982
78.982
162.883
RN 100-1000D
m/z

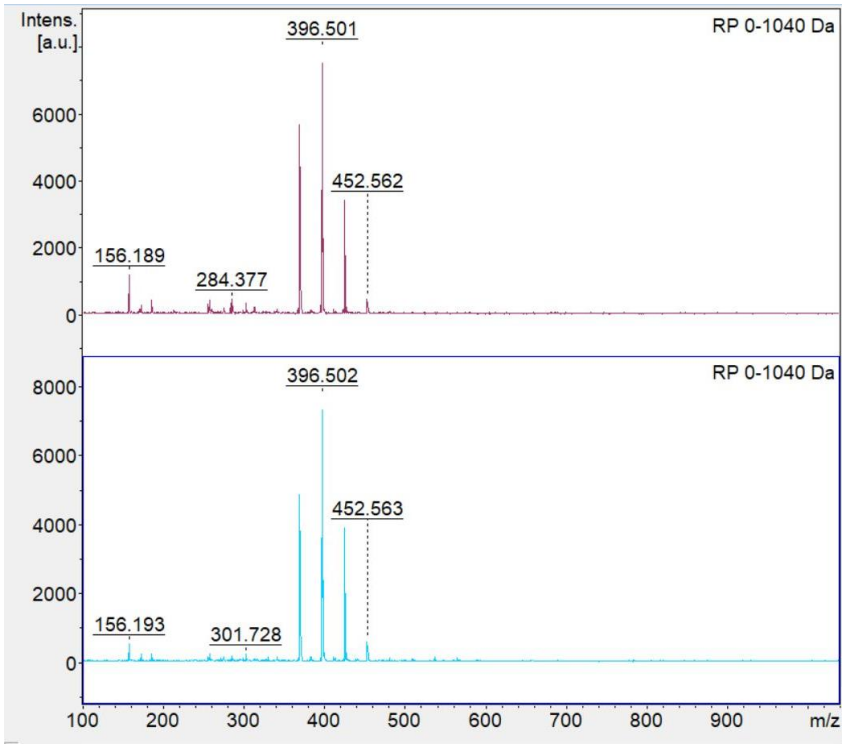
Intens.
[a.u.]
396.501
452.562
156.189
284.377
RP 0-1040 Da
396.502
452.563
156.193
301.728
RP 0-1040 Da
m/z

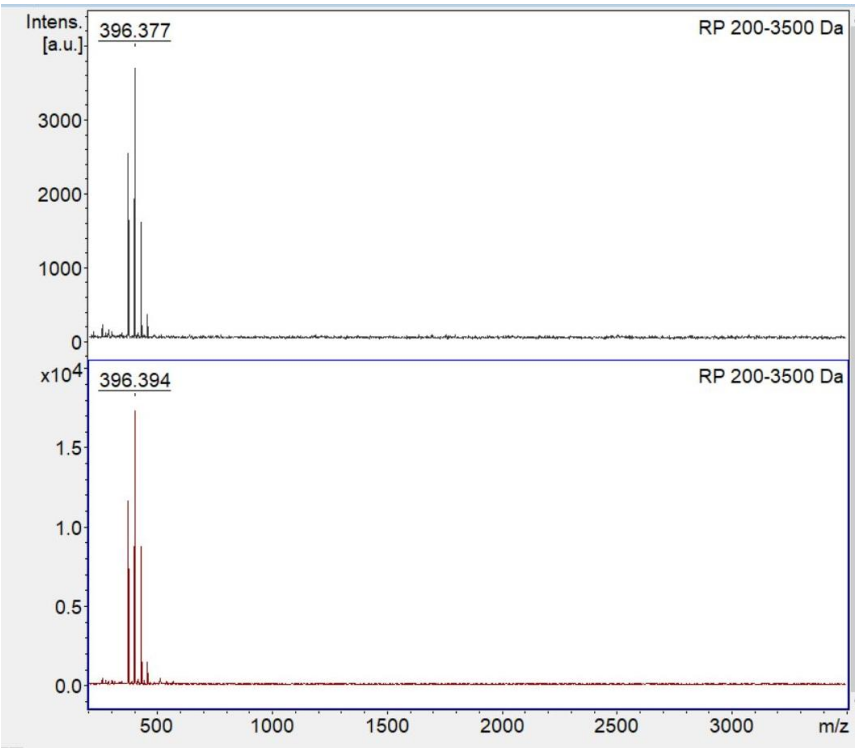

Figure 95: Figure containing three pairs of mass spectra of TEVA Resin in 3 M hydrochloric acid analyzed using MALDI-TOF-MS, plotted as m/z or mass-to-charge ratio versus intensity. The top graph in each pair is the sample that received 50 kGy gamma exposure. The first pair of graphs is with the mass spectrometer with negative high voltage applied, the middle pair illustrates the same region with positive high voltage applied, and the last pair examines a wider mass range using the positive high voltage.

Figure 96 specifically examines low mass-to-charge ratio fragments of TEVA Resin in 3 M hydrochloric acid, with irradiated and unirradiated paired spectra for ease of comparison. The pair of reflector negative spectra illustrating the lower mass to charge ratio region below show the same tendency as the previous figure: there are notable peaks at 214 and 288 m/z in the mass spectrum collected from the irradiated sample but not in the unirradiated control sample. The pair of reflector positive spectra in the figure below differs in that there is a peak at 171 m/z in the irradiated sample but not in the unirradiated control.

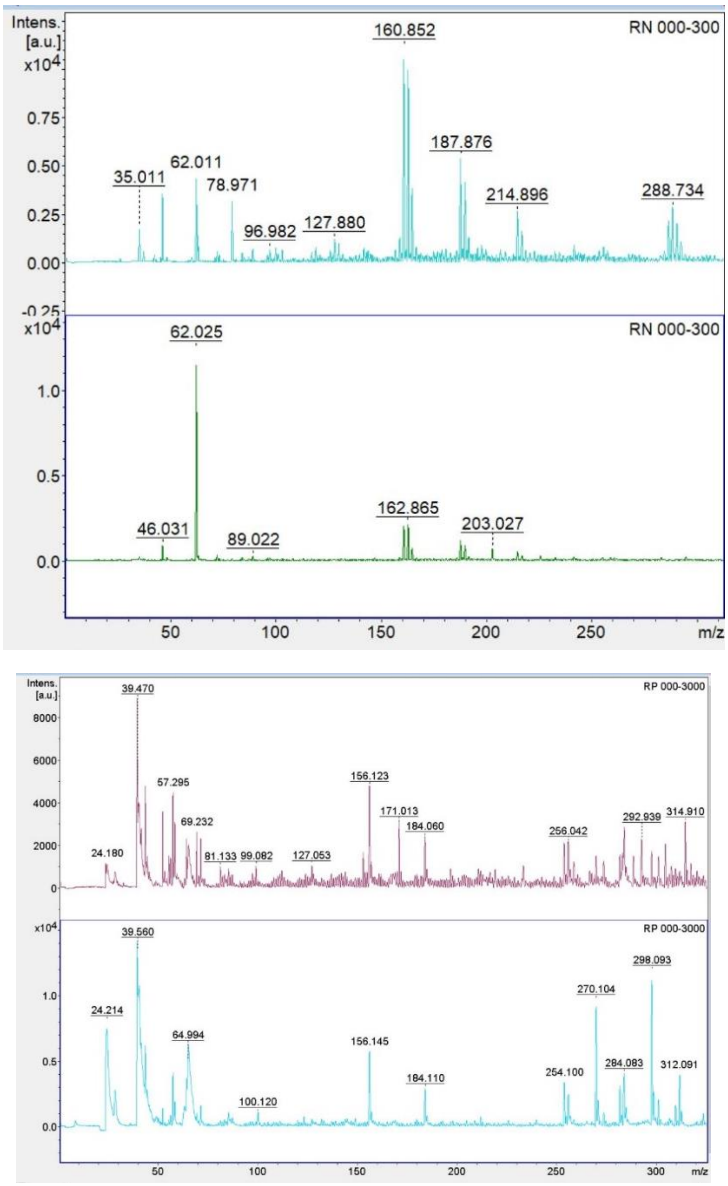

Figure 96: Figure containing two pairs of mass spectra of TEVA Resin in 3 M hydrochloric acid analyzed using MALDI-TOF-MS, plotted as m/z or mass-to-charge ratio versus intensity. The top graph in each pair is the sample that received 50 kGy gamma exposure. The first pair of graphs is with the mass spectrometer with negative high voltage applied, and the bottom pair examines the same region with positive high voltage applied.

The spectra showing TEVA Resin irradiated in water and dry are in Appendix D.

7.3.3: Fragmentation of UTEVA Resin

Specifics of the more general analysis of UTEVA Resin via MALDI-TOF-MS are in section 6.3. The figure 97 below shows the impact of irradiation on UTEVA Resin. Each pair of spectra is

comprised of the mass spectrum generated from the sample irradiated with 50 kGy gamma radiation (top) and the unirradiated control that went through identical chemical processing (bottom). Figure 97 illustrates a wide mass range for UTEVA Resin in 3 M nitric acid. In the pair of reflector negative spectra presented in the figure below, there are peaks at 363 and 597 m/z in the spectrum generated from the irradiated sample that are not present in the spectrum generated from the unirradiated sample. The 363 and 597 m/z peaks are possibly complexes that formed after some of the DAAP extractant molecules broke under radiolysis. There is a notable peak at 292 m/z in the spectrum generated from the unirradiated sample (figure 97) that is likely the DAAP extractant itself which is not present in the spectrum generated from the irradiated sample. In both pairs of reflector positive spectra, there is a marked increase in the magnitude of the peak at 331 m/z in the spectrum generated from the unirradiated sample compared to the spectrum generated from the irradiated sample.

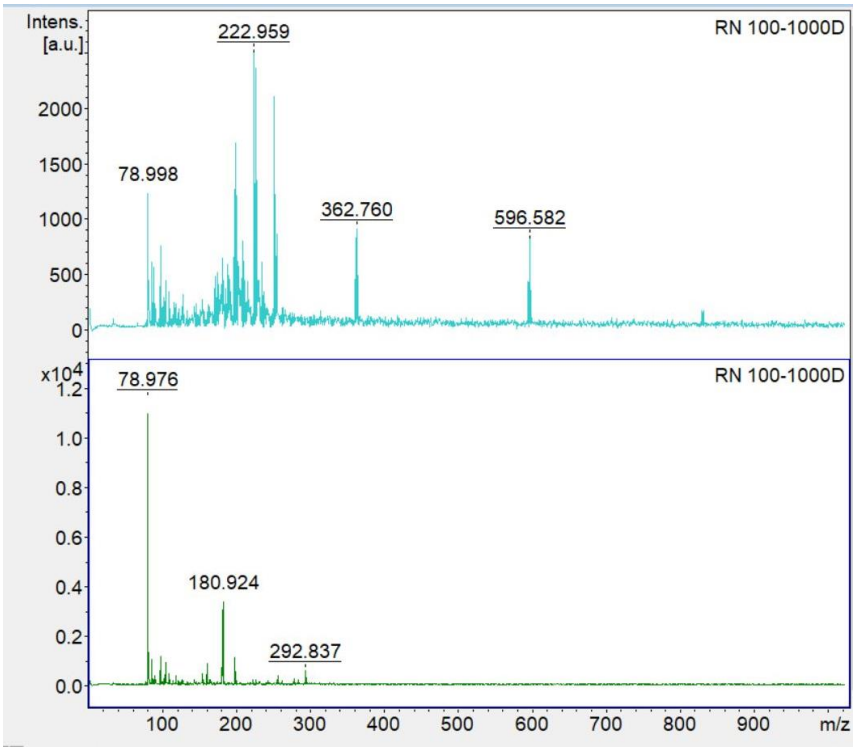

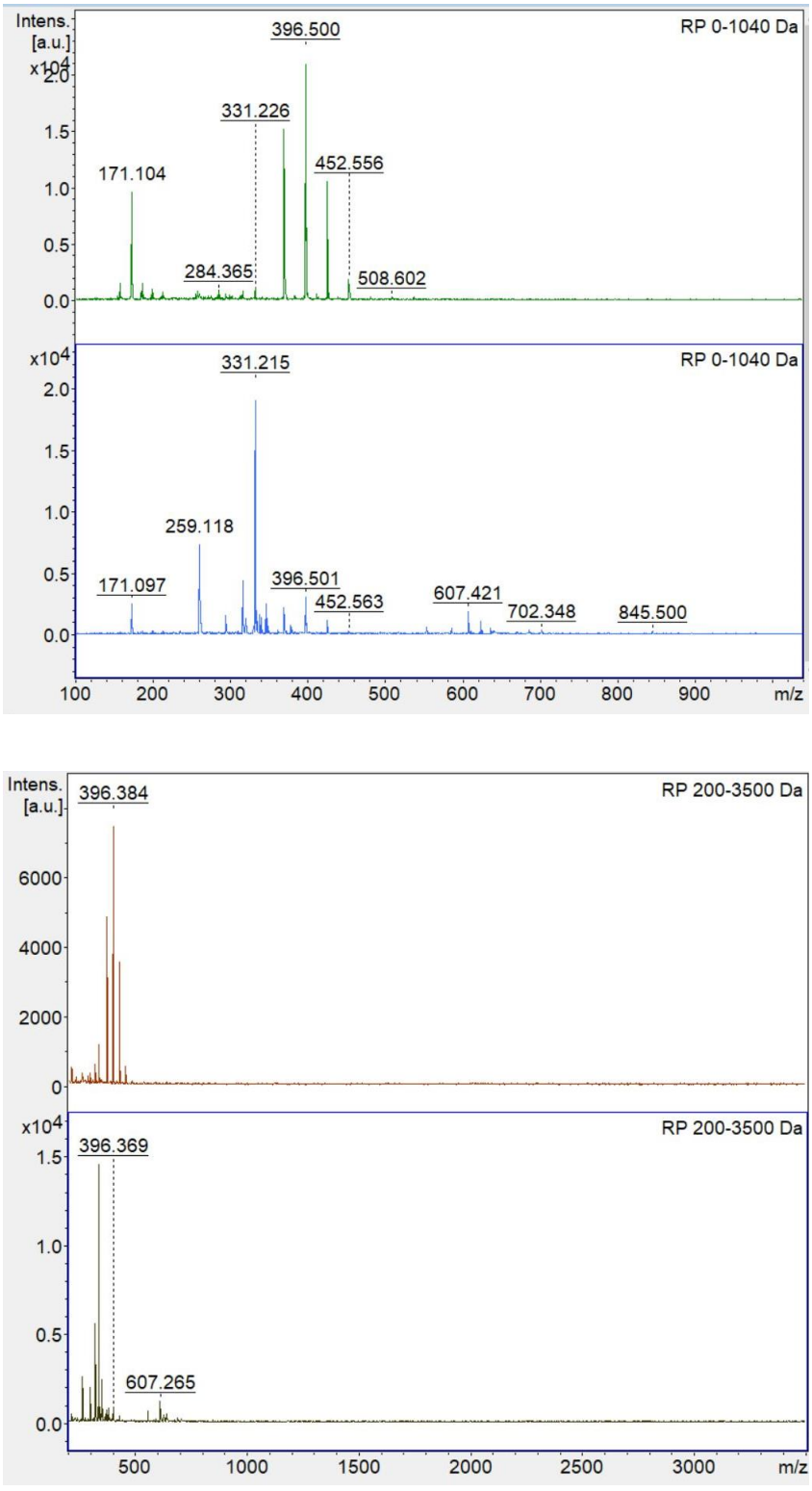

Figure 97: Figure containing three pairs of mass spectra of UTEVA Resin in 3 M nitric acid analyzed using MALDI-TOF-MS, plotted as m/z or mass-to-charge ratio versus intensity. The top graph in each pair is the sample that received 50 kGy gamma exposure. The first pair of graphs is with the mass spectrometer with negative high voltage applied, the middle pair examines the same region with high voltage applied, and the last pair examines a wider mass range using the positive high voltage.

Figure 98 specifically examines low mass-to-charge ratio fragments of UTEVA Resin in 3 M nitric acid, with irradiated and unirradiated paired spectra for ease of comparison. In the spectrum generated from the irradiated sample of UTEVA Resin in 3 M nitric acid, there are detectable peaks at 221 and 283 m/z that are not present in the spectrum generated from the unirradiated control sample. There are no detectable differences between the reflector positive spectra for irradiated and unirradiated UTEVA Resin in 3 M nitric acid below a mass to charge ratio of 300.

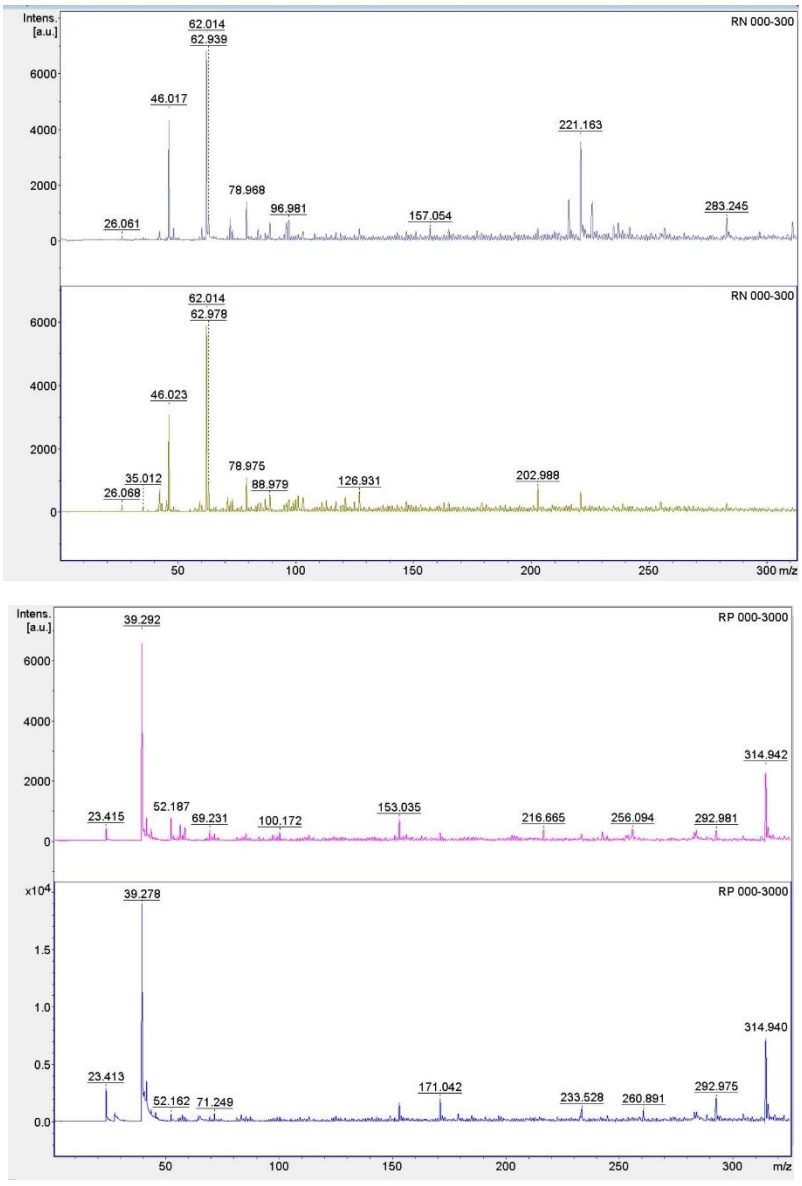

Figure 98: Figure containing two pairs of mass spectra of UTEVA Resin in 3 M nitric acid analyzed using MALDI-TOF-MS, plotted as m/z or mass-to-charge ratio versus intensity. The top graph in each pair is the sample that received 50 kGy gamma exposure. The first pair of graphs is with the mass spectrometer with negative high voltage applied, and the bottom pair illustrates the same region with positive high voltage applied.

The spectra of UTEVA Resin irradiated in 3 M hydrochloric acid, water, and without any aqueous layer (i.e., dry) did not present major detectable differences between the irradiated and unirradiated spectra contained in Appendix D.

7.3.4: Fragmentation of ACTINIDE Resin

Specifics of the more general analysis of the Actinide (DIPEX) Resin via MALDI-TOF-MS are in Section 6.3. Figure 99 shows the impact of irradiation on Actinide Resin. Each pair of spectra is comprised of the mass spectrum generated from the sample irradiated with 50 kGy gamma radiation (top) and the unirradiated control that went through identical chemical processing (bottom). Exposure to 50 kGy gamma radiation did not have marked effects on the retention of plutonium on the Actinide Resin. Overt differences between the mass spectra generated from the irradiated and the unirradiated Actinide (DIPEX) Resin samples was considered unlikely.

Figure 99 illustrates the wide mass range of the mass spectra gathered for Actinide Resin in 3 M nitric acid. The reflector negative spectrum generated from the irradiated sample has markedly more peaks in the 200-300 m/z range than the spectrum generated from the unirradiated sample. The spectrum generated from the irradiated sample also has peaks at 823 and 852 m/z that are not present in the unirradiated control sample of Actinide Resin in 3 M nitric acid. Both the spectrum generated from the irradiated sample of Actinide Resin in 3 M nitric acid and the spectrum generated from the unirradiated control sample show a main peak at 439 m/z and more peaks in the 600-800 m/z range in sequence. This could indicate that the DIPEX extractant

is more likely to interact with the polymer backbone of the resin; however, more study is needed.

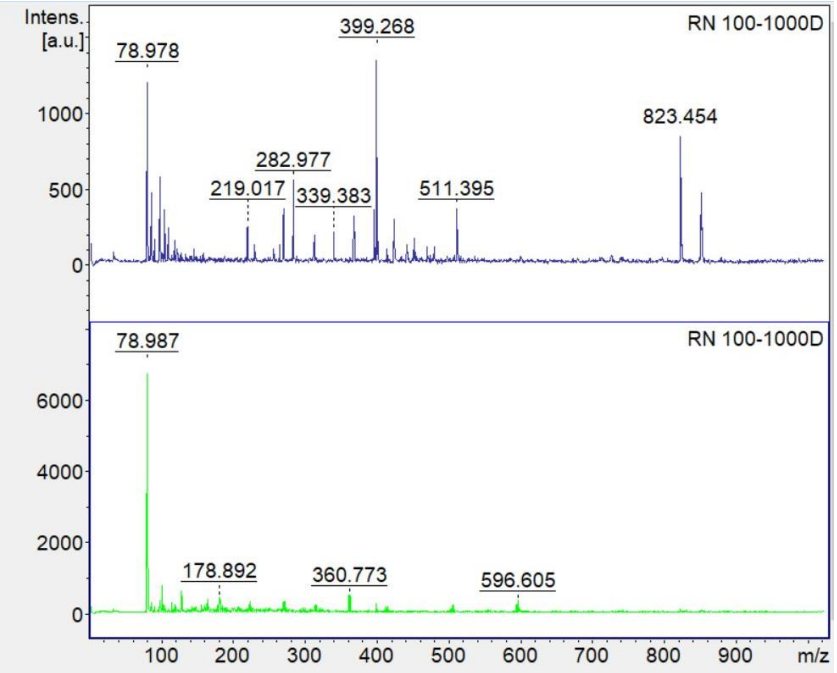

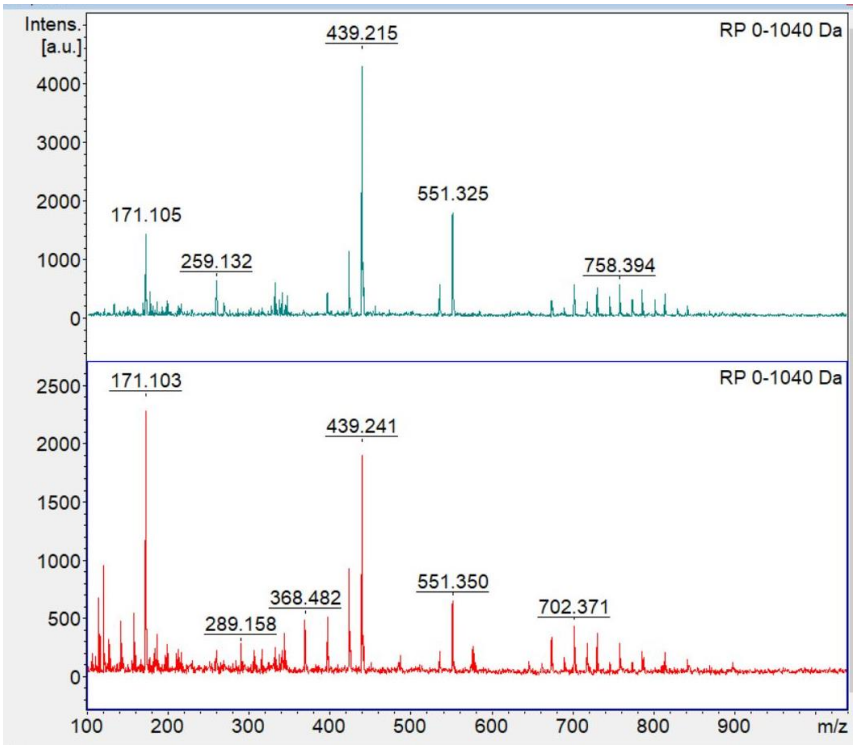

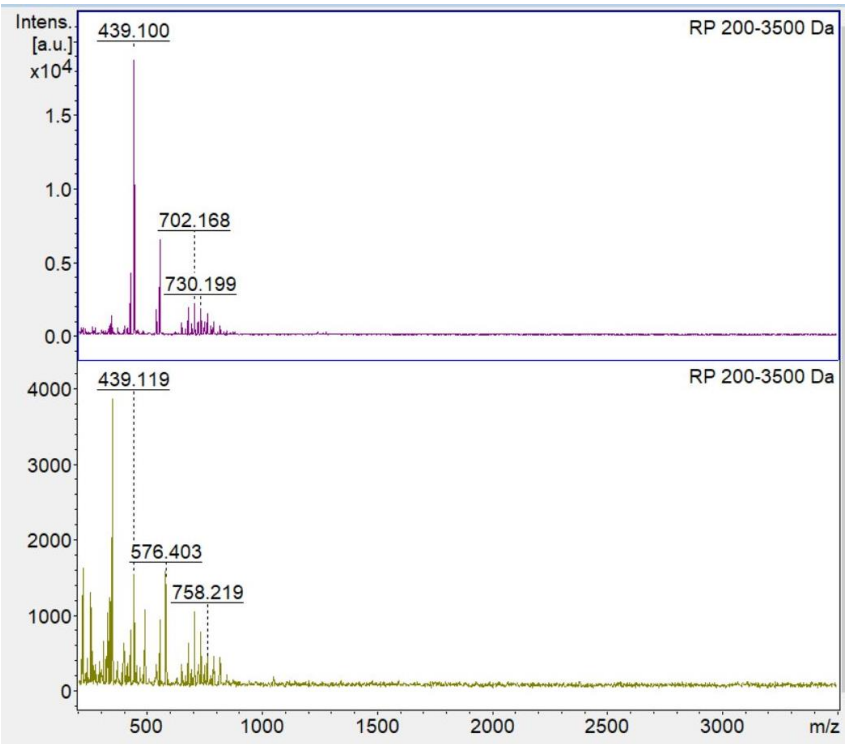

Figure 99: Figure containing three pairs of mass spectra of Actinide Resin in 3 M nitric acid analyzed using MALDI-TOF-MS, plotted as m/z or mass-to-charge ratio versus intensity. The top graph in each pair is the sample that received 50 kGy gamma exposure. The first pair of graphs is with the mass spectrometer with negative high voltage applied, the middle pair examines the same region with high voltage applied, and the last pair examines a wider mass range using the positive high voltage.

Figure 100 specifically examines low mass-to-charge ratio fragments of Actinide Resin in 3 M nitric acid, with irradiated and unirradiated paired spectra for ease of comparison.

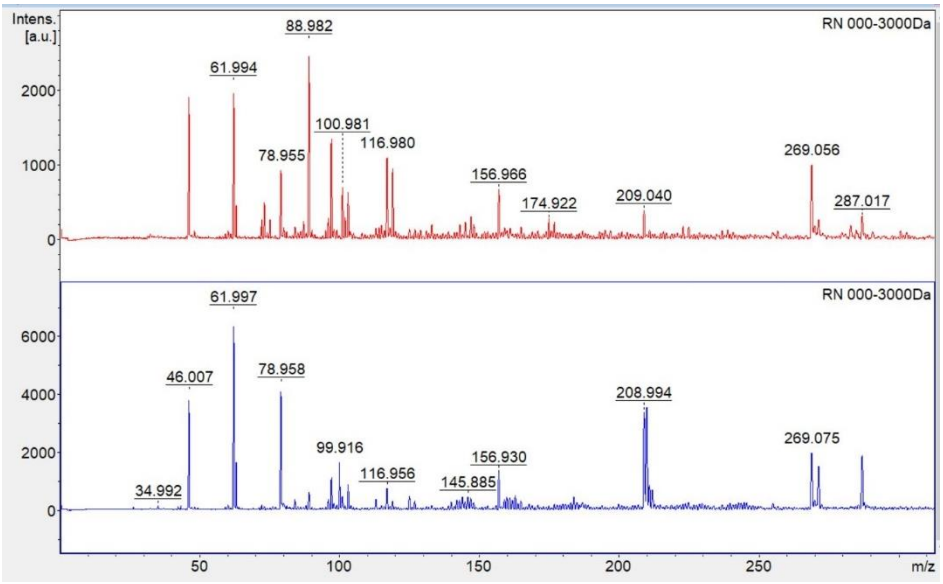

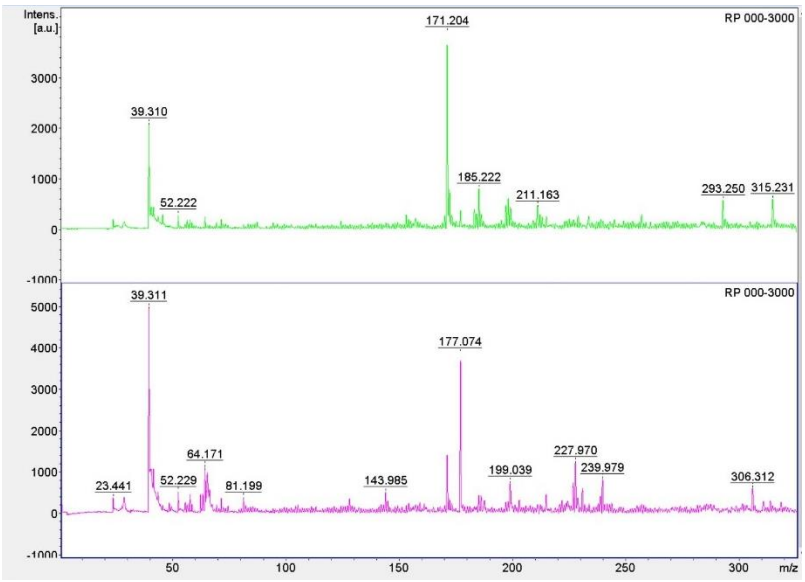

Figure 100: Figure containing two pairs of mass spectra of Actinide Resin in 3 M nitric acid analyzed using MALDI-TOF-MS, plotted as m/z or mass-to-charge ratio versus intensity. The top graph in each pair is the sample that received 50 kGy gamma exposure. The first pair of graphs is with the mass spectrometer with negative high voltage applied, and the bottom pair illustrates the same region with positive high voltage applied.

The spectra generated from the samples of the Actinide Resin irradiated in 3 M hydrochloric acid, water, and dry are in Appendix D as they did not demonstrate changes between the spectra generated from the irradiated and the unirradiated samples beyond what is demonstrated by the samples of the Actinide Resin shown in Figures 99 and 100.

7.4: Conclusions

Overall, MALDI can serve as a helpful tool for diagnosing changes in mass spectra from ionizing radiation. Ideally, a higher radiation dose would be used to interrogate the resins themselves. Generally, 50 kGy ionizing gamma radiation appears to have limited or no impact on the inert polymer backbone of extraction chromatographic resins. Within each irradiation condition, there may be small differences. TRU in hydrochloric acid and UTEVA and TEVA in nitric acid differences between the irradiated and unirradiated samples in the acid condition accompanied by changes in plutonium retention. Samples irradiated dry tended to result in even fewer

differences between the mass spectra generated for the irradiated and the unirradiated samples. This supports the hypothesis that changes inflicted upon materials by radiolysis are due to chemically reactive species in solution rather than the ionizing radiation interacting directly with the resin.

CONCLUSIONS

Herein is an executive summary of the conclusions from the entirety of this work.

The Cs-137 Irradiator in Room 470 of the Molecular and Radiological Biosciences Building at Colorado State University in Fort Collins, CO was characterized using Fricke Dosimetry. The dose rates in the locations most proximal to the source along with the position of the source when it is deployed were experimentally determined to be 8 Gy/min in the top row of the sample carousel and 6.6 Gy/min in the bottom row of the sample carousel.

The retention of plutonium was investigated on four irradiated extraction chromatography resins: TRU Resin, TEVA Resin, UTEVA Resin, and the Actinide Resin. The Actinide Resin proved the least susceptible to changes in plutonium retention from increasing absorbed dose of ionizing radiation up to 50 kGy. TRU, TEVA, and UTEVA Resins were all affected by the ionizing radiation to some degree. The retention of plutonium was enhanced as a result of increasing absorbed dose. Since there was no common impact across all resins, it is likely that the inert support, Amberchrom CG71, which all four resins share, is generally not changed by ionizing gamma radiation up to 50 kGy. TRU Resin is most affected in hydrochloric acid systems. TEVA and UTEVA Resins are more affected in nitric acid systems. There was no experimentally defined direct correlation between the concentration of the acid to the magnitude of the change on the resin.

Surface characterization of extraction chromatography materials is possible and effective when performed using FTIR. Mass spectra of extraction chromatography resins can be generated

using MALDI-TOF-MS. These spectra can be used to determine shifts in irradiated/unirradiated samples in terms of both the extractant and the polymer backbone.

FUTURE DIRECTIONS

There are several ways in which this research can be continued by further researchers. The first is using different types of radiation, such as those with higher linear energy transfer like charged particle irradiations, to determine differences in how the materials are affected. Another is contacting different analytes such as americium or uranium with the resins studied in this work to determine whether there are differences in how those heavy metals are retained versus how the plutonium was retained. A third manner in which this research may be continued is by the use of more resins, such as LN, DGA, or TK series resins that are also commercially available from either Eichrom of Triskem. Another manner in which this research can be continued is through the use of more surface functionalization analysis techniques: x-ray photoelectron spectroscopy (XPS), scanning electron microscopy (SEM), transmission electron microscopy (TEM), and atomic force microscopy (AFM).

REFERENCES

1. Rodgriguez, C. Pin and J. 15.8 Separation Methods Based on Liquid-Liquid Extraction, Extraction Chromatography, and Other Miscellaneous Solid Phase Extraction Processes. *Treatise of Geochemistry, 2nd Ed.* s.l. : Elsevier Ltd., 2014.

2. Triskem International. *Extraction Chromatography Technical Documentation - All Resins.* s.l. : Triskem International.

3. Robert M. Silverstein, G. Clayton Bassler, and Terence C. Morrill. *Spectrometric Identification of Organic Compounds, 4th Ed.* 4. New York : John Wiley & Sons, 1981.

4. Marie Curie Biographical. *NobelPrize.org.* [Online] 1903. [Cited: 09 15, 2023.] https://www.nobelprize.org/prizes/physics/1903/marie-curie/biographical/.

5. Hou, Jukka Lehto and Xiaolin. *Chemistry and Analysis of Radionuclides: Laboratory Techniques and Methodology.* Weinheim : Wiley-VCH Verlag GmbH & Co., 2011.

6. Lewis, Jason S., Windhorst, Albert D., and Zeglis, Brian M., [ed.]. *Radiopharmaceutical Chemistry.* s.l. : Spring Nature Switzerland, 2019.

7. IAEA (International Atomic Energy Agency). https://www-nds.iaea.org/relnsd/vcharthtml/VChartHTML.html. *IAEA Live Chart of Nuclides.* [Online]

8. Eichrom Technologies. TRU Resin. *Eichrom Technologies.* [Online] https://www.eichrom.com/products/tru-resin.

9. Morss, Norman M. Edelstein and Lester R. Radioelements: Actinides. [book auth.] Frank Rosch. *Nuclear- and Radiochemistry Volume 2: Modern Applications, 2nd extended edition.* Mainz : DE GRUYTER, 2022, Vol. 2, 9.

10. Attila Vertes, Sandor Nagy, Zoltan Klencsar, Rezso G. Lovas, Frank Rosch. *Handbook of Nuclear Chemistry, 2nd Ed.: Chemical Applications of Nuclear Reactions and Radiations.* s.l. : Springer Reference, 2011. Vol. 3.

11. *Generation of high atomic and molecular Rydberg states. In: Dobo J, SChiller R (eds) Proceedings of the 5th Tihany symposium on radiation chemistry.* J, Bednar. Budapest : s.n., 1983.

12. *Gamma radiation induces hydrogen absorption by copper in water.* Claudio M. Lousada, I. L. Soroka, Yuriy Yagodzinskyy, and Nadezda V. Tarakina. April 2006, Nature Portfolio: Scientific Reports, Vol. 6, pp. 1-8.

13. *Ion Yields and Fragmentation Processes in the Radiolysis of HCl and DCl.* Peter F. Carr, Patricia Christensen, Derek E. Wilson, and David A. Armstrong. 3, s.l. : National Research Council of Canada, 1974, Vol. 52.

14. Random House. dictionary.com. [Online] Random House. www.dictionary.com.

15. Harris, Daniel C. *Quantitative Chemical Analysis, 6th Ed.* New York : W.H. Freeman and Co., 2003.

16. Rohana Liyanage and Jackson O. Lay, Jr. An Introduction to MALDI-TOF MS. [book auth.] Jackson O. Lay, Jr., and J.D. Winefordner Charles L. Wilkins. *Identification of Mocroorganisms by Mass Spectrometry.* Hoboken : John Wiley and Sons, Inc., 2006.

17. Del Guerra, Alberto and Daniele Panetta. Radiation Measurement. [book auth.] Frank Rosch. *Nuclear- and Radiochemistry. Vol. 2 Modern Applications.* 2nd, extended edition. s.l. : DE GRUYTER, 2022, Vol. 2, 1, pp. 1-44.

18. (youtube), U.S. EPA. *Radionuclides in Drinking Water: 4.2 Liquid Scintillation Counting.* [web] January 19, 2017.

19. Sehested, K. The Fricke Dosimeter. [book auth.] R.J. Berry, and Marcel Dekker N.W. Holm. *Manual on Radiation Dosimetry.* 1970, pp. 313-317.

20. International, ASTM. *Standard Practice for Using the Fricke Dosimetry System.* West Conshohocken : ASTM International, 2018. ISO/ASTM 51026:2015(E).

21. Eichrom Technologies. TEVA Resin. *Eichrom Technologies.* [Online] https://www.eichrom.com/products/teva-resin/.

22. —. UTEVA Resin. *Eichrom Technologies.* [Online] https://www.eichrom.com/products/uteva-resin/.

23. —. Actinide Resin. *Eichrom TEchnologies.* [Online] https://www.eichrom.com/products/actinide-resin/.

24. *Laser desorption ionization of red phosphorus clusters and their use for mass calibration in time-of-flight mass spectrometry.* Katerina Sladkova, Jan Houska, Josef Havel. 19, s.l. : Wiley, October 1, 2009, RAPID COMMUNICATIONS IN MASS SPECTROMETRY, Vol. 23, pp. 3114-3118.

25. *Gamma Radiolysis of Phenyl-Substituted TODGAs: Part II .* Christopher Zarzana, et al. 5, 2023, Solvent Extraction and Ion Exchange, Vol. 41, pp. 582-605.

26. *Gamma Radiolysis of Phenyl-Substituted TODGAs: Part I.* Christopher Zarzana, et al. 5, 2023, Solvent Extraction and Ion Exchange, Vol. 41, pp. 564-581.

27. *Exploring how exposure to radiolysis and harsh chemical reagents impact americium-241 extraction chromatography.* Brian t. ARko, David Dan, Sara Adelman, David B. Kimball, Stosh A. Kozimor, Marki M. Martinez, Tara MAsteren, DAniel L. Huber, Veronika Mocko, Jung Rim, Jenifer C. Shafer, Benjamin W. Stein, and E. Miller Wylie. s.l. : Royal Society of Chemistry, 2023, Materials Advances, Vol. 4, pp. 265-283.

28. *Radiation stability of diglycolamide functionalized calix[4]arenes in ionic liquid: Solvent extraction, EPR and GC-MS studies.* A. Sengupta, P.K. Mohapatra, A.B. Patil, R.M. Kadam, and W. Verboom. s.l. : Elsevier Ltd., 2016, SEparation and Purification Technology, Vol. 162, pp. 77-863.

29. *Gamma radiolytic stability of the novel modified diglycolamide 2,2'-oxybis(N,N-didecylpropanamide) (mTDDGA) for grouped actinide extraction.* Bart Verlinden, Karen Van Hecke, Andreas Wilden, Michelle Hupert, Beatrix Santiago-Schubel, Richard J. M. Egberink, Willem Verboom, Piotr M. Kowalski, Giuseppe Modolo, Marc Verwerft, Koen Binnemans, and Thomas Cardinaels. s.l. : Royal Society of Chemistry, 2022, RSC Advances, Vol. 12, pp. 12416-12426.

30. *Gamma and beta radiolysis of tri-iso-amyl phosphate: Degredation of tri-iso-amyl phosphate and formation of di-ido-amyl phosphoric acid.* Fengzhen Li, Yilin Qin, Wei Liao, Feize Li, Tu Lan, Songdong Ding, Jiali Liao, Jijun Yang, Yuanyou Yang, Wen Feng, and Ning Liu. s.l. : Elsevier Ltd., 2022, Radiation Physics and Chemistry, Vol. 199, p. 110354.

31. *Grafted mesoporous silicas for radionuclide uptake: Radiolytic stability under electron irradiation.* Guillaume Zante, Vincent Bouniol, Saad Sene, Cyrielle Rey, Jeremy Causse, Joulia Larionova, Yannick Guari, Xavier Deschanels, and Sophie Le Caer. s.l. : Elsevier Ltd., 2022, Microporous and Mesoporous Materials, Vol. 336, p. 111851.

32. *Effect of irradiation on the hydrodynamic parameters and extraction efficiency of several frequently used ionic liquids.* P.K. Verma, R.B> Gujar, A.S. Kanekar, Y.K. Bhardwaj, and P.K. Mohapatra. s.l. : Elsevier Ltd., 2019, RAdiation Physics and Chemistry, Vol. 158, pp. 180-187.

33. *Catalytic degredation of lindane using gamma radiations: Degredation products.* Abdul Ghaffar, Tabata Masaaki, Rukhsanda Aziz, and Saima Sarfaz. s.l. : Elsevier Ltd., 2023, RAdiation Physics and Chemistry, Vol. 205, p. 110741.

34. *Gamma radiolysis of hydrophilic diglycolamide ligands in concentrated aqueous nitrate solution.* Gregory P. Horne, Andreas Wilden, Stephen P. Mezyk, Liam Twight, Michelle Hupert, Andrea Stark, Willem Verboom, Bruce J. Mincher, and Giuseppe Modolo. s.l. : Royal Society of Chemistry, 2019, Dalton Transactions, Vol. 48, pp. 17005-17013.

35. *Radiolytic degredation of a new diglycol-diamide ligand for actinide and lanthanide co-extraction from spent nuclear fuel.* Annalisa Ossola, Elena Macerata, Dario A. Tinonin, Federica Faroldi, Marco Giola, Mario Mariani, and Alessandro Casnati. s.l. : Elsevier Ltd., 2016, Radiation Physics and Chemistry, Vol. 124, pp. 246-251.

APPENDIX A: PICTURES OF IRRADIATION FACILITIES

Pictures of Irradiator

Pictures of Irradiation Chamber

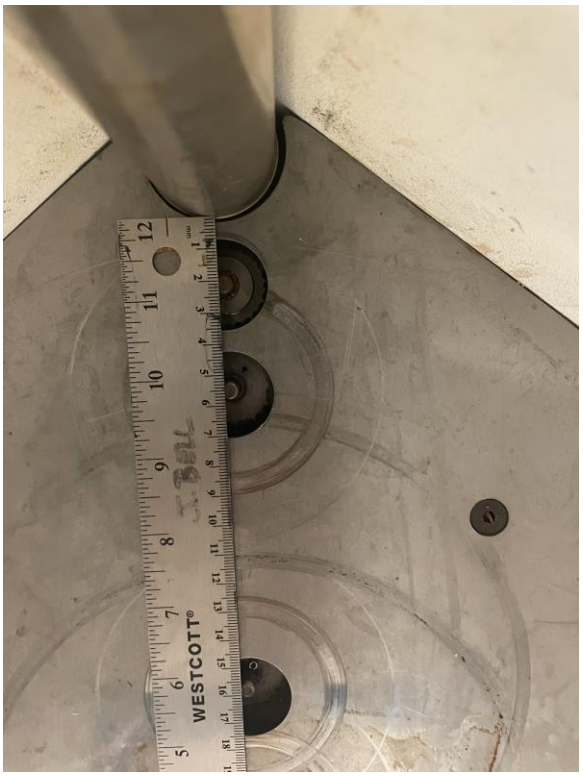
WESTCOTT


WESTCOTT
STAINLESS STEEL
U.S.A.

Pictures of Sample Carousel


mm
1
2
3
4
5
6
7
10
11

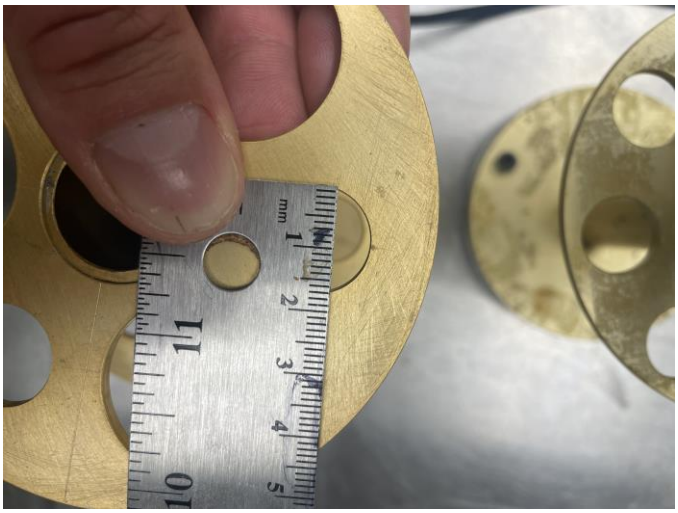

Pictures of 3D Printed Sample Holder

APPENDIX B: DATA FOR IRRADIATOR CHARACTERIZATION

Below are the data tables for the irradiation conditions. The first (table 5) was included in the body of Chapter 1. The others, however, were placed within this Appendix.

Table 32: Top Row of the Sample Carousel, 18-minute irradiation

	1	2	3	4	5	6	7	8	average	std dev
Wavelengt	Abs	Abs	Abs	Abs	Abs	Abs	Abs	Abs	Abs	
305	0.809332	0.764575	0.843757	0.848194	0.850992	0.847934	0.855006	0.861229	0.835127	0.03247
304.9	0.810619	0.765619	0.845266	0.84963	0.85237	0.849626	0.856666	0.862621	0.836552	0.032637
304.8	0.811795	0.766983	0.846722	0.850688	0.853694	0.850906	0.857827	0.864106	0.83784	0.032633
304.7	0.813341	0.76799	0.848156	0.851973	0.854794	0.852233	0.859253	0.865297	0.83913	0.032687
304.6	0.813823	0.76905	0.849537	0.853518	0.856579	0.853595	0.860718	0.866777	0.84045	0.032944
304.5	0.815643	0.770217	0.850835	0.854681	0.857895	0.855297	0.861955	0.868552	0.841885	0.032991
304.4	0.816962	0.771216	0.852282	0.856011	0.859148	0.856417	0.863367	0.869747	0.843144	0.033074
304.3	0.818141	0.772477	0.853514	0.857319	0.860475	0.85798	0.864773	0.871299	0.844497	0.033153
304.2	0.819728	0.773831	0.854961	0.858685	0.861885	0.85968	0.866386	0.872953	0.846014	0.033212
304.1	0.821252	0.775561	0.856776	0.860498	0.863744	0.861575	0.867869	0.874704	0.847747	0.033243
304	0.822788	0.776579	0.858024	0.861781	0.865295	0.862804	0.86899	0.875746	0.849001	0.033269
303.9	0.824059	0.777993	0.859518	0.863451	0.866658	0.864553	0.870515	0.877438	0.850523	0.03336
303.8	0.825435	0.779582	0.860946	0.864905	0.868363	0.866048	0.871997	0.878976	0.852032	0.033358
303.7	0.827073	0.780627	0.862945	0.866446	0.869793	0.867863	0.873483	0.880438	0.853583	0.033514
303.6	0.828515	0.782144	0.864247	0.868019	0.870996	0.868911	0.874876	0.881964	0.854959	0.033458
303.5	0.829982	0.783177	0.8654	0.869113	0.872511	0.870581	0.876555	0.883083	0.8563	0.033554
303.4	0.831521	0.784599	0.867284	0.871081	0.874636	0.872428	0.878066	0.884438	0.858007	0.033664
303.3	0.832954	0.786019	0.86879	0.872406	0.876175	0.873838	0.879785	0.886694	0.859583	0.033788
303.2	0.834553	0.78727	0.870651	0.87409	0.877662	0.875631	0.881604	0.888253	0.861214	0.03393
303.1	0.836066	0.788639	0.872234	0.87536	0.879227	0.877071	0.883135	0.889921	0.862707	0.033983
303	0.837231	0.790087	0.874268	0.877568	0.880831	0.879079	0.884827	0.892009	0.864487	0.034218
302.9	0.839083	0.79169	0.875834	0.879041	0.882509	0.880951	0.88659	0.893751	0.866181	0.034233
302.8	0.840897	0.79309	0.87741	0.880819	0.884452	0.882837	0.888167	0.895609	0.86791	0.034348
302.7	0.842562	0.794518	0.879274	0.882359	0.886074	0.884616	0.889597	0.8974	0.86955	0.034423
302.6	0.844183	0.796037	0.881063	0.884435	0.887976	0.886552	0.891703	0.899211	0.871395	0.034587
302.5	0.845834	0.797553	0.882787	0.886272	0.889976	0.888332	0.893226	0.900888	0.873108	0.034666
302.4	0.847676	0.799116	0.884662	0.887912	0.891853	0.890263	0.895118	0.902864	0.874933	0.034771
302.3	0.849284	0.800687	0.886356	0.889862	0.893555	0.892022	0.897135	0.904613	0.876689	0.03487
302.2	0.850826	0.802313	0.888242	0.891623	0.895521	0.893776	0.898763	0.906335	0.878425	0.03494
302.1	0.853032	0.80366	0.89008	0.893352	0.897284	0.896251	0.900679	0.908408	0.880343	0.035115
302	0.854786	0.805587	0.891745	0.895349	0.899355	0.89794	0.902803	0.910146	0.882214	0.035117
	0.830612	0.783822	0.866567	0.870208	0.873622	0.871535	0.877466	0.88437	**0.857275**	**0.033749**
								0.857275		

Table 33: Bottom Row of the Sample Carousel, 18-minute irradiation

	9	10	11	12	13	14	15	16	average	std dev
Wavelengt	Abs	Abs	Abs	Abs	Abs	Abs	Abs	Abs	Abs	
305	0.476582	0.641562	0.821933	0.866553	0.699398	0.730726	0.606427	0.818703	0.707736	0.130521
304.9	0.477276	0.642293	0.82325	0.867825	0.700382	0.731687	0.607194	0.819719	0.708703	0.130732
304.8	0.477781	0.643059	0.824695	0.869408	0.701297	0.732679	0.60786	0.820938	0.709715	0.131095
304.7	0.478275	0.643992	0.825797	0.871029	0.702325	0.733754	0.608626	0.822172	0.710746	0.131405
304.6	0.478709	0.644713	0.827512	0.872523	0.703214	0.734681	0.60924	0.823215	0.711726	0.131791
304.5	0.479396	0.645697	0.82866	0.873783	0.704284	0.735755	0.610148	0.824556	0.712785	0.131988
304.4	0.479926	0.646312	0.829795	0.87557	0.705128	0.736966	0.610767	0.825467	0.713741	0.132327
304.3	0.480207	0.647279	0.831214	0.87691	0.706423	0.737786	0.611412	0.826684	0.714739	0.132681
304.2	0.480874	0.648283	0.832931	0.878509	0.707588	0.738945	0.61208	0.828328	0.715942	0.133077
304.1	0.481636	0.649331	0.834425	0.880113	0.708621	0.740131	0.612984	0.82963	0.717109	0.133352
304	0.482014	0.650211	0.835468	0.881452	0.709438	0.741015	0.613732	0.831032	0.718045	0.133658
303.9	0.482684	0.651031	0.83712	0.883263	0.710797	0.742285	0.614484	0.83223	0.719237	0.134033
303.8	0.483211	0.652055	0.838526	0.884935	0.7119	0.74344	0.615423	0.833566	0.720382	0.134369
303.7	0.483767	0.652869	0.839979	0.886393	0.712794	0.74444	0.616076	0.834955	0.721409	0.134718
303.6	0.484175	0.653567	0.841316	0.888253	0.713987	0.745756	0.616751	0.836273	0.72251	0.135162
303.5	0.484682	0.654455	0.842638	0.889833	0.715011	0.746634	0.617566	0.837825	0.72358	0.135521
303.4	0.485179	0.655252	0.843747	0.891144	0.716335	0.747681	0.618307	0.838951	0.724575	0.135773
303.3	0.485899	0.656233	0.845354	0.892975	0.716978	0.748708	0.618617	0.840071	0.725604	0.136162
303.2	0.486282	0.656915	0.847035	0.894966	0.718492	0.74994	0.619582	0.841646	0.726857	0.136674
303.1	0.48686	0.657912	0.848643	0.896607	0.719643	0.75114	0.620356	0.843112	0.728034	0.137054
303	0.487339	0.658825	0.850287	0.898536	0.720779	0.752418	0.621445	0.844466	0.729262	0.137474
302.9	0.488083	0.660003	0.851633	0.900218	0.721932	0.753621	0.622154	0.845926	0.730446	0.13778
302.8	0.488599	0.660917	0.853417	0.902313	0.723097	0.754902	0.623111	0.847245	0.7317	0.138247
302.7	0.489019	0.662011	0.855065	0.90406	0.724441	0.7562	0.62389	0.849107	0.732974	0.138731
302.6	0.489848	0.662774	0.856963	0.905932	0.725432	0.757505	0.62483	0.850434	0.734215	0.139112
302.5	0.490407	0.664126	0.858186	0.907857	0.726725	0.758579	0.625608	0.852036	0.73544	0.139484
302.4	0.490947	0.665026	0.860273	0.909748	0.728137	0.760044	0.626697	0.853702	0.736822	0.139977
302.3	0.491621	0.665937	0.861675	0.91183	0.729292	0.761411	0.627424	0.855327	0.738065	0.14042
302.2	0.492155	0.666972	0.863613	0.913294	0.730346	0.762499	0.628325	0.856514	0.739215	0.14077
302.1	0.492998	0.668034	0.865157	0.915677	0.731807	0.763972	0.62901	0.858576	0.740654	0.141287
302	0.493589	0.668985	0.867162	0.917634	0.733435	0.765214	0.630218	0.860229	0.742058	0.141743
		0.65473	0.843338	0.890617	0.715467	0.747113	0.617753	0.83815	**0.724001**	**0.135714**
								0.758167		

Table 34:Top Row of the Sample Carousel, 15-minute irradiation. This irradiation condition was removed from the study after outlier testing. It was determined that the Fricke solution was insufficiently aerated.

	17	18	19	20	21	22	23	24	average	std dev
Wavelengt	Abs	Abs	Abs	Abs	Abs	Abs	Abs	Abs	Abs	
305	0.28711	0.425342	0.487457	0.342252	0.073548	0.266755	0.325572	0.375736	0.322972	0.123841
304.9	0.287348	0.425754	0.487967	0.34265	0.073688	0.267021	0.325974	0.376304	0.323338	0.123964
304.8	0.287826	0.426189	0.488525	0.343101	0.073808	0.267232	0.32639	0.376733	0.323725	0.12409
304.7	0.288066	0.426792	0.489236	0.343308	0.074008	0.267657	0.326794	0.377176	0.32413	0.124234
304.6	0.288343	0.426962	0.489606	0.343675	0.07389	0.267719	0.327012	0.377451	0.324332	0.124369
304.5	0.28877	0.427666	0.490427	0.344108	0.074201	0.268007	0.327457	0.378044	0.324835	0.124529
304.4	0.28891	0.428013	0.490962	0.344319	0.074154	0.268298	0.327598	0.378184	0.325055	0.124674
304.3	0.289026	0.428474	0.491501	0.344644	0.074254	0.268578	0.328008	0.378519	0.325375	0.124808
304.2	0.289503	0.429046	0.492118	0.345119	0.074485	0.268835	0.328597	0.378922	0.325828	0.124926
304.1	0.289875	0.429641	0.492899	0.345257	0.074444	0.269309	0.328729	0.37961	0.32622	0.125156
304	0.290071	0.429933	0.493534	0.345779	0.074537	0.269376	0.329108	0.379916	0.326532	0.125303
303.9	0.290327	0.43052	0.49402	0.346094	0.074743	0.269678	0.329404	0.380164	0.326869	0.125398
303.8	0.290631	0.431282	0.494757	0.34644	0.07466	0.269954	0.329818	0.380666	0.327276	0.125661
303.7	0.290928	0.431806	0.495368	0.346917	0.074716	0.270199	0.329836	0.381123	0.327612	0.125833
303.6	0.29128	0.43223	0.496096	0.347239	0.07478	0.270405	0.330498	0.381583	0.328014	0.126012
303.5	0.291633	0.432834	0.496533	0.347736	0.074987	0.270665	0.330718	0.381901	0.328376	0.126106
303.4	0.291693	0.433501	0.49732	0.347905	0.074951	0.270869	0.331075	0.382226	0.328692	0.126354
303.3	0.292014	0.433819	0.497726	0.348367	0.074902	0.270903	0.331376	0.382715	0.328978	0.126508
303.2	0.292197	0.434351	0.498206	0.348452	0.074933	0.271414	0.331642	0.382989	0.329273	0.126632
303.1	0.292404	0.434731	0.499031	0.349119	0.074925	0.271581	0.331774	0.383455	0.329628	0.12686
303	0.292784	0.435323	0.499616	0.34935	0.075046	0.271894	0.332353	0.383764	0.330016	0.126996
302.9	0.293129	0.435888	0.500241	0.349694	0.075268	0.272071	0.332946	0.384499	0.330467	0.127146
302.8	0.293633	0.436405	0.500968	0.350254	0.075236	0.272451	0.33302	0.385022	0.330874	0.127353
302.7	0.293925	0.436932	0.501795	0.350572	0.075295	0.272793	0.333421	0.385402	0.331267	0.127553
302.6	0.294277	0.437446	0.502577	0.350821	0.07553	0.273127	0.333945	0.386078	0.331725	0.127707
302.5	0.294584	0.438046	0.503231	0.351662	0.07553	0.273467	0.33419	0.386543	0.332157	0.127915
302.4	0.295012	0.43868	0.503967	0.351966	0.075609	0.273703	0.334788	0.387083	0.332601	0.128115
302.3	0.295132	0.439441	0.504808	0.352324	0.075783	0.274092	0.335152	0.387456	0.333024	0.128317
302.2	0.295557	0.43991	0.505724	0.352676	0.075863	0.274342	0.335505	0.387724	0.333412	0.128515
302.1	0.29598	0.440586	0.506203	0.353105	0.075909	0.274555	0.335859	0.388485	0.333835	0.128697
302	0.296205	0.441149	0.506889	0.353542	0.076022	0.275061	0.336432	0.388801	0.334263	0.12885
	0.291554	0.432861	0.496752	0.347692	0.074829	0.27071	0.330806	0.382073	**0.32841**	**0.126207**
								0.32841		

Table 35: Bottom Row of the Sample Carousel, 15-minute irradiation

	25	26	27	28	29	30	31	32	average	std dev
Wavelengt	Abs	Abs	Abs	Abs	Abs	Abs	Abs	Abs	Abs	
305	0.494979	0.323082	0.573972	0.78266	0.438539	0.76883	0.760326	0.791859	0.616781	0.183844
304.9	0.495451	0.323413	0.5747	0.783679	0.438818	0.770302	0.761328	0.793426	0.617639	0.184291
304.8	0.495889	0.32365	0.575621	0.785086	0.439632	0.771128	0.762534	0.794579	0.618515	0.184622
304.7	0.496697	0.324084	0.576334	0.786842	0.439997	0.773036	0.763902	0.795894	0.619598	0.185156
304.6	0.49724	0.324479	0.577256	0.788038	0.440365	0.774403	0.765069	0.79712	0.620496	0.185546
304.5	0.49795	0.324868	0.577859	0.789562	0.440963	0.775743	0.766325	0.798588	0.621482	0.185981
304.4	0.498526	0.325168	0.578843	0.790962	0.441543	0.777104	0.767469	0.799875	0.622436	0.186389
304.3	0.499308	0.325344	0.579907	0.792732	0.441882	0.779242	0.768935	0.801107	0.623557	0.187005
304.2	0.499851	0.325736	0.580676	0.793895	0.442868	0.780068	0.770321	0.802749	0.624521	0.187327
304.1	0.500402	0.326247	0.581747	0.795623	0.443053	0.782219	0.771734	0.804381	0.625676	0.187955
304	0.501163	0.326668	0.58264	0.79711	0.4439	0.783603	0.772927	0.805589	0.6267	0.188292
303.9	0.501788	0.326887	0.583354	0.798593	0.444427	0.784857	0.774465	0.806963	0.627667	0.188784
303.8	0.502377	0.327318	0.584188	0.800108	0.444921	0.786881	0.775921	0.808386	0.628762	0.189325
303.7	0.502981	0.327767	0.585062	0.801778	0.445447	0.788454	0.777305	0.809836	0.629829	0.189817
303.6	0.503838	0.327958	0.586329	0.803282	0.446041	0.789713	0.778616	0.811294	0.630884	0.190254
303.5	0.504324	0.328534	0.586979	0.804705	0.446584	0.791595	0.78017	0.812833	0.631965	0.19077
303.4	0.504807	0.328625	0.587867	0.806257	0.447292	0.792888	0.781545	0.813921	0.6329	0.19123
303.3	0.505562	0.32896	0.588716	0.807904	0.447594	0.794505	0.782812	0.815806	0.633982	0.191813
303.2	0.506036	0.329371	0.589718	0.809944	0.44835	0.796581	0.784522	0.81719	0.635214	0.192425
303.1	0.506769	0.329791	0.590645	0.8113	0.449035	0.797964	0.785907	0.818595	0.636251	0.192818
303	0.507411	0.330363	0.591421	0.813223	0.449547	0.799641	0.787272	0.820346	0.637403	0.193368
302.9	0.508289	0.33063	0.592575	0.81517	0.450123	0.801311	0.788698	0.821981	0.638597	0.193936
302.8	0.508835	0.331103	0.593553	0.816893	0.450946	0.803268	0.790479	0.823773	0.639856	0.194527
302.7	0.509542	0.331518	0.594234	0.818558	0.451569	0.805153	0.792136	0.825631	0.641043	0.195132
302.6	0.510217	0.331906	0.595199	0.8205	0.452035	0.807155	0.793713	0.827122	0.642231	0.19575
302.5	0.511134	0.332426	0.596578	0.822479	0.452881	0.809114	0.795368	0.828763	0.643593	0.196277
302.4	0.511902	0.332799	0.59739	0.824333	0.453375	0.811046	0.79711	0.83081	0.644846	0.196965
302.3	0.512616	0.333063	0.598473	0.826197	0.453785	0.812653	0.798666	0.832486	0.645992	0.197576
302.2	0.513228	0.333616	0.599303	0.828105	0.454466	0.814504	0.800523	0.834225	0.647246	0.19818
302.1	0.51406	0.33391	0.600526	0.830194	0.455342	0.81634	0.802252	0.836224	0.648606	0.198823
302	0.514868	0.33452	0.601493	0.832227	0.455814	0.818601	0.804087	0.838253	0.649983	0.199522
	0.504453	0.32851	0.587199	0.80574	0.446811	0.79219	0.780724	0.813536	**0.632395**	**0.191087**
								0.632395		

Table 36: Top Row of the Sample Carousel, 12-minute irradiation

	33	34	35	36	37	38	39	40	average	std dev
Wavelengt	Abs	Abs	Abs	Abs	Abs	Abs	Abs	Abs	Abs	
305	0.580977	0.662914	0.653607	0.663861	0.577626	0.614254	0.64528	0.669838	0.633545	0.03761
304.9	0.581931	0.664091	0.654872	0.664975	0.578308	0.61529	0.646506	0.671207	0.634647	0.037798
304.8	0.583013	0.665285	0.655942	0.666539	0.579462	0.616448	0.647711	0.672291	0.635836	0.03785
304.7	0.583923	0.666754	0.657342	0.667839	0.580645	0.617722	0.64884	0.673551	0.637077	0.037968
304.6	0.585272	0.668225	0.658541	0.669027	0.581457	0.618749	0.650031	0.674704	0.638251	0.038055
304.5	0.585958	0.669534	0.659963	0.670641	0.582908	0.619968	0.651673	0.676249	0.639612	0.038247
304.4	0.586955	0.670748	0.661408	0.672023	0.583738	0.621188	0.652465	0.677431	0.640745	0.038386
304.3	0.588319	0.672285	0.662703	0.673436	0.58496	0.622588	0.654113	0.678845	0.642156	0.038453
304.2	0.589314	0.67403	0.664044	0.674878	0.586149	0.623629	0.655212	0.680385	0.643455	0.03865
304.1	0.590481	0.675458	0.665799	0.676626	0.587409	0.624904	0.656451	0.68165	0.644847	0.038781
304	0.591525	0.676673	0.667113	0.677985	0.588364	0.62621	0.65801	0.682998	0.64611	0.03892
303.9	0.592671	0.67828	0.668765	0.679417	0.58975	0.627604	0.659221	0.684634	0.647543	0.039045
303.8	0.593665	0.67987	0.670015	0.681016	0.590652	0.628963	0.660352	0.685917	0.648806	0.039241
303.7	0.594976	0.681384	0.671402	0.682777	0.5921	0.630255	0.661991	0.68758	0.650308	0.039356
303.6	0.595969	0.683208	0.67323	0.683967	0.593257	0.63131	0.663455	0.68885	0.651656	0.039556
303.5	0.597121	0.684598	0.674617	0.685421	0.594061	0.632812	0.664806	0.690289	0.652966	0.039732
303.4	0.598258	0.68617	0.67616	0.687117	0.595326	0.633689	0.666011	0.69188	0.654327	0.039934
303.3	0.599174	0.687856	0.677791	0.688625	0.596434	0.635433	0.66767	0.693471	0.655807	0.040168
303.2	0.600552	0.689665	0.679363	0.690356	0.597699	0.636855	0.668839	0.695116	0.657306	0.040322
303.1	0.601728	0.690987	0.680972	0.69171	0.598943	0.638272	0.670488	0.696376	0.658684	0.040392
303	0.603109	0.692861	0.682627	0.693474	0.600342	0.639698	0.672119	0.698277	0.660313	0.040588
302.9	0.604166	0.694698	0.684188	0.695226	0.601471	0.641313	0.67365	0.699921	0.661829	0.04084
302.8	0.605677	0.696655	0.686053	0.696985	0.602817	0.642909	0.675146	0.70162	0.663483	0.041001
302.7	0.606906	0.698114	0.687725	0.698851	0.604292	0.644185	0.676961	0.703247	0.665035	0.041159
302.6	0.608188	0.699995	0.689435	0.700661	0.605725	0.645503	0.678548	0.704966	0.666628	0.04136
302.5	0.60929	0.701941	0.691018	0.702493	0.606967	0.647433	0.680445	0.706692	0.668285	0.041606
302.4	0.610981	0.703851	0.693148	0.704141	0.608474	0.649028	0.681975	0.708597	0.670024	0.041729
302.3	0.612342	0.705485	0.694979	0.706071	0.609978	0.650284	0.683866	0.71007	0.671634	0.041878
302.2	0.613442	0.70747	0.696593	0.707892	0.611074	0.652054	0.6854	0.711895	0.673228	0.042172
302.1	0.614768	0.709382	0.698634	0.709996	0.612471	0.653533	0.687014	0.713966	0.674971	0.042471
302	0.616163	0.711321	0.700581	0.711768	0.614122	0.655315	0.689056	0.715571	0.676737	0.042595
	0.597639	0.685477	0.67544	0.686316	0.594741	0.633464	0.66559	0.691228	**0.653737**	**0.039867**
								0.653737		

Table 37: Bottom Row of the Sample Carousel, 12-minute irradiation

	41	42	43	44	45	46	47	48	average	std dev
Wavelengt	Abs	Abs	Abs	Abs	Abs	Abs	Abs	Abs	Abs	
305	0.243567	0.427217	0.581762	0.653872	0.37586	0.580371	0.667813	0.701706	0.529021	0.162743
304.9	0.243741	0.427847	0.583028	0.655066	0.376271	0.581212	0.668804	0.70281	0.529847	0.163103
304.8	0.244043	0.428168	0.583777	0.656358	0.376886	0.582156	0.669921	0.704327	0.530704	0.163501
304.7	0.244297	0.428819	0.5848	0.657666	0.377331	0.583125	0.671408	0.705608	0.531632	0.163929
304.6	0.244718	0.429345	0.585874	0.658875	0.377641	0.584277	0.672371	0.706802	0.532488	0.164267
304.5	0.244829	0.430229	0.587049	0.66019	0.378258	0.585263	0.673656	0.708364	0.53348	0.164714
304.4	0.245149	0.430503	0.588065	0.661226	0.378738	0.586195	0.674719	0.709591	0.534273	0.165063
304.3	0.245481	0.431409	0.589123	0.662535	0.379154	0.58757	0.67625	0.710875	0.5353	0.165478
304.2	0.245679	0.432074	0.59035	0.664095	0.37984	0.588301	0.677403	0.712404	0.536268	0.16591
304.1	0.245994	0.432514	0.591466	0.665588	0.380274	0.589741	0.678916	0.71417	0.537333	0.166466
304	0.246274	0.433341	0.592554	0.666898	0.380826	0.590759	0.680168	0.715432	0.538281	0.166831
303.9	0.246476	0.433881	0.593544	0.668155	0.381217	0.591876	0.681604	0.717208	0.539245	0.167358
303.8	0.246815	0.434832	0.595026	0.669529	0.38197	0.592938	0.682962	0.718314	0.540298	0.167687
303.7	0.247037	0.435317	0.596242	0.671196	0.382399	0.594068	0.684402	0.720225	0.54136	0.168286
303.6	0.247347	0.436224	0.597191	0.672393	0.383001	0.595223	0.685383	0.721601	0.542295	0.168601
303.5	0.247538	0.436681	0.598143	0.673492	0.383305	0.596211	0.686831	0.723272	0.543184	0.169111
303.4	0.247942	0.437181	0.599126	0.675079	0.38385	0.597486	0.688196	0.724613	0.544184	0.169539
303.3	0.248091	0.43796	0.600404	0.676742	0.384602	0.598591	0.689681	0.726333	0.5453	0.170063
303.2	0.248326	0.438459	0.601764	0.678243	0.38497	0.599781	0.691282	0.727912	0.546342	0.170626
303.1	0.248543	0.439157	0.602991	0.679655	0.385489	0.600787	0.692708	0.729519	0.547356	0.171114
303	0.24896	0.440074	0.604075	0.681062	0.386015	0.602414	0.694114	0.731184	0.548487	0.171559
302.9	0.249299	0.440584	0.605453	0.682833	0.386814	0.603251	0.695777	0.732958	0.549621	0.172089
302.8	0.249765	0.441322	0.606848	0.684797	0.38746	0.604876	0.697498	0.734787	0.550919	0.17266
302.7	0.250052	0.442251	0.608052	0.686081	0.387873	0.606081	0.698738	0.736512	0.551955	0.173113
302.6	0.250445	0.442935	0.609417	0.687915	0.388514	0.607373	0.700631	0.738361	0.553199	0.173701
302.5	0.250848	0.443495	0.610743	0.689609	0.389298	0.608726	0.70223	0.740164	0.554389	0.174221
302.4	0.250872	0.444411	0.612107	0.691337	0.389684	0.61015	0.703768	0.742376	0.555588	0.174921
302.3	0.251483	0.445208	0.613548	0.693012	0.390295	0.611543	0.70547	0.744015	0.556822	0.175385
302.2	0.251604	0.445782	0.614763	0.694603	0.391056	0.612694	0.707222	0.745978	0.557963	0.175995
302.1	0.252082	0.446524	0.616104	0.696353	0.391702	0.614078	0.708516	0.747827	0.559148	0.176477
302	0.252312	0.447277	0.617584	0.69805	0.39239	0.615246	0.710717	0.749783	0.56042	0.177131
	0.247729	0.436807	0.598741	0.674597	0.383645	0.59685	0.687715	0.724033	**0.543765**	**0.169408**
								0.543765		

Table 38: Top Row of the Sample Carousel, 9-minute irradiation

	49	50	51	52	53	54	55	56	average	std dev
Wavelengt	Abs	Abs	Abs	Abs	Abs	Abs	Abs	Abs	Abs	
305	0.547959	0.587728	0.562872	0.549762	0.367061	0.387906	0.510723	0.528196	0.505276	0.082246
304.9	0.548935	0.589094	0.564201	0.550784	0.367471	0.388354	0.51166	0.529245	0.506218	0.082587
304.8	0.549868	0.590099	0.565249	0.551875	0.367981	0.388972	0.51274	0.530121	0.507113	0.082785
304.7	0.551288	0.591663	0.566566	0.552984	0.368541	0.389644	0.513365	0.53131	0.50817	0.083114
304.6	0.552277	0.59302	0.567678	0.554161	0.369077	0.390283	0.51477	0.532132	0.509175	0.083371
304.5	0.553146	0.594247	0.568781	0.555328	0.369637	0.391044	0.515523	0.533281	0.510123	0.083575
304.4	0.554456	0.5953	0.570095	0.55642	0.37012	0.391314	0.516564	0.534207	0.51106	0.083915
304.3	0.555731	0.596888	0.571167	0.557695	0.370972	0.392098	0.517624	0.535537	0.512214	0.084141
304.2	0.55688	0.59829	0.572422	0.558946	0.371396	0.392642	0.518753	0.536436	0.513221	0.084483
304.1	0.558285	0.599943	0.573952	0.560265	0.372108	0.393265	0.519591	0.537583	0.514374	0.084835
304	0.559365	0.601117	0.575142	0.561491	0.372502	0.393896	0.520773	0.538945	0.515404	0.085139
303.9	0.56073	0.602775	0.576592	0.562699	0.373105	0.394704	0.521831	0.539849	0.516536	0.085453
303.8	0.561878	0.604228	0.577688	0.563703	0.373725	0.395193	0.522806	0.541157	0.517547	0.085746
303.7	0.563289	0.605737	0.579289	0.565293	0.374246	0.395607	0.524003	0.54237	0.518729	0.0862
303.6	0.564546	0.607487	0.580066	0.566512	0.374756	0.396573	0.524686	0.543317	0.519743	0.086441
303.5	0.565663	0.608378	0.581949	0.567683	0.375267	0.396973	0.525877	0.544279	0.520758	0.086776
303.4	0.566874	0.610341	0.582957	0.568792	0.37593	0.397791	0.527151	0.545706	0.521943	0.087076
303.3	0.568259	0.611755	0.584744	0.570206	0.376445	0.398571	0.528274	0.547002	0.523157	0.087449
303.2	0.56995	0.613436	0.585925	0.571735	0.377171	0.399139	0.52909	0.548081	0.524316	0.087813
303.1	0.571077	0.614941	0.587303	0.57294	0.377824	0.399996	0.530464	0.549549	0.525512	0.088082
303	0.572672	0.616676	0.588674	0.574489	0.378469	0.400584	0.531643	0.550647	0.526732	0.088487
302.9	0.57396	0.618291	0.590503	0.575732	0.379196	0.401334	0.532481	0.551925	0.527928	0.088825
302.8	0.575526	0.620252	0.591927	0.57723	0.379834	0.402047	0.534093	0.553396	0.529288	0.089255
302.7	0.57684	0.621902	0.593283	0.578551	0.38036	0.402986	0.53516	0.554511	0.530449	0.089564
302.6	0.578758	0.623748	0.595183	0.580299	0.380932	0.403607	0.536352	0.55578	0.531832	0.090095
302.5	0.580285	0.625516	0.596616	0.581598	0.381593	0.404441	0.537473	0.557458	0.533122	0.090454
302.4	0.581681	0.627258	0.598415	0.583218	0.382262	0.405294	0.539137	0.558623	0.534486	0.09084
302.3	0.583332	0.629239	0.599915	0.584736	0.382938	0.406066	0.540088	0.559982	0.535787	0.091258
302.2	0.584823	0.631198	0.601655	0.586075	0.383476	0.406718	0.541428	0.56142	0.537099	0.091736
302.1	0.586581	0.633028	0.603074	0.587791	0.384242	0.40749	0.542803	0.562667	0.538459	0.092124
302	0.588231	0.634945	0.605193	0.589312	0.384897	0.408556	0.54415	0.56417	0.539932	0.09255
	0.566553	0.60963	0.582551	0.568332	0.375598	0.397519	0.526486	0.545125	**0.521474**	**0.086981**
								0.521474		

Table 39: Bottom Row of the Sample Carousel, 9-minute irradiation

	57	58	59	60	61	62	63	64	average	std dev
Wavelengt	Abs	Abs	Abs	Abs	Abs	Abs	Abs	Abs	Abs	
305	0.585655	0.5172	0.427112	0.500114	0.515483	0.443649	0.512896	0.491561	0.499209	0.048687
304.9	0.586772	0.518016	0.427624	0.500878	0.516372	0.444284	0.513903	0.492151	0.5	0.048873
304.8	0.588049	0.518984	0.428561	0.501817	0.517233	0.444966	0.514583	0.493055	0.500906	0.04899
304.7	0.589352	0.520191	0.429033	0.502857	0.518542	0.445736	0.515758	0.493977	0.501931	0.04925
304.6	0.590743	0.521044	0.429818	0.50366	0.519457	0.446622	0.516255	0.494657	0.502782	0.049389
304.5	0.592099	0.522317	0.430649	0.504647	0.520458	0.447247	0.517377	0.495396	0.503774	0.049601
304.4	0.593295	0.523281	0.431295	0.505699	0.521622	0.447914	0.518286	0.496395	0.504723	0.049783
304.3	0.594765	0.52436	0.432043	0.506626	0.522609	0.448909	0.519616	0.497271	0.505775	0.049975
304.2	0.596157	0.525505	0.432644	0.5076	0.523796	0.449609	0.520265	0.498082	0.506707	0.050216
304.1	0.597614	0.526642	0.433591	0.508843	0.525035	0.450624	0.521385	0.49893	0.507833	0.050369
304	0.599037	0.527793	0.434336	0.509593	0.526066	0.451276	0.522194	0.499923	0.508777	0.050588
303.9	0.600481	0.528917	0.435246	0.510899	0.527021	0.452297	0.523633	0.500896	0.509924	0.05074
303.8	0.602014	0.530251	0.435909	0.511718	0.528208	0.45296	0.524635	0.501946	0.510955	0.051027
303.7	0.603525	0.531324	0.436857	0.512887	0.529556	0.454003	0.525509	0.502767	0.512053	0.051182
303.6	0.604914	0.532314	0.43755	0.51365	0.530332	0.454666	0.526506	0.503584	0.51294	0.051393
303.5	0.606366	0.533435	0.438179	0.514984	0.531657	0.455331	0.527374	0.504453	0.513972	0.051662
303.4	0.607894	0.534379	0.439148	0.515738	0.532835	0.456334	0.528428	0.505356	0.515014	0.051813
303.3	0.609457	0.535692	0.440075	0.516833	0.53392	0.457281	0.529529	0.506465	0.516156	0.052003
303.2	0.61127	0.536908	0.440817	0.518061	0.535262	0.458096	0.530806	0.507414	0.517329	0.052335
303.1	0.61288	0.538003	0.441734	0.519014	0.536521	0.458896	0.531939	0.508369	0.51842	0.052565
303	0.614321	0.539277	0.442738	0.520216	0.537598	0.460149	0.532825	0.509226	0.519544	0.052656
302.9	0.616232	0.540598	0.443383	0.521391	0.538781	0.460757	0.534015	0.510449	0.520701	0.053054
302.8	0.617793	0.541994	0.444433	0.522776	0.540293	0.461881	0.53542	0.511375	0.521996	0.053232
302.7	0.619677	0.543332	0.44519	0.523787	0.541486	0.462945	0.536385	0.512447	0.523156	0.053524
302.6	0.621369	0.544722	0.446165	0.525005	0.543055	0.463902	0.537667	0.513497	0.524423	0.053772
302.5	0.623269	0.545972	0.447062	0.526475	0.544199	0.464953	0.53894	0.514558	0.525678	0.054046
302.4	0.625283	0.547292	0.448025	0.527664	0.545754	0.466077	0.540154	0.515857	0.527013	0.054339
302.3	0.626971	0.54866	0.448769	0.528789	0.547033	0.466855	0.541052	0.516915	0.528131	0.054634
302.2	0.628771	0.549919	0.449576	0.530058	0.548524	0.467819	0.542388	0.517886	0.529368	0.054938
302.1	0.630633	0.55137	0.450711	0.531271	0.549721	0.468825	0.543638	0.518978	0.530643	0.055172
302	0.632759	0.552953	0.451559	0.532599	0.551044	0.469715	0.544755	0.520241	0.531953	0.055556
	0.607401	0.533956	0.438704	0.51536	0.532241	0.455954	0.528004	0.50497	**0.514574**	**0.051786**
								0.514574		

Table 40: Top Row of the Sample Carousel, 6-minute irradiation

	65	66	67	68	69	70	71	72	average	std dev
wavelengt	Abs	Abs	Abs	Abs	Abs	Abs	Abs	Abs	Abs	
305	0.404813	0.44238	0.445102	0.452668	0.288142	0.366775	0.419892	0.218616	0.379799	0.084747
304.9	0.405631	0.443322	0.445801	0.453581	0.288648	0.367605	0.420756	0.218938	0.380535	0.084944
304.8	0.40662	0.444209	0.447151	0.455072	0.28923	0.368227	0.421677	0.219064	0.381406	0.085336
304.7	0.407209	0.445339	0.448291	0.455848	0.289712	0.369031	0.422547	0.219439	0.382177	0.085566
304.6	0.408322	0.446628	0.449256	0.457234	0.290157	0.369694	0.423346	0.219645	0.383035	0.08594
304.5	0.409015	0.447683	0.450553	0.458152	0.290698	0.370679	0.424291	0.220111	0.383898	0.086168
304.4	0.409909	0.448647	0.451709	0.459147	0.291194	0.37113	0.425214	0.220176	0.384641	0.086515
304.3	0.411031	0.449971	0.452413	0.460447	0.291492	0.371968	0.426264	0.220738	0.385541	0.086793
304.2	0.411806	0.450779	0.454101	0.461543	0.292088	0.372902	0.427008	0.22089	0.38639	0.087128
304.1	0.412802	0.452355	0.454701	0.462999	0.292585	0.373609	0.428013	0.221276	0.387292	0.087452
304	0.413728	0.453437	0.456393	0.464011	0.293231	0.374439	0.429057	0.221415	0.388214	0.087831
303.9	0.414706	0.454903	0.45726	0.465097	0.293649	0.375197	0.429927	0.221922	0.389083	0.088096
303.8	0.415579	0.455831	0.45883	0.46635	0.294258	0.376261	0.430806	0.222293	0.390026	0.088399
303.7	0.416719	0.457279	0.459939	0.467653	0.294656	0.376953	0.431933	0.222627	0.39097	0.088791
303.6	0.417499	0.45844	0.460952	0.46869	0.295282	0.377605	0.432719	0.222783	0.391746	0.089085
303.5	0.418388	0.459728	0.462298	0.470111	0.295706	0.378557	0.433652	0.223004	0.392681	0.089499
303.4	0.419222	0.46089	0.463467	0.471076	0.296115	0.379513	0.434527	0.223421	0.393529	0.089766
303.3	0.420502	0.462274	0.464914	0.472523	0.296716	0.380274	0.435734	0.223593	0.394566	0.090229
303.2	0.421614	0.463688	0.46606	0.473898	0.297155	0.381066	0.436645	0.223968	0.395512	0.090595
303.1	0.422474	0.464814	0.467431	0.474937	0.297775	0.382097	0.437771	0.224442	0.396468	0.090858
303	0.423851	0.466177	0.468747	0.47653	0.298517	0.382916	0.438983	0.224744	0.397558	0.091268
302.9	0.424666	0.467775	0.470088	0.477797	0.299024	0.383787	0.440064	0.224825	0.398503	0.091729
302.8	0.425865	0.46918	0.471609	0.479442	0.299584	0.384858	0.441073	0.225503	0.399639	0.092073
302.7	0.427039	0.470523	0.472809	0.480776	0.300199	0.385789	0.442129	0.225707	0.400621	0.092461
302.6	0.428173	0.472027	0.474523	0.482172	0.300805	0.38667	0.443426	0.226156	0.401744	0.092881
302.5	0.429091	0.473727	0.475943	0.483734	0.301464	0.387735	0.444681	0.226285	0.402833	0.093373
302.4	0.430623	0.475251	0.477427	0.485209	0.302051	0.388784	0.445773	0.226902	0.404003	0.093736
302.3	0.431599	0.47667	0.47843	0.486443	0.302693	0.38978	0.446878	0.227266	0.40497	0.094045
302.2	0.432939	0.478082	0.480195	0.488057	0.303314	0.390592	0.447968	0.227669	0.406102	0.094495
302.1	0.434163	0.479597	0.481498	0.489597	0.303909	0.391768	0.4493	0.228114	0.407243	0.09489
302	0.435308	0.481202	0.483382	0.491321	0.304442	0.392746	0.450589	0.228304	0.408412	0.095461
	0.419062	0.460413	0.462944	0.470713	0.295951	0.379	0.434279	0.223221	**0.393198**	**0.089682**
								0.393198		

Table 41: Bottom Row of the Sample Carousel, 6-minute irradiation

	73	74	75	76	77	78	79	80	average	std dev
Wavelengt	Abs	Abs	Abs	Abs	Abs	Abs	Abs	Abs	Abs	
305	0.486975	0.489327	0.478525	0.47978	0.42648	0.419803	0.4939	0.461138	0.466991	0.028837
304.9	0.488066	0.490644	0.479671	0.480908	0.427285	0.420753	0.494838	0.462164	0.468041	0.02894
304.8	0.489382	0.491835	0.480839	0.482059	0.428129	0.421398	0.496083	0.463189	0.469114	0.029157
304.7	0.490644	0.493147	0.481964	0.483306	0.429142	0.422393	0.497205	0.464104	0.470238	0.029258
304.6	0.491791	0.494413	0.483448	0.484513	0.429859	0.423207	0.49861	0.46529	0.471391	0.029492
304.5	0.493335	0.49575	0.484644	0.48573	0.430922	0.424201	0.499719	0.466359	0.472583	0.02961
304.4	0.494397	0.497098	0.485733	0.486882	0.431787	0.424949	0.501097	0.467273	0.473652	0.029808
304.3	0.495878	0.498354	0.487169	0.488303	0.432924	0.426036	0.502191	0.468616	0.474934	0.029891
304.2	0.497277	0.499772	0.488495	0.48953	0.433942	0.42714	0.50374	0.469385	0.47616	0.030062
304.1	0.498804	0.501463	0.489861	0.490909	0.435051	0.428005	0.505317	0.470764	0.477522	0.030311
304	0.500125	0.502547	0.491189	0.49216	0.435885	0.42887	0.506421	0.471872	0.478634	0.030463
303.9	0.501601	0.504386	0.49277	0.49352	0.437194	0.429923	0.508046	0.473223	0.480083	0.030659
303.8	0.503175	0.50544	0.494245	0.494998	0.438253	0.430952	0.509577	0.47428	0.481365	0.03083
303.7	0.504569	0.507017	0.495705	0.496437	0.439128	0.431731	0.511053	0.475535	0.482647	0.03112
303.6	0.505846	0.508452	0.49697	0.49779	0.440178	0.432909	0.512324	0.476475	0.483868	0.03122
303.5	0.507559	0.509833	0.498262	0.499025	0.441303	0.433591	0.513635	0.477654	0.485108	0.031451
303.4	0.508941	0.511303	0.499742	0.500242	0.442223	0.434873	0.515331	0.478742	0.486425	0.031623
303.3	0.51058	0.512828	0.501345	0.501766	0.443363	0.435958	0.516842	0.479926	0.487826	0.031829
303.2	0.511885	0.514536	0.502684	0.503277	0.444919	0.436937	0.518253	0.48141	0.489238	0.031923
303.1	0.513678	0.516265	0.504255	0.504767	0.445628	0.437837	0.519916	0.482555	0.490613	0.032313
303	0.515375	0.517626	0.505727	0.506202	0.447119	0.439286	0.521442	0.484047	0.492103	0.032329
302.9	0.517005	0.51923	0.507359	0.507726	0.448275	0.440163	0.522914	0.485301	0.493497	0.032583
302.8	0.518757	0.521283	0.509089	0.509407	0.4496	0.441434	0.525029	0.486923	0.49519	0.03286
302.7	0.520267	0.522604	0.510719	0.510808	0.450773	0.442754	0.526558	0.487999	0.49656	0.032969
302.6	0.522093	0.524338	0.512519	0.512604	0.451922	0.443725	0.528389	0.489552	0.498143	0.033299
302.5	0.523971	0.526273	0.514169	0.514247	0.453178	0.44497	0.530359	0.491029	0.499775	0.033575
302.4	0.525987	0.527988	0.516096	0.515835	0.454679	0.446338	0.532067	0.492546	0.501442	0.033741
302.3	0.527921	0.529824	0.517564	0.517562	0.456001	0.447369	0.533698	0.49375	0.502961	0.034009
302.2	0.529385	0.531337	0.519338	0.519202	0.456972	0.44848	0.535604	0.495072	0.504424	0.034287
302.1	0.531263	0.533264	0.520964	0.520688	0.458478	0.449735	0.537485	0.496683	0.50607	0.034483
302	0.533388	0.535367	0.522975	0.522553	0.459923	0.451259	0.539241	0.498104	0.507852	0.034712
	0.508385	0.510759	0.499162	0.499766	0.441952	0.434419	0.514738	0.478418	**0.48595**	**0.031537**
								0.48595		

Table 42: Top Row of the Sample Carousel, 3-minute irradiation

	81	82	83	84	85	86	87	88	avg	std dev
wavelengt	Abs	Abs	Abs	Abs	Abs	Abs	Abs	Abs	Abs	std dev
305	0.380845	0.373045	0.370261	0.389155	0.359585	0.358151	0.366878	0.369136	0.370882	0.01033
304.9	0.382121	0.37406	0.371284	0.390295	0.360594	0.359386	0.36795	0.370036	0.371966	0.01036
304.8	0.383224	0.374893	0.372476	0.391442	0.361734	0.360483	0.36905	0.371365	0.373083	0.010353
304.7	0.384481	0.375953	0.373608	0.392719	0.363268	0.361799	0.370132	0.372649	0.374326	0.010311
304.6	0.38578	0.377051	0.374799	0.393942	0.364168	0.363081	0.371558	0.37361	0.375499	0.010354
304.5	0.387015	0.378005	0.376042	0.395148	0.365518	0.364221	0.372874	0.375008	0.376729	0.010331
304.4	0.388214	0.37917	0.377147	0.396347	0.366696	0.365542	0.373905	0.376142	0.377895	0.010325
304.3	0.389649	0.380422	0.378511	0.397662	0.368269	0.366718	0.375292	0.377492	0.379252	0.01032
304.2	0.391166	0.381523	0.379751	0.399101	0.369365	0.368085	0.376622	0.378753	0.380546	0.010403
304.1	0.392356	0.382617	0.381129	0.400333	0.370977	0.36957	0.37824	0.380174	0.381925	0.010267
304	0.393631	0.383917	0.382084	0.401585	0.372223	0.371017	0.379383	0.381325	0.383146	0.010251
303.9	0.395252	0.38498	0.383536	0.402884	0.373768	0.372364	0.380894	0.382871	0.384569	0.010232
303.8	0.396676	0.386196	0.384799	0.404185	0.375243	0.373744	0.382399	0.384455	0.385962	0.010194
303.7	0.398238	0.387485	0.386247	0.405851	0.376644	0.375155	0.38374	0.385931	0.387411	0.010285
303.6	0.399308	0.388728	0.387378	0.406841	0.378166	0.376651	0.385264	0.387102	0.38868	0.010099
303.5	0.40111	0.389865	0.388669	0.408271	0.379334	0.377889	0.386514	0.388297	0.389993	0.010244
303.4	0.402289	0.390991	0.389909	0.409399	0.380896	0.379359	0.388119	0.389997	0.39137	0.010092
303.3	0.403847	0.392389	0.39142	0.411119	0.382594	0.381058	0.38948	0.391418	0.392916	0.010104
303.2	0.405459	0.393561	0.392859	0.412382	0.384218	0.382664	0.391259	0.393052	0.394432	0.010013
303.1	0.406643	0.394903	0.394166	0.413839	0.385462	0.384172	0.39243	0.394328	0.395743	0.010014
303	0.408592	0.39627	0.395867	0.415536	0.387225	0.38573	0.394376	0.396265	0.397483	0.010056
302.9	0.410209	0.397421	0.397388	0.417169	0.388825	0.387381	0.39604	0.39789	0.39904	0.010067
302.8	0.412033	0.398936	0.399047	0.418638	0.390742	0.389185	0.397705	0.399501	0.400723	0.009987
302.7	0.413614	0.400281	0.400498	0.420029	0.392379	0.390805	0.399261	0.401243	0.402264	0.009932
302.6	0.415327	0.401643	0.401904	0.421882	0.393953	0.392679	0.400999	0.402984	0.403921	0.009979
302.5	0.417042	0.403133	0.403596	0.423571	0.395813	0.394217	0.403069	0.404696	0.405642	0.009975
302.4	0.418875	0.404838	0.40528	0.425134	0.39761	0.396137	0.404868	0.406709	0.407432	0.009905
302.3	0.420566	0.406074	0.406907	0.426747	0.39964	0.397995	0.40656	0.408452	0.409118	0.009831
302.2	0.422234	0.407532	0.40813	0.428474	0.401054	0.399452	0.408104	0.410183	0.410645	0.009944
302.1	0.424192	0.408899	0.410125	0.430234	0.402885	0.401471	0.410088	0.412248	0.412518	0.009927
302	0.426117	0.41067	0.411866	0.432021	0.40525	0.403512	0.412088	0.413984	0.414438	0.009826
	0.40181	0.390498	0.38957	0.409095	0.380455	0.379022	0.387585	0.38959	**0.390953**	**0.010139**
								0.390953		

Table 43: Bottom Row of the Sample Carousel, 3-minute irradiation

	89	90	91	92	93	94	95	96	average	std dev
Wavelengt	Abs	Abs	Abs	Abs	Abs	Abs	Abs	Abs	Abs	
305	0.385845	0.364951	0.362114	0.393221	0.347238	0.325157	0.387223	0.407066	0.371602	0.026878
304.9	0.386943	0.366136	0.363132	0.394266	0.347936	0.325667	0.388464	0.408131	0.372584	0.027076
304.8	0.388308	0.367166	0.364258	0.395518	0.348866	0.326664	0.38958	0.409238	0.3737	0.027165
304.7	0.38949	0.368439	0.36557	0.396556	0.34964	0.327461	0.390828	0.410688	0.374834	0.027343
304.6	0.390692	0.369739	0.366629	0.3977	0.350291	0.328238	0.39168	0.411657	0.375828	0.027446
304.5	0.391993	0.37062	0.367809	0.398967	0.351295	0.329039	0.392797	0.413293	0.376977	0.027672
304.4	0.393033	0.372129	0.369076	0.400058	0.351913	0.329855	0.394004	0.414279	0.378044	0.027768
304.3	0.394633	0.373596	0.370402	0.401329	0.353087	0.330748	0.395205	0.415641	0.37933	0.027903
304.2	0.395798	0.374742	0.371852	0.402544	0.353795	0.331395	0.396486	0.416904	0.380439	0.028115
304.1	0.397179	0.376241	0.373343	0.404141	0.355015	0.332523	0.397737	0.418375	0.381819	0.028222
304	0.398507	0.377433	0.37456	0.405198	0.35556	0.333312	0.398832	0.419844	0.382906	0.028449
303.9	0.400022	0.378773	0.375903	0.40681	0.35669	0.334249	0.40015	0.421201	0.384225	0.028624
303.8	0.401468	0.380307	0.37736	0.407952	0.357695	0.335265	0.401608	0.422616	0.385534	0.02875
303.7	0.403051	0.381876	0.379036	0.40943	0.358471	0.336167	0.40294	0.42418	0.386894	0.028994
303.6	0.404401	0.383197	0.380193	0.410674	0.359547	0.336991	0.404155	0.425671	0.388104	0.029176
303.5	0.405478	0.384518	0.381676	0.411842	0.360533	0.337771	0.405316	0.426851	0.389248	0.029278
303.4	0.407186	0.385921	0.38306	0.413221	0.361433	0.338633	0.406662	0.428403	0.390565	0.029529
303.3	0.408739	0.387506	0.384672	0.414635	0.36225	0.339421	0.408161	0.430036	0.391927	0.029818
303.2	0.410366	0.389248	0.386213	0.416268	0.363565	0.340598	0.409426	0.431748	0.393429	0.029965
303.1	0.411824	0.390608	0.38767	0.417543	0.364335	0.341571	0.410806	0.433126	0.394685	0.030147
303	0.413676	0.392497	0.389387	0.419229	0.365681	0.342473	0.412207	0.434979	0.396266	0.030411
302.9	0.415225	0.393999	0.390924	0.420785	0.366564	0.343435	0.413819	0.436522	0.397659	0.030661
302.8	0.417161	0.395873	0.392932	0.422546	0.367582	0.344597	0.415237	0.438255	0.399273	0.030895
302.7	0.418546	0.397377	0.394313	0.42388	0.368783	0.345562	0.416714	0.440043	0.400652	0.031101
302.6	0.420501	0.399223	0.396188	0.425558	0.369809	0.346529	0.418412	0.441858	0.40226	0.031418
302.5	0.422451	0.401175	0.397872	0.427297	0.370995	0.347786	0.419916	0.443722	0.403902	0.031643
302.4	0.424274	0.403002	0.399886	0.429031	0.372069	0.348708	0.421556	0.445514	0.405505	0.031951
302.3	0.425809	0.404745	0.40178	0.43046	0.373326	0.349779	0.422926	0.447266	0.407012	0.032115
302.2	0.427739	0.40658	0.403317	0.432362	0.374381	0.35088	0.424447	0.449267	0.408622	0.032449
302.1	0.429486	0.408331	0.405444	0.43405	0.375502	0.351973	0.426325	0.451006	0.410265	0.032703
302	0.431756	0.410394	0.407358	0.435891	0.376761	0.35339	0.428012	0.453067	0.412079	0.032961
	0.406825	0.385688	0.382707	0.41287	0.360987	0.338253	0.406182	0.428079	**0.390199**	**0.029569**
								0.390199		

Table 44: Fricke Unirradiated Sample Blanks for the Determination of the Initial Absorbance

	97	98	99	100	Avg	std dev
wavelengt	Abs	Abs	Abs	Abs	Abs	
305	0.285168	0.274533	0.286315	0.270822	0.279209	0.007707
304.9	0.28621	0.275621	0.287509	0.271847	0.280296	0.007751
304.8	0.287355	0.276545	0.288619	0.272911	0.281357	0.007814
304.7	0.288763	0.277998	0.28996	0.274542	0.282816	0.007705
304.6	0.289869	0.278995	0.290925	0.275656	0.283861	0.007681
304.5	0.291078	0.280214	0.292182	0.276709	0.285046	0.007749
304.4	0.29213	0.281487	0.293445	0.277825	0.286222	0.007746
304.3	0.293543	0.282792	0.294742	0.279438	0.287629	0.00766
304.2	0.294807	0.284179	0.296044	0.280586	0.288904	0.007689
304.1	0.296281	0.285696	0.297519	0.281843	0.290335	0.007759
304	0.297642	0.287058	0.29902	0.28315	0.291717	0.007822
303.9	0.299251	0.2884	0.300328	0.284675	0.293163	0.007813
303.8	0.300421	0.28975	0.301698	0.286001	0.294468	0.007781
303.7	0.302046	0.291219	0.303234	0.287436	0.295984	0.007854
303.6	0.303428	0.292575	0.304563	0.289138	0.297426	0.007728
303.5	0.304857	0.29386	0.305917	0.290441	0.298769	0.007781
303.4	0.306256	0.295435	0.307348	0.291942	0.300245	0.007717
303.3	0.307866	0.296801	0.308716	0.29333	0.301678	0.007774
303.2	0.3094	0.298696	0.310485	0.295071	0.303413	0.007696
303.1	0.310699	0.299933	0.311784	0.296366	0.304696	0.007711
303	0.312542	0.301781	0.313615	0.298122	0.306515	0.007737
302.9	0.314065	0.30332	0.315352	0.299713	0.308112	0.007775
302.8	0.316068	0.305389	0.317349	0.301391	0.310049	0.007878
302.7	0.317515	0.306937	0.31873	0.302961	0.311536	0.007793
302.6	0.319665	0.308748	0.320569	0.304822	0.313451	0.007871
302.5	0.321218	0.310545	0.322446	0.306489	0.315175	0.00788
302.4	0.323206	0.312238	0.324342	0.308517	0.317076	0.007896
302.3	0.324811	0.314023	0.325865	0.310343	0.31876	0.007754
302.2	0.326658	0.315799	0.327658	0.312137	0.320563	0.007772
302.1	0.328558	0.317609	0.329707	0.314023	0.322474	0.00784
302	0.330411	0.319567	0.331497	0.316106	0.324395	0.007717
	0.305864	0.295088	0.307016	0.291431	**0.29985**	**0.007769**
				0.29985		

APPENDIX C: DATA FOR PLUTONIUM RETENTION MEASUREMENTS

Table 45: Table giving labeling schema for samples and a record of what the conditions of irradiation or kinetics study were for every individual sample pertaining to the retention of plutonium presented here. This table also includes the samples that were disqualified from the study for reasons that include but are not limited to: the use of an incompatible filter material (i.e. PES), experimental process error, the discovered fact that microcentrifuge tubes cannot withstand 50 kGy of gamma radiation without significant embrittlement, and failures with the extended use of the pneumatics of the Cs-137 irradiator.

sample ID	solution	acid concentration / M	irradiation time / min	Irradiation Dose / Gy	note
TRU-01	nitric acid	3	0	0	PES filter
TRU-02	nitric acid	3	0	0	PES filter
TRU-03	nitric acid	3	0	0	PES filter
TRU-04	nitric acid	3	0	0	PES filter
TRU-05	nitric acid	3	1.25	10	PES filter
TRU-06	nitric acid	3	1.25	10	PES filter
TRU-07	nitric acid	3	1.25	10	PES filter
TRU-08	nitric acid	3	1.25	10	PES filter
TRU-09	hydrochloric acid	3	0	0	PES filter
TRU-10	hydrochloric acid	3	0	0	PES filter
TRU-11	hydrochloric acid	3	0	0	PES filter
TRU-12	hydrochloric acid	3	0	0	PES filter
TRU-13	hydrochloric acid	3	1.25	10	PES filter
TRU-14	hydrochloric acid	3	1.25	10	PES filter
TRU-15	hydrochloric acid	3	1.25	10	PES filter
TRU-16	hydrochloric acid	3	1.25	10	PES filter
TRU-17	nitric acid	3	12.5	100	PES filter
TRU-18	nitric acid	3	12.5	100	PES filter
TRU-19	nitric acid	3	12.5	100	PES filter
TRU-20	nitric acid	3	12.5	100	PES filter
TRU-21	nitric acid	3	125	1000	PES filter
TRU-22	nitric acid	3	125	1000	PES filter
TRU-23	nitric acid	3	125	1000	PES filter
TRU-24	nitric acid	3	125	1000	PES filter
TRU-25	hydrochloric acid	3	12.5	100	PES filter
TRU-26	hydrochloric acid	3	12.5	100	PES filter
TRU-27	hydrochloric acid	3	12.5	100	PES filter
TRU-28	hydrochloric acid	3	12.5	100	PES filter
TRU-29	hydrochloric acid	3	125	1000	PES filter
TRU-30	hydrochloric acid	3	125	1000	PES filter
TRU-31	hydrochloric acid	3	125	1000	PES filter
TRU-32	hydrochloric acid	3	125	1000	PES filter

TRU-33	water	N/A			
TRU-34	water	N/A			
TRU-35	water	N/A			
TRU-36	water	N/A			
TRU-37	water	N/A			
TRU-38	water	N/A			
TRU-39	water	N/A			
TRU-40	water	N/A			
TRU-41	nitric acid	3	1250	10000	PES filter
TRU-42	nitric acid	3	1250	10000	PES filter
TRU-43	nitric acid	3	1250	10000	PES filter
TRU-44	nitric acid	3	1250	10000	PES filter
TRU-45	nitric acid	3	0	0	PES filter
TRU-46	nitric acid	3	0	0	PES filter
TRU-47	nitric acid	3	0	0	PES filter
TRU-48	nitric acid	3	0	0	PES filter
TRU-49	water	N/A			
TRU-50	water	N/A			
TRU-51	water	N/A			
TRU-52	water	N/A			
TRU-53	water	N/A			
TRU-54	water	N/A			
TRU-55	water	N/A			
TRU-56	water	N/A			
TRU-57	hydrochloric acid	3	1250	10000	PES filter
TRU-58	hydrochloric acid	3	1250	10000	PES filter
TRU-59	hydrochloric acid	3	1250	10000	PES filter
TRU-60	hydrochloric acid	3	1250	10000	PES filter
TRU-61	hydrochloric acid	3	0	0	PES filter
TRU-62	hydrochloric acid	3	0	0	PES filter
TRU-63	hydrochloric acid	3	0	0	PES filter
TRU-64	hydrochloric acid	3	REMOVED/syringe filter failure	0	PES filter
TRU-65	nitric acid	3	6250	50000	PES filter
TRU-66	nitric acid	3	6250	50000	PES filter
TRU-67	nitric acid	3	6250	50000	PES filter
TRU-68	nitric acid	3	6250	50000	PES filter
TRU-69	nitric acid	3	0	0	PES filter
TRU-70	nitric acid	3	0	0	PES filter
TRU-71	nitric acid	3	0	0	PES filter
TRU-72	nitric acid	3	0	0	PES filter
TRU-73	hydrochloric acid	3	6250	50000	PES filter
TRU-74	hydrochloric acid	3	6250	50000	PES filter

TRU-75	hydrochloric acid	3	6250	50000	PES filter
TRU-76	hydrochloric acid	3	6250	50000	PES filter
TRU-77	hydrochloric acid	3	0	0	PES filter
TRU-78	hydrochloric acid	3	0	0	PES filter
TRU-79	hydrochloric acid	3	0	0	PES filter
TRU-80	hydrochloric acid	3	0	0	PES filter
TRU-81	nitric acid	3	0	0	PTFE filter
TRU-82	nitric acid	3	0	0	PTFE filter
TRU-83	nitric acid	3	0	0	PTFE filter
TRU-84	nitric acid	3	0	0	PTFE filter
TRU-85	nitric acid	3	1.25	10	PTFE filter
TRU-86	nitric acid	3	1.25	10	PTFE filter
TRU-87	nitric acid	3	1.25	10	PTFE filter
TRU-88	nitric acid	3	1.25	10	PTFE filter
TRU-89	nitric acid	3	12.5	100	PTFE filter
TRU-90	nitric acid	3	12.5	100	PTFE filter
TRU-91	nitric acid	3	12.5	100	PTFE filter
TRU-92	nitric acid	3	12.5	100	PTFE filter
TRU-93	nitric acid	3	125	1000	PTFE filter
TRU-94	nitric acid	3	125	1000	PTFE filter
TRU-95	nitric acid	3	125	1000	PTFE filter
TRU-96	nitric acid	3	125	1000	PTFE filter
TRU-97	nitric acid	3	1250	10000	PTFE filter
TRU-98	nitric acid	3	1250	10000	PTFE filter
TRU-99	nitric acid	3	1250	10000	PTFE filter
TRU-100	nitric acid	3	1250	10000	PTFE filter
TRU-101	nitric acid	3	0	0	PTFE filter
TRU-102	nitric acid	3	0	0	PTFE filter
TRU-103	nitric acid	3	0	0	PTFE filter
TRU-104	nitric acid	3	0	0	PTFE filter
TRU-105	hydrochloric acid	3	0	0	PTFE filter
TRU-106	hydrochloric acid	3	0	0	PTFE filter
TRU-107	hydrochloric acid	3	0	0	PTFE filter
TRU-108	hydrochloric acid	3	0	0	PTFE filter
TRU-109	hydrochloric acid	3	1.25	10	PTFE filter
TRU-110	hydrochloric acid	3	1.25	10	PTFE filter
TRU-111	hydrochloric acid	3	1.25	10	PTFE filter
TRU-112	hydrochloric acid	3	1.25	10	PTFE filter
TRU-113	hydrochloric acid	3	12.5	100	PTFE filter
TRU-114	hydrochloric acid	3	12.5	100	PTFE filter
TRU-115	hydrochloric acid	3	12.5	100	PTFE filter
TRU-116	hydrochloric acid	3	12.5	100	PTFE filter
TRU-117	hydrochloric acid	3	125	1000	PTFE filter

TRU-118	hydrochloric acid	3	125	1000	PTFE filter
TRU-119	hydrochloric acid	3	125	1000	PTFE filter
TRU-120	hydrochloric acid	3	125	1000	PTFE filter
TRU-121	hydrochloric acid	3	1250	10000	PTFE filter
TRU-122	hydrochloric acid	3	1250	10000	PTFE filter
TRU-123	hydrochloric acid	3	1250	10000	PTFE filter
TRU-124	hydrochloric acid	3	1250	10000	PTFE filter
TRU-125	hydrochloric acid	3	0	0	PTFE filter
TRU-126	hydrochloric acid	3	0	0	PTFE filter
TRU-127	hydrochloric acid	3	0	0	PTFE filter
TRU-128	hydrochloric acid	3	0	0	PTFE filter
TRU-129	nitric acid	1	0	0	PTFE filter
TRU-130	nitric acid	1	0	0	PTFE filter
TRU-131	nitric acid	1	0	0	PTFE filter
TRU-132	nitric acid	1	0	0	PTFE filter
TRU-133	nitric acid	1	1.25	10	PTFE filter
TRU-134	nitric acid	1	1.25	10	PTFE filter
TRU-135	nitric acid	1	1.25	10	PTFE filter
TRU-136	nitric acid	1	1.25	10	PTFE filter
TRU-137	nitric acid	1	12.5	100	PTFE filter
TRU-138	nitric acid	1	12.5	100	PTFE filter
TRU-139	nitric acid	1	12.5	100	PTFE filter
TRU-140	nitric acid	1	12.5	100	PTFE filter
TRU-141	nitric acid	1	125	1000	PTFE filter
TRU-142	nitric acid	1	125	1000	PTFE filter
TRU-143	nitric acid	1	125	1000	PTFE filter
TRU-144	nitric acid	1	125	1000	PTFE filter
TRU-145	nitric acid	1	1250	10000	PTFE filter
TRU-146	nitric acid	1	1250	10000	PTFE filter
TRU-147	nitric acid	1	1250	10000	PTFE filter
TRU-148	nitric acid	1	1250	10000	PTFE filter
TRU-149	nitric acid	1	0	0	PTFE filter
TRU-150	nitric acid	1	0	0	PTFE filter
TRU-151	nitric acid	1	0	0	PTFE filter
TRU-152	nitric acid	1	0	0	PTFE filter
TRU-153	hydrochloric acid	1	0	0	PTFE filter
TRU-154	hydrochloric acid	1	0	0	PTFE filter
TRU-155	hydrochloric acid	1	0	0	PTFE filter
TRU-156	hydrochloric acid	1	0	0	PTFE filter
TRU-157	hydrochloric acid	1	1.25	10	PTFE filter
TRU-158	hydrochloric acid	1	1.25	10	PTFE filter
TRU-159	hydrochloric acid	1	1.25	10	PTFE filter
TRU-160	hydrochloric acid	1	1.25	10	PTFE filter

TRU-161	hydrochloric acid	1	12.5	100	PTFE filter
TRU-162	hydrochloric acid	1	12.5	100	PTFE filter
TRU-163	hydrochloric acid	1	12.5	100	PTFE filter
TRU-164	hydrochloric acid	1	12.5	100	PTFE filter
TRU-165	hydrochloric acid	1	125	1000	PTFE filter
TRU-166	hydrochloric acid	1	125	1000	PTFE filter
TRU-167	hydrochloric acid	1	125	1000	PTFE filter
TRU-168	hydrochloric acid	1	125	1000	PTFE filter
TRU-169	hydrochloric acid	1	1250	10000	PTFE filter
TRU-170	hydrochloric acid	1	1250	10000	PTFE filter
TRU-171	hydrochloric acid	1	1250	10000	PTFE filter
TRU-172	hydrochloric acid	1	1250	10000	PTFE filter
TRU-173	hydrochloric acid	1	0	0	PTFE filter
TRU-174	hydrochloric acid	1	0	0	PTFE filter
TRU-175	hydrochloric acid	1	0	0	PTFE filter
TRU-176	hydrochloric acid	1	0	0	PTFE filter
TRU-177	hydrochloric acid	3	1250	10000	THIS CONDITION WAS RERUN DUE TO IRREGULAR RESULT ON FIRST RUN
TRU-178	hydrochloric acid	3	1250	10000	
TRU-179	hydrochloric acid	3	1250	10000	
TRU-180	hydrochloric acid	3	1250	10000	
TRU-181	hydrochloric acid	3	0	0	
TRU-182	hydrochloric acid	3	0	0	
TRU-183	hydrochloric acid	3	0	0	
TRU-184	hydrochloric acid	3	0	0	
TRU-185	nitric acid	3	N/A kinetics		0
TRU-186	nitric acid	3	N/A kinetics		0
TRU-187	nitric acid	3	N/A kinetics		0
TRU-188	nitric acid	3	N/A kinetics		0
TRU-189	nitric acid	3	N/A kinetics		1
TRU-190	nitric acid	3	N/A kinetics		1
TRU-191	nitric acid	3	N/A kinetics		1
TRU-192	nitric acid	3	N/A kinetics		1
TRU-193	nitric acid	3	N/A kinetics		3
TRU-194	nitric acid	3	N/A kinetics		3
TRU-195	nitric acid	3	N/A kinetics		3
TRU-196	nitric acid	3	N/A kinetics		3
TRU-197	nitric acid	3	N/A kinetics		7

TRU-198	nitric acid	3	N/A kinetics		7
TRU-199	nitric acid	3	N/A kinetics		7
TRU-200	nitric acid	3	N/A kinetics		7
TRU-201	nitric acid	3	N/A kinetics		14
TRU-202	nitric acid	3	N/A kinetics		14
TRU-203	nitric acid	3	N/A kinetics		14
TRU-204	nitric acid	3	N/A kinetics		14
TRU-205	nitric acid	3	N/A kinetics		22
TRU-206	nitric acid	3	N/A kinetics		22
TRU-207	nitric acid	3	N/A kinetics		22
TRU-208	nitric acid	3	N/A kinetics		22
TRU-209	hydrochloric acid	3	N/A kinetics		0
TRU-210	hydrochloric acid	3	N/A kinetics		0
TRU-211	hydrochloric acid	3	N/A kinetics		0
TRU-212	hydrochloric acid	3	N/A kinetics		0
TRU-213	hydrochloric acid	3	N/A kinetics		1
TRU-214	hydrochloric acid	3	N/A kinetics		1
TRU-215	hydrochloric acid	3	N/A kinetics		1
TRU-216	hydrochloric acid	3	N/A kinetics		1
TRU-217	hydrochloric acid	3	N/A kinetics		3
TRU-218	hydrochloric acid	3	N/A kinetics		3
TRU-219	hydrochloric acid	3	N/A kinetics		3
TRU-220	hydrochloric acid	3	N/A kinetics		3
TRU-221	hydrochloric acid	3	N/A kinetics		7
TRU-222	hydrochloric acid	3	N/A kinetics		7
TRU-223	hydrochloric acid	3	N/A kinetics		7
TRU-224	hydrochloric acid	3	N/A kinetics		7
TRU-225	hydrochloric acid	3	N/A kinetics		14
TRU-226	hydrochloric acid	3	N/A kinetics		14
TRU-227	hydrochloric acid	3	N/A kinetics		14
TRU-228	hydrochloric acid	3	N/A kinetics		14
TRU-229	hydrochloric acid	3	N/A kinetics		22
TRU-230	hydrochloric acid	3	N/A kinetics		22
TRU-231	hydrochloric acid	3	N/A kinetics		22
TRU-232	hydrochloric acid	3	N/A kinetics		22
TRU-233	nitric acid	1	N/A kinetics		0
TRU-234	nitric acid	1	N/A kinetics		0
TRU-235	nitric acid	1	N/A kinetics		0
TRU-236	nitric acid	1	N/A kinetics		0
TRU-237	nitric acid	1	N/A kinetics		1
TRU-238	nitric acid	1	N/A kinetics		1
TRU-239	nitric acid	1	N/A kinetics		1
TRU-240	nitric acid	1	N/A kinetics		1

TRU-241	nitric acid	1	N/A kinetics		3
TRU-242	nitric acid	1	N/A kinetics		3
TRU-243	nitric acid	1	N/A kinetics		3
TRU-244	nitric acid	1	N/A kinetics		3
TRU-245	nitric acid	1	N/A kinetics		7
TRU-246	nitric acid	1	N/A kinetics		7
TRU-247	nitric acid	1	N/A kinetics		7
TRU-248	nitric acid	1	N/A kinetics		7
TRU-249	nitric acid	1	N/A kinetics		14
TRU-250	nitric acid	1	N/A kinetics		14
TRU-251	nitric acid	1	N/A kinetics		14
TRU-252	nitric acid	1	N/A kinetics		14
TRU-253	nitric acid	1	N/A kinetics		22
TRU-254	nitric acid	1	N/A kinetics		22
TRU-255	nitric acid	1	N/A kinetics		22
TRU-256	nitric acid	1	N/A kinetics		22
TRU-257	hydrochloric acid	1	N/A kinetics		0
TRU-258	hydrochloric acid	1	N/A kinetics		0
TRU-259	hydrochloric acid	1	N/A kinetics		0
TRU-260	hydrochloric acid	1	N/A kinetics		0
TRU-261	hydrochloric acid	1	N/A kinetics		1
TRU-262	hydrochloric acid	1	N/A kinetics		1
TRU-263	hydrochloric acid	1	N/A kinetics		1
TRU-264	hydrochloric acid	1	N/A kinetics		1
TRU-265	hydrochloric acid	1	N/A kinetics		3
TRU-266	hydrochloric acid	1	N/A kinetics		3
TRU-267	hydrochloric acid	1	N/A kinetics		3
TRU-268	hydrochloric acid	1	N/A kinetics		3
TRU-269	hydrochloric acid	1	N/A kinetics		7
TRU-270	hydrochloric acid	1	N/A kinetics		7
TRU-271	hydrochloric acid	1	N/A kinetics		7
TRU-272	hydrochloric acid	1	N/A kinetics		7
TRU-273	hydrochloric acid	1	N/A kinetics		14
TRU-274	hydrochloric acid	1	N/A kinetics		14
TRU-275	hydrochloric acid	1	N/A kinetics		14
TRU-276	hydrochloric acid	1	N/A kinetics		14
TRU-277	hydrochloric acid	1	N/A kinetics		22
TRU-278	hydrochloric acid	1	N/A kinetics		22
TRU-279	hydrochloric acid	1	N/A kinetics		22
TRU-280	hydrochloric acid	1	N/A kinetics		22
TRUB-01	nitric acid	3	6622.5	50000	
TRUB-02	nitric acid	3	6622.5	50000	
TRUB-03	nitric acid	3	6622.5	50000	

TRUB-04	nitric acid	3	6622.5	50000	
TRUB-05	nitric acid	3	0	0	
TRUB-06	nitric acid	3	0	0	
TRUB-07	nitric acid	3	0	0	
TRUB-08	nitric acid	3	0	0	
TRUB-09	hydrochloric acid	3	6622.5	50000	
TRUB-10	hydrochloric acid	3	6622.5	50000	
TRUB-11	hydrochloric acid	3	6622.5	50000	
TRUB-12	hydrochloric acid	3	6622.5	50000	Removed due
TRUB-13	hydrochloric acid	3	0	0	To process error
TRUB-14	hydrochloric acid	3	0	0	
TRUB-15	hydrochloric acid	3	0	0	
TRUB-16	hydrochloric acid	3	0	0	
TRUB-17	nitric acid	1	6622.5	50000	
TRUB-18	nitric acid	1	6622.5	50000	
TRUB-19	nitric acid	1	6622.5	50000	
TRUB-20	nitric acid	1	6622.5	50000	
TRUB-21	nitric acid	1	0	0	
TRUB-22	nitric acid	1	0	0	
TRUB-23	nitric acid	1	0	0	
TRUB-24	nitric acid	1	0	0	
TRUB-25	hydrochloric acid	1	6622.5	50000	
TRUB-26	hydrochloric acid	1	6622.5	50000	
TRUB-27	hydrochloric acid	1	6622.5	50000	
TRUB-28	hydrochloric acid	1	6622.5	50000	
TRUB-29	hydrochloric acid	1	0	0	
TRUB-30	hydrochloric acid	1	0	0	
TRUB-31	hydrochloric acid	1	0	0	
TRUB-32	hydrochloric acid	1	0	0	
TEVA-01	nitric acid	3	0	0	
TEVA-02	nitric acid	3	0	0	
TEVA-03	nitric acid	3	0	0	
TEVA-04	nitric acid	3	0	0	
TEVA-05	nitric acid	3	1.25	10	
TEVA-06	nitric acid	3	1.25	10	
TEVA-07	nitric acid	3	1.25	10	
TEVA-08	nitric acid	3	1.25	10	
TEVA-09	nitric acid	3	12.5	100	
TEVA-10	nitric acid	3	12.5	100	
TEVA-11	nitric acid	3	12.5	100	
TEVA-12	nitric acid	3	12.5	100	
TEVA-13	nitric acid	3	125	1000	

TEVA-14	nitric acid	3	125	1000	
TEVA-15	nitric acid	3	125	1000	
TEVA-16	nitric acid	3	125	1000	
TEVA-17	nitric acid	3	1250	10000	
TEVA-18	nitric acid	3	1250	10000	
TEVA-19	nitric acid	3	1250	10000	
TEVA-20	nitric acid	3	1250	10000	
TEVA-21	nitric acid	3	0	0	
TEVA-22	nitric acid	3	0	0	
TEVA-23	nitric acid	3	0	0	
TEVA-24	nitric acid	3	0	0	
TEVA-25	hydrochloric acid	3	0	0	
TEVA-26	hydrochloric acid	3	0	0	
TEVA-27	hydrochloric acid	3	0	0	
TEVA-28	hydrochloric acid	3	0	0	
TEVA-29	hydrochloric acid	3	1.25	10	
TEVA-30	hydrochloric acid	3	1.25	10	
TEVA-31	hydrochloric acid	3	1.25	10	
TEVA-32	hydrochloric acid	3	1.25	10	
TEVA-33	hydrochloric acid	3	12.5	100	
TEVA-34	hydrochloric acid	3	12.5	100	
TEVA-35	hydrochloric acid	3	12.5	100	
TEVA-36	hydrochloric acid	3	12.5	100	
TEVA-37	hydrochloric acid	3	125	1000	
TEVA-38	hydrochloric acid	3	125	1000	
TEVA-39	hydrochloric acid	3	125	1000	
TEVA-40	hydrochloric acid	3	125	1000	
TEVA-41	hydrochloric acid	3	1250	10000	
TEVA-42	hydrochloric acid	3	1250	10000	
TEVA-43	hydrochloric acid	3	1250	10000	
TEVA-44	hydrochloric acid	3	1250	10000	
TEVA-45	hydrochloric acid	3	0	0	
TEVA-46	hydrochloric acid	3	0	0	
TEVA-47	hydrochloric acid	3	0	0	
TEVA-48	hydrochloric acid	3	0	0	
TEVA-49	nitric acid	3	6250	50000	eliminated from study
TEVA-50	nitric acid	3	6250	50000	due to radiolytic embrittlement of tubes
TEVA-51	nitric acid	3	6250	50000	and irregular results due to freezing

TEVA-52	nitric acid	3	6250	50000	
TEVA-53	nitric acid	3	0	0	
TEVA-54	nitric acid	3	0	0	
TEVA-55	nitric acid	3	0	0	
TEVA-56	nitric acid	3	0	0	
TEVA-57	hydrochloric acid	3	6250	50000	
TEVA-58	hydrochloric acid	3	6250	50000	
TEVA-59	hydrochloric acid	3	6250	50000	
TEVA-60	hydrochloric acid	3	6250	50000	
TEVA-61	hydrochloric acid	3	0	0	
TEVA-62	hydrochloric acid	3	0	0	
TEVA-63	hydrochloric acid	3	0	0	
TEVA-64	hydrochloric acid	3	0	0	
TEVA-65	nitric acid	1	0	0	
TEVA-66	nitric acid	1	0	0	
TEVA-67	nitric acid	1	0	0	
TEVA-68	nitric acid	1	0	0	
TEVA-69	nitric acid	1	1.25	10	
TEVA-70	nitric acid	1	1.25	10	
TEVA-71	nitric acid	1	1.25	10	
TEVA-72	nitric acid	1	1.25	10	
TEVA-73	nitric acid	1	12.5	100	
TEVA-74	nitric acid	1	12.5	100	
TEVA-75	nitric acid	1	12.5	100	
TEVA-76	nitric acid	1	12.5	100	
TEVA-77	nitric acid	1	125	1000	
TEVA-78	nitric acid	1	125	1000	
TEVA-79	nitric acid	1	125	1000	
TEVA-80	nitric acid	1	125	1000	
TEVA-81	nitric acid	1	1250	10000	
TEVA-82	nitric acid	1	1250	10000	
TEVA-83	nitric acid	1	1250	10000	
TEVA-84	nitric acid	1	1250	10000	
TEVA-85	nitric acid	1	0	0	
TEVA-86	nitric acid	1	0	0	
TEVA-87	nitric acid	1	0	0	
TEVA-88	nitric acid	1	0	0	
TEVA-89	hydrochloric acid	1	0	0	
TEVA-90	hydrochloric acid	1	0	0	
TEVA-91	hydrochloric acid	1	0	0	
TEVA-92	hydrochloric acid	1	0	0	
TEVA-93	hydrochloric acid	1	1.25	10	
TEVA-94	hydrochloric acid	1	1.25	10	

TEVA-95	hydrochloric acid	1	1.25	10	
TEVA-96	hydrochloric acid	1	1.25	10	
TEVA-97	hydrochloric acid	1	12.5	100	
TEVA-98	hydrochloric acid	1	12.5	100	
TEVA-99	hydrochloric acid	1	12.5	100	
TEVA-100	hydrochloric acid	1	12.5	100	
TEVA-101	hydrochloric acid	1	125	1000	
TEVA-102	hydrochloric acid	1	125	1000	
TEVA-103	hydrochloric acid	1	125	1000	
TEVA-104	hydrochloric acid	1	125	1000	
TEVA-105	hydrochloric acid	1	1250	10000	
TEVA-106	hydrochloric acid	1	1250	10000	
TEVA-107	hydrochloric acid	1	1250	10000	
TEVA-108	hydrochloric acid	1	1250	10000	
TEVA-109	hydrochloric acid	1	0	0	
TEVA-110	hydrochloric acid	1	0	0	
TEVA-111	hydrochloric acid	1	0	0	
TEVA-112	hydrochloric acid	1	0	0	
TEVA-113	hydrochloric acid	3	1250	10000	
TEVA-114	hydrochloric acid	3	1250	10000	
TEVA-115	hydrochloric acid	3	1250	10000	
TEVA-116	hydrochloric acid	3	1250	10000	
TEVA-117	hydrochloric acid	3	0	0	
TEVA-118	hydrochloric acid	3	0	0	
TEVA-119	hydrochloric acid	3	0	0	
TEVA-120	hydrochloric acid	3	0	0	
TEVA-121	nitric acid	3	N/A kinetics		0
TEVA-122	nitric acid	3	N/A kinetics		0
TEVA-123	nitric acid	3	N/A kinetics		0
TEVA-124	nitric acid	3	N/A kinetics		0
TEVA-125	nitric acid	3	N/A kinetics		1
TEVA-126	nitric acid	3	N/A kinetics		1
TEVA-127	nitric acid	3	N/A kinetics		1
TEVA-128	nitric acid	3	N/A kinetics		1
TEVA-129	nitric acid	3	N/A kinetics		3
TEVA-130	nitric acid	3	N/A kinetics		3
TEVA-131	nitric acid	3	N/A kinetics		3
TEVA-132	nitric acid	3	N/A kinetics		3
TEVA-133	nitric acid	3	N/A kinetics		7
TEVA-134	nitric acid	3	N/A kinetics		7
TEVA-135	nitric acid	3	N/A kinetics		7
TEVA-136	nitric acid	3	N/A kinetics		7
TEVA-137	nitric acid	3	N/A kinetics		14

TEVA-138	nitric acid	3	N/A kinetics		14
TEVA-139	nitric acid	3	N/A kinetics		14
TEVA-140	nitric acid	3	N/A kinetics		14
TEVA-141	nitric acid	3	N/A kinetics		22
TEVA-142	nitric acid	3	N/A kinetics		22
TEVA-143	nitric acid	3	N/A kinetics		22
TEVA-144	nitric acid	3	N/A kinetics		22
TEVAB-01	nitric acid	3	6622.5	50000	
TEVAB-02	nitric acid	3	6622.5	50000	
TEVAB-03	nitric acid	3	6622.5	50000	
TEVAB-04	nitric acid	3	6622.5	50000	
TEVAB-05	nitric acid	3	0	0	
TEVAB-06	nitric acid	3	0	0	
TEVAB-07	nitric acid	3	0	0	
TEVAB-08	nitric acid	3	0	0	
TEVAB-09	hydrochloric acid	3	6622.5	50000	
TEVAB-10	hydrochloric acid	3	6622.5	50000	
TEVAB-11	hydrochloric acid	3	6622.5	50000	
TEVAB-12	hydrochloric acid	3	6622.5	50000	
TEVAB-13	hydrochloric acid	3	0	0	
TEVAB-14	hydrochloric acid	3	0	0	
TEVAB-15	hydrochloric acid	3	0	0	
TEVAB-16	hydrochloric acid	3	0	0	
TEVAB-17	nitric acid	1	6622.5	50000	
TEVAB-18	nitric acid	1	6622.5	50000	
TEVAB-19	nitric acid	1	6622.5	50000	
TEVAB-20	nitric acid	1	6622.5	50000	
TEVAB-21	nitric acid	1	0	0	
TEVAB-22	nitric acid	1	0	0	
TEVAB-23	nitric acid	1	0	0	
TEVAB-24	nitric acid	1	0	0	
TEVAB-25	hydrochloric acid	1	6622.5	50000	
TEVAB-26	hydrochloric acid	1	6622.5	50000	
TEVAB-27	hydrochloric acid	1	6622.5	50000	
TEVAB-28	hydrochloric acid	1	6622.5	50000	
TEVAB-29	hydrochloric acid	1	0	0	
TEVAB-30	hydrochloric acid	1	0	0	
TEVAB-31	hydrochloric acid	1	0	0	
TEVAB-32	hydrochloric acid	1	0	0	
UTEVA-01	nitric acid	3	0	0	
UTEVA-02	nitric acid	3	0	0	
UTEVA-03	nitric acid	3	0	0	
UTEVA-04	nitric acid	3	0	0	

UTEVA-05	nitric acid	3	1.25	10	
UTEVA-06	nitric acid	3	1.25	10	
UTEVA-07	nitric acid	3	1.25	10	
UTEVA-08	nitric acid	3	1.25	10	
UTEVA-09	nitric acid	3	12.5	100	
UTEVA-10	nitric acid	3	12.5	100	
UTEVA-11	nitric acid	3	12.5	100	
UTEVA-12	nitric acid	3	12.5	100	
UTEVA-13	nitric acid	3	125	1000	
UTEVA-14	nitric acid	3	125	1000	
UTEVA-15	nitric acid	3	125	1000	
UTEVA-16	nitric acid	3	125	1000	
UTEVA-17	nitric acid	3	1250	10000	
UTEVA-18	nitric acid	3	1250	10000	
UTEVA-19	nitric acid	3	1250	10000	
UTEVA-20	nitric acid	3	1250	10000	
UTEVA-21	nitric acid	3	0	0	
UTEVA-22	nitric acid	3	0	0	
UTEVA-23	nitric acid	3	0	0	
UTEVA-24	nitric acid	3	0	0	
UTEVA-25	hydrochloric acid	3	0	0	
UTEVA-26	hydrochloric acid	3	0	0	
UTEVA-27	hydrochloric acid	3	0	0	
UTEVA-28	hydrochloric acid	3	0	0	
UTEVA-29	hydrochloric acid	3	1.25	10	
UTEVA-30	hydrochloric acid	3	1.25	10	
UTEVA-31	hydrochloric acid	3	1.25	10	
UTEVA-32	hydrochloric acid	3	1.25	10	
UTEVA-33	hydrochloric acid	3	12.5	100	
UTEVA-34	hydrochloric acid	3	12.5	100	
UTEVA-35	hydrochloric acid	3	12.5	100	
UTEVA-36	hydrochloric acid	3	12.5	100	
UTEVA-37	hydrochloric acid	3	125	1000	
UTEVA-38	hydrochloric acid	3	125	1000	
UTEVA-39	hydrochloric acid	3	125	1000	
UTEVA-40	hydrochloric acid	3	125	1000	
UTEVA-41	hydrochloric acid	3	1250	10000	
UTEVA-42	hydrochloric acid	3	1250	10000	
UTEVA-43	hydrochloric acid	3	1250	10000	
UTEVA-44	hydrochloric acid	3	1250	10000	
UTEVA-45	hydrochloric acid	3	0	0	
UTEVA-46	hydrochloric acid	3	0	0	
UTEVA-47	hydrochloric acid	3	0	0	

UTEVA-48	hydrochloric acid	3	0	0	
UTEVA-49	nitric acid	1	0	0	
UTEVA-50	nitric acid	1	0	0	
UTEVA-51	nitric acid	1	0	0	
UTEVA-52	nitric acid	1	0	0	
UTEVA-53	nitric acid	1	1.25	10	
UTEVA-54	nitric acid	1	1.25	10	
UTEVA-55	nitric acid	1	1.25	10	
UTEVA-56	nitric acid	1	1.25	10	
UTEVA-57	nitric acid	1	12.5	100	
UTEVA-58	nitric acid	1	12.5	100	
UTEVA-59	nitric acid	1	12.5	100	
UTEVA-60	nitric acid	1	12.5	100	
UTEVA-61	nitric acid	1	125	1000	
UTEVA-62	nitric acid	1	125	1000	
UTEVA-63	nitric acid	1	125	1000	
UTEVA-64	nitric acid	1	125	1000	
UTEVA-65	nitric acid	1	1250	10000	
UTEVA-66	nitric acid	1	1250	10000	
UTEVA-67	nitric acid	1	1250	10000	
UTEVA-68	nitric acid	1	1250	10000	
UTEVA-69	nitric acid	1	0	0	
UTEVA-70	nitric acid	1	0	0	
UTEVA-71	nitric acid	1	0	0	
UTEVA-72	nitric acid	1	0	0	
UTEVA-73	hydrochloric acid	1	0	0	
UTEVA-74	hydrochloric acid	1	0	0	
UTEVA-75	hydrochloric acid	1	0	0	
UTEVA-76	hydrochloric acid	1	0	0	
UTEVA-77	hydrochloric acid	1	1.25	10	
UTEVA-78	hydrochloric acid	1	1.25	10	
UTEVA-79	hydrochloric acid	1	1.25	10	
UTEVA-80	hydrochloric acid	1	1.25	10	
UTEVA-81	hydrochloric acid	1	12.5	100	
UTEVA-82	hydrochloric acid	1	12.5	100	
UTEVA-83	hydrochloric acid	1	12.5	100	
UTEVA-84	hydrochloric acid	1	12.5	100	
UTEVA-85	hydrochloric acid	1	125	1000	
UTEVA-86	hydrochloric acid	1	125	1000	
UTEVA-87	hydrochloric acid	1	125	1000	
UTEVA-88	hydrochloric acid	1	125	1000	
UTEVA-89	hydrochloric acid	1	1250	10000	
UTEVA-90	hydrochloric acid	1	1250	10000	

UTEVA-91	hydrochloric acid	1	1250	10000	
UTEVA-92	hydrochloric acid	1	1250	10000	
UTEVA-93	hydrochloric acid	1	0	0	
UTEVA-94	hydrochloric acid	1	0	0	
UTEVA-95	hydrochloric acid	1	0	0	
UTEVA-96	hydrochloric acid	1	0	0	
UTEVA-97	hydrochloric acid	3	N/A kinetics		0
UTEVA-98	hydrochloric acid	3	N/A kinetics		0
UTEVA-99	hydrochloric acid	3	N/A kinetics		0
UTEVA-100	hydrochloric acid	3	N/A kinetics		0
UTEVA-101	hydrochloric acid	3	N/A kinetics		1
UTEVA-102	hydrochloric acid	3	N/A kinetics		1
UTEVA-103	hydrochloric acid	3	N/A kinetics		1
UTEVA-104	hydrochloric acid	3	N/A kinetics		1
UTEVA-105	hydrochloric acid	3	N/A kinetics		3
UTEVA-106	hydrochloric acid	3	N/A kinetics		3
UTEVA-107	hydrochloric acid	3	N/A kinetics		3
UTEVA-108	hydrochloric acid	3	N/A kinetics		3
UTEVA-109	hydrochloric acid	3	N/A kinetics		7
UTEVA-110	hydrochloric acid	3	N/A kinetics		7
UTEVA-111	hydrochloric acid	3	N/A kinetics		7
UTEVA-112	hydrochloric acid	3	N/A kinetics		7
UTEVA-113	hydrochloric acid	3	N/A kinetics		14
UTEVA-114	hydrochloric acid	3	N/A kinetics		14
UTEVA-115	hydrochloric acid	3	N/A kinetics		14
UTEVA-116	hydrochloric acid	3	N/A kinetics		14
UTEVA-117	hydrochloric acid	3	N/A kinetics		22
UTEVA-118	hydrochloric acid	3	N/A kinetics		22
UTEVA-119	hydrochloric acid	3	N/A kinetics		22
UTEVA-120	hydrochloric acid	3	N/A kinetics		22
UTEVAB-01	nitric acid	3	6622.5	50000	
UTEVAB-02	nitric acid	3	6622.5	50000	
UTEVAB-03	nitric acid	3	6622.5	50000	
UTEVAB-04	nitric acid	3	6622.5	50000	
UTEVAB-05	nitric acid	3	0	0	
UTEVAB-06	nitric acid	3	0	0	
UTEVAB-07	nitric acid	3	0	0	
UTEVAB-08	nitric acid	3	0	0	
UTEVAB-09	hydrochloric acid	3	6622.5	50000	
UTEVAB-10	hydrochloric acid	3	6622.5	50000	
UTEVAB-11	hydrochloric acid	3	6622.5	50000	
UTEVAB-12	hydrochloric acid	3	6622.5	50000	
UTEVAB-13	hydrochloric acid	3	0	0	

UTEVAB-14	hydrochloric acid	3	0	0	
UTEVAB-15	hydrochloric acid	3	0	0	
UTEVAB-16	hydrochloric acid	3	0	0	
UTEVAB-17	nitric acid	1	6622.5	50000	
UTEVAB-18	nitric acid	1	6622.5	50000	
UTEVAB-19	nitric acid	1	6622.5	50000	
UTEVAB-20	nitric acid	1	6622.5	50000	
UTEVAB-21	nitric acid	1	0	0	
UTEVAB-22	nitric acid	1	0	0	
UTEVAB-23	nitric acid	1	0	0	
UTEVAB-24	nitric acid	1	0	0	
UTEVAB-25	hydrochloric acid	1	6622.5	50000	
UTEVAB-26	hydrochloric acid	1	6622.5	50000	
UTEVAB-27	hydrochloric acid	1	6622.5	50000	
UTEVAB-28	hydrochloric acid	1	6622.5	50000	
UTEVAB-29	hydrochloric acid	1	0	0	
UTEVAB-30	hydrochloric acid	1	0	0	
UTEVAB-31	hydrochloric acid	1	0	0	
UTEVAB-32	hydrochloric acid	1	0	0	
AC-01	nitric acid	3	0	0	
AC-02	nitric acid	3	0	0	
AC-03	nitric acid	3	0	0	
AC-04	nitric acid	3	0	0	
AC-05	nitric acid	3	1.25	10	
AC-06	nitric acid	3	1.25	10	
AC-07	nitric acid	3	1.25	10	
AC-08	nitric acid	3	1.25	10	
AC-09	nitric acid	3	12.5	100	
AC-10	nitric acid	3	12.5	100	
AC-11	nitric acid	3	12.5	100	
AC-12	nitric acid	3	12.5	100	
AC-13	nitric acid	3	125	1000	
AC-14	nitric acid	3	125	1000	
AC-15	nitric acid	3	125	1000	
AC-16	nitric acid	3	125	1000	
AC-17	nitric acid	3	1250	10000	
AC-18	nitric acid	3	1250	10000	
AC-19	nitric acid	3	1250	10000	
AC-20	nitric acid	3	1250	10000	
AC-21	nitric acid	3	0	0	
AC-22	nitric acid	3	0	0	
AC-23	nitric acid	3	0	0	
AC-24	nitric acid	3	0	0	

AC-25	hydrochloric acid	3	0	0	
AC-26	hydrochloric acid	3	0	0	
AC-27	hydrochloric acid	3	0	0	
AC-28	hydrochloric acid	3	0	0	
AC-29	hydrochloric acid	3	1.25	10	
AC-30	hydrochloric acid	3	1.25	10	
AC-31	hydrochloric acid	3	1.25	10	
AC-32	hydrochloric acid	3	1.25	10	
AC-33	hydrochloric acid	3	12.5	100	
AC-34	hydrochloric acid	3	12.5	100	
AC-35	hydrochloric acid	3	12.5	100	
AC-36	hydrochloric acid	3	12.5	100	
AC-37	hydrochloric acid	3	125	1000	
AC-38	hydrochloric acid	3	125	1000	
AC-39	hydrochloric acid	3	125	1000	
AC-40	hydrochloric acid	3	125	1000	
AC-41	hydrochloric acid	3	1250	10000	
AC-42	hydrochloric acid	3	1250	10000	
AC-43	hydrochloric acid	3	1250	10000	
AC-44	hydrochloric acid	3	1250	10000	
AC-45	hydrochloric acid	3	0	0	
AC-46	hydrochloric acid	3	0	0	
AC-47	hydrochloric acid	3	0	0	
AC-48	hydrochloric acid	3	0	0	
AC-49	nitric acid	1	0	0	
AC-50	nitric acid	1	0	0	
AC-51	nitric acid	1	0	0	
AC-52	nitric acid	1	0	0	
AC-53	nitric acid	1	1.25	10	
AC-54	nitric acid	1	1.25	10	
AC-55	nitric acid	1	1.25	10	
AC-56	nitric acid	1	1.25	10	
AC-57	nitric acid	1	12.5	100	
AC-58	nitric acid	1	12.5	100	
AC-59	nitric acid	1	12.5	100	
AC-60	nitric acid	1	12.5	100	
AC-61	nitric acid	1	125	1000	
AC-62	nitric acid	1	125	1000	
AC-63	nitric acid	1	125	1000	
AC-64	nitric acid	1	125	1000	
AC-65	nitric acid	1	1250	10000	
AC-66	nitric acid	1	1250	10000	
AC-67	nitric acid	1	1250	10000	

AC-68	nitric acid	1	1250	10000	
AC-69	nitric acid	1	0	0	
AC-70	nitric acid	1	0	0	
AC-71	nitric acid	1	0	0	
AC-72	nitric acid	1	0	0	
AC-73	hydrochloric acid	1	0	0	
AC-74	hydrochloric acid	1	0	0	
AC-75	hydrochloric acid	1	0	0	
AC-76	hydrochloric acid	1	0	0	
AC-77	hydrochloric acid	1	1.25	10	
AC-78	hydrochloric acid	1	1.25	10	
AC-79	hydrochloric acid	1	1.25	10	
AC-80	hydrochloric acid	1	1.25	10	
AC-81	hydrochloric acid	1	12.5	100	
AC-82	hydrochloric acid	1	12.5	100	
AC-83	hydrochloric acid	1	12.5	100	
AC-84	hydrochloric acid	1	12.5	100	
AC-85	hydrochloric acid	1	125	1000	
AC-86	hydrochloric acid	1	125	1000	
AC-87	hydrochloric acid	1	125	1000	
AC-88	hydrochloric acid	1	125	1000	
AC-89	hydrochloric acid	1	1250	10000	
AC-90	hydrochloric acid	1	1250	10000	
AC-91	hydrochloric acid	1	1250	10000	
AC-92	hydrochloric acid	1	1250	10000	
AC-93	hydrochloric acid	1	0	0	
AC-94	hydrochloric acid	1	0	0	
AC-95	hydrochloric acid	1	0	0	
AC-96	hydrochloric acid	1	0	0	
AC-97	hydrochloric acid	3	N/A kinetics		0
AC-98	hydrochloric acid	3	N/A kinetics		0
AC-99	hydrochloric acid	3	N/A kinetics		0
AC-100	hydrochloric acid	3	N/A kinetics		0
AC-101	hydrochloric acid	3	N/A kinetics		1
AC-102	hydrochloric acid	3	N/A kinetics		1
AC-103	hydrochloric acid	3	N/A kinetics		1
AC-104	hydrochloric acid	3	N/A kinetics		1
AC-105	hydrochloric acid	3	N/A kinetics		3
AC-106	hydrochloric acid	3	N/A kinetics		3
AC-107	hydrochloric acid	3	N/A kinetics		3
AC-108	hydrochloric acid	3	N/A kinetics		3
AC-109	hydrochloric acid	3	N/A kinetics		7
AC-110	hydrochloric acid	3	N/A kinetics		7

AC-111	hydrochloric acid	3	N/A kinetics		7
AC-112	hydrochloric acid	3	N/A kinetics		7
AC-113	hydrochloric acid	3	N/A kinetics		14
AC-114	hydrochloric acid	3	N/A kinetics		14
AC-115	hydrochloric acid	3	N/A kinetics		14
AC-116	hydrochloric acid	3	N/A kinetics		14
AC-117	hydrochloric acid	3	N/A kinetics		22
AC-118	hydrochloric acid	3	N/A kinetics		22
AC-119	hydrochloric acid	3	N/A kinetics		22
AC-120	hydrochloric acid	3	N/A kinetics		22
AC-B-01	nitric acid	3	6622.5	50000	
AC-B-02	nitric acid	3	6622.5	50000	
AC-B-03	nitric acid	3	6622.5	50000	
AC-B-04	nitric acid	3	6622.5	50000	
AC-B-05	nitric acid	3	0	0	
AC-B-06	nitric acid	3	0	0	
AC-B-07	nitric acid	3	0	0	
AC-B-08	nitric acid	3	0	0	
AC-B-09	hydrochloric acid	3	6622.5	50000	
AC-B-10	hydrochloric acid	3	6622.5	50000	
AC-B-11	hydrochloric acid	3	6622.5	50000	
AC-B-12	hydrochloric acid	3	6622.5	50000	
AC-B-13	hydrochloric acid	3	0	0	
AC-B-14	hydrochloric acid	3	0	0	
AC-B-15	hydrochloric acid	3	0	0	
AC-B-16	hydrochloric acid	3	0	0	
~~AC-B-17~~	~~nitric acid~~	~~1~~	~~6622.5~~	~~50000~~	Batch
~~AC-B-18~~	~~nitric acid~~	~~1~~	~~6622.5~~	~~50000~~	Scrapped
~~AC-B-19~~	~~nitric acid~~	~~1~~	~~6622.5~~	~~50000~~	Due to
~~AC-B-20~~	~~nitric acid~~	~~1~~	~~6622.5~~	~~50000~~	Malfunction
~~AC-B-21~~	~~nitric acid~~	~~1~~	~~0~~	~~0~~	With
~~AC-B-22~~	~~nitric acid~~	~~1~~	~~0~~	~~0~~	Irradiator
~~AC-B-23~~	~~nitric acid~~	~~1~~	~~0~~	~~0~~	Sample
~~AC-B-24~~	~~nitric acid~~	~~1~~	~~0~~	~~0~~	Holder
~~AC-B-25~~	~~hydrochloric acid~~	~~1~~	~~6622.5~~	~~50000~~	Rotation
~~AC-B-26~~	~~hydrochloric acid~~	~~1~~	~~6622.5~~	~~50000~~	-
~~AC-B-27~~	~~hydrochloric acid~~	~~1~~	~~6622.5~~	~~50000~~	-
~~AC-B-28~~	~~hydrochloric acid~~	~~1~~	~~6622.5~~	~~50000~~	-
~~AC-B-29~~	~~hydrochloric acid~~	~~1~~	~~0~~	~~0~~	-
~~AC-B-30~~	~~hydrochloric acid~~	~~1~~	~~0~~	~~0~~	-
~~AC-B-31~~	~~hydrochloric acid~~	~~1~~	~~0~~	~~0~~	-
~~AC-B-32~~	~~hydrochloric acid~~	~~1~~	~~0~~	~~0~~	-
AC-B-33	nitric acid	1	6622.5	50000	

AC-B-34	nitric acid	1	6622.5	50000	
AC-B-35	nitric acid	1	6622.5	50000	
AC-B-36	nitric acid	1	6622.5	50000	
AC-B-37	nitric acid	1	0	0	
AC-B-38	nitric acid	1	0	0	
AC-B-39	nitric acid	1	0	0	
AC-B-40	nitric acid	1	0	0	
AC-B-41	hydrochloric acid	1	6622.5	50000	
AC-B-42	hydrochloric acid	1	6622.5	50000	
AC-B-43	hydrochloric acid	1	6622.5	50000	
AC-B-44	hydrochloric acid	1	6622.5	50000	
AC-B-45	hydrochloric acid	1	0	0	
AC-B-46	hydrochloric acid	1	0	0	
AC-B-47	hydrochloric acid	1	0	0	
AC-B-48	hydrochloric acid	1	0	0	

S#	SAMPLE ID	COUNT TIME / MIN	CPMA	SIS	MESSAGES	Group
1	HNO3 STD-1	60	4193	243.22		1
2	HNO3 STD-2	60	4190	236.39		1
3	HNO3 STD-3	60	4183	235.25		1
4	HNO3 STD-4	60	4200	232.15		1
5	HCl STD-1	60	3180	678.86		2
6	HCl STD-2	60	3182	684.63		2
7	HCl STD-3	60	3163	685.47		2
8	HCl STD-4	60	3178	688.8		2
9	TRU081	60	110	453.28		3
10	TRU082	60	109	484.33		3
11	TRU083	60	109	461.46		3
12	TRU084	60	111	495.31		3
13	TRU085	60	110	512.57		4
14	TRU086	60	112	466.93		4
15	TRU087	60	110	512.45		4
16	TRU088	60	108	487.05		4
17	TRU089	60	107	447.03		5
18	TRU090	60	110	486.64		5
19	TRU091	60	109	468.22		5
20	TRU092	60	109	500.46		5
21	TRU093	60	107	461.08		6
22	TRU094	60	107	433.96		6
23	TRU095	60	108	477.75		6
24	TRU096	60	108	442.31		6

25	TRU097	60	105	432.94		7
26	TRU098	60	104	410.41		7
27	TRU099	60	105	426.29		7
28	TRU100	60	109	424.4		7
29	TRU101	60	111	479.19		8
30	TRU102	60	103	427.1		8
31	TRU103	60	105	433.55		8
32	TRU104	60	113	526.67		8
~~33~~	~~TRU065~~	~~60~~	~~338~~	~~645.85~~		~~9~~
~~34~~	~~TRU066~~	~~60~~	~~710~~	~~632.6~~		~~9~~
~~35~~	~~TRU067~~	~~60~~	~~412~~	~~653.69~~		~~9~~
~~36~~	~~TRU068~~	~~60~~	~~1316~~	~~628.16~~		~~9~~
~~37~~	~~TRU069~~	~~60~~	~~1164~~	~~627.11~~		~~10~~
~~38~~	~~TRU070~~	~~60~~	~~774~~	~~635.85~~		~~10~~
~~39~~	~~TRU071~~	~~60~~	~~886~~	~~634.46~~		~~10~~
~~40~~	~~TRU072~~	~~60~~	~~912~~	~~634.24~~		~~10~~
41	TRU105	60	504	674.47		11
42	TRU106	60	625	678.41		11
43	TRU107	60	577	669.69		11
44	TRU108	60	831	652.41		11
45	TRU109	60	542	671.92		12
46	TRU110	60	646	682.39		12
47	TRU111	60	561	669.74		12
48	TRU112	60	716	674.56		12
49	TRU113	60	468	659.68		13
50	TRU114	60	432	684.63		13
51	TRU115	60	441	674.91		13
52	TRU116	60	481	664.22		13
53	TRU117	60	485	686.38		14
54	TRU118	60	330	674.32		14
55	TRU119	60	363	679.35		14
56	TRU120	60	315	687.93		14
57	TRU121	60	203	688.48		15
58	TRU122	60	186	692.34		15
59	TRU123	60	256	663.86		15
60	TRU124	60	205	681.4		15
61	TRU125	60	1299	667.67		16
62	TRU126	60	1049	667.41		16
63	TRU127	60	973	680.6		16
64	TRU128	60	1318	642.8		16
~~65~~	~~TRU073~~	~~60~~	~~113~~	~~637.16~~		~~17~~
~~66~~	~~TRU074~~	~~60~~	~~112~~	~~651.34~~		~~17~~
~~67~~	~~TRU075~~	~~60~~	~~116~~	~~614.25~~		~~17~~

~~68~~	~~TRU076~~	~~60~~	~~111~~	~~632.08~~		~~17~~
~~69~~	~~TRU077~~	~~60~~	~~113~~	~~643.12~~		~~18~~
~~70~~	~~TRU078~~	~~60~~	~~116~~	~~664.34~~		~~18~~
~~71~~	~~TRU079~~	~~60~~	~~114~~	~~662.61~~		~~18~~
~~72~~	~~TRU080~~	~~60~~	~~115~~	~~641.28~~		~~18~~

Group	Dw	Sdev (1 sigma)	t-test, two tailed, unequal variance
3	489.2468	4.426168	
4	488.1446	7.545476	0.811
5	493.9523	5.986464	0.257
6	499.8872	2.792158	0.009
7	508.6503	10.88971	0.03
8	498.2246	22.85592	
~~9~~	~~85.54326~~	~~55.32013~~	
~~10~~	~~41.14358~~	~~9.975569~~	
11	49.02598	13.80656	
12	49.57207	8.814369	
13	73.13569	4.663446	0.007
14	96.67266	20.92045	0.014
15	182.0492	26.21357	0.001
16	17.1519	5.682034	0.001
~~17~~	~~354.8214~~	~~7.086469~~	
~~18~~	~~349.8461~~	~~4.170419~~	

S#	SAMPLE ID	Count time / min	CPMA	SIS		Group
1	HNO3 STD-1	60	4175	163.03		1
2	HNO3 STD-2	60	4180	163.71		1
3	HNO3 STD-3	60	4169	155.5		1
4	HNO3 STD-4	60	4196	168.19		1
5	TRUB-01	60	111	657.61		2
6	TRUB-02	60	114	627.77		2
7	TRUB-03	60	108	658.47		2
8	TRUB-04	60	115	643.41		2
9	TRUB-05	60	119	647.11		3
10	TRUB-06	60	121	643.71		3
11	TRUB-07	60	119	634.63		3
12	TRUB-08	60	113	645.9		3
13	HCl STD-1	60	3154	664.57		4
14	HCl STD-2	60	3175	670.9		4

15	HCl STD-3	60	3165	678.85		4
16	HCl STD-4	60	3175	680.28		4
17	TRUB-09	60	910	598.6		5
18	TRUB-10	60	192	666.53		5
19	TRUB-11	60	1240	597.85		5
20	TRUB-14	60	1249	594.47		6
21	TRUB-15	60	1000	606.56		6
22	TRUB-16	60	1396	611.13		6

Group	average	SDEV
1	**2786.667**	**11.57584**
2	112	3.162278
3	118	3.464102
4	**2111.5**	**10.01249**
5	780.6667	535.837
6	1215	200.1774

Group	Dw	Sdev	t-test, two tailed, unequal variance
2	477.9196	14.19091	
3	452.6291	14.2011	0.045
5	80.13699	103.9429	
6	15.43059	6.151666	0.394

S#	SAMPLE ID	COUNT TIME/MIN	CPMA	SIS	MESSAGES
1	A-HNO3 STD-A	60	2058	605.02	
2	B-HNO3 STD-B	60	2070	617.56	
3	C-HNO3 STD-C	60	2061	618.28	
4	D-HNO3 STD-D	60	2059	622.14	
5	TRUB-17	60	106	721.47	
6	TRUB-18	60	106	717.09	
7	TRUB-19	60	104	737.79	
8	TRUB-20	60	103	708.78	
9	TRUB-21	60	128	705.12	
10	TRUB-22	60	123	702.52	
11	TRUB-23	60	117	709.33	
12	TRUB-24	60	119	713.46	
13	E-HCl STD-E	60	4016	673.41	
14	F-HCl STD-F	60	4019	662	
15	G-HCl STD-G	60	4031	659.41	
16	H-HCl STD-H	60	4044	659.24	
17	TRUB-25	60	394	697.08	
18	TRUB-26	60	508	702.08	
19	TRUB-27	60	343	712.95	

20	TRUB-28	60	1089	681.85	
21	TRUB-29	60	2094	666.58	
22	TRUB-30	60	1938	660.17	
23	TRUB-31	60	1837	669.85	
24	TRUB-32	60	1941	655.15	

Group	average	sdev
1	2062	5.477226
2	104.75	1.5
3	121.75	4.856267
4	4027.5	12.76715
5	583.5	343.9869
6	1952.5	105.9953

Group	Dw	sdev	t-test, two tailed, unequal variance
2	242.5067	3.769247	
3	206.0842	8.903988	0.002
5	91.96853	46.70918	
6	7.563068	1.471832	0.036

s#	SAMPLE ID	Time / min	CPMA	SIS		Group
1	HNO3 STD-1	60	4193	243.22		1
2	HNO3 STD-2	60	4190	236.39		1
3	HNO3 STD-3	60	4183	235.25		1
4	HNO3 STD-4	60	4200	232.15		1
5	HCl STD-1	60	3180	678.86		2
6	HCl STD-2	60	3182	684.63		2
7	HCl STD-3	60	3163	685.47		2
8	HCl STD-4	60	3178	688.8		2
1	TEVA01	60	75.42	310.37		3
2	TEVA02	60	78.55	312.99		3
3	TEVA03	60	76.95	301.95		3
4	TEVA04	60	74.65	290.35		3
5	TEVA05	60	88.45	338.73		4
6	TEVA06	60	77.22	269.18		4
7	TEVA07	60	75.23	286.8		4
8	TEVA08	60	74.77	297.91		4
9	TEVA09	60	71.13	281.05		5
10	TEVA10	60	66.42	270.23		5
11	TEVA11	60	67	269.73		5
12	TEVA12	60	75.2	275.81		5
13	TEVA13	60	62.77	232.44		6
14	TEVA14	60	62.85	238.21		6
15	TEVA15	60	63.13	227.74		6
16	TEVA16	60	61.92	227.89		6

17	TEVA17	60	62.28	212.33		7
18	TEVA18	60	59.73	219.33		7
19	TEVA19	60	59.32	205.59		7
20	TEVA20	60	57.67	198.46		7
21	TEVA21	60	74.32	293.75		8
22	TEVA22	60	72.95	273.77		8
23	TEVA23	60	70.03	272.56		8
24	TEVA24	60	71.78	277.28		8
25	TEVA25	60	1394.32	545.02		9
26	TEVA26	60	1404.42	544.7		9
27	TEVA27	60	1448.25	552.78		9
28	TEVA28	60	1281.45	526.28		9
29	TEVA29	60	1463.62	531.51		10
30	TEVA30	60	1479.43	543.13		10
31	TEVA31	60	1293.43	496.25		10
32	TEVA32	60	1416.88	534.96		10
33	TEVA33	60	1352.43	515.31		11
34	TEVA34	60	1408.98	520.03		11
35	TEVA35	60	1435.47	542.82		11
36	TEVA36	60	1420.58	527.62		11
37	TEVA37	60	1527	637.73		12
38	TEVA38	60	1437	636.02		12
39	TEVA39	60	1520	645.7		12
40	TEVA40	60	1445	648.14		12
41	TEVA41	60	1407	661.54		13
42	TEVA42	60	1462	651.32		13
43	TEVA43	60	1390	658.96		13
44	TEVA44	60	1476	646.38		13
45	TEVA45	60	1528	657.79		14
46	TEVA46	60	1544	645.62		14
47	TEVA47	60	1547	649.42		14
48	TEVA48	60	1525	645.26		14
~~49~~	~~TEVA49~~	~~60~~	~~117~~	~~627.78~~		~~15~~
~~50~~	~~TEVA50~~	~~60~~	~~109~~	~~699.74~~		~~15~~
~~51~~	~~TEVA51~~	~~60~~	~~109~~	~~673~~		~~15~~
~~52~~	~~TEVA52~~	~~60~~	~~109~~	~~718.13~~		~~15~~
~~53~~	~~TEVA53~~	~~60~~	~~187~~	~~685.16~~		~~16~~
~~54~~	~~TEVA54~~	~~60~~	~~158~~	~~651.48~~		~~16~~
~~55~~	~~TEVA55~~	~~60~~	~~236~~	~~627.16~~		~~16~~
~~56~~	~~TEVA56~~	~~60~~	~~189~~	~~635.61~~		~~16~~
~~57~~	~~TEVA57~~	~~60~~	~~890~~	~~683.09~~		~~17~~
~~58~~	~~TEVA58~~	~~60~~	~~801~~	~~635.51~~		~~17~~
~~59~~	~~TEVA59~~	~~60~~	~~928~~	~~641.38~~		~~17~~

~~60~~	~~TEVA60~~	~~60~~	~~740~~	~~695.23~~		~~17~~
~~61~~	~~TEVA61~~	~~60~~	~~806~~	~~660.02~~		~~18~~
~~62~~	~~TEVA62~~	~~60~~	~~732~~	~~703.86~~		~~18~~
~~63~~	~~TEVA63~~	~~60~~	~~794~~	~~691.94~~		~~18~~
~~64~~	~~TEVA64~~	~~60~~	~~740~~	~~705.09~~		~~18~~

Group	average	sdev
1	2794.333	7.047458
2	2117.167	8.655441
3	76.3925	1.727008
4	78.9175	6.443329
5	69.9375	4.087284
6	62.6675	0.521688
7	59.75	1.907232
8	72.27	1.818663
9	1382.11	71.07216
10	1413.34	84.23559
11	1404.365	36.28126
12	1482.25	47.82869
13	1433.75	41.68433
14	1536	11.10555
~~15~~	~~111~~	~~4~~
~~16~~	~~192.5~~	~~32.27486~~
~~17~~	~~839.75~~	~~85.1758~~
~~18~~	~~768~~	~~37.41657~~

Group	Dw	sdev	t-test, two tailed, unequal variance
3	711.8515	16.45333	
4	691.4756	54.07213	0.515
5	781.1034	45.85767	0.05
6	871.8432	7.47007	0
7	916.0496	29.5852	0
8	753.6726	19.54561	
9	10.69985	1.637282	
10	10.04353	1.874609	0.617
11	10.16663	0.794714	0.587
12	8.589263	0.922627	0.078
13	9.552029	0.859896	0.016
14	7.56836	0.199325	
~~15~~	~~542.2072~~		
~~16~~	~~299.9481~~		
~~17~~	~~45.63561~~		
~~18~~	~~52.70182~~		

s#	SAMPLE ID	time	CPMA	SIS		Group
1	HNO3 STD-1	60	4225	387.59		1
2	HNO3 STD-2	60	4204	383.74		1
3	HNO3 STD-3	60	4228	367.28		1
4	HNO3 STD-4	60	4225	362.92		1
5	UTEVA-01	60	402	604.96		2
6	UTEVA-02	60	574	607.13		2
7	UTEVA-03	60	474	611.19		2
8	UTEVA-04	60	472	629.05		2
9	UTEVA-05	60	544	602		3
10	UTEVA-06	60	660	588.36		3
11	UTEVA-07	60	390	617.77		3
12	UTEVA-08	60	355	638.2		3

13	UTEVA-09	60	275	638.53		4
14	UTEVA-10	60	352	623.73		4
15	UTEVA-11	60	302	643.46		4
16	UTEVA-12	60	313	659.63		4
17	UTEVA-13	60	488	615.48		5
18	UTEVA-14	60	452	618.6		5
19	UTEVA-15	60	378	600.64		5
20	UTEVA-16	60	433	619.04		5
21	UTEVA-17	60	212	607.42		6
22	UTEVA-18	60	246	628.3		6
23	UTEVA-19	60	241	594.94		6
24	UTEVA-20	60	283	642.15		6
25	UTEVA-21	60	318	647.56		7
26	UTEVA-22	60	310	628.62		7
27	UTEVA-23	60	374	636.11		7
28	UTEVA-24	60	424	623.65		7
29	TEVA-B-01	60	108	672.29		8
30	TEVA-B-02	60	105	653.51		8
31	TEVA-B-03	60	110	599.41		8
32	TEVA-B-04	60	107	627.55		8
33	TEVA-B-05	60	237	583.96		9
34	TEVA-B-06	60	145	603.55		9
35	TEVA-B-07	60	143	611.67		9
36	TEVA-B-08	60	218	578.45		9
37	UTEVA-B-01	60	190	684.9		10
38	UTEVA-B-02	60	146	669.74		10
39	UTEVA-B-03	60	178	645.57		10
40	UTEVA-B-04	60	165	663.98		10
41	UTEVA-B-05	60	344	607.66		11
42	UTEVA-B-06	60	260	680.58		11
43	UTEVA-B-07	60	306	639.09		11
44	UTEVA-B-08	60	348	631.19		11
45	HCl STD-1	60	3182	828.71		12
46	HCl STD-2	60	3254	879.06		12
47	HCl STD-3	60	3120	910.21		12
48	HCl STD-4	60	3322	924.25		12
49	UTEVA-25	60	1328	701.83		13
50	UTEVA-26	60	1302	702.43		13
51	UTEVA-27	60	1242	713.07		13
52	UTEVA-28	60	1263	654.69		13
53	UTEVA-29	60	1262	699.94		14
54	UTEVA-30	60	1231	693.53		14
55	UTEVA-31	60	1160	712.73		14

56	UTEVA-32	60	1274	719.58		14
57	UTEVA-33	60	1200	719.1		15
58	UTEVA-34	60	1039	720.49		15
59	UTEVA-35	60	1180	720.34		15
60	UTEVA-36	60	1299	722.68		15
61	UTEVA-37	60	1206	716.85		16
62	UTEVA-38	60	1289	710.32		16
63	UTEVA-39	60	1225	646.92		16
64	UTEVA-40	60	1325	711.67		16
65	UTEVA-41	60	1360	708.26		17
66	UTEVA-42	60	1225	705.03		17
67	UTEVA-43	60	1183	695.37		17
68	UTEVA-44	60	1221	720.13		17
69	UTEVA-45	60	1298	715.82		18
70	UTEVA-46	60	1256	714.75		18
71	UTEVA-47	60	1305	707.42		18
72	UTEVA-48	60	1448	706.91		18
73	TEVA-B-09	60	1416	635.94		19
74	TEVA-B-10	60	1393	630.57		19
75	TEVA-B-11	60	1360	634.51		19
76	TEVA-B-12	60	1193	656.21		19
77	TEVA-B-13	60	1188	646.6		20
78	TEVA-B-14	60	1591	609.09		20
79	TEVA-B-15	60	1370	627.84		20
80	TEVA-B-16	60	1192	637.67		20
81	UTEVA-B-09	60	612	719.6		21
82	UTEVA-B-10	60	552	744.28		21
83	UTEVA-B-11	60	834	714.19		21
84	UTEVA-B-12	60	903	693.52		21
85	UTEVA-B-13	60	677	744.06		22
86	UTEVA-B-14	60	902	713.87		22
87	UTEVA-B-15	60	652	748.85		22
88	UTEVA-B-16	60	935	717.31		22

Group	average	sdev
1	**2813.667**	**11.09054**
2	480.5	70.75545
3	487.25	141.434
4	310.5	31.94266
5	437.75	45.90116

group	Dw	Sdev	t-test, two tailed, unequal variance
2	98.99098	17.12573	
3	102.8783	34.25984	0.848
4	162.6551	18.47484	0.002
5	109.6614	14.16105	0.375
6	211.6347	27.26239	0.008

6	245.5	29.14904
7	356.5	53.25098
8	107.5	2.081666
09	185.75	48.83561
10	169.75	18.83923
11	314.5	40.96747
12	**2146.333**	**87.56521**
13	1283.75	38.57784
14	1231.75	51.14929
15	1179.5	107.1463
16	1261.25	55.37975
17	1247.25	77.5129
18	1326.75	83.67945
19	1340.5	100.9835
20	1335.25	190.4545
21	725.25	169.5708
22	791.5	147.6177

7	140.4177	22.98908	
8	503.6202	10.1432	0.015
9	299.2967	83.03243	
10	314.7006	38.4828	
11	161.4065	25.42323	0.001
13	13.46111	1.004048	
14	14.89657	1.491309	0.168
15	16.62801	3.444667	0.162
16	14.08405	1.489334	0.517
17	14.51228	2.044298	0.194
18	12.44703	1.952094	
19	12.16931	2.593103	0.868
20	12.61503	4.370632	
21	41.72898	14.54381	0.527
22	35.68675	10.38875	

s#	SAMPLE ID	time	CPMA	SIS		Group
1	A: 1 M HNO3 STD	60	2073	609.95		1
2	B: 1 M HNO3 STD	60	2084	608.26		1
3	C: 1 M HNO3 STD	60	2067	613.23		1
4	D: 1 M HNO3 STD	60	2077	613.84		1
5	TRU-129	60	109	737.27		2
6	TRU-130	60	113	729.84		2
7	TRU-131	60	109	768.31		2
8	TRU-132	60	110	725.54		2
9	TRU-133	60	104	756.54		3
10	TRU-134	60	111	737.47		3
11	TRU-135	60	110	764.92		3
12	TRU-136	60	109	736.99		3
13	TRU-137	60	106	709.12		4
14	TRU-138	60	111	712.95		4
15	TRU-139	60	109	741.6		4
16	TRU-140	60	117	708		4
17	TRU-141	60	106	753.95		5
18	TRU-142	60	114	739.22		5
19	TRU-143	60	112	734.93		5
20	TRU-144	60	109	712.52		5
21	TRU-145	60	114	691.75		6
22	TRU-146	60	119	760.81		6

23	TRU-147	60	114	721.26		6
24	TRU-148	60	109	743.87		6
25	TRU-149	60	115	710.19		7
26	TRU-150	60	118	726.07		7
27	TRU-151	60	110	736.36		7
28	TRU-152	60	116	726.88		7
29	TEVA-65	60	578	692.91		8
30	TEVA-66	60	494	683.06		8
31	TEVA-67	60	552	658.79		8
32	TEVA-68	60	576	677.26		8
33	TEVA-69	60	557	678.4		9
34	TEVA-70	60	497	690.74		9
35	TEVA-71	60	521	672.48		9
36	TEVA-72	60	470	674.22		9
37	TEVA-73	60	222	713.95		10
38	TEVA-74	60	474	686.6		10
39	TEVA-75	60	342	678.22		10
40	TEVA-76	60	511	674.35		10
41	TEVA-77	60	314	685.57		11
42	TEVA-78	60	547	660.66		11
43	TEVA-79	60	208	698.25		11
44	TEVA-80	60	150	697.52		11
45	TEVA-81	60	153	719.55		12
46	TEVA-82	60	117	731.38		12
47	TEVA-83	60	126	701.56		12
48	TEVA-84	60	134	707.64		12
49	TEVA-85	60	551	661.54		13
50	TEVA-86	60	594	673.01		13
51	TEVA-87	60	401	729.14		13
52	TEVA-88	60	374	743.02		13
53	TEVA-B-17	60	115	728.31		14
54	TEVA-B-18	60	109	761.5		14
55	TEVA-B-19	60	113	728.29		14
56	TEVA-B-20	60	112	747.1		14
57	TEVA-B-21	60	533	699.16		15
58	TEVA-B-22	60	301	665.7		15
59	TEVA-B-23	60	367	704.19		15
60	TEVA-B-24	60	381	717.27		15
61	UTEVA-B-17	60	399	728.14		16
62	UTEVA-B-18	60	307	725.73		16
63	UTEVA-B-19	60	314	731.93		16
64	UTEVA-B-20	60	479	712.76		16
65	UTEVA-B-21	60	646	743.46		17

66	UTEVA-B-22	60	452	749.19		17
67	UTEVA-B-23	60	716	719.02		17
68	UTEVA-B-24	60	510	726.67		17
69	E: 1 M HCl STD	60	4032	671.65		18
70	F: 1 M HCl STD	60	4036	664.48		18
71	G: 1 M HCl STD	60	4045	662.97		18
72	H: 1 M HCl STD	60	4066	658.67		18
73	TRU-153	60	1395	739.53		19
74	TRU-154	60	1147	766.75		19
75	TRU-155	60	1882	696.95		19
76	TRU-156	60	1368	739.14		19
77	TRU-157	60	1797	713.5		20
78	TRU-158	60	1292	734.88		20
79	TRU-159	60	1396	739.72		20
80	TRU-160	60	1402	753.45		20
81	TRU-161	60	1307	740.23		21
82	TRU-162	60	1392	741.96		21
83	TRU-163	60	1648	723.58		21
84	TRU-164	60	1310	757.45		21
85	TRU-165	60	1412	751.47		22
86	TRU-166	60	1104	759.35		22
87	TRU-167	60	1848	709.87		22
88	TRU-168	60	1260	734.84		22
89	TRU-169	60	1310	734.23		23
90	TRU-170	60	1231	748.47		23
91	TRU-171	60	1353	758.05		23
92	TRU-172	60	1420	725.05		23
93	TRU-173	60	1556	713		24
94	TRU-174	60	1441	741.18		24
95	TRU-175	60	1127	755.66		24
96	TRU-176	60	1261	741.39		24
97	TEVA-089	60	1885	700.03		25
98	TEVA-090	60	1820	705.83		25
99	TEVA-091	60	1959	698.52		25
100	TEVA-092	60	1034	756.44		25
101	TEVA-093	60	1141	759.11		26
102	TEVA-094	60	1964	709.33		26
103	TEVA-095	60	1932	697.32		26
104	TEVA-096	60	2075	659.93		26
105	TEVA-097	60	1570	682.79		27
106	TEVA-098	60	2004	668.49		27
107	TEVA-099	60	1796	713.08		27
108	TEVA-100	60	1895	7001.05		27

109	TEVA-101	60	1796	721.61		28
110	TEVA-102	60	1894	711.81		28
111	TEVA-103	60	1955	719.97		28
112	TEVA-104	60	1951	707		28
113	TEVA-105	60	1854	691.83		29
114	TEVA-106	60	1762	716.58		29
115	TEVA-107	60	1905	710.2		29
116	TEVA-108	60	1863	693.81		29
117	TEVA-109	60	1924	708.22		30
118	TEVA-110	60	2067	708.64		30
119	TEVA-111	60	1947	708.92		30
120	TEVA-112	60	1885	711.67		30
121	TEVA-B-25	60	1861	696.34		31
122	TEVA-B-26	60	1682	728.4		31
123	TEVA-B-27	60	1248	775.59		31
124	TEVA-B-28	60	1108	738.41		31
125	TEVA-B-29	60	2015	690.21		32
126	TEVA-B-30	60	1688	672.95		32
127	TEVA-B-31	60	1294	722.9		32
128	TEVA-B-32	60	2136	703.44		32
129	UTEVA-B-25	60	1409	763.4		33
130	UTEVA-B-26	60	1541	768.57		33
131	UTEVA-B-27	60	1549	773.96		33
132	UTEVA-B-28	60	1311	785.82		33
133	UTEVA-B-29	60	1652	760.49		34
134	UTEVA-B-30	60	1687	750.57		34
135	UTEVA-B-31	60	1560	763.68		34
136	UTEVA-B-32	60	1558	786.54		34

Group	AVERAGE	SDEV
1	**1383.5**	**7.135592**
2	110.25	1.892969
3	108.5	3.109126
4	110.75	4.645787
5	110.25	3.5
6	114	4.082483
7	114.75	3.40343
8	550	39.1578
9	511.25	36.93576
10	387.25	131.9024

Group	Dw	Sdev	t-test, two tailed, unequal variance
2	231.0298	4.249947	
3	235.1839	7.485829	0.381
4	230.1665	10.31912	0.885
5	231.166	8.019375	0.977
6	222.9532	8.713022	0.78
7	221.295	7.290417	
8	30.51228	3.807424	
9	34.33316	3.897906	0.21
10	59.51758	32.2929	0.17
11	94.05039	57.78933	0.115

11	304.75	175.1939
12	132.5	15.32971
13	480	108.8026
14	112.25	2.5
15	395.5	98.0799
16	374.75	81.11052
17	581	121.2875
18	**2696.5**	**15.17399**
19	1448	309.9279
20	1471.75	222.6363
21	1414.25	160.7324
22	1406	320.3748
23	1328.5	79.20648
24	1346.25	190.0094
25	1674.5	430.7594
26	1778	429.0649
27	1816.25	184.843
28	1899	74.10353
29	1846	60.24948
30	1955.75	78.45753
31	1474.75	354.9942
32	1783.25	377.0848
33	1452.5	114.1038
34	1614.25	65.38285

12	190.8603	23.47572	0
13	39.94668	13.56842	
14	226.5957	5.5291	0
15	52.96509	16.41882	
16	56.34147	15.5224	0.032
17	29.23745	10.35847	
19	18.439	7.535111	
20	17.21272	5.031843	0.797
21	18.47443	4.006724	0.994
22	19.75704	8.290556	0.822
23	20.70407	2.449578	0.993
24	20.67628	5.849392	
25	14.48199	11.81435	
26	12.15732	10.10556	0.775
27	9.93711	3.205486	0.505
28	8.43247	1.138489	0.382
29	9.238342	0.9735	0.066
30	7.607551	1.078902	
31	18.23212	9.264731	0.296
32	11.4096	7.421877	
33	17.30617	3.008065	0.077
34	13.44967	1.348635	

s#	SAMPLE ID	time	CPMA	SIS		Group
1	1: 3 M HNO3 STD	60	4182	99.24		1
2	2: 3 M HNO3 STD	60	4193	136.85		1
3	3: 3 M HNO3 STD	60	4198	153.38		1
4	4: 3 M HNO3 STD	60	4185	142.3		1
5	AC-01	60	104	693.84		2
6	AC-02	60	102	737.87		2
7	AC-03	60	105	716.12		2
8	AC-04	60	102	704.09		2
9	AC-05	60	101	725.49		3
10	AC-06	60	104	676.25		3
11	AC-07	60	106	740.3		3
12	AC-08	60	102	719.34		3
13	AC-09	60	103	722.64		4
14	AC-10	60	103	714.52		4
15	AC-11	60	102	685.92		4

16	AC-12	60	104	714.61		4
17	AC-13	60	106	710.95		5
18	AC-14	60	101	717.61		5
19	AC-15	60	103	705.71		5
20	AC-16	60	104	677.8		5
21	AC-17	60	102	671.02		6
22	AC-18	60	104	685.83		6
23	AC-19	60	103	683.46		6
24	AC-20	60	103	705		6
25	AC-21	60	103	722.29		7
26	AC-22	60	104	734.17		7
27	AC-23	60	104	706.94		7
28	AC-24	60	102	741.15		7
29	5: 3 M HCl STD	60	3177	910.65		8
30	6: 3 M HCl STD	60	3254	917.39		8
31	7: 3 M HCl STD	60	3135	892.59		8
32	8: 3 M HCl STD	60	3322	921.45		8
33	AC-25	60	105	751.02		9
34	AC-26	60	105	731.84		9
35	AC-27	60	104	747.07		9
36	AC-28	60	102	743		9
37	AC-29	60	104	739.05		10
38	AC-30	60	106	731.45		10
39	AC-31	60	107	724.93		10
40	AC-32	60	103	751.26		10
41	AC-33	60	105	740.48		11
42	AC-34	60	106	720.58		11
43	AC-35	60	103	761.92		11
44	AC-36	60	107	708.64		11
45	AC-37	60	106	720.74		12
46	AC-38	60	102	738.28		12
47	AC-39	60	104	746.74		12
48	AC-40	60	106	718.04		12
49	AC-41	60	105	739.97		13
50	AC-42	60	106	735.42		13
51	AC-43	60	102	756.36		13
52	AC-44	60	106	743.54		13
53	AC-45	60	104	753.91		14
54	AC-46	60	103	747.43		14
55	AC-47	60	103	741.53		14
56	AC-48	60	104	742.4		14

Group	AVERAGE	SDEV
1	**2793**	**7.325754**
2	103.25	1.5
3	103.25	2.217356
4	103	0.816497
5	103.5	2.081666
6	103	0.816497
7	103.25	0.957427
8	**2148**	**82.90155**
9	104	1.414214
10	105	1.825742
11	105.25	1.707825
12	104.5	1.914854
13	104.75	1.892969
14	103.5	0.57735

Group	Dw	sdev	t-test, two tailed, unequal variance
2	521.1024	7.840389	
3	521.2032	11.56583	0.989
4	522.3557	4.299639	0.791
5	519.874	10.86254	0.861
6	522.3557	4.299639	0.708
7	521.052	5.037268	
9	393.1348	5.672831	
10	389.2357	7.116669	0.426
11	388.2521	6.666459	0.308
12	391.2049	7.595482	0.55
13	390.2213	7.526665	0.292
14	395.0822	2.315438	

s#	SAMPLE ID	time	CPMA	SIS		Group
1	1: 3 M HNO3 STD	60	4179	133.27		1
2	2: 3 M HNO3 STD	60	4192	172.31		1
3	3: 3 M HNO3 STD	60	4197	197.93		1
4	4: 3 M HNO3 STD	60	4194	183.14		1
5	AC-B-01	60	105	701.64		2
6	AC-B-02	60	105	710.72		2
7	AC-B-03	60	106	709.91		2
8	AC-B-04	60	107	691.53		2
9	AC-B-05	60	106	731.18		3
10	AC-B-06	60	108	723.1		3
11	AC-B-07	60	107	717.9		3
12	AC-B-08	60	103	734.05		3
13	5: 3 M HCl STD	60	3164	890.73		4
14	6: 3 M HCl STD	60	3217	888.11		4
15	7: 3 M HCl STD	60	3133	899.5		4
16	8: 3 M HCl STD	60	3313	924.56		4
17	AC-B-10	60	108	722.97		5
18	AC-B-11	60	105	756.87		5
19	AC-B-12	60	103	746.25		5
20	AC-B-13	60	105	740.22		6
21	AC-B-14	60	107	760.76		6
22	AC-B-15	60	106	731.01		6
23	AC-B-16	60	104	749.24		6

24	A: 1 M HNO3 STD	60	2061	599.23		7
25	B: 1 M HNO3 STD	60	2085	602.54		7
26	C: 1 M HNO3 STD	60	2081	609.9		7
27	D: 1 M HNO3 STD	60	2077	605.74		7
28	UT-49	60	486	676.43		8
29	UT-50	60	796	558.95		8
30	UT-51	60	671	703.07		8
31	UT-52	60	863	688.26		8
32	UT-53	60	847	702.47		9
33	UT-54	60	768	677.61		9
34	UT-55	60	438	717.32		9
35	UT-56	60	658	714.09		9
36	UT-57	60	820	694.2		10
37	UT-58	60	734	699.74		10
38	UT-59	60	642	707.03		10
39	UT-60	60	353	722.08		10
40	UT-61	60	605	711.62		11
41	UT-62	60	504	715.96		11
42	UT-63	60	350	696.65		11
43	UT-64	60	374	700.1		11
44	UT-65	60	324	714.11		12
45	UT-66	60	361	698.44		12
46	UT-67	60	329	695.52		12
47	UT-68	60	266	709.79		12
48	UT-69	60	526	720.68		13
49	UT-70	60	457	670.26		13
50	UT-71	60	573	704.78		13
51	UT-72	60	493	696.58		13
52	E: 1 M HCl STD	60	4027	661.23		14
53	F: 1 M HCl STD	60	4041	658.37		14
54	G: 1 M HCl STD	60	4042	649		14
55	H: 1 M HCl STD	60	4054	653.8		14
56	UT-73	60	1695	733.86		15
57	UT-74	60	1725	719.29		15
58	UT-75	60	1791	722.8		15
59	UT-76	60	1933	715.91		15
60	UT-77	60	1865	745.21		16
61	UT-78	60	1872	752.35		16
62	UT-79	60	1847	708.82		16
63	UT-80	60	1880	712.31		16
64	UT-81	60	1895	693.62		17
65	UT-82	60	1885	734.63		17
66	UT-83	60	1831	720.78		17

67	UT-84	60	1672	736.15		17
68	UT-85	60	1712	735.14		18
69	UT-86	60	1763	729.08		18
70	UT-87	60	1958	725.78		18
71	UT-88	60	1903	730.23		18
72	UT-89	60	1730	717.79		19
73	UT-90	60	1839	713.05		19
74	UT-91	60	1877	747.26		19
75	UT-92	60	1931	733.59		19
76	UT-93	60	1816	729.35		20
77	UT-94	60	1865	739.12		20
78	UT-95	60	1943	693.45		20
79	UT-96	60	1888	695.78		20

Group	average	SDEV
1	**2793.667**	**7.937254**
2	105.75	0.957427
3	106	2.160247
4	**2137.833**	**78.86856**
5	105.3333	2.516611
6	105.5	1.290994
7	**1384**	**10.51982**
8	704	165.6885
9	677.75	177.6333
10	637.25	202.9604
11	458.25	118.9464
12	320	39.55587
13	512.25	49.33812
14	**2694**	**11.04536**
15	1786	105.8867
16	1866	14.07125
17	1820.75	103.074
18	1834	115.5595
19	1844.25	85.00735
20	1878	52.71938

Group	Dw	sdev	t-test, two tailed, unequal variance
2	508.3855	4.765568	0.86
3	507.2733	10.88029	
5	386.0709	9.659213	0.911
6	385.3214	4.960417	
8	21.26366	11.14711	
9	23.49623	13.69547	0.809
10	28.24903	20.47232	0.577
11	43.44228	15.72652	0.066
12	67.57547	11.64739	0.006
13	34.41143	5.208399	
15	10.24498	1.732825	
16	8.875834	0.218526	0.212
17	9.666924	1.760481	0.656
18	9.466143	1.857262	0.562
19	9.262766	1.37875	0.518
20	8.707033	0.804685	

s#	SAMPLE ID	time	CPMA	SIS		Group
1	A: 1 M HNO3 STD	60	2071	604.55		1
2	B: 1 M HNO3 STD	60	2081	606.42		1

3	C: 1 M HNO3 STD	60	2077	608.92		1
4	D: 1 M HNO3 STD	60	2077	605.61		1
5	AC-49	60	105	732.75		2
6	AC-50	60	105	723.53		2
7	AC-51	60	102	748.68		2
8	AC-52	60	105	736.44		2
9	AC-53	60	102	719.31		3
10	AC-54	60	105	752.37		3
11	AC-55	60	102	754.21		3
12	AC-56	60	103	767.57		3
13	AC-57	60	102	750.14		4
14	AC-58	60	104	738.92		4
15	AC-59	60	104	747.36		4
16	AC-60	60	104	714.15		4
17	AC-61	60	102	736.32		5
18	AC-62	60	106	774.01		5
19	AC-63	60	103	745.65		5
20	AC-64	60	105	730.58		5
21	AC-65	60	107	706.4		6
22	AC-66	60	105	748.3		6
23	AC-67	60	107	741.77		6
24	AC-68	60	104	746.59		6
25	AC-69	60	102	738.07		7
26	AC-70	60	106	776.71		7
27	AC-71	60	105	718.19		7
28	AC-72	60	103	740.47		7
29	E: 1 M HCl STD	60	4062	645.53		8
30	F: 1 M HCl STD	60	4056	645.1		8
31	G: 1 M HCl STD	60	4040	649.66		8
32	H: 1 M HCl STD	60	4046	654.4		8
33	AC-73	60	104	751.89		9
34	AC-74	60	105	712.6		9
35	AC-75	60	106	750.6		9
36	AC-76	60	104	733.82		9
37	AC-77	60	106	765.76		10
38	AC-78	60	99	771.58		10
39	AC-79	60	104	722.48		10
40	AC-80	60	104	750.89		10
41	AC-81	60	106	751.2		11
42	AC-82	60	106	737.16		11
43	AC-83	60	104	753.59		11
44	AC-84	60	106	734.99		11
45	AC-85	60	105	717.36		12

46	AC-86	60	108	707.84		12
47	AC-87	60	104	735.99		12
48	AC-88	60	106	748.73		12
49	AC-89	60	105	709.35		13
50	AC-90	60	107	777.39		13
51	AC-91	60	105	744.19		13
52	AC-92	60	103	743.19		13
53	AC-93	60	102	745.43		14
54	AC-94	60	104	775.35		14
55	AC-95	60	105	716.05		14
56	AC-96	60	105	738.3		14

Group	AVERAGE	SDEV
1	1384.333	4.123106
2	104.25	1.5
3	103	1.414214
4	103.5	1
5	104	1.825742
6	105.75	1.5
7	104	1.825742
8	2700.667	9.865766
9	104.75	0.957427
10	103.25	2.986079
11	105.5	1
12	105.75	1.707825
13	105	1.632993
14	104	1.414214

Group	Dw	Sdev	t-test, two tailed, unequal variance
2	245.6213	3.877683	
3	248.8402	3.656001	0.273
4	247.5229	2.609979	0.451
5	246.2794	4.675175	0.836
6	241.852	3.724195	0.191
7	246.2794	4.675175	
9	495.6727	4.695141	
10	503.4668	15.45484	0.396
11	492.0096	4.899614	0.322
12	490.8638	8.201997	0.358
13	494.5061	8.003939	0.394
14	499.4318	7.132415	

s#	SAMPLE ID	time	CPMA	SIS		Group
1	A: 1 M HNO3 STD	60	2075	609.51		1
2	B: 1 M HNO3 STD	60	2092	613.71		1
3	C: 1 M HNO3 STD	60	2088	611.68		1
4	D: 1 M HNO3 STD	60	2094	613.3		1
5	AC-B-33	60	103	712		2
6	AC-B-34	60	103	739.3		2
7	AC-B-35	60	105	731.81		2
8	AC-B-36	60	103	734.76		2
9	AC-B-37	60	103	753.19		3
10	AC-B-38	60	107	761.54		3

11	AC-B-39	60	103	748.36		3
12	AC-B-40	60	105	762.68		3
13	E: 1 M HCl STD	60	4030	660.12		4
14	F: 1 M HCl STD	60	4041	656.7		4
15	G: 1 M HCl STD	60	4049	654.89		4
16	H: 1 M HCl STD	60	4052	656.03		4
17	AC-B-41	60	106	758.51		5
18	AC-B-42	60	102	752.72		5
19	AC-B-43	60	104	765.01		5
20	AC-B-44	60	104	760.88		5
21	AC-B-45	60	103	773.43		6
22	AC-B-46	60	103	746.37		6
23	AC-B-47	60	102	766.95		6
23	AC-B-48	60	104	747.38		6

Group	average	SDEV
1	1391.5	8.539126
2	103.5	1
3	104.5	1.914854
4	2695.333	9.831921
5	104	1.632993
6	103	0.816497

Group	Dw	sdev	t-test, two tailed, unequal variance
2	248.9075	2.573278	0.403
3	246.3824	4.843955	
5	498.4292	8.142559	0.333
6	503.3903	4.149287	

s#	SAMPLE ID	time	CPMA	SIS		Group
1	5: 3 M HCl STD	60	3191	925.17		1
2	6: 3 M HCl STD	60	3256	929.53		1
3	7: 3 M HCl STD	60	3127	901.95		1
4	8: 3 M HCl STD	60	3314	922.6		1
5	TEVA-113	60	1387	647.64		2
6	TEVA-114	60	1410	634.29		2
7	TEVA-115	60	1398	626.21		2
8	TEVA-116	60	1439	646.21		2
9	TEVA-117	60	1410	650.84		3
10	TEVA-118	60	1379	649.1		3
11	TEVA-119	60	1389	646.98		3
12	TEVA-120	60	1441	655.43		3
13	TRU-177	60	610	557.32		4
14	TRU-178	60	401	672.15		4
15	TRU-179	60	629	650.71		4

16	TRU-180	60	839	642.53		4
17	TRU-181	60	1271	644.44		5
18	TRU-182	60	1249	648.77		5
19	TRU-183	60	1530	660.25		5
20	TRU-184	60	1152	667.75		5

Group	AVERAGE	SDEV
1	2148	80.84141
2	1408.5	22.39792
3	1404.75	27.40286
4	619.75	178.9811
5	1300.5	161.4982

Group	Dw	t-test, two tailed, unequal variance
2	15.7508	0.833
3	15.87293	
4	73.97741	0.038
5	19.55017	

Kinetics studies

S#	SAMPLE ID	COUNT TIME/MIN	CPMA	SIS	MESSAGES	Group
1	1: 3 M HNO3 STD	60	4173	69.3		1
2	2: 3 M HNO3 STD	60	4176	98.29		1
3	3: 3 M HNO3 STD	60	4199	101.23		1
4	4: 3 M HNO3 STD	60	4166	99.59		1
5	TRU-185	60	116	687.65		2
6	TRU-186	60	112	693.22		2
7	TRU-187	60	111	676.64		2
8	TRU-188	60	114	706.51		2
9	TRU-201	60	124	666.36		3
10	TRU-202	60	118	664.97		3
11	TRU-203	60	115	673.65		3
12	TRU-204	60	116	663.55		3
13	TRU-217	60	118	671.41		4
14	TRU-218	60	117	655.92		4
15	TRU-219	60	115	654.5		4
16	TRU-220	60	106	681.13		4
17	TRU-233	60	114	672.21		5
18	TRU-234	60	116	691.03		5
19	TRU-235	60	115	676.46		5
20	TRU-236	60	117	652.98		5
21	TRU-249	60	110	710.39		6
22	TRU-250	60	114	703.61		6

23	TRU-251	60	106	707.8		6
24	TRU-252	60	109	684.78		6
25	TRU-265	60	107	679		7
26	TRU-266	60	107	691.92		7
27	TRU-267	60	110	699		7
28	TRU-268	60	108	706.92		7
29	5: 3 M HCl STD	60	3197	927.48		8
30	6: 3 M HCl STD	60	3255	929.66		8
31	7: 3 M HCl STD	60	3122	898.79		8
32	8: 3 M HCl STD	60	3311	928.22		8
33	TRU-189	60	1001	644.02		9
34	TRU-190	60	1269	614.54		9
35	TRU-191	60	851	689.05		9
36	TRU-192	60	1362	671.54		9
37	TRU-205	60	1340	677.96		10
38	TRU-206	60	1411	683		10
39	TRU-207	60	1445	686.16		10
40	TRU-208	60	1444	687.66		10
41	TRU-221	60	1395	679.68		11
42	TRU-222	60	1429	692.02		11
43	TRU-223	60	1472	681.77		11
44	TRU-224	60	1175	655.11		11
45	TRU-237	60	1246	679.37		12
46	TRU-238	60	1495	677.88		12
47	TRU-239	60	926	647.45		12
48	TRU-240	60	1442	638.82		12
49	TRU-253	60	1273	629.61		13
50	TRU-254	60	1381	619.2		13
51	TRU-255	60	1391	606.02		13
52	TRU-256	60	1437	675.92		13
53	TRU-269	60	1246	618.93		14
54	TRU-270	60	1223	674.4		14
55	TRU-271	60	1437	634.92		14
56	TRU-272	60	1190	653.6		14
57	A: 1 M HNO3 STD	60	2058	608.44		15
58	B: 1 M HNO3 STD	60	2085	603.95		15
59	C: 1 M HNO3 STD	60	2074	610.78		15
60	D: 1 M HNO3 STD	60	2071	610.44		15
61	TRU-193	60	109	723.56		16
62	TRU-194	60	114	723.7		16
63	TRU-195	60	116	726.77		16
64	TRU-196	60	128	722.17		16
65	TRU-209	60	115	725.78		17

66	TRU-210	60	120	735.16		17
67	TRU-211	60	116	733.6		17
68	TRU-212	60	108	717.92		17
69	TRU-225	60	126	723.67		18
70	TRU-226	60	119	732.85		18
71	TRU-227	60	120	708.05		18
72	TRU-228	60	131	737.73		18
73	TRU-241	60	121	714.5		19
74	TRU-242	60	123	749.16		19
75	TRU-243	60	117	746.03		19
76	TRU-244	60	121	736.23		19
77	TRU-257	60	122	736.79		20
78	TRU-258	60	114	754.4		20
79	TRU-259	60	119	738.06		20
80	TRU-260	60	111	763.17		20
81	TRU-273	60	108	745.55		21
82	TRU-274	60	117	735.8		21
83	TRU-275	60	117	723.94		21
84	TRU-276	60	113	740.9		21
85	E: 1 M HCl STD	60	4033	660.61		22
86	F: 1 M HCl STD	60	4028	654.87		22
87	G: 1 M HCl STD	60	4045	653.63		22
88	H: 1 M HCl STD	60	4042	655.12		22
89	TRU-197	60	1677	707.82		23
90	TRU-198	60	1900	738.52		23
91	TRU-199	60	1753	739.36		23
92	TRU-200	60	1566	740.37		23
93	TRU-213	60	1743	722.42		24
94	TRU-214	60	1619	708.57		24
95	TRU-215	60	1799	680.7		24
96	TRU-216	60	1346	733.68		24
97	TRU-229	60	1664	734.19		25
98	TRU-230	60	2032	691.35		25
99	TRU-231	60	1441	725.8		25
100	TRU-232	60	1993	675.63		25
101	TRU-245	60	2042	732.43		26
102	TRU-246	60	1742	684.61		26
103	TRU-247	60	2054	698.22		26
104	TRU-248	60	1944	695.82		26
105	TRU-261	60	1570	739.3		27
106	TRU-262	60	1730	715.65		27
107	TRU-263	60	1614	714.3		27
108	TRU-264	60	1686	731.39		27

109	TRU-277	60	1185	715.48		28
110	TRU-278	60	1572	733.46		28
111	TRU-279	60	1725	725.71		28
112	TRU-280	60	1347	728.64		28

Group	AVERAGE	SDEV
1	**2785.667**	**14.29452**
2	113.25	2.217356
3	118.25	4.031129
4	114	5.477226
5	115.5	1.290994
6	109.75	3.304038
7	108	1.414214
8	**2147.5**	**80.89654**
9	1120.75	236.1389
10	1410	49.26797
11	1367.75	132.3061
12	1277.25	257.4948
13	1370.5	69.42382
14	1274	111.0705
15	**1381.333**	**11.10555**
16	116.75	8.057088
17	114.75	4.99166
18	124	5.597619
19	120.5	2.516611
20	116.5	4.932883
21	113.75	4.272002
22	**2691.333**	**7.874008**
23	1724	140.226
24	1626.75	201.7133
25	1782.5	281.2028
26	1945.5	144.3364
27	1650	71.62867
28	1457.25	238.8394

Group	Dw	TTEST
2	707.9249	
3	676.723	0.076
4	703.0702	0.859
5	693.5498	0.142
6	731.4579	0.137
7	743.7963	0.008
9	27.48383	
10	15.69149	0.124
11	17.10291	0.162
12	20.4404	0.446
13	17.00839	0.152
14	20.56907	0.28
16	324.9465	
17	331.1329	0.716
18	304.1935	0.185
19	313.9004	0.388
20	325.7082	0.999
21	334.3077	0.563
23	16.83295	
24	19.6327	0.451
25	15.29593	0.849
26	11.5009	0.076
27	18.93333	0.416
28	25.40573	0.136

S#	SAMPLE ID	COUNT TIME/MIN	CPMA	SIS	MESSAGES	Group
1	9: 3 M HNO3 STD	60	4238	509.13		1
2	10: 3 M HNO3 STD	60	4206	470.53		1
3	11: 3 M HNO3 STD	60	4215	519.51		1

4	12: 3 M HNO3 STD	60	4251	513.72		1
5	TEVA-121	60	140	694.09		2
6	TEVA-122	60	147	674.53		2
7	TEVA-123	60	137	711.83		2
8	TEVA-124	60	139	689.92		2
9	TEVA-125	60	127	709.26		3
10	TEVA-126	60	155	666.48		3
11	TEVA-127	60	130	685.56		3
12	TEVA-128	60	139	684.07		3
13	TEVA-129	60	120	712.6		4
14	TEVA-130	60	119	700.37		4
15	TEVA-131	60	128	718.62		4
16	TEVA-132	60	119	702.57		4
17	13: 3 M HCl STD	60	3656	655.9		5
18	14: 3 M HCl STD	60	3548	667.39		5
19	15: 3 M HCl STD	60	3639	69.6		5
20	16: 3 M HCl STD	60	3653	636.28		5
21	UT-97	60	1575	700.25		6
22	UT-98	60	1714	689.43		6
23	UT-99	60	1794	659.77		6
24	UT-100	60	1733	701.59		6
25	UT-101	60	1668	646.35		7
26	UT-102	60	1739	652.86		7
27	UT-103	60	1734	655.63		7
28	UT-104	60	1832	703.32		7
29	UT-105	60	1791	693.7		8
30	UT-106	60	1889	698.31		8
31	UT-107	60	1857	700.55		8
32	UT-108	60	1915	670.75		8
33	AC-97	60	90	803.39		9
34	AC-98	60	89	761.99		9
35	AC-99	60	89	796.65		9
36	AC-100	60	88	800.76		9
37	AC-101	60	90	768		10
38	AC-102	60	93	769.6		10
39	AC-103	60	91	802.15		10
40	AC-104	60	91	786.72		10
41	AC-105	60	91	760.42		11
42	AC-106	60	90	725.06		11
43	AC-107	60	92	750.24		11
44	AC-108	60	91	763.36		11
1	TEVA-133	60	84	850.21		12
2	TEVA-134	60	87	802.38		12

3	TEVA-135	60	89	836.73		12
4	TEVA-136	60	88	805.21		12
5	TEVA-137	60	81	829.05		13
6	TEVA-138	60	97	838.41		13
7	TEVA-139	60	80	845.93		13
8	TEVA-140	60	93	760.93		13
9	TEVA-141	60	78	829.79		14
10	TEVA-142	60	79	884.05		14
11	TEVA-143	60	80	863.93		14
12	TEVA-144	60	93	829.98		14
13	UT-109	60	1735	661.36		15
14	UT-110	60	1740	710.38		15
15	UT-111	60	1794	695.57		15
16	UT-112	60	1814	692.68		15
17	UT-113	60	1727	682.69		16
18	UT-114	60	1806	648.39		16
19	UT-115	60	1751	699.39		16
20	UT-116	60	1460	700.94		16
21	UT-117	60	1838	651.44		17
22	UT-118	60	1819	667.44		17
23	UT-119	60	1765	648.39		17
24	UT-120	60	1870	691.91		17
25	AC-109	60	60	977.56		18
26	AC-110	60	65	868.17		18
27	AC-111	60	59	961.93		18
28	AC-112	60	61	934.94		18
29	AC-113	60	59	996.96		19
30	AC-114	60	57	1002.53		19
31	AC-115	60	72	784.61		19
32	AC-116	60	61	921.51		19
33	AC-117	60	59	959.76		20
34	AC-118	60	62	940.87		20
35	AC-119	60	58	1025.21		20
36	AC-120	60	59	939.31		20

Group	AVERAGE	SDEV
1	**2818.333**	**20.66398**
2	140.75	4.349329
3	137.75	12.57975
4	121.5	4.358899
5	**2416**	**51.20547**

Group	Dw	TTEST
2	570.7105	
3	583.7931	0.598
4	665.8848	0.001
6	12.53521	
7	11.57751	0.513

6	1704	92.52387
7	1743.25	67.43577
8	1863	53.54126
9	89	0.816497
10	91.25	1.258306
11	91	0.816497
12	87	2.160247
13	87.75	8.539126
14	82.5	7.047458
15	1770.75	39.30543
16	1686	154.253
17	1823	44.02272
18	61.25	2.629956
19	62.25	6.70199
20	59.5	1.732051

8	8.904992	0.045
9	784.382	
10	764.3014	0.027
11	766.4835	0.013
12	941.8391	0
13	933.5328	0.003
14	994.8485	0.001
15	10.93181	0.261
16	12.98932	0.803
17	9.75864	0.092
18	1153.347	0.001
19	1134.337	0.008
20	1188.151	0

APPENDIX D: AUXILIARY SPECTRA FOR FTIR AND MALDI ANALYSES

Spectra from Chapter 5

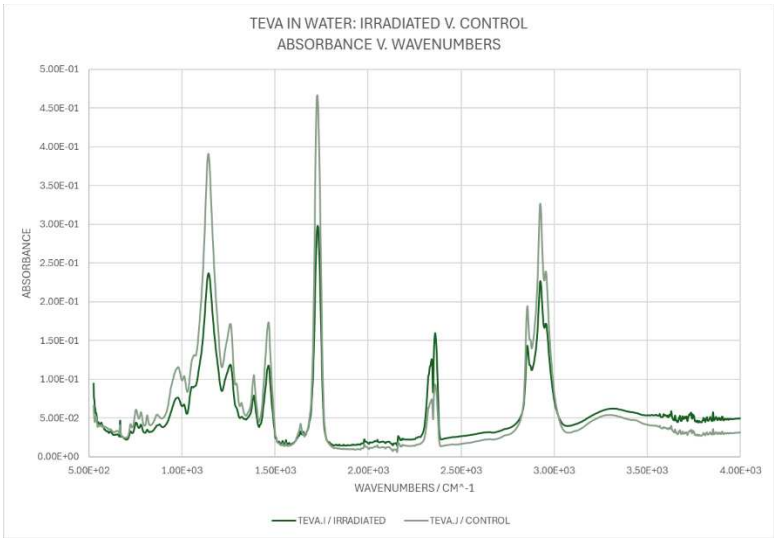

Figure 101: Graph showing FTIR absorbance for 50 kGy irradiated and unirradiated TEVA Resin in water in absorbance versus wavenumbers.

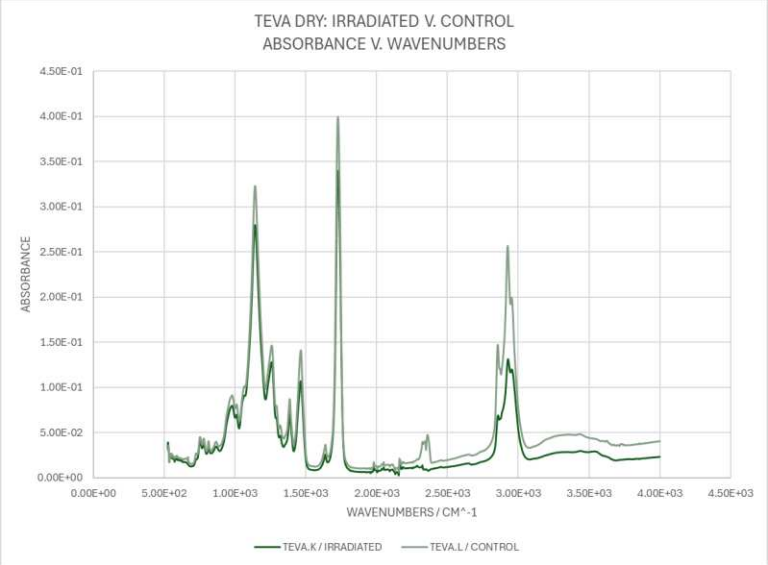

Figure 102: Graph showing FTIR absorbance for 50 kGy irradiated and unirradiated TEVA Resin dry in absorbance versus wavenumbers.

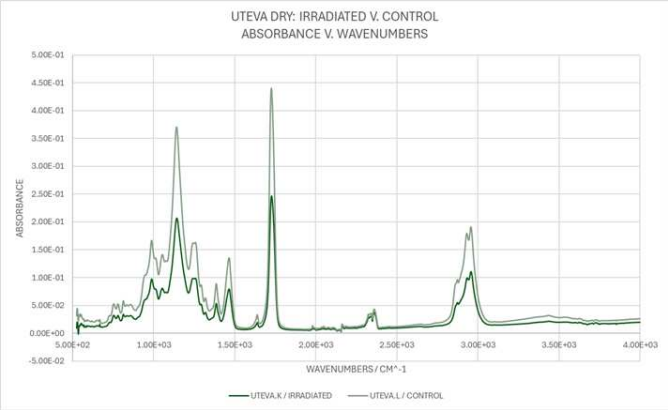

Figure 103: Graph showing FTIR absorbance for 50 kGy irradiated and unirradiated UTEVA Resin dry in absorbance versus wavenumbers.

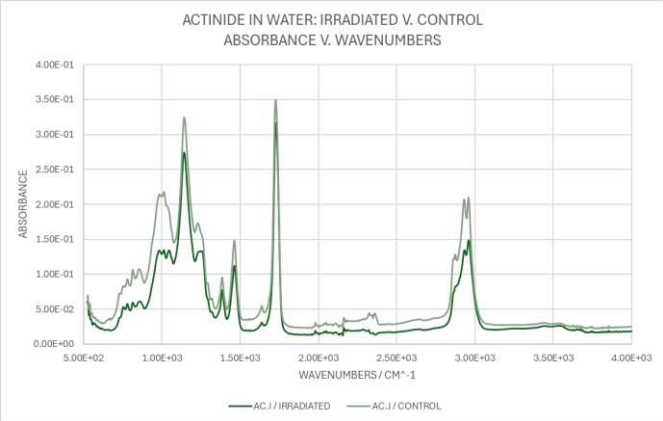

Figure 104: Graph showing FTIR absorbance for 50 kGy irradiated and unirradiated Actinide Resin in water in absorbance versus wavenumbers.

Spectra from Chapter 6

Figure 105 illustrates the mass spectra generated for TRU Resin in 3 M hydrochloric acid. The spectral features previously discussed for the previous figure are also present in the reflector positive spectra shown below.

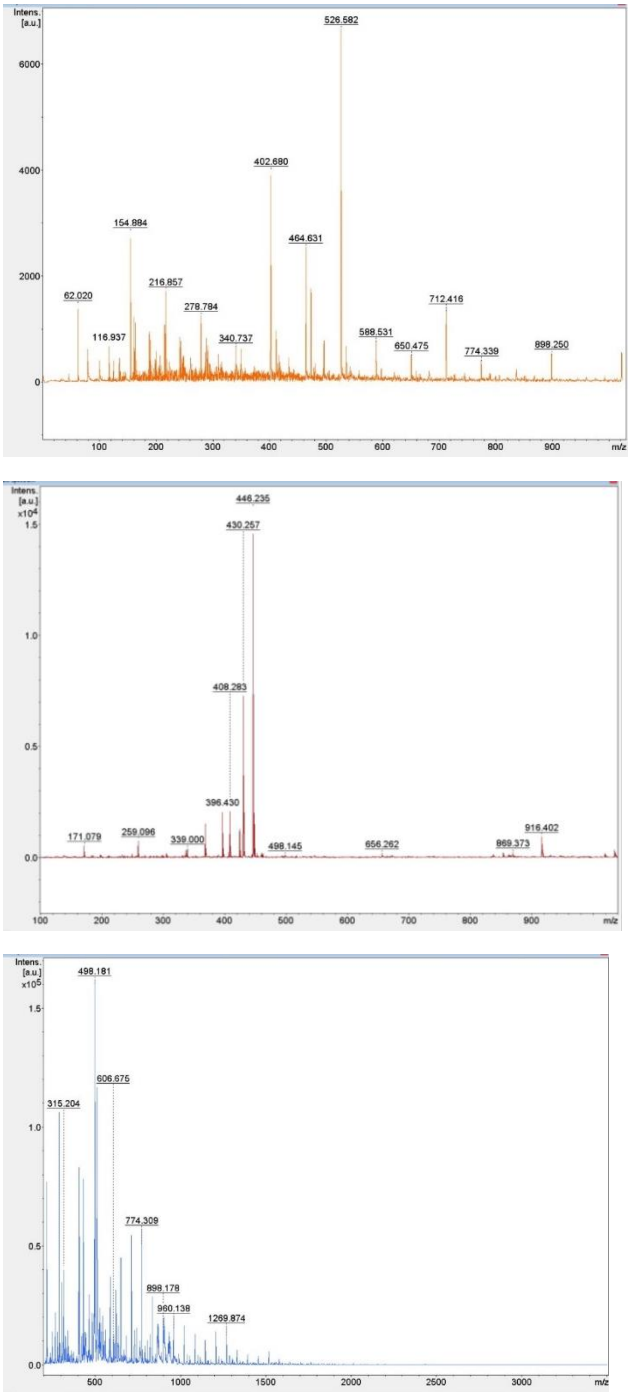

Figure 105: Figure containing three mass spectra of TRU Resin in 3 M hydrochloric acid analyzed using MALDI-TOF-MS, plotted as m/z or mass-to-charge ratio versus intensity. The first graph is with the mass spectrometer with negative high voltage applied, the middle graph examines the same region with high voltage applied, and the last graph examines a wider mass range using the positive high voltage.

Figure 106 illustrates the mass spectra generated for dry TRU Resin beads applied directly to the stainless-steel target plate with no liquid pre-conditioning. The peak at 283 m/z in the reflector

negative spectrum below is likely TBP complexed with a water molecule that lost a proton during the desorption/ionization process. The same spectral features at 408, 430, and 446 discussed previously for reflector positive spectra are also present in the following figure.

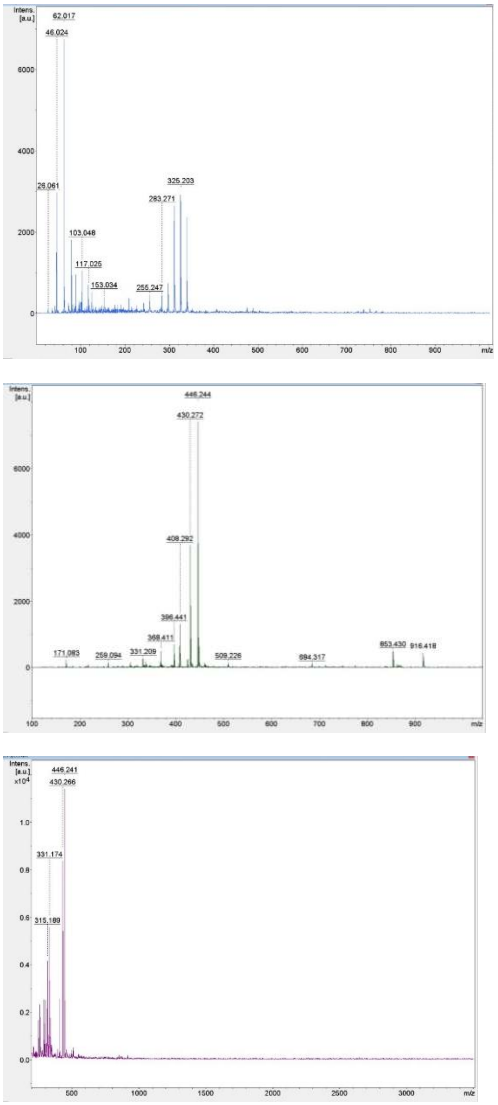

Figure 106: Figure containing three mass spectra of dry TRU Resin analyzed using MALDI-TOF-MS, plotted as m/z or mass-to-charge ratio versus intensity. The first graph is with the mass spectrometer with negative high voltage applied, the middle graph examines the same region with high voltage applied, and the last graph examines a wider mass range using the positive high voltage.

Figure 107 shows those mass spectra generated for TEVA Resin in 3 M nitric acid. Similar spectral features as in the TEVA Resin in water are shown for the TEVA Resin in 3 M nitric acid.

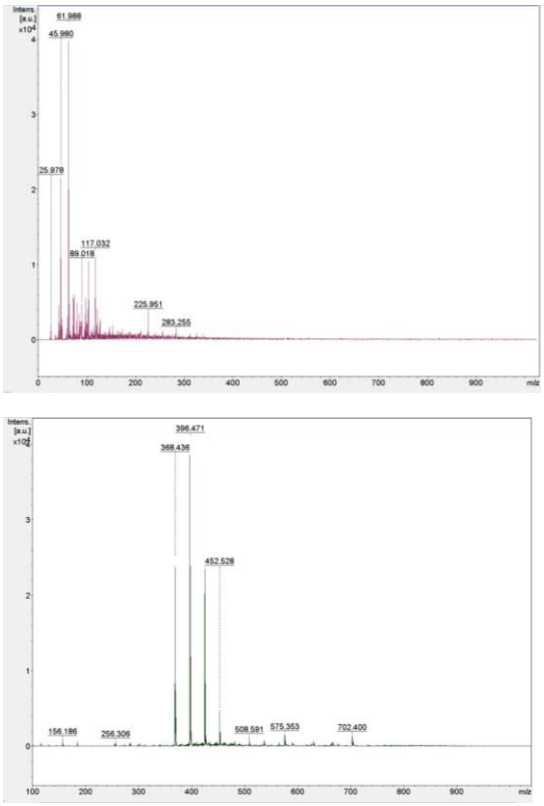

Figure 107: Figure containing two mass spectra of TEVA Resin in 3 M nitric acid analyzed using MALDI-TOF-MS, plotted as m/z or mass-to-charge ratio versus intensity. The first graph is with the mass spectrometer with negative high voltage applied, and the second graph illustrates the same region with positive high voltage applied.

Figure 108 shows those mass spectra generated for TEVA Resin in 3 M hydrochloric acid. Features in both the reflector negative and reflector positive spectra resemble those of the reflector negative and reflector positive spectra collected for TEVA Resin in 3 M nitric acid and water.

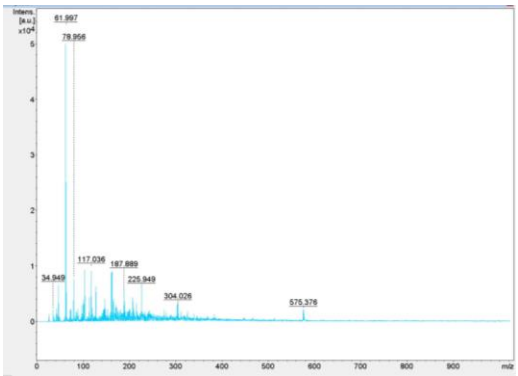

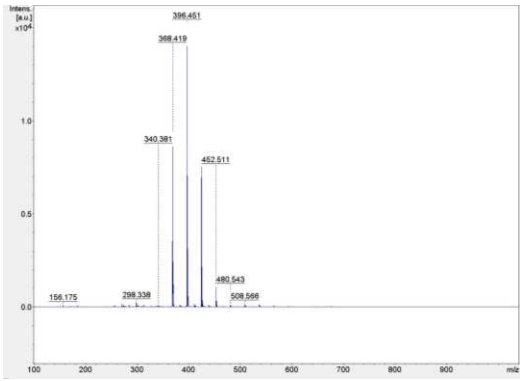

Figure 108: Figure containing two mass spectra of TEVA Resin in 3 M hydrochloric acid analyzed using MALDI-TOF-MS, plotted as m/z or mass-to-charge ratio versus intensity. The first graph is with the mass spectrometer with negative high voltage applied, and the second graph examines the same region with positive high voltage applied.

Figure 109 shows those mass spectra generated for dry TEVA Resin. While there is increased noise in the reflector negative spectrum collected from the dry TEVA Resin, the spectral features are still similar to those of previously collected TEVA Resin spectra. The reflector positive spectrum collected for dry TEVA Resin has similar spectral features to other TEVA Resin spectra collected with positive high voltage applied.

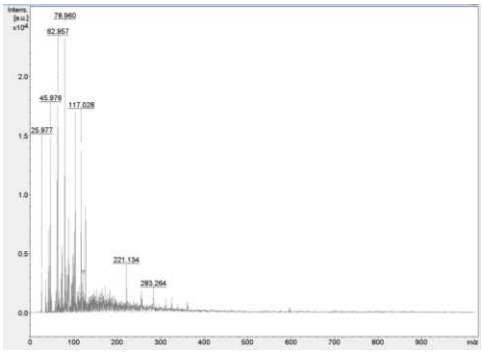

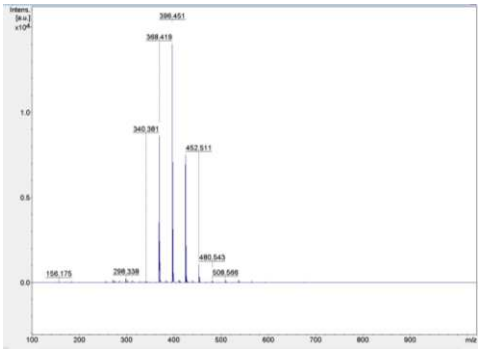

Figure 109: Figure containing two mass spectra of dry TEVA Resin analyzed using MALDI-TOF-MS, plotted as m/z or mass-to-charge ratio versus intensity. The first graph is with the mass spectrometer with negative high voltage applied, and the second graph illustrates the same region with positive high voltage applied.

Figure 110 shows the gathered mass spectra of dry UTEVA Resin. The spectral features in the dry UTEVA Resin generally resemble those of the UTEVA Resin in water and 3 M hydrochloric acid.

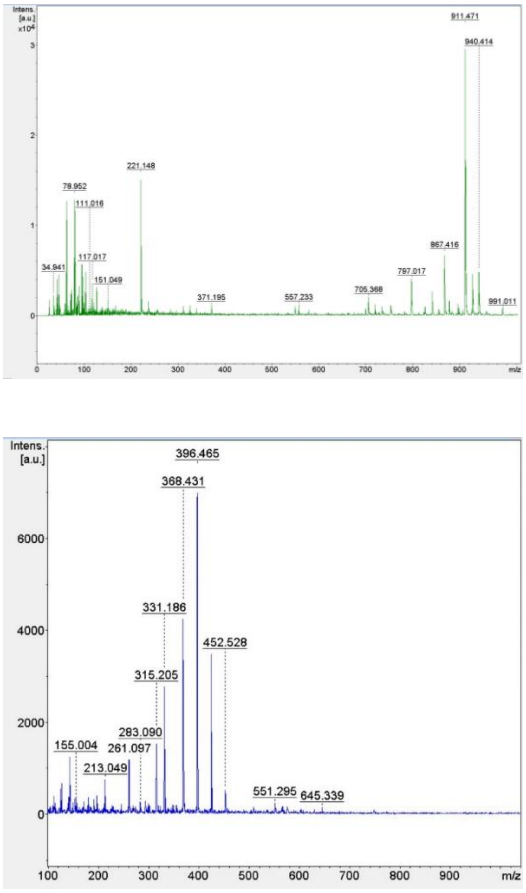

Figure 110: Figure containing two mass spectra of dry UTEVA Resin analyzed using MALDI-TOF-MS, plotted as m/z or mass-to-charge ratio versus intensity. The first graph is with the mass spectrometer with negative high voltage applied, and the second graph examines the same region with positive high voltage applied.

Figure 111 contains the spectra generated for the Actinide Resin in 3 M hydrochloric acid. The spectra generated for the Actinide Resin in 3 M HCl show similar spectral features to those in the spectra generated for the Actinide Resin in 3 M HNO_3 and water.

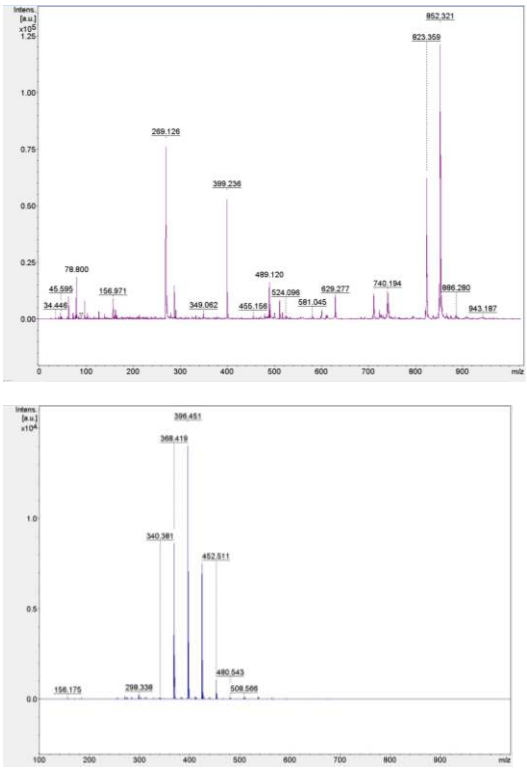

Figure 111: Figure containing two mass spectra of the Actinide Resin in 3 M hydrochloric acid analyzed using MALDI-TOF-MS, plotted as m/z or mass-to-charge ratio versus intensity. The first graph is with the mass spectrometer with negative high voltage applied, and the second graph illustrates the same region with positive high voltage applied.

Figure 112 contains the spectra generated for dry Actinide Resin applied directly to the stainless-steel target plate. The spectra generated for the dry Actinide Resin show similar spectral features to those of the mass spectra generated for the Actinide Resin in water, hydrochloric acid, and nitric acid.

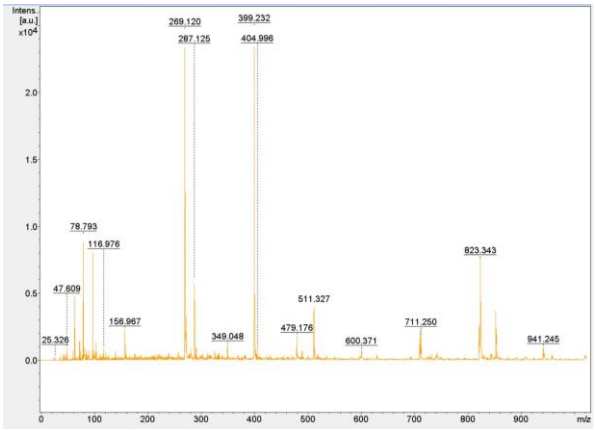

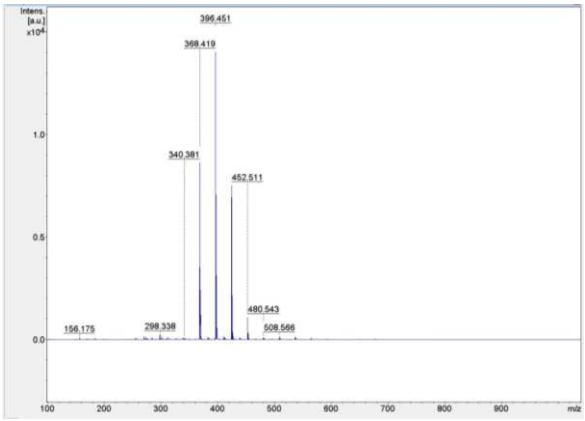

Figure 112: Figure containing two mass spectra of the dry Actinide Resin analyzed using MALDI-TOF-MS, plotted as m/z or mass-to-charge ratio versus intensity. The first graph is with the mass spectrometer with negative high voltage applied, and the second graph examines the same region with positive high voltage applied.

Spectra from Chapter 7

This first pair of graphs within figure 113 show a look at a wide mass range for the impacts of irradiation on TRU Resin in 3 M nitric acid. The spectra with the negative high voltage applied show that the irradiated sample is more readily desorbed and ionized by the MALDI.

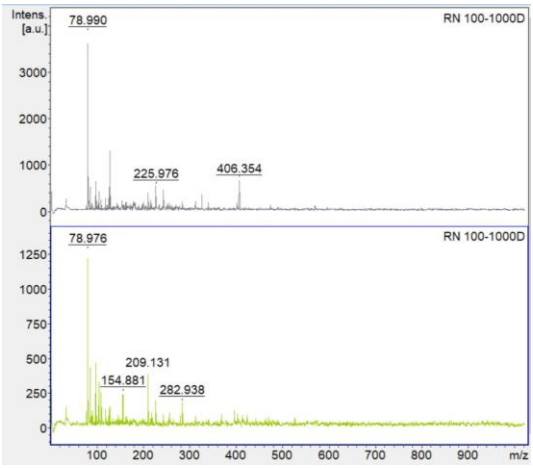

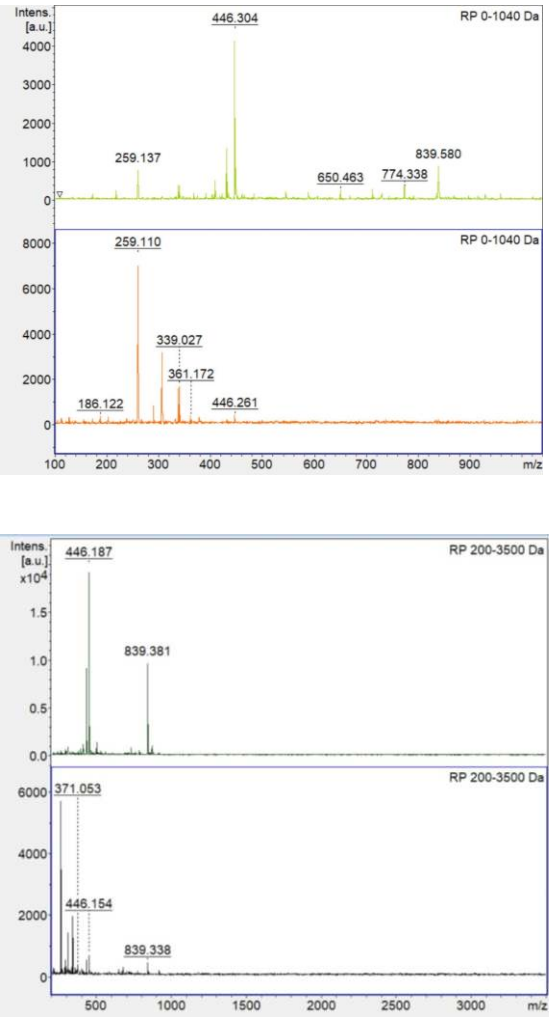

Figure 113: Figure containing three pairs of mass spectra of TRU Resin in 3 M nitric acid analyzed using MALDI-TOF-MS, plotted as m/z or mass-to-charge ratio versus intensity. The top graph in each pair is the sample that received 50 kGy gamma exposure. The first pair of graphs is with the mass spectrometer with negative high voltage applied, the middle pair illustrates the same region with high voltage applied, and the last pair examines a wider mass range using the positive high voltage.

Figure 114 specifically examines low mass-to-charge ratio fragments of TRU Resin in 3 M nitric acid, with irradiated and unirradiated paired spectra for ease of comparison. The first pair of spectra in the figure below show the same spectral features as the first pair of spectra in the previous figure where the irradiated sample was more readily ionized and desorbed by the MALDI's laser. In the spectra gathered with the positive high voltage applied, there is a peak at 171 m/z in the unirradiated sample's spectrum that does not appear in the spectrum gathered for the irradiated sample.

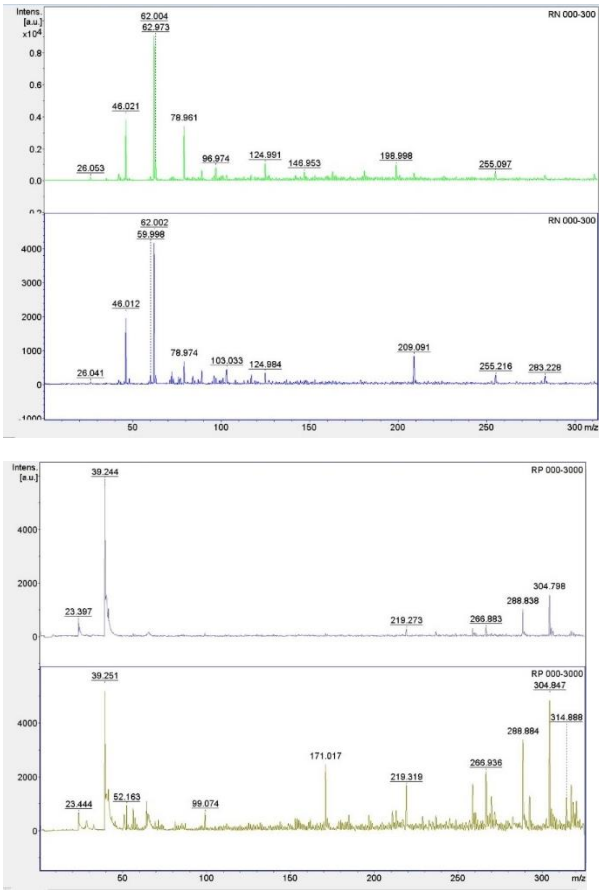

Figure 114: Figure containing two pairs of mass spectra of TRU Resin in 3 M nitric acid analyzed using MALDI-TOF-MS, plotted as m/z or mass-to-charge ratio versus intensity. The top graph in each pair is the sample that received 50 kGy gamma exposure. The first pair of graphs is with the mass spectrometer with negative high voltage applied, and the bottom pair examines the same region with positive high voltage applied.

Figure 115 shows TRU Resin in water, with paired spectra of the irradiated sample and the unirradiated control baseline sample.

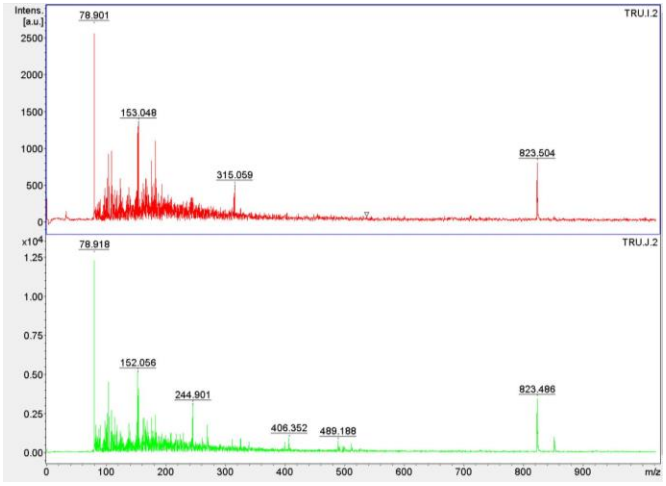

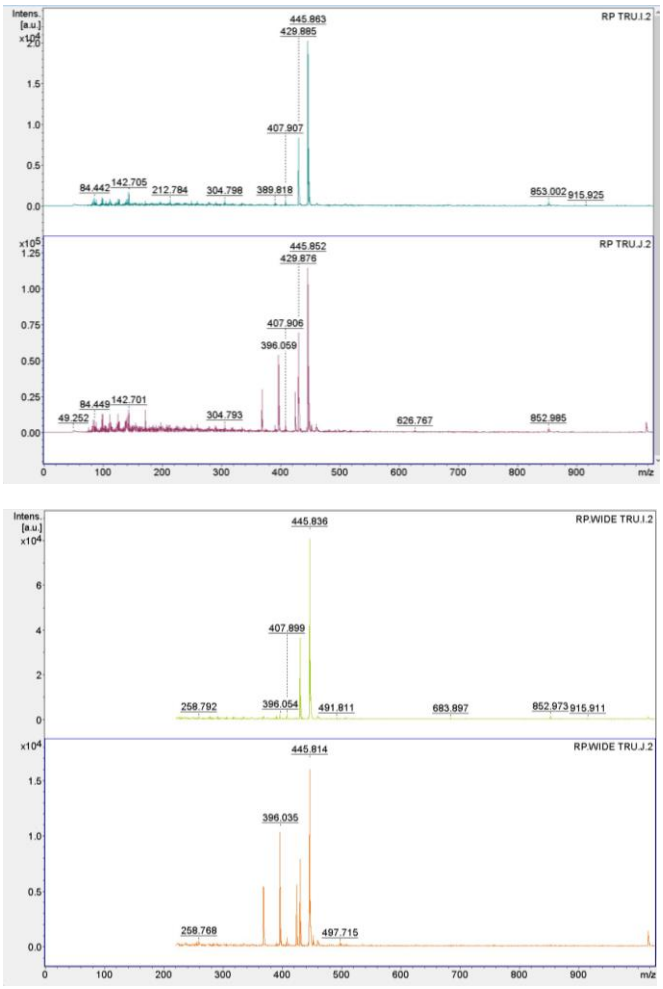

Figure 115: Figure containing three pairs of mass spectra of TRU Resin in water analyzed using MALDI-TOF-MS, plotted as m/z or mass-to-charge ratio versus intensity. The top graph in each pair is the sample that received 50 kGy gamma exposure. The first pair of graphs is with the mass spectrometer with negative high voltage applied, the middle pair illustrates the same region with high voltage applied, and the last pair examines a wider mass range using the positive high voltage.

Figure 116 specifically examines low mass-to-charge ratio fragments of TRU Resin in water, with irradiated and unirradiated paired spectra for ease of comparison.

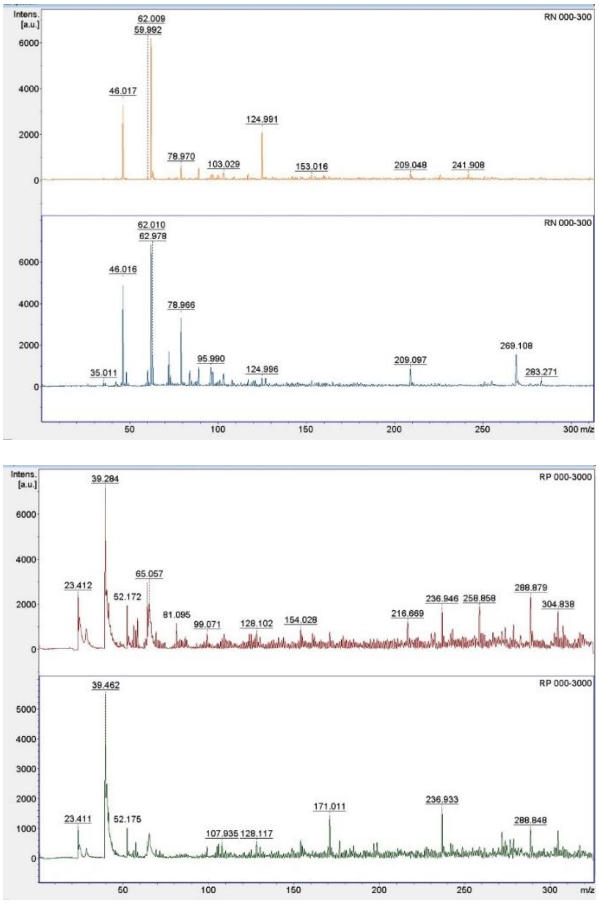

Figure 116: Figure containing two pairs of mass spectra of TRU Resin in water analyzed using MALDI-TOF-MS, plotted as m/z or mass-to-charge ratio versus intensity. The top graph in each pair is the sample that received 50 kGy gamma exposure. The first pair of graphs is with the mass spectrometer with negative high voltage applied, and the bottom pair examines the same region with positive high voltage applied.

Figure 117 shows the TEVA Resin in water, with paired spectra of the irradiated sample and the unirradiated control baseline sample.

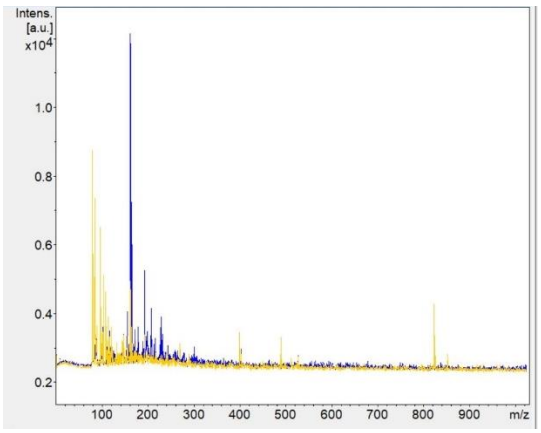

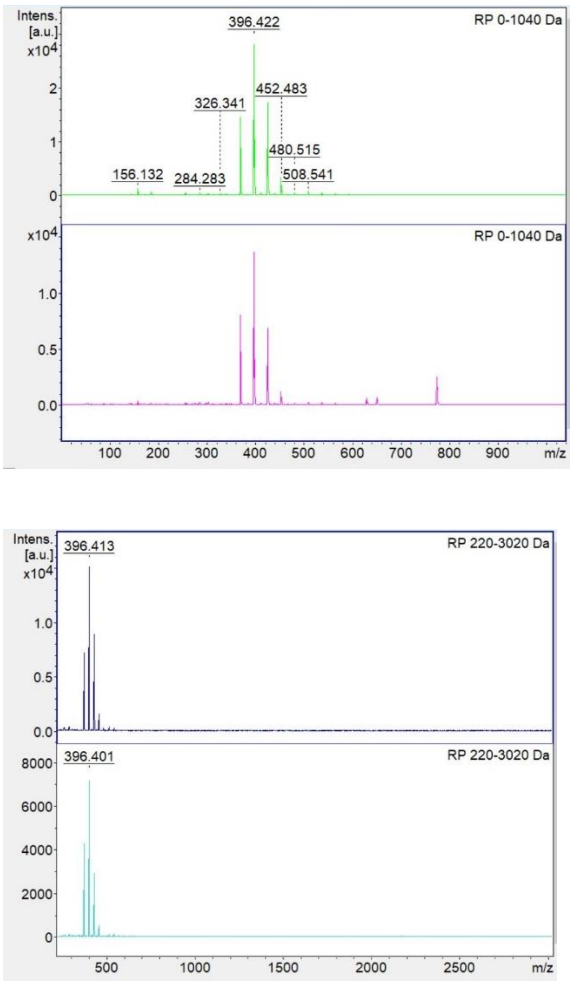

Figure 117: Figure containing three pairs of mass spectra of TEVA Resin in water analyzed using MALDI-TOF-MS, plotted as m/z or mass-to-charge ratio versus intensity. The top graph in each pair is the sample that received 50 kGy gamma exposure. The first pair of graphs is with the mass spectrometer with negative high voltage applied, the middle pair examines the same region with high voltage applied, and the last pair examines a wider mass range using the positive high voltage.

Figure 118 specifically examines low mass-to-charge ratio fragments of TEVA Resin in water, with irradiated and unirradiated paired spectra for ease of comparison.

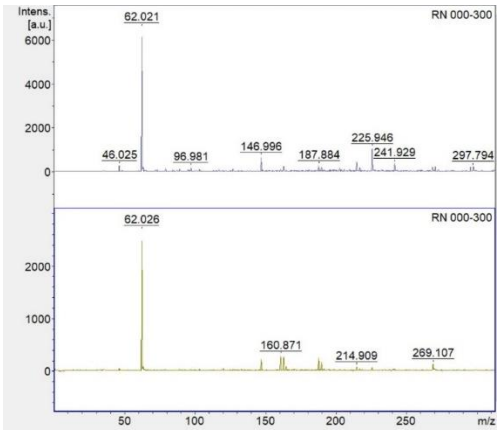

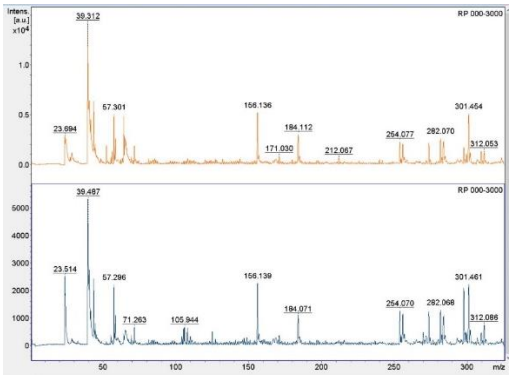

Figure 118: Figure containing two pairs of mass spectra of TEVA Resin in water analyzed using MALDI-TOF-MS, plotted as m/z or mass-to-charge ratio versus intensity. The top graph in each pair is the sample that received 50 kGy gamma exposure. The first pair of graphs is with the mass spectrometer with negative high voltage applied, and the bottom pair illustrates the same region with positive high voltage applied.

Figure 119 illustrates the dry TEVA Resin, with paired spectra of the irradiated sample and the unirradiated control baseline sample.

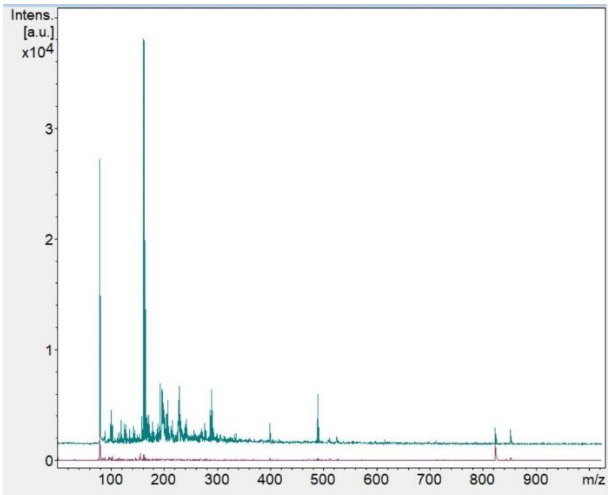

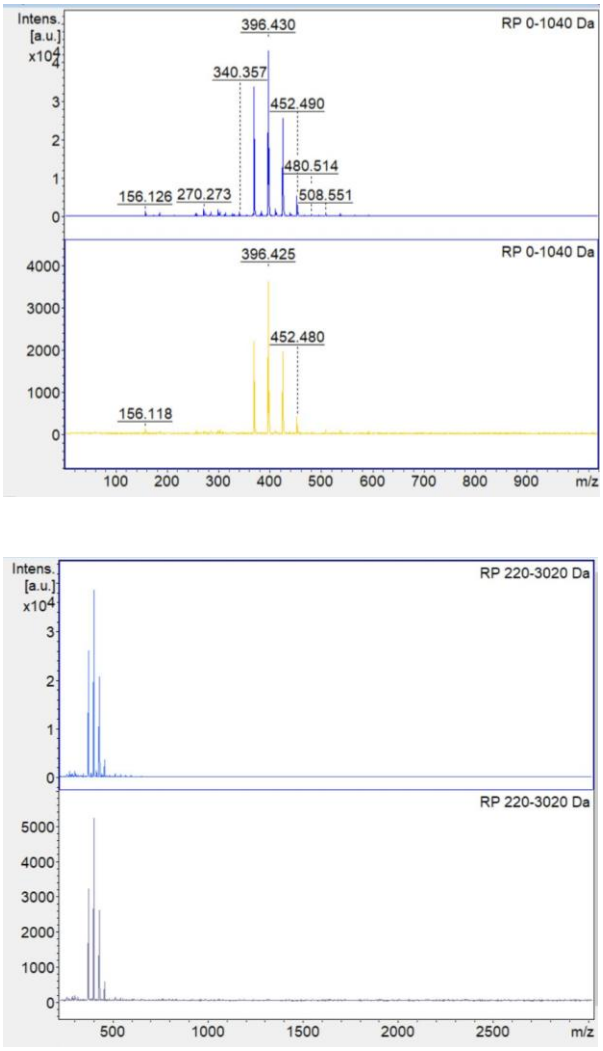

Figure 119: Figure containing three pairs of mass spectra of dry TEVA Resin analyzed using MALDI-TOF-MS, plotted as m/z or mass-to-charge ratio versus intensity. The top graph in each pair is the sample that received 50 kGy gamma exposure. The first pair of graphs is with the mass spectrometer with negative high voltage applied, the middle pair examines the same region with high voltage applied, and the last pair examines a wider mass range using the positive high voltage.

Figure 120 specifically examines low mass-to-charge ratio fragments of dry TEVA Resin, with irradiated and unirradiated paired spectra for ease of comparison.

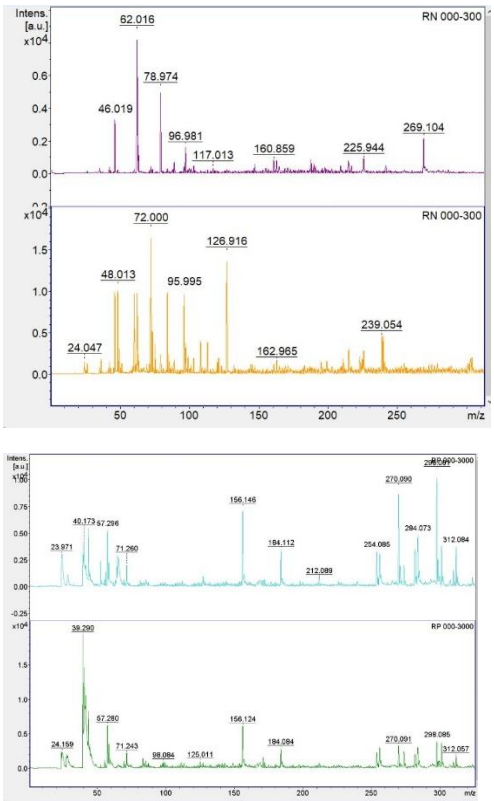

Figure 120: Figure containing two pairs of mass spectra of dry TEVA Resin analyzed using MALDI-TOF-MS, plotted as m/z or mass-to-charge ratio versus intensity. The top graph in each pair is the sample that received 50 kGy gamma exposure. The first pair of graphs is with the mass spectrometer with negative high voltage applied, and the bottom pair examines the same region with positive high voltage applied.

Figure 121 illustrates the UTEVA Resin in 3 M hydrochloric acid, with paired spectra of the irradiated sample and the unirradiated control baseline sample.

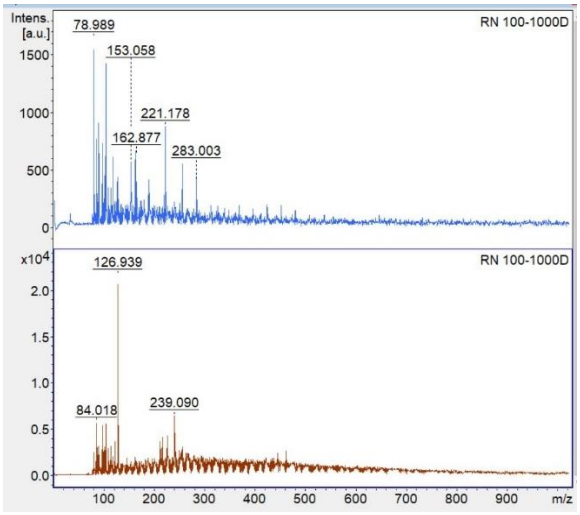

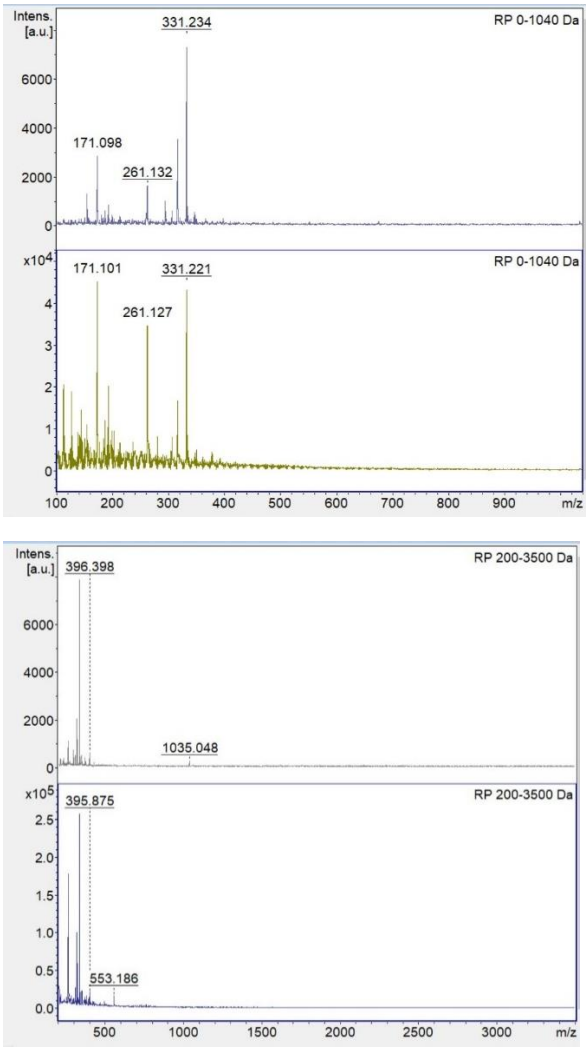

Figure 121: Figure containing three pairs of mass spectra of UTEVA Resin in 3 M hydrochloric acid analyzed using MALDI-TOF-MS, plotted as m/z or mass-to-charge ratio versus intensity. The top graph in each pair is the sample that received 50 kGy gamma exposure. The first pair of graphs is with the mass spectrometer with negative high voltage applied, the middle pair illustrates the same region with high voltage applied, and the last pair examines a wider mass range using the positive high voltage.

Figure 122 specifically examines low mass-to-charge ratio fragments of UTEVA Resin in 3 M hydrochloric acid, with irradiated and unirradiated paired spectra for ease of comparison.

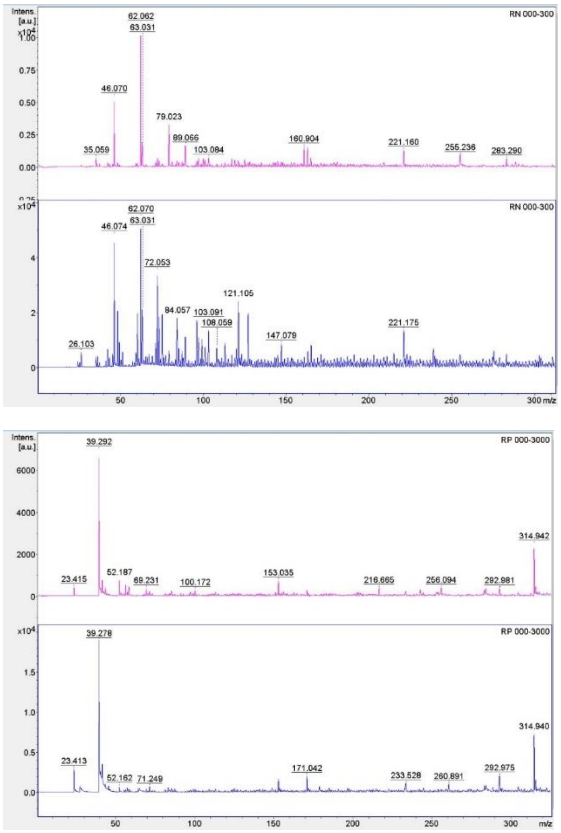

Figure 122: Figure containing two pairs of mass spectra of UTEVA Resin in 3 M hydrochloric acid analyzed using MALDI-TOF-MS, plotted as m/z or mass-to-charge ratio versus intensity. The top graph in each pair is the sample that received 50 kGy gamma exposure. The first pair of graphs is with the mass spectrometer with negative high voltage applied, and the bottom pair illustrates the same region with positive high voltage applied.

Figure 123 illustrates the UTEVA Resin in water, with paired spectra of the irradiated sample and the unirradiated control baseline sample.

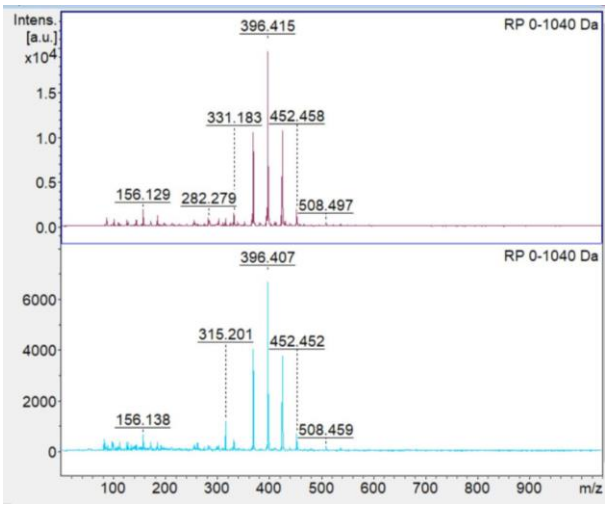

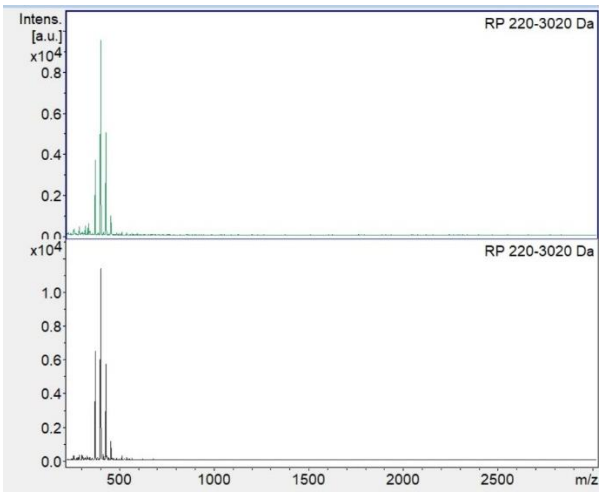

Figure 123: Figure containing two pairs of mass spectra of UTEVA Resin in water analyzed using MALDI-TOF-MS, plotted as m/z or mass-to-charge ratio versus intensity. The top graph in each pair is the sample that received 50 kGy gamma exposure. The first pair of graphs is with the mass spectrometer with positive high voltage applied, and the second pair examines a wider mass range using the positive high voltage.

Figure 124 specifically examines low mass-to-charge ratio fragments of UTEVA Resin in water, with irradiated and unirradiated paired spectra for ease of comparison.

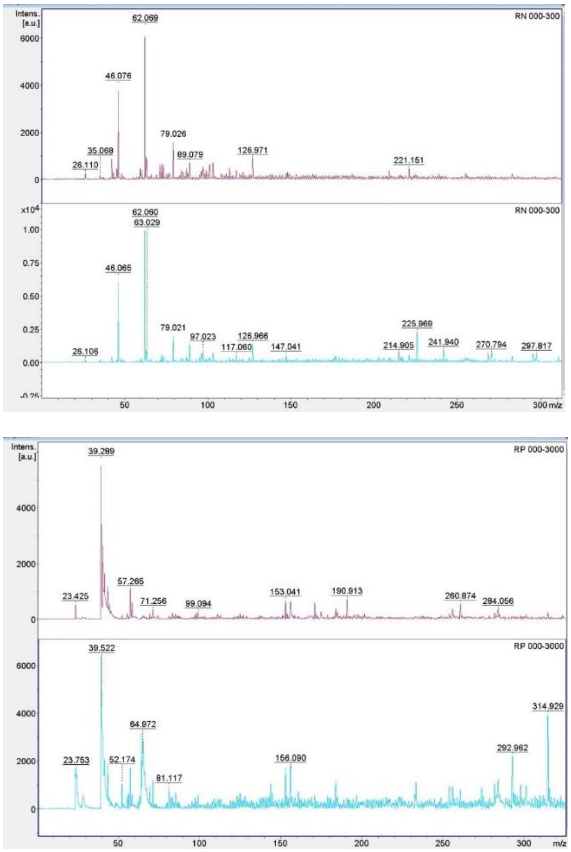

Figure 124: Figure containing two pairs of mass spectra of UTEVA Resin in water analyzed using MALDI-TOF-MS, plotted as m/z or mass-to-charge ratio versus intensity. The top graph in each pair is the sample that received 50 kGy gamma exposure. The first pair of graphs is with the mass spectrometer with negative high voltage applied, and the bottom pair examines the same region with positive high voltage applied.

Figure 125 illustrates the dry UTEVA Resin, with paired spectra of the irradiated sample and the unirradiated control baseline sample.

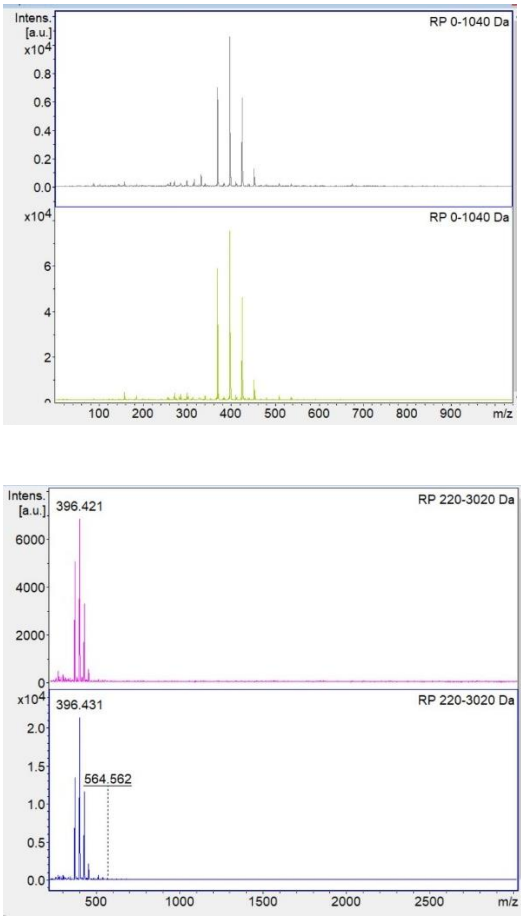

Figure 125: Figure containing two pairs of mass spectra of dry UTEVA Resin analyzed using MALDI-TOF-MS, plotted as m/z or mass-to-charge ratio versus intensity. The top graph in each pair is the sample that received 50 kGy gamma exposure. The first pair of graphs is with the mass spectrometer with positive high voltage applied, and the second pair examines a wider mass range using the positive high voltage.

Figure 126 specifically examines low mass-to-charge ratio fragments of dry UTEVA Resin, with irradiated and unirradiated paired spectra for ease of comparison.

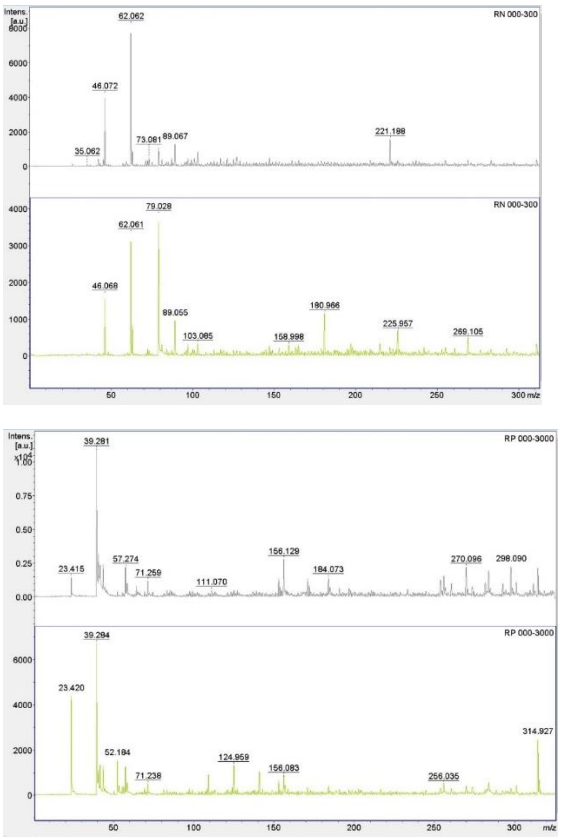

Figure 126: Figure containing two pairs of mass spectra of dry UTEVA Resin analyzed using MALDI-TOF-MS, plotted as m/z or mass-to-charge ratio versus intensity. The top graph in each pair is the sample that received 50 kGy gamma exposure. The first pair of graphs is with the mass spectrometer with negative high voltage applied, and the bottom pair examines the same region with positive high voltage applied.

Figure 127 illustrates the Actinide Resin in 3 M hydrochloric acid, with paired spectra of the irradiated sample and the unirradiated control baseline sample.

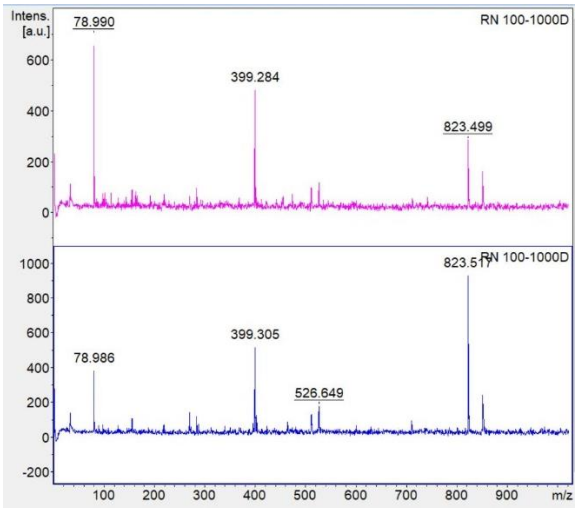

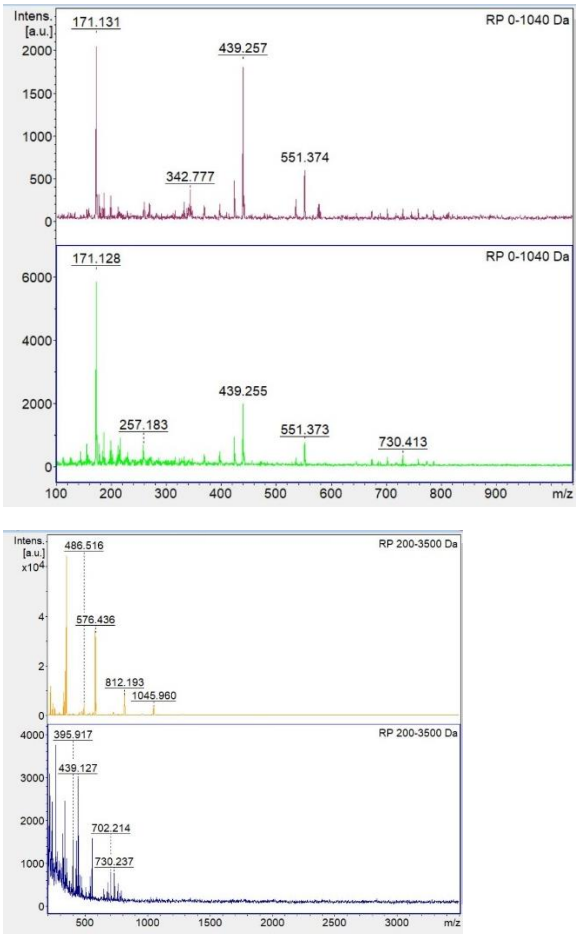

Figure 127: Figure containing three pairs of mass spectra of Actinide Resin in 3 M hydrochloric acid analyzed using MALDI-TOF-MS, plotted as m/z or mass-to-charge ratio versus intensity. The top graph in each pair is the sample that received 50 kGy gamma exposure. The first pair of graphs is with the mass spectrometer with negative high voltage applied, the middle pair illustrates the same region with high voltage applied, and the last pair examines a wider mass range using the positive high voltage.

Figure 128 specifically examines low mass-to-charge ratio fragments of Actinide Resin in 3 M hydrochloric acid, with irradiated and unirradiated paired spectra for ease of comparison.

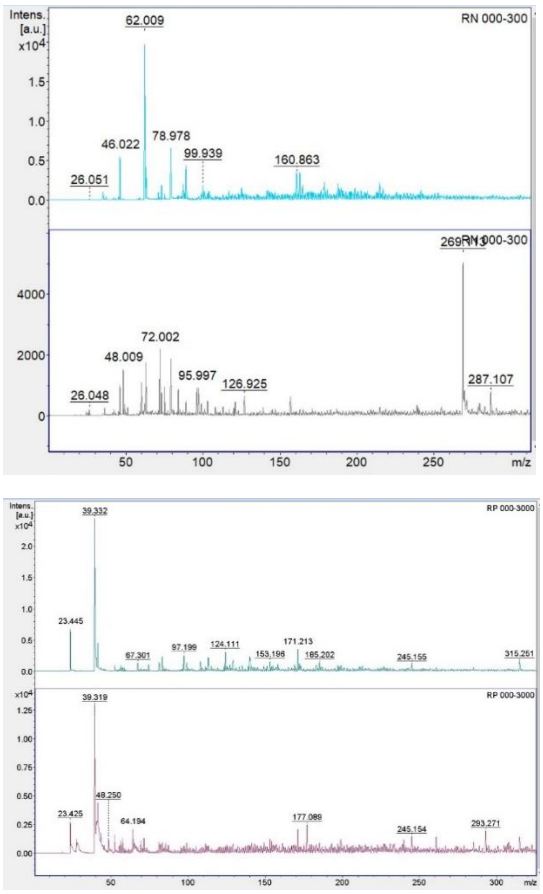

Figure 128: Figure containing two pairs of mass spectra of Actinide Resin in 3 M hydrochloric acid analyzed using MALDI-TOF-MS, plotted as m/z or mass-to-charge ratio versus intensity. The top graph in each pair is the sample that received 50 kGy gamma exposure. The first pair of graphs is with the mass spectrometer with negative high voltage applied, and the bottom pair illustrates the same region with positive high voltage applied.

Figure 129 illustrates the Actinide Resin in water, with paired spectra of the irradiated sample and the unirradiated control baseline sample.

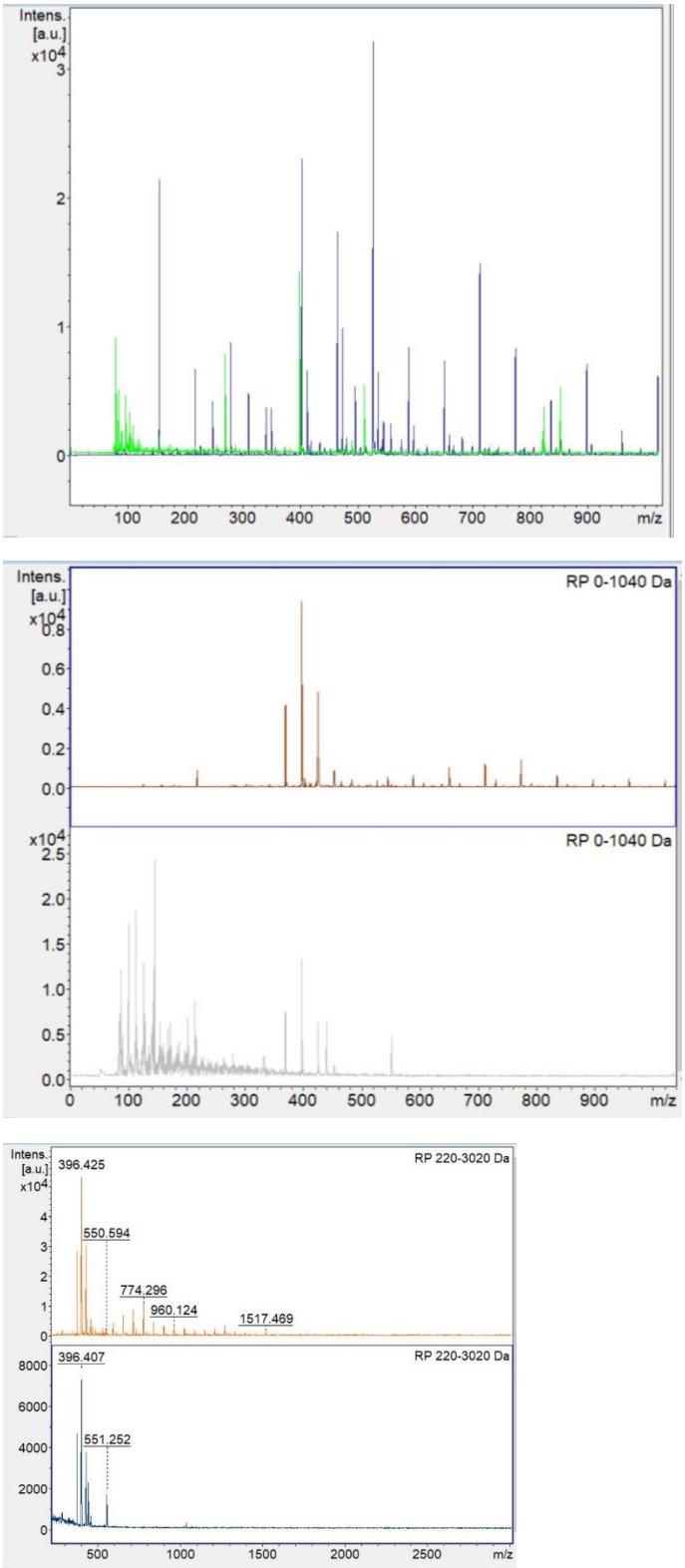

Figure 129: Figure containing three pairs of mass spectra of Actinide Resin in water analyzed using MALDI-TOF-MS, plotted as m/z or mass-to-charge ratio versus intensity. The top graph in each pair is the sample that received 50 kGy gamma exposure. The first pair of graphs is with the mass spectrometer with negative high voltage applied, the middle pair examines the same region with high voltage applied, and the last pair examines a wider mass range using the positive high voltage.

Figure 130 specifically examines low mass-to-charge ratio fragments of Actinide Resin in water, with irradiated and unirradiated paired spectra for ease of comparison.

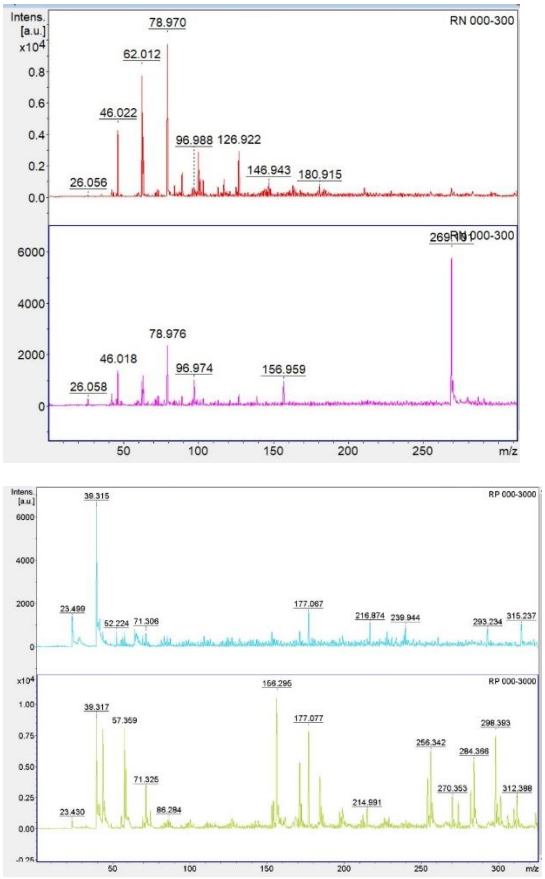

Figure 130: Figure containing two pairs of mass spectra of Actinide Resin in water analyzed using MALDI-TOF-MS, plotted as m/z or mass-to-charge ratio versus intensity. The top graph in each pair is the sample that received 50 kGy gamma exposure. The first pair of graphs is with the mass spectrometer with negative high voltage applied, and the bottom pair examines the same region with positive high voltage applied.

Figure 131 illustrates the dry Actinide Resin, with paired spectra of the irradiated sample and the unirradiated control baseline sample.

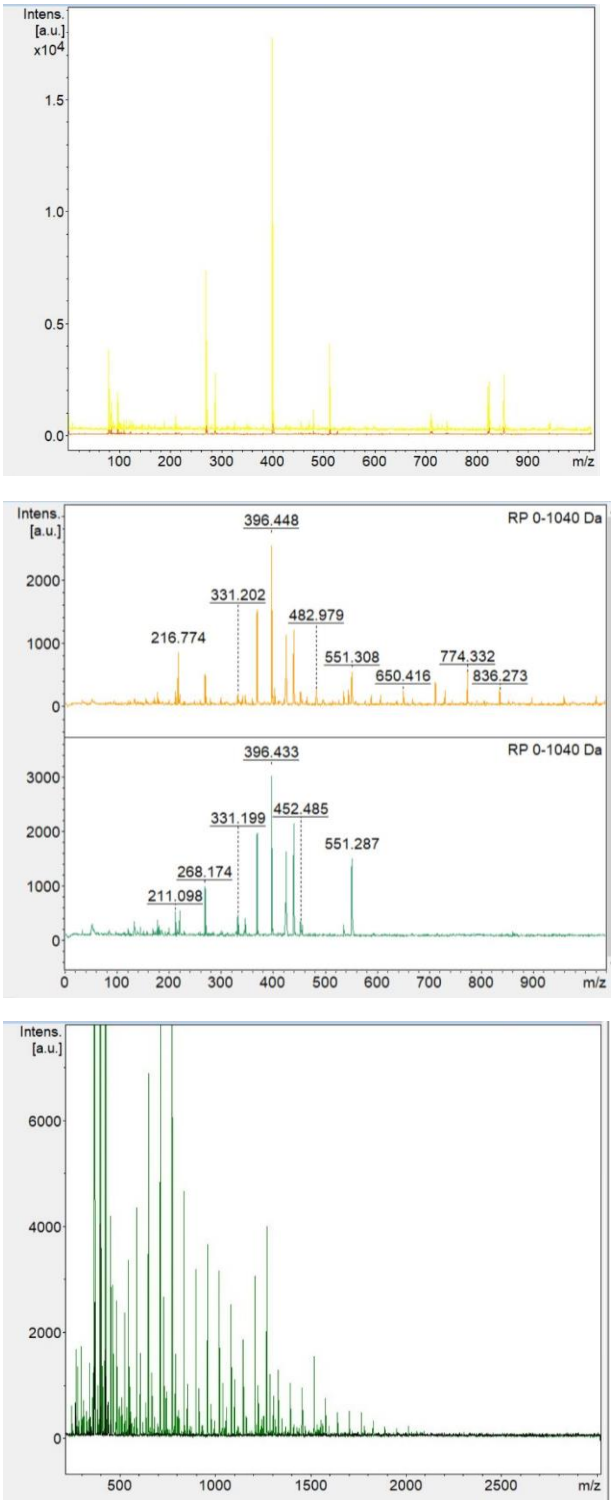

Figure 131: Figure containing three pairs of mass spectra of dry Actinide Resin analyzed using MALDI-TOF-MS, plotted as m/z or mass-to-charge ratio versus intensity. The top graph in each pair is the sample that received 50 kGy gamma exposure. The first pair of graphs is with the mass spectrometer with negative high voltage applied, the middle pair illustrates the same region with high voltage applied, and the last pair examines a wider mass range using the positive high voltage.

Figure 132 specifically examines low mass-to-charge ratio fragments of the dry Actinide Resin, with irradiated and unirradiated paired spectra for ease of comparison.

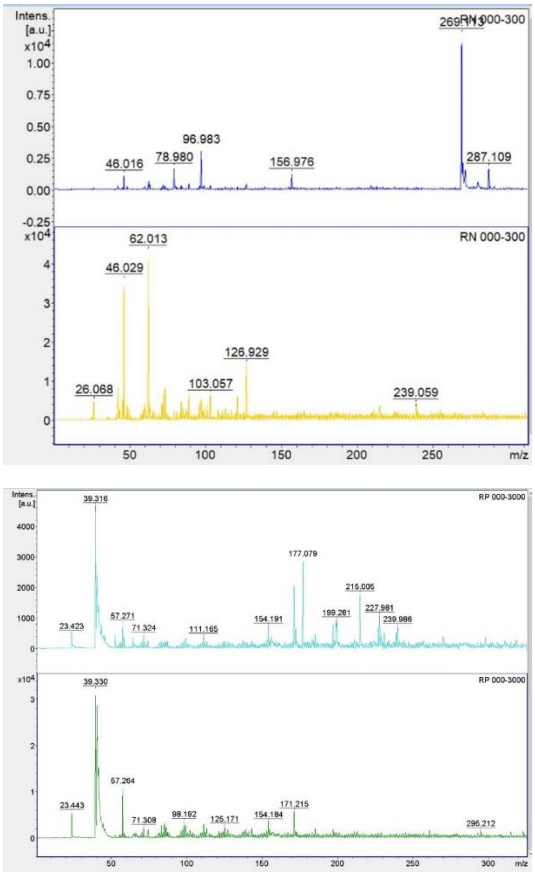

Figure 132: Figure containing two pairs of mass spectra of dry Actinide Resin analyzed using MALDI-TOF-MS, plotted as m/z or mass-to-charge ratio versus intensity. The top graph in each pair is the sample that received 50 kGy gamma exposure. The first pair of graphs is with the mass spectrometer with negative high voltage applied, and the bottom pair examines the same region with positive high voltage applied.

AFM: atomic force microscopy.

Analytical Resources Core (ARC): an analytical facility maintained by CSU that allows for the use of specialized analytical equipment. RRID: SCR_021758.

Attenuated Total Reflectance (ATR): a technique that, when used with FTIR, combines infrared spectroscopy with ATR sampling to analyze the molecular composition of materials.

Becquerel (Bq): an SI unit of radioactivity equal to one decay per second.

BPHA: N-benzoyl-N-phenylhydroxylamine, an organic chelating agent.

Cesium-137: a radioisotope of Cesium (atomic number 55), also written as $^{137}_{55}Cs$, ^{137}Cs, 137Cs, and Cs-137.

CMPO: octyl phenyl-N, N-di-isobutyl carbamoyl phosphine oxide, an organic extractant in the TRU Resin.

Colorado State University (CSU): university at which this research is being conducted.

Curie (Ci): a unit of radioactivity equal to 3.7×10^{10} Bq.

DAAP: diamyl amyl phosphonate, the organic extractant in the UTEVA Resin, also known as DPPP.

DIPEX: abbreviation for P, P'-di(2-ethylhexyl) methane-di-phosphonic acid, an organic extractant in the Actinide Resin, also known as bis(2-ethylhexyl) methane-di-phosphonic acid.

di-phosphonic acid (HEDPA): an organic extractant.

Distribution ratio (D) or (D_w): is the ratio of the concentration or amount of a particular analyte present in one phase of an extraction divided by that present in the other phase of an extraction. D_w is specifically the distribution ratio by weight. Most commonly, within the scope of this work, this is used to show the amount of analyte retained on an extraction chromatographic resin divided by the amount of an analyte that was still present in the aqueous phase after a separatory process was carried out.

DPPP: dipentyl pentyl phosphonate, also referenced as DP(PP) or DAAP, the organic extractant in the UTEVA Resin.

EB: electron bombardment, a method of ionization used in mass spectrometry.

EI: electron impact, a method of ionization used in mass spectrometry.

Environmental and Radiological Health Sciences (ERHS): department at Colorado State University (CSU) in which this research is being conducted.

Fourier-Transform Infrared Spectroscopy (FTIR): a technique used to obtain an infrared spectrum of absorption or emission of solid, liquid, or gas.

Gray (Gy): a unit of absorbed dose.

GC: gas chromatography

GC-MS: gas chromatography-mass spectrometry

HDEHP: di-2-ethylhexyl orthophosphoric acid, an organic extractant.

HEDPA: di-phosphonic acid, an organic extractant

HPLC: high performance liquid chromatography

IAEA: International Atomic Energy Agency.

IBMK: isobutyl methyl ketone, an organic solvent.

LC-MS: liquid chromatography-mass spectrometry.

LET: linear energy transfer

LSC: liquid scintillation counting.

MALDI-TOF-MS-MS: Matrix Assisted Laser Desorption Ionization Time of Flight Mass Spectrometer Mass Spectrometer.

MDP: methane-di-phosphonic acid, an organic extractant noted for its actinide and lanthanide affinity.

Meters (m): the SI base unit of length.

Molar (M): a unit of concentration, mol/L, moles per liter.

Nanometers (nm): a metric unit of length, equivalent to 10^{-9} meters.

Plutonium (Pu): chemical element with atomic number 94.

Plutonium-239: an isotope of plutonium, also written as ${}^{239}_{94}Pu$, ${}^{239}Pu$, 239Pu, and Pu-239.

SEM: scanning electron microscopy.

TBP: tri-n-butyl phosphate, an organic solvent in the TRU Resin.

TEM: transmission electron microscopy.

TEVA: extraction chromatography resin known for extracting TEtraValent Actinide materials.

TOPO: trioctyl-phosphine oxide, an organic solvent.

TTA: thenoyltrifluoroacetone, an organic chelating agent.

UTEVA: extraction chromatography resin known for extracting Uranium and TEtraValent Actinide materials.

XPS: x-ray photoelectron spectroscopy.